

Silver-containing diamond-like carbon deposited by plasma as versatile antibacterial coatings

**Thèse en cotutelle
Doctorat en génie des matériaux et de la métallurgie**

Maxime Cloutier

Université Laval
Québec, Canada
Philosophiae doctor (Ph.D.)

et

Université Pierre et Marie Curie
Paris, France
Docteur

© Maxime Cloutier, 2017

Silver-containing diamond-like carbon deposited by plasma as versatile antibacterial coatings

**Thèse en cotutelle
Doctorat en génie des matériaux et de la métallurgie**

Maxime Cloutier

Sous la direction de :

Diego Mantovani, directeur de recherche

Michael Tatoulian, directeur de cotutelle

Résumé

Les infections associées au milieu hospitalier demeurent une cause majeure de mortalité et de morbidité dans le monde, malgré plusieurs décennies dédiées à promouvoir une meilleure surveillance et des méthodes de désinfection plus complètes. La capacité des bactéries pathogènes à survivre sur des substrats solides a été identifiée comme un facteur clé de la pathogénèse de ces infections, en multipliant les sources de transmission et de contamination. Au niveau de la recherche, cette situation s'est récemment traduite par un intérêt marqué pour le développement de revêtements antibactériens novateurs pouvant constituer une ligne de défense complémentaire contre la colonisation bactérienne de surfaces, pourvu qu'ils puissent résister à l'environnement rigoureux des établissements de santé.

Dans cette thèse, nous avons émis l'hypothèse qu'un revêtement antibactérien avec une stabilité supérieure pouvait être déposé en utilisant un procédé plasma modulable, de sorte que les propriétés du revêtement résultant pourraient être adaptées aux exigences de différentes situations ou applications. Par conséquent, des revêtements nanocomposites de carbone amorphe adamantin contenant de l'argent (Ag-DLC) ont été développés et étudiés comme plate-forme polyvalente pour des surfaces antibactériennes. L'intérêt de ce matériau réside dans la combinaison des excellentes propriétés mécaniques, de la résistance à l'usure et de l'inertie chimique du carbone amorphe adamantin avec les propriétés antibactériennes à large spectre des nanomatériaux d'argent au sein d'un même revêtement déposé par plasma.

Ce travail a d'abord identifié les défis de conception spécifiquement associés au développement de revêtements antibactériens pour le milieu hospitalier. Des analyses approfondies des revêtements Ag-DLC ont ensuite démontré une bonne efficacité antibactérienne *in vitro* ainsi qu'une stabilité des propriétés, de la structure et de l'état chimique des revêtements dans le temps. L'étendue de la polyvalence des revêtements Ag-DLC a été évaluée au travers de l'identification des mécanismes de croissance principaux, permettant d'obtenir des informations essentielles sur la façon dont les propriétés des films, telles que la dureté, la teneur et la distribution d'argent, pouvaient être contrôlées en ajustant des paramètres spécifiques du dépôt plasma. De plus, un traitement de surface *in situ* a été développé pour surmonter les problèmes de délamination et a montré la capacité de favoriser l'adhérence de

revêtements DLC sur des substrats métalliques. Dans l'ensemble, cette étude a mis en évidence l'importance de la stabilité dans l'application des revêtements antibactériens et a démontré le vaste potentiel des procédés plasma pour le dépôt de revêtements antibactériens stables avec des propriétés adaptables.

Abstract

Healthcare-associated infections remain a major cause of mortality and morbidity worldwide, with a substantial financial burden on society, despite decades of monitoring and disinfection efforts. The ability of pathogenic bacteria to survive on solid substrates has emerged as a key contributing factor in the pathogenesis of these infections by multiplying the sources of transmission and contamination. This has prompted investigations into the development of innovative antibacterial coatings, which could provide a complementary barrier against bacterial colonization of surfaces provided that they can withstand the harsh operating environment of healthcare facilities.

In this thesis, we hypothesized that an antibacterial coating with superior stability could be deposited using a tailorable plasma process, so that the resulting coatings' properties could be adapted to match the requirements of different situations or applications. Therefore, silver-containing diamond-like carbon (Ag-DLC) nanocomposite coatings were developed and investigated as a versatile platform material for antibacterial surfaces. The interest of this material lies in the combination of the excellent mechanical properties, wear-resistance and chemical inertness of diamond-like carbon with the broad-spectrum antibacterial properties of silver nanomaterials in a single, plasma-deposited coating.

This work first identified the specific design challenges associated with the development of antibacterial coatings for healthcare environments. Thorough investigations of Ag-DLC coatings then revealed good antibacterial efficacy *in vitro* as well as stability of the coatings' properties, structure, and chemistry over time. The extent of the tailorability of Ag-DLC coatings was also assessed through the identification of the main growth mechanisms, providing insights on how the film's properties, such as the hardness, silver content, and silver distribution, could be controlled by adjusting specific plasma deposition parameters. Furthermore, an *in situ* interface plasma treatment was developed to overcome delamination issues and showed the ability to promote the adhesion of high stress DLC coatings on metallic substrates. Overall, this study highlighted the importance of stability in the application of antibacterial coatings and demonstrated the vast potential of plasma processes for the deposition of stable antibacterial coatings with tunable properties.

Table of contents

Résumé.....	iii
Abstract	v
List of tables	x
List of figures	xi
Abbreviations & Symbols	xvi
Acknowledgements	xviii
Foreword	xxi
1 Introduction	1
1.1 Context and motivation	1
1.2 Challenge	3
1.2.1 Healthcare-associated infections	3
1.2.2 Role of surfaces	6
1.2.3 Prevention strategies.....	9
1.2.4 Bacteria.....	10
1.2.5 Antimicrobial agents.....	14
1.3 Proposed platform	18
1.3.1 Surface engineering by plasma	19
1.3.2 Deposition techniques	25
1.3.3 Diamond-Like Carbon	28
1.4 Summary of approach and research objectives.....	33
2 Antibacterial coatings: challenges, perspectives and opportunities	35
2.1 Résumé.....	37
2.2 Abstract	38
2.3 Antibacterial surfaces in health applications	39
2.3.1 Advances in biomedical engineering prompted by the development of new materials	39
2.3.2 Nosocomial infections and the role of surfaces	39
2.3.3 Importance of antibacterial coatings.....	40
2.4 Relevance of release-based antibacterial coatings.....	45
2.4.1 Recent developments in antibacterial strategies.....	45
2.4.2 Key challenges	46
2.5 Release-based coatings	46
2.6 Control of release kinetics.....	48
2.6.1 Passive approaches.....	48
2.6.2 Active approaches – stimuli-responsive materials.....	51
2.6.3 Bacterial triggers approaches	52
2.7 Multifunctional coatings	55

2.7.1 Multi-release coatings.....	55
2.7.2 Multi-approach coatings.....	55
2.7.3 Multi-property (smart) coatings	56
2.8 Long-term stability	57
2.9 Conclusions and perspectives.....	61
3 Adhesion enhancement of DLC coatings on 316L stainless steel surfaces by <i>in situ</i> plasma carburation	63
3.1 Résumé.....	64
3.2 Abstract	65
3.3 Introduction.....	66
3.4 Materials & Methods.....	67
3.4.1 Sample preparation.....	67
3.4.2 Characterization	68
3.4.3 Adhesion tests.....	68
3.5 Results and discussions	69
3.5.1 Effect of interfacial treatment on composition.....	69
3.5.2 Depth profiling	74
3.5.3 Adhesion measurements.....	75
3.6 Conclusions	77
4 Controlled distribution and clustering of silver in Ag-DLC nanocomposite coatings using a hybrid plasma approach	79
4.1 Résumé.....	80
4.2 Abstract	81
4.3 Introduction.....	83
4.4 Experimental.....	84
4.5 Results.....	86
4.5.1 General composition and morphology of Ag-DLC coatings	86
4.5.2 Effect of silver ion flux.....	89
4.5.3 Effect of ion energy	91
4.6 Discussion	93
4.7 Conclusions	96
4.8 Acknowledgements	97
5 On the long term antibacterial features of silver-doped diamond-like carbon coatings deposited via a hybrid plasma process.....	98
5.1 Résumé.....	99
5.2 Abstract	100
5.3 Background	101
5.4 Materials &Methods.....	104
5.4.1 Materials.....	104

5.4.2	Plasma deposition of thin film.....	104
5.4.3	X-Ray Photoelectron Spectroscopy	104
5.4.4	Silver release analysis	106
5.4.5	Bacterial strain and culture preparation	106
5.4.6	Antibacterial activity test	106
5.4.7	Live/dead bacterial viability assay	106
5.4.8	Modified Kirby-Bauer diffusion test.....	107
5.5	Results and discussion	108
5.5.1	Chemical composition.....	108
5.5.2	Antibacterial activity evaluation	110
5.5.3	Release of silver ions from the coating.....	112
5.6	Conclusions	114
5.7	Competing interests.....	115
5.8	Authors' contributions	115
5.9	Acknowledgements	115
6	Long-term stability of hydrogenated DLC coatings: Effects of ageing on the structural, chemical and mechanical properties.....	116
6.1	Résumé.....	117
6.2	Abstract	118
6.3	Introduction.....	119
6.4	Materials & Methods.....	120
6.4.1	Sample preparation and storage	120
6.4.2	Characterisation	121
6.5	Results and discussion	122
6.5.1	Structural properties	122
6.5.2	Surface chemistry	125
6.5.3	Surface morphology	127
6.5.4	Mechanical properties.....	128
6.5.5	Tribological properties	131
6.6	Conclusion	132
6.7	Acknowledgment	133
7	General discussion	134
7.1	Summary and significance of contribution.....	134
7.2	Ag-DLC as a tunable platform	137
7.2.1	Choice of substrates.....	137
7.2.2	Structure and mechanical properties	138
7.2.3	Silver ions release.....	139

7.2.4 Antibacterial properties.....	140
7.3 Investigated areas of applications of Ag-DLC coatings	141
7.3.1 Healthcare environmental surfaces	141
7.3.2 Catalytic coating for depollution.....	142
7.4 Limitations.....	143
7.4.1 Limitations of this study.....	143
7.4.2 Limitations of Ag-DLC coatings	144
8 Conclusions and perspectives	146
9 References.....	147
Annexes	174
A. Stability and robustness assessment of Ag-DLC coatings	174
Abstract	175
Introduction.....	175
Experimental.....	176
Ag-DLC coatings deposition.....	176
Stability and robustness assessment.....	177
Conclusions	178
B. Report on the performances of Ag-DLC as catalytic coatings in an ozonation process	180
Context.....	180
Materials & Methods.....	181
Catalysis of ozone degradation	182
Catalyst in the degradation of a model pollutant.....	184
Stability of silver as a catalyst.....	185
Stability of Ag-DLC coatings under water flow	187
Conclusions	189
C. List of publications	190
D. List of scientific communications.....	192

List of tables

Table 1.1: Modes of transmission of pathogens. Adapted from [23, 31]	6
Table 1.2: Key factors facilitating surface-mediated transmission of infections.	7
Table 1.3: Ionization potential and dissociation energy of relevant atoms and molecules. Data from [99-101]	21
Table 1.4: Important parameters of plasma discharges and their respective impact on the deposition process. The selected examples are taken from DLC literature.....	27
Table 1.5: Interface modification strategies for the optimisation of adhesion strength.	32
Table 2.1: Main antibacterial compounds in release-based coatings	42
Table 2.2: Uses of plasma processes for antibacterial coatings and surfaces	59
Table 3.1 : Plasma treatment parameters	68
Table 3.2 : Chemical surface composition of untreated and treated samples measured by XPS.	72
Table 5.1: Critical properties to consider in the design of antibacterial coatings. Comparison between implantable devices and environmental surfaces.	103
Table 6.1: Hardness of DLC films measured by nanoindentation	131
Table B.1: Contact angle (water) of stainless steel and Ag-DLC coatings before and after 24h exposure to water flow	189

List of figures

Figure 1.1 : Pathogens associated with four of the most common HAIs in intensive care unit surveillance, 2003 (adapted from [20]). Gram-negative bacterial species are shown in color, gram-positive species are shown in black and white.....	4
Figure 1.2: Persistence of relevant pathogens on environmental surfaces (adapted from [26]). The estimated survival time, in months, is based on the average life of infective strains on dry, inanimate surfaces at room temperature. The reported persistence for <i>Klebsiella pneumoniae</i> (30 months) and <i>Salmonella typhimurium</i> (50 months) are not shown to their full extent in the graph.	8
Figure 1.3: The multiplication of pathogen reservoirs and infection transmission routes due to contaminated surfaces (adapted from [27]).	8
Figure 1.4: Cell wall structure of Gram-negative and Gram-positive bacteria (from [53]).....	11
Figure 1.5 : Model of the development of biofilms from planktonic cells and dispersal of bacteria from a mature biofilm [55].	12
Figure 1.6: Genetic and biochemical mechanisms of the development of bacteria resistance to biocidal metals (from [65]).	13
Figure 1.7: Mechanisms of action of silver against bacteria (from [78])	15
Figure 1.8: High-angle angular dark-field scanning TEM (HAADF STEM) images showing the interactions of silver nanoparticles with bacteria: (left) <i>E. coli</i> , (middle) <i>S. typhus</i> , (right) <i>P. aeruginosa</i> (adapted from [71]).....	16
Figure 1.9: Maxwellian energy distribution of electrons in a weakly ionized plasma (from [98]). Another function that can be used to describe electron energy distribution is the Druyvesteyn function.	21
Figure 1.10: Ion energy distributions for an Ar plasma at different rf-bias power showing the characteristic double energy peak of ions [103]......	22
Figure 1.11: Range of energies and densities for various species found in CCP (left) and ICP (right) processing plasmas (low pressure, RF discharges). From [96]	26
Figure 1.12 : (left) Parallel plate reactor (for CCP) and (right) inductively driven planar source (for ICP) [96, 124].	27
Figure 1.13: Ternary diagram of Diamond-Like Carbon. [140].....	29
Figure 1.14: a) Subplantation and relaxation processes leading to the formation of sp ³ bonding in a:C-H film [125]; b) Sp ³ fraction as a function of the bias voltage/ion energy [144]; c) The various plasma-surface processes playing in a role in the deposition of DLC [125].....	31
Figure 1.15: Graphical representation of the different topics addressed in this doctoral thesis.....	34
Figure 2.1: Schematics and images illustrating various passive strategies to control the release kinetics and antibacterial properties of coatings. a) AFM images showing the change of topography and nanotexture of Ti surfaces after an acid etching treatment [227]. b) SEM micrographs of cyclodextrin-based hydrogels with tunable porosity [228]. Porous coatings with a lower crosslinking density exhibit faster release kinetics than more crosslinked hydrogels. c) The deposition of a thin plasma polymer film can be used as a diffusion barrier for release-based antibacterial coating, enabling the	

control of the antibacterial agents rate of release by adjusting its thickness [229]. d) SEM images of TiO₂ nanotubes (NTs) used as tunable reservoirs for Ag NPs [230]. e) Other special architectures, such as dendrimers, can be used for loading and delivery of antibacterial compounds from a coating [221]. Figures reproduced with permission from Elsevier (a-b, d-e). ©2009 ACS (c) 50

Figure 2.2: Designing antibacterial coatings within a 4D perspective. The design strategies to control the release of antibacterial agents over space and time can be grouped under three main categories. a) Passive approaches. By tuning the coating's properties, it is possible to impose specific preloaded release kinetics, giving the possibility to produce a variety a release profiles, including rapid bursts (left) or linear release (right) from AB coatings. b) Active approaches. External stimuli can be used to trigger the local release of embedded compounds. c) Bacterial triggers approaches. Bacteria-responsive coatings release antibacterial agents locally when challenged by bacteria. Inset: examples of representative release profiles for each approach, showing the release rate as a function of time. 54

Figure 2.3: Control of release kinetics - Bacteria-triggered release. Coatings have been engineered to release antibacterial agents when subjected to two different bacterial triggers, the acidification of the local environment from bacterial metabolism and bacteria secreted enzymes. When challenged, the antibacterial compounds can be released by different mechanisms from simple bond cleavage to charge balance within the coating. 54

Figure 3.1 : a) XPS core-level spectra of C1s after plasma carburation treatment b) Example of decomposed spectrum. The c) Comparison of the C-Me/C-C ratio for the different treatment biases..... 71

Figure 3.2 : XPS core level spectra of C1s at the interface of samples treated with (a)-100V and (b)-250V plasma carburation treatment recorded at take-off angles from 15° to 80°. 72

Figure 3.3 : XPS core-level spectra of (a) Cr2p and (b) Fe2p after plasma carburation treatment. 73

Figure 3.4 : a) XPS depth profile of a DLC coated, interface treated sample (V_b=-650V). b) Evolution of the atomic concentration of the main metals (Fe and Cr) with the C-Me contribution measured using the C1s peak. 75

Figure 3.5 : Maximum tensile strength recorded during the pull-off experiment for specimens treated with etching (black, left) and plasma carburation at -650V (red, right). Each bar represents an individual DLC deposition and is the average of at least two pull-off tests. 76

Figure 3.6 : Optical micrograph showing a combination of adhesive and cohesive failure of an interface-treated (-650V) DLC coating after a pull-off test. The different zones observed are 1) 316L substrate (adhesive failure), 2) damaged DLC film (cohesive failure), and 3) intact DLC film. The stud initially covered zone 1 and 2. Scale bar, 250µm..... 76

Figure 3.7 : Representative optical micrographs showing the self-delamination and peeling of DLC coatings occurring for non-treated interfaces. Scale bar, 100µm. 77

Figure 4.1 : Graphical abstract 82

Figure 4.2: Example of XPS depth profile of Ag-DLC films (V_b =-100V, V_{Ag} =-750V) showing (a) the atomic percentages (at.%) of carbon, silver, oxygen and silicon with a zoom-in (inset) on the first 200s of sputtering, (b) the Ag3d5 peak binding energy, and

(c) the evolution of the silver modified Auger parameter as a function of the profiling time..... 87

Figure 4.3: (a, b) Representative SEM images (n=4) of Ag-DLC coatings. ($V_{Ag} = -750V$, $V_b = -100V$). c) Size distribution histogram of silver clusters ($N=1197$, $\square d = 1 \text{ nm}$). Dotted curves show the best fit simulated LND functions for each mode (M1 and M2) of the bimodal distribution. The solid curve is the sum of the two components. Counting was limited to particle diameter above 4.5 nm due to image resolution limits..... 88

Figure 4.4 : AFM topography (left panels) and phase contrast (right panels) images of DLC (a, b) and Ag-DLC coatings (c, d). Representative images taken from n =5. Please note the scale height/phase differences..... 89

Figure 4.5 : Effect of the variation of the silver target bias /silver flux on silver distribution in Ag-DLC films. a) Representative silver concentration profiles (n=2) measured by XPS profiling. b) Surface and bulk concentrations for each condition. Bulk Ag concentration corresponds to the average value between 200 and 300 s sputtering time..... 90

Figure 4.6 : Effect of Ag flux on silver clusters size and density in Ag-DLC. Representative AFM height images ($1 \times 1 \square m$, n=3) of coatings deposited with (a) low (-400V) and (b) high (-750V) silver target bias (V_{Ag}). 91

Figure 4.7: Representative XPS depth profile (n=3) analysis showing the effect of the ion energy (V_b) on silver dispersion and clustering in Ag-DLC samples. (a) Silver concentration (at.%) profiles, (b) Binding energy and (c) FWHM of the $Ag_{3d_{5/2}}$ peak for different substrate bias. Higher FWHM /BE shifts indicate the presence of smaller clusters. 92

Figure 4.8: Effect of ion energy on silver surface distribution and cluster size in a-C:H:Ag films. Representative AFM height images ($1 \times 1 \square m$, n=3) of coatings deposited at a substrate bias (V_b) of (a) 0V (b) -50V (c) -100V and (d) -150V substrate bias (V_b). Please note the scale height differences..... 93

Figure 4.9: Schematics of silver distribution for two different growth modes of a-C:H:Ag. Hydrocarbon ions subplantation leads to subsurface film densification and growth. The process also induces a thermally activated diffusion of Ag which, combined with the inability of Ag atoms to implant in the film due to their size, ultimately causes Ag segregation at the surface of Ag-DLC coatings where it diffuses to form nanoclusters. Surface growth occurs at all deposition biases (V_b) but is the only mode of growth in polymer-like coatings. This leads to a more uniform distribution of Ag through the coatings depth, with less fluctuation in cluster size. 96

Figure 5.1 : a) Deposition procedure of the Ag-DLC films b) Schematic of the plasma reactor 1. Quartz window, 2. Spiral antenna, 3. Matching and tuning networks, 4. RF generator (13,56 MHz, Max: 1000 W) of the ICP plasma source, 5a. VLF generator (3 kHz) for biasing of the silver target, 5b. Heating current supply 6. Vacuum system (throttle valve + turbo mechanical pump + primary mechanical pump), 7. LF generator (90 kHz) for biasing of the sample holder, 8. Sample holder (4 inches diameter), 9. Reactor door and observation window, 10. Silver target (silver wire 99,99% purity, biased and heated), 11. Mass flow controllers, 12. Gas cylinders. 105

Figure 5.2: Results of XPS analyzes: a) typical XPS survey of Ag-DLC (Ag 2.4 at.%), b) Silver concentration (at.%) of Ag-DLC films for different negative bias on the silver cathode and c) Depth profile showing the position of $Ag_{3d_{5/2}}$ peak (black squares) and oxygen concentration (red triangles) . In inset, high resolution Ag_{3d} peak showing the influence of the oxidation state on the peak position. 109

Figure 5.3 : Antibacterial activity of Ag-DLC coatings against *E. coli*. Fluorescent optical micrographs showing the distribution of Live (green)/Dead (red)-stained cells on a) uncoated silicon and b) 2.4at.% Ag-DLC coated silicon. c) Quantitative antibacterial activity test of Ag-DLC with different silver concentration. 111

Figure 5.4: a) Silver release (in $\mu\text{g/L}$ or ppb) from Ag-DLC (1.7 at% silver) coatings in deionized water, for up to two weeks. b) Modified Kirby-Bauer diffusion test with a 2.4 at% Ag-DLC coating at the middle. 112

Figure 6.1: Single-wavelength Raman spectroscopy ($\lambda=488$ nm) analysis of DLC samples. a) Typical Raman spectra showing both deconvoluted peaks and the fitted linear background. b) Pos(G) c) I(D)/I(G) ratio d) FWHM(G) and e) hydrogen content of as-deposited (squares) and aged (triangles) DLC films as a function of deposition power. 125

Figure 6.2: Representative XPS survey spectra of DLC films (deposition power 200 W) before and after ageing. Only carbon (C1s) and oxygen (O1s) were detected on both samples. 125

Figure 6.3: High resolution (HR) XPS analysis of the investigated films. a) HR XPS C(1s) spectrum of the DLC films with corresponding peak deconvolution (deposition power 150 W, post-ageing). b) Proportion of oxygen components of the C(1s) peak for the as-deposited and aged DLC films. 127

Figure 6.4: Representative water contact angle measurements of a) as-deposited ($81\pm 3^\circ$) and b) aged DLC coatings ($65\pm 3^\circ$)..... 127

Figure 6.5: Characteristic tapping mode AFM height images ($1\ \mu\text{m} \times 1\ \mu\text{m}$) of DLC films a) as-deposited and b) aged (deposition power 250 W). Please note that the vertical scale bars represents only 1 nm, for both images. 128

Figure 6.6: Compressive stress measured experimentally in as-deposited (square, black) and aged (triangle, red) DLC coatings, as a function of deposition power. 130

Figure 6.7 : Representative nanoscale friction measurements (deposition power 150 W) of as-deposited (square, black) and aged (triangle, red)..... 131

Figure 7.1: The different investigated strategies for the controlled release of Ag^+ ions from silver-based plasma coatings. 140

Figure A.1: Silver concentration (measured by XPS) as a function of sputtering depth for coatings deposited at 0V (red circles) and -100V (black square) bias voltage. The hardness and silver ion release values for each conditions are also shown. Both coatings were deposited at the same silver flux, [H] and [CH] concentrations. 177

Figure A.2 Representative SEM images of a) $V_b=0\text{V}$ coating after 20 wear cycles and b) $V_b=-100\text{V}$ coating after 1000 wear cycles. c) Silver content at the surface of 0V, 50 and 100V Ag-DLC coatings for an increasing number of cleaning cycles. 178

Figure B.1 Schematic of the setup used in the ozone degradation experiment. 182

Figure B.2 : Typical reaction kinetics of ozone in solution, measured by UV-Spectroscopy. Because of the upper sensitivity detection limit of the setup, the initial stage of the decomposition kinetics could not be observed and were labeled over-saturation stage. 183

Figure B.3 : Ozone decomposition curves when in contact the different silver-based catalyst investigated. The time constants presented on the right figure are associated with the first-order decomposition kinetics measured in the second stage (decomposition stage) of the experiment. 184

Figure B.4 : Degradation of pyruvic acid after 1 hour. 185

Figure B.5 : Representative images of sputtered silver coatings (on COC substrates) after 1 cycle of ozonation experiment..... 186

Figure B.6 : Representative images of Ag-DLC coatings on stainless steel before (as-deposited) and after ozonation. Top pictures are optical microscopy (zoomed X20). 186

Figure B.7 : Optical microscopy images (50X) of Ag-DLC coated microchannels after 24h under a dynamic water flow. (Top) Inside of microchannels (Bottom) Ridge between pairs of microchannels..... 187

Abbreviations & Symbols

Below is a list of abbreviations and terms used throughout this project. The large majority of the listed abbreviations are already defined in the body of the thesis but are grouped here for ease of reference.

AB: Antibacterial

a-C: Amorphous carbon

a-C:H: Hydrogenated amorphous carbon

AFM: Atomic force microscopy

Ag-DLC: Silver-containing diamond-like carbon

AMP: Antimicrobial peptides

BE: Binding energy

CFU: Colony-forming unit

DC: Direct current

DLC: Diamond-like carbon

FWHM: Full width at half maximum

GF-AAS: Graphite furnace atomic absorption spectroscopy

HAI: Healthcare-associated infection

ICP: Inductively-coupled plasma

IED: Ion energy distribution

LbL: Layer-by-layer

LND: Lognormal distribution

LTE: Local thermodynamic equilibrium

LOD: Limit of detection

LOL: Limit of linearity

LOQ: Limit of quantification

MRSA : Methicillin-resistant staphylococcus aureus

NP: Nanoparticle

PECVD: Plasma-enhancement chemical vapor deposition

PEG: Polyethylene glycol

PEM: Polyelectrolyte multilayer

PVD: Physical vapor deposition

QAC: Quaternary ammonium compound

QS: Quorum-sensing

RF: Radio frequency

ROS: Reactive oxygen species

SEM: Scanning electron microscopy

SS316L: Stainless steel 316L

VLF: Very-low frequency

XPS: X-ray photoelectron spectroscopy

α' : Modified Auger parameter

R_{RMS} : Root mean squared roughness

σ_M : Geometric standard deviation or shape parameter

T_e : Electron temperature

V_{Ag} : Bias voltage applied to the silver target

V_b : Bias voltage applied to the substrate holder

Acknowledgements

A ma femme H el ena et   mes parents, Ann et Richard,
Cette th ese est autant votre r eussite que la mienne, merci.

To my wife H el ena and to my parents, Ann and Richard,
This thesis is as much your success as it is mine, thank you.

Autant le travail d'écriture d'une thèse peut être un exercice solitaire et qui rejoint, au final, qu'un nombre très restreint de lecteurs, autant la thèse elle-même n'est possible que par l'apport et le soutien d'une foule de personnes. Ces quelques lignes sont dédiées à tous ceux qui ont contribué, de près ou de loin, au succès de mon parcours doctoral.

Je tiens à remercier tout d'abord mes superviseurs, Pr Diego Mantovani et Pr Michael Tatoulian, pour la confiance qu'ils m'ont accordée en acceptant de mettre en place et d'encadrer ce travail doctoral. Votre accessibilité, votre ouverture, et votre soutien continu (même pour régler mes trop nombreux soucis administratifs) ont contribué autant que votre créativité et votre encadrement scientifique à la réalisation de cette thèse. Mais surtout, vous avez réussi à créer, chacun de votre côté, des laboratoires où la science autant que les relations humaines sont mis de l'avant et dans lesquels j'ai eu un plaisir réel à évoluer durant les dernières années.

Un grand merci aux nombreuses personnes ayant eu la tâche (que j'espère n'avoir pas trop rendue ingrate) de me superviser à une certaine étape de mon parcours scientifique : Dr Pascale Chevallier, Pr Paul De Koninck, Dr Cédric Guyon, Dr François Lewis, Dr Stéphanie Ognier, Dr Andranik Sarkissian, et Dr Stéphane Turgeon. Le chemin est assez long et complexe entre le baccalauréat et la fin du doctorat. Vous m'avez aidé à le parcourir à ma façon, tout en m'évitant pas mal d'embûches.

Bien qu'on réussisse à s'éloigner de notre laboratoire quelques journées par année, le quotidien d'un doctorant y reste malgré tout lié. Je veux donc remercier du fond du cœur tous les collègues avec lesquels j'ai pu échanger, apprendre, et grandir durant mon passage. A mes collègues de Paris – Alex, Bradley, Cédric, Dia, Diane, Eric, Fred, Olivier, Mengxue, Rafik, Simon, Xi et j'en passe - merci pour l'accueil toujours chaleureux, les discussions, les vendredis gras, les soirées, et les énigmes. Les moments passés chez vous ont toujours paru trop courts. A mes collègues de Québec (il y en a beaucoup trop pour tous les nommer) – Andrée-Anne, Audrey, Bernard, Carlo, Caroline, Daniele, Éléonore, Essowe, Farid, Fred, Gad, Jean, Julien, Laurence, Linda, Livia, Lucie, Mahrokh, Marie, Mathieu, Meryem, Morgane, Myriam, Nina, Olivier, Pascale, Ranna, Sébastien, Sergio, Stéphane, Vanessa et les autres. Vous avez toujours réussi à faire de notre petit centre de recherche un endroit où l'on prenait plaisir à y retourner jour après jour, malgré l'absence de soleil!

Une pensée bien spéciale aussi à ceux et celles qui ont été présents pendant une bonne partie de mon parcours. J'espère bien que nos routes continueront à se croiser régulièrement dans l'avenir. Pascale – Merci pour m'avoir pris sous ton aile dès mon premier stage, pour tes conseils, ton soutien et pour toutes les fois où tu as passé mes échantillons XPS en priorité! Stéphane – Le seul probablement toujours partant pour discuter science, système à vide ou DLC! Merci pour ta rigueur et ton sens du savoir-faire, des qualités qui j'espère auront déteint un peu sur moi. Olivier – Mon « analogue » DLC côté français, mais surtout quelqu'un avec qui j'ai eu plaisir fou sur deux continents. Merci pour toutes les discussions, les voyages, les soirées et pour l'accueil. Tu reviens au Québec quand tu veux! Éléonore et Vanessa – Vous veniez presque toujours en paire donc aussi bien vous garder comme cela. Je vous ai peut-être fait vieillir prématurément avec toutes les mini crises cardiaques créées en me croisant dans les corridors. Merci de m'avoir enduré depuis le début et pour tous les souvenirs.

Un merci du fond du cœur à mes parents, Ann et Richard. Outre votre contribution génétique non négligeable, vous avez aussi su instiller en moi une curiosité, un désir d'apprendre et une certaine forme d'entêtement dès mon plus jeune âge qui ont fait de moi la personne que je suis aujourd'hui. Ça a sans doute contribué plus que tous autres facteurs à la réussite de ce doctorat. Je vous confie maintenant (en partie) la tâche de faire de même avec la prochaine génération.

Une pensée spéciale à mon fils, Félix, et à son petit frère qui s'en vient, qui ont fait des derniers mois de ma thèse une période beaucoup moins stressante que je ne l'aurais imaginé initialement.

Enfin, mes derniers remerciements vont à mon extraordinaire femme, Héléna, qui a parcouru tout ce chemin (et bien plus) avec moi. Je ne t'ai pas fait la vie facile avec mes habitudes nocturnes, mon horaire de travail bizarre et mes allers-retours entre la France et le Québec. Merci pour tes sacrifices, tes conseils, ton aide, pour m'avoir épaulé et supporté pendant les hauts et les bas de ma thèse, et pour m'avoir constamment démontré que la vie est toujours plus belle lorsqu'elle est partagée avec toi. C'est la seule raison pour laquelle tu n'auras pas besoin de m'appeler Dr Cloutier!

Foreword

From the reader's perspective, the study presented herein could be looked at strictly as a work on antibacterial surfaces and plasma deposition. However, from the author's standpoint, it should also be seen through a broader lens, particularly in regard to the objective and scope of the research effort. Instead of focusing strictly on an optimisation process, this thesis was aimed at addressing the challenge of creating a flexible and tunable material platform, capable of exhibiting multiple properties or functions. As such, its potential resides not only in finding application in different fields, from water decontamination to antibacterial hospital surfaces, but also in our ability to adapt the produced materials' properties to match specific aspects of a chosen environment. Therefore, this thesis explores the ways in which we can understand, improve and control the properties of the Ag-DLC nanocoatings rather than evaluating their performances in a particular setting.

The intrinsic multidisciplinary and breadth of work that characterize this project called for its realisation in a strongly collaborative environment. For this reason, this thesis was pursued as a "cotutelle" between the Laboratory for Biomaterials and Bioengineering (LBB) at Université Laval (Québec, Canada) and the Laboratoire Procédés, Plasmas, Microsystèmes (2PM) at Université Pierre et Marie Curie (UMPC-Sorbonne, Paris, France). The rich collaborative history, complementarity of expertise and quality of research teams in both laboratories were paramount in the realisation of this thesis.

This work is not an extension of previous research from either groups but rather a new investigation. Therefore, the general objectives of the thesis were to first synthesize Ag-DLC coatings using a plasma-based deposition process and then investigate their potential as a material platform through the exploration of four different aspects: i) the interface between metallic substrates and DLC coatings; ii) the analysis of growth mechanisms and distribution

of silver; iii) the measurement of silver-release and antibacterial properties; iv) the evaluation of long-term stability. These results are presented as four published articles making up chapters 3, 4, 5 and 6, respectively, of the current thesis. In addition, the field of antibacterial coatings and the role that silver and plasma-based coatings like Ag-DLC can potentially play within that field have been reviewed and published in a comprehensive review article, presented in chapter 2. Additional unpublished materials that bear relevance to this thesis are presented at the end of this manuscript in annexes.

Further details on the published articles integrated to this thesis are given below.

Chapter 2: Antibacterial Coatings: Challenges, Perspectives, and Opportunities

Authors: Cloutier, M., Mantovani, D., Rosei, F.

Published October 2015 in Trends in Biotechnology, 33 (11), 637-652.

All authors jointly identified the scope of the review article. MC reviewed the literature and wrote the manuscript, under the supervision of DM and FR.

Chapter 3: Adhesion enhancement of DLC coatings on 316L stainless steel surfaces by in situ plasma carburation

Authors: Cloutier, M. Turgeon, S., Chevallier, P., Tatoulian, M., Mantovani, D.

Journal: Applied Surface Science (to be submitted)

MC designed and performed all the experiments, analyzed the data and wrote the manuscript.

MC and ST came up with the original idea for plasma carburation. ST and PC helped with the

acquisition and analysis of XPS. MT and DM edited the manuscript. All authors discussed the results and implications and commented on the manuscript at all stages.

Chapter 4: Controlled Distribution and Clustering of Silver in Ag-DLC Nanocomposite Coatings Using a Hybrid Plasma Approach

Authors: Cloutier, M. Turgeon, S., Busby, Y., Tatoulian, M., Pireaux, J.J., Mantovani, D.

Published July 2016 in: ACS Applied Materials & Interfaces, 8 (32), 21020-21027.

MC designed and performed all the experiments, analyzed data and wrote the manuscript.

MC and ST designed the study. MC, ST and YB planned and performed the XPS experiments and analyzed the results. MC wrote the manuscript. JJP provided conceptual advice on the XPS investigation. All authors discussed the results and implications and commented on the manuscript at all stages.

Chapter 5: On the long term antibacterial features of silver-doped diamondlike carbon coatings deposited via a hybrid plasma process

Authors: Cloutier, M. Tolouci, R., Lesage, O., Lévesque, L., Turgeon, S., Tatoulian, M., Mantovani, D.

Published June 2014 in Biointerphases, 9 (2), 029013.

MC, OL and ST designed the study. MT and DM supervised the project. MC, RT, OL and ST performed non-biological experiments. LL designed and performed the antibacterial tests and helped in the results analysis. MC and OL wrote the manuscript. All authors discussed the results and edited the manuscript.

Chapter 6: Long-term stability of hydrogenated DLC coatings: Effects of aging on the structural, chemical and mechanical properties

Authors: Cloutier, M., Harnagea, C., Hale, P., Seddiki, O., Rosei, F., Mantovani, D.

Published September 2014 in *Diamond and Related Materials*, 48, 65-72.

MC designed the experiments. PH and OS carried out the first set (year 0) of experiments. MC performed the second set (year 3) of experiment and analyzed the data. CH performed the friction experiments. MC wrote the manuscript. CH, FR and DM oversaw the redaction and edited the manuscript.

1 Introduction

1.1 Context and motivation

Healthcare associated infections (HAIs) continue to be a major public health concern in healthcare units worldwide and has been attracting the attention of public health stakeholders for several decades. Although it is difficult to evaluate, their cost, both human and financial, remains staggering, even in this day and age. The number of HAIs in the US, makes it one of the most common adverse event in healthcare. A 2011 survey in acute care hospitals revealed an estimated 725 000 HAIs cases, amongst which 75 000 resulted in deaths [1]. This number goes up to 1.7 million cases of HAIs and 99 000 death annually, when considering the entire healthcare system [2]. Similarly high prevalence rates of HAIs are reported throughout developed countries, 5.4% in France and 8.0 % in Canada, with some units (*e.g.* pediatric intensive care, transplant units) experiencing rates close to 30% [3-6]. In low- and middle-income countries, the consequences of HAIs are even more dire, with an average prevalence rate of 15.5% [5]. While negligible compared to morbidity and mortality, the economic impacts of bacteria related diseases also put an additional burden on the healthcare system and global productivity of communities. Estimates of annual direct costs of HAIs vary due to differences in methodologies but remain significant in all cases; between 7 and 23 billion USD [2, 7] and up to 7 billion € in Europe [5, 8]. Furthermore, the topic of HAIs has become highly politicised during the last decade, negatively impacting the perception of healthcare systems and tarnishing the image of medical practitioners around the world [9].

Lately, clinical and epidemiological evidences have further underlined the importance of a new area of concern in the fight against HAIs [10-12]. Pathogens are capable of surviving for weeks on environmental surfaces (inanimate objects in the immediate vicinity of a patient such as bed rails, lavatory sinks, over-bed tables, floors, etc.), which become reservoirs of pathogens. Healthcare workers, visitors or the patients themselves may contaminate their hands or gloves by touching contaminated surfaces, thereby multiplying the potential sources of pathogen transmission to patients [13-15].

The use of antibacterial surfaces has been advocated as a viable solution to reduce the risks posed by contaminated environmental surfaces. In this case, however, their design entails a number of stringent requirements, different from those of surfaces intended for medical

devices applications. For them to be effective in near-patient clinical areas, such antibacterial surfaces must be used in conjunction with, and therefore resist, frequent cleaning and disinfection procedures. Thus, they must exhibit chemical stability, good wear-resistance, and superior mechanical properties, in conjunction with long-term antibacterial properties.

1.2 Challenge

1.2.1 Healthcare-associated infections

1.2.1.1 Historical perspective

While many bacteria are either beneficial or harmless to the human body, history has shown the dire consequences that some pathogens can have. Famous examples of deadly bacteria abound: the Black Death (*Yersinia Pestis*), one of the most devastating pandemics in human history that peaked during the middle of the 14th century, typhus (*Rickettsia*), with known outbreaks ranging from the Classical Greece to the second world war and tuberculosis (*Mycobacterium tuberculosis*), which was a major killer in Europe in the past and still causes many deaths in Africa. Despite an increasing knowledge of microorganisms, marked by Antonie van Leeuwenhoek's first observation of unicellular organisms in 1674, Louis Pasteur's experiments regarding germ theory in the early 1860s and Robert Koch's postulates formulated in 1884 establishing a causal relationship between an infection and a causative microbe [16], and the consequent establishment of modern hygiene practices, pathogens are still a major cause of disease and death nowadays.

1.2.1.2 Definition and classification of HAIs

Healthcare-associated infections¹ (HAIs) are defined as infections acquired while receiving medical treatment in a healthcare facility [17]. As presented previously, HAIs are a major cause of morbidity and mortality, as well as a significant financial burden. Their existence obviously predates any modern literature, but the role of pathogens in HAIs has been closely monitored by public health agencies since the inception of global surveillance programs in the 1970s. While the term pathogen used previously actually englobes all types of infecting organisms such as bacteria, viruses, fungi or even prions, HAIs are for the vast majority caused by bacteria. A notable exception is the norovirus, the most common cause of viral gastroenteritis in humans [18]. Clinically, HAIs are classified based on the location of the infection. Common examples include urinary tract infections (UTI), pneumonia, bloodstream infections (BI), surgical site infections (SSI) and *C. difficile* infections [17].

¹ Other common names include hospital-acquired infections and nosocomial infections.

Any pathogenic organism may theoretically cause an HAI under the right conditions, but 8 pathogens account for about 80% of all HAIs [19]. Furthermore, each bacteria is not restricted to a single type of infection, each of them has been reported as a causative pathogen for all of the most noteworthy HAIs (Figure 1.1). In general, pathogen distribution and prevalence amongst infected patients have been showed to vary with time, location/department type and patient type, amongst other factors [6, 20-22].

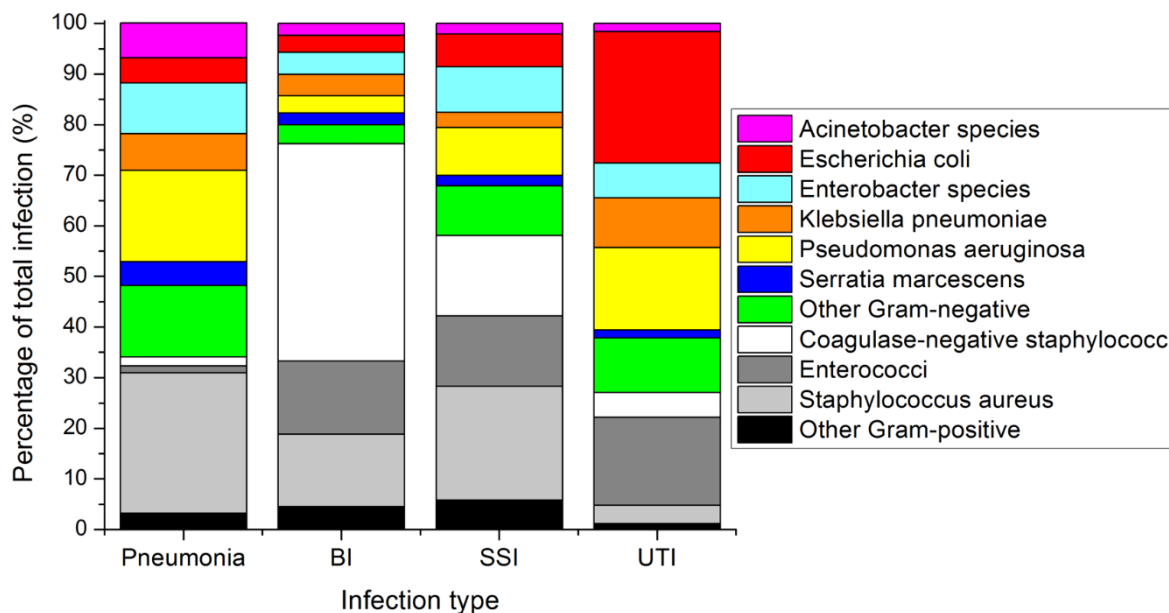


Figure 1.1: Pathogens associated with four of the most common HAIs in intensive care unit surveillance, 2003 (adapted from [20]). Gram-negative bacterial species are shown in color, gram-positive species are shown in black and white.

1.2.1.3 Etiology of HAIs

The development of an infection entails the presence of three elements: a source of pathogens, a susceptible host, and a mode of transmission for the infectious agent [23]. Public health researchers and agencies have looked within this epidemiology triad to develop infection prevention strategies.

Sources

Major sources of infection agents in healthcare settings are either humans, (patients, healthcare workers or visitors), inanimate environmental surfaces or the endogenous flora of patients [23]. Although one of the primary source in healthcare settings, carriage of pathogens by human is

typically short-lived. However, some human sources, such as incubating, asymptomatic or transiently colonized carriers, are considerably more difficult to detect than carriers with active infections [23, 24]. Epidemiological and clinical studies have confirmed the role of environmental surfaces as reservoirs of pathogens [25-27]. Since surfaces also play an important role in infection transmission, this topic will be discussed in more details in section 1.2.2.

Transmission

There are six possible modes of transmission for infection-causing pathogens (Table 1.1). The role of direct, droplet and airborne transmission in the spread of HAIs have been well-recognized for several decades. Bacterial infections are more commonly passed on by direct contact, usually by the hand of healthcare workers [28]. This has resulted in the implementation of several strategies targeting these modes of transmission, with programs to improve compliance with hand hygiene best practices as their cornerstone [29, 30]. However, the role of surfaces, and consequently of indirect contact transmission, have emerged much more recently. Researchers have shown that several pathogens can contaminate hospital surfaces and play an important role in transmission events of HAIs. This will be described in more details below. Lastly, although they are important from an epidemiological standpoint, neither vehicle nor vector-borne transmission play a significant role in the transmission of HAIs.

Table 1.1: Modes of transmission of pathogens. Adapted from [23, 31]

Mode of transmission		Description	Important dissemination factors
Contact	Direct	Person to person transmission without intermediate object/person.	Ungloved contact, skin cuts or abrasions
	Indirect	Contact with a contaminated intermediate object, usually inanimate or contaminated gloves.	Near-patient surfaces (tables, beds, floors), patient-care devices
	Droplet	Transmission through large (>5µm) particles.	Coughing, sneezing or talking.
Non-contact	Airborne	Transmission via droplet nuclei (<5µm) or dust particles.	Ventilation systems.
	Vector-borne	Insect or animal vectors	Mosquitoes, flies, rats, etc.
	Vehicle	Single contaminated source spreading the infection (e.g. infected batch of food)	Food, water, medication, etc.

Host

The susceptibility of the host, the final link in the infection chain, is linked with genetic and intrinsic factors such as age, severity of underlying illness, loss of skin, and degree of immunosuppression [32]. Furthermore, a patient’s susceptibility of contracting an HAI has been also strongly correlated with the use of indwelling medical devices. Catheter-associated UTIs remain one of the most common healthcare infections [33]. Similarly, the use of ventilators and central venous catheters have been respectively associated with an increased incidence and severity of pneumonia and BIs [5, 34, 35].

1.2.2 Role of surfaces

The intricate array of events leading to a patient being infected has complicated the estimation of the full extent of the role played by environmental surfaces in the spread of HAIs. Most of the epidemiological proofs linking pathogens found on environmental surfaces with specific infections has been indirect. Weber et al. have showed patient-to-patient transmission to be directly proportional to the local level of environmental contamination [36]. Likewise, many

studies have linked improved room disinfection procedures to lower incidence of HAIs [12, 37-39]. Still, the substantial body of evidence accumulated over the last decade have led the scientific and medical communities to recognize the key role of environmental surface in the transmission of HAIs. Key factors influencing HAIs transmission via surfaces are presented in Table 1.2.

Table 1.2: Key factors facilitating surface-mediated transmission of infections.

Factor	Examples	Refs
Persistence of numerous key pathogens on environmental surfaces for several months	<i>E. Coli</i> can persist for up to 16 months on dry inanimate surfaces (see further examples in Figure 1.2)	[26, 36]
High proportion of near-patient surfaces contaminated by pathogens	Estimated mean MRSA contamination rates of common surfaces in clinical areas: floor (35%), overbed table (40%), siderails (27%) room door handle (22%), sink taps (24%).	[10, 12, 40]
Low threshold for minimum infective dose	10 CFU inoculum of staphylococci have the potential to cause an infection	[10, 15]
Relative inefficiency of current disinfection procedures to remove pathogens from surfaces	<i>C. difficile</i> was cultured from 44% of surfaces in 9 rooms after bleach disinfection was implemented during an outbreak	[27, 41]
Rapid transfer from surfaces to hand (and vice versa)	46% glove contamination rate from touching bedrails of VRE patients	[42, 43]

Environmental surfaces contribute to the multiplication of infection pathways to patients. They may act as reservoirs or as transient sources of pathogens, from which patients or healthcare workers may get contaminated (Figure 1.3). Studies have shown contamination by pathogens of numerous near-patient surfaces including, but not limited to, door handles, clothes and linens (bed sheets, patient gowns, healthcare workers clothes), hospital beds (including overbed table, siderails), bathroom surfaces (sink, bathroom door handle) and portable equipment [10, 28]. The majority of these surfaces are likely to be touched by hands

on a daily basis. Operating rooms have also encountered environmental surface contamination issues, with floors and anesthesia equipment showing high contamination rates [44].

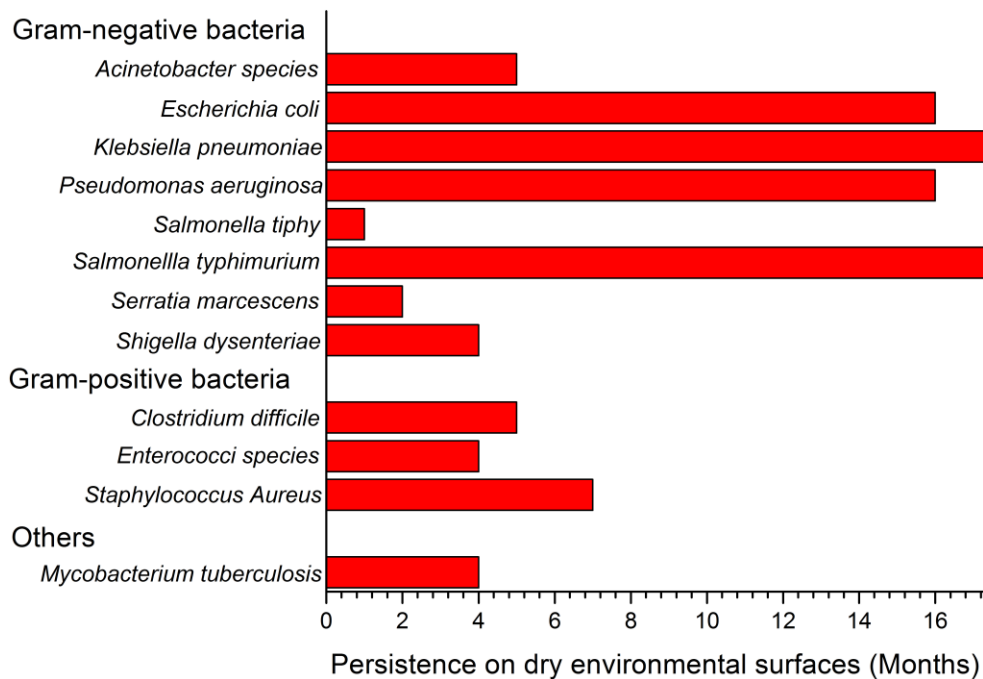


Figure 1.2: Persistence of relevant pathogens on environmental surfaces (adapted from [26]). The estimated survival time, in months, is based on the average life of infective strains on dry, inanimate surfaces at room temperature. The reported persistence for *Klebsiella pneumoniae* (30 months) and *Salmonella typhimurium* (50 months) are not shown to their full extent in the graph.

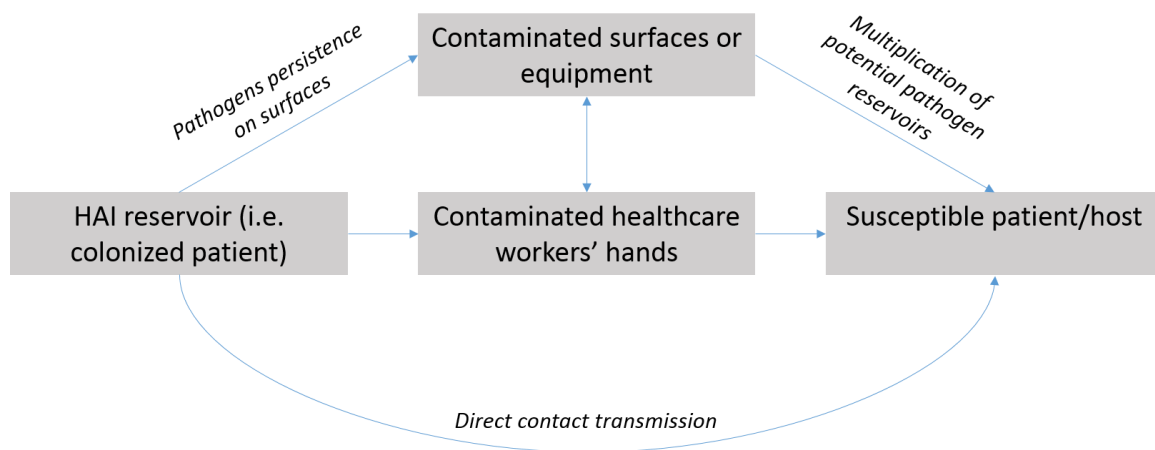


Figure 1.3: The multiplication of pathogen reservoirs and infection transmission routes due to contaminated surfaces (adapted from [27]).

1.2.3 Prevention strategies

Increased recognition of the importance of environmental surfaces in the transmission of HAIs have spurred the search for new ways of preventing bacterial colonization of surfaces in healthcare settings. The inanimate environment is probably one of the transmission factors that can be managed most efficiently with proper preparation [44]. It is estimated that as many as 55% to 70% of HAIs may be preventable if necessary measures are undertaken to reduce the level of contamination currently found on environmental surfaces [7]. The inhomogeneity and variations in pathogens distribution have led scientists to call for the use of broad, horizontal approaches, which can target multiple bacterial species at the same time for infection prevention, rather than vertical, species-specific interventions [45].

Several potential approaches of decreasing the level of contamination of environmental surfaces in healthcare settings have been proposed. Integrating more thorough and frequent cleaning protocols, using disinfectants rather than detergent and water, is seen as the most affordable approach [46]. Studies have shown decreases in surface contamination and reductions of HAIs after substituting detergent-based cleanings with active oxygen-based compounds or hypochlorite solutions [47, 48]. However, there are several issues with disinfectant approaches. First, high levels of compliance (>80%) are needed to ensure reduction of HAIs [48]. Based on similar experiences and due to the complexity of the hospital environment, these compliance levels are not sustainable on the long term [49]. Second, the use of a cleaning agent that is not completely effective against a target microorganism can spread pathogens to other surfaces [27]. Third, metals and equipment may get damaged by using liquid disinfectants, especially if they contain chlorine [50]. Finally, the liberal use of disinfectants, which are discharged into the environment, may foster the development of resistance in bacteria and have other, more general environmentally damaging effects in addition to being potentially harmful to users [27].

Novel environmental decontamination technologies such as ultraviolet germicidal irradiation have been studied as potential dry disinfection technologies, circumventing a lot of the issues plaguing traditional disinfectants. However, their ineffectiveness at eliminating pathogens not in a direct line of sight of the generator make them an incomplete solution [51].

A principle that have progressively taken hold among the different interested parties and experts is that infection prevention must be viewed as a holistic process. Therefore, it is better

serve by a comprehensive multibarrier approach, where disinfection control programs are combined with antibacterial surfaces. The development of antibacterial coatings for near patient areas can play an important role in the global mitigation strategy of HAIs, by reducing microbial loads on a surface without outside intervention. Therefore, such coating would provide an additional, complementary barrier to pathogen transmission, while acting in conjunction with normal cleaning and disinfection procedures. The suitability of engineered materials for such task typically depends on their stability and general ability to withstand harsh operating conditions. Chapter 2 presents a complete literature review of antibacterial coatings.

1.2.4 Bacteria

1.2.4.1 Generalities

As one of the first life forms to emerge on our planet, bacteria constitute a large and diverse domain of prokaryotic (unicellular) microorganisms, englobing millions of species. Typically between 0.5 and 5 μm in length, bacteria display a wide variety of morphologies: spherical (cocci), rod-shaped (bacilli), curved-rods (vibrio), spiral-shaped (spirilla), etc. Bacterial populations can reach extremely rapid growth, achieved through binary fission of individual unicellular organism. Under optimal conditions, populations of HAI-relevant bacteria like *E. Coli* and *S. Aureus* can double in 17 and 27 minutes, respectively [52].

The bacterial cell is surrounded by a lipid membrane, encasing the cytoplasm of the cell and acting as a barrier to hold all of its components (nutrients, proteins, etc.) within it. Unlike eukaryotes, bacteria do not have nucleus. Their genetic material is loosely located in the cytoplasm and consists of a single circular DNA chromosome. In addition to the cell membrane, most bacteria also possess a cell wall. Differences in cell wall's structure and composition is the basis for one of the most common classification dichotomy within the bacteria domain: gram-negative (thin cell wall) and gram-positive (thick cell wall) bacteria (Figure 1.4). Differences in structure usually induce differences in antibiotic susceptibility and should be taken into account when developing antibacterial approaches.

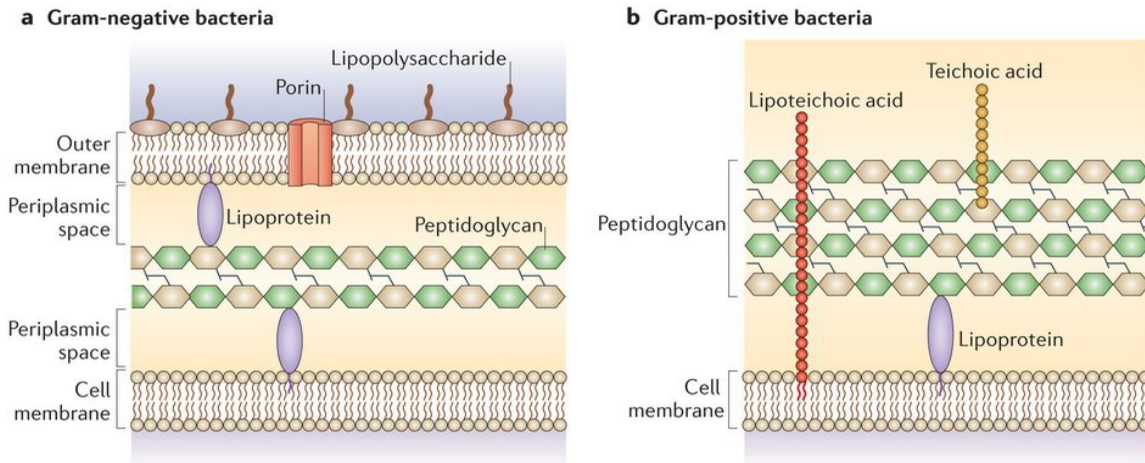


Figure 1.4: Cell wall structure of Gram-negative and Gram-positive bacteria (from [53])

1.2.4.2 Biofilms

Bacteria undergo major changes during their transition from the planktonic state, where cells are isolated and free in the environment, to a sessile state (attached to a surface) [54]. In the latter case, the microorganisms can form a complex community, with new phenotypic characteristics, called a biofilm. Biofilms constitute a protected mode of growth that allows survival of bacteria in a hostile environment [55, 56]. Planktonic bacteria are exposed to harmful agents in their environment, such as biocides or antimicrobial agents in clinical/industrial settings or even phages in nature. Inversely, once on a surface, the cells are embedded within a self-produced matrix of Extracellular Polymeric Substances (EPS), isolating them from the outside and preventing penetration of antibacterial agents in the full depth of the biofilm [55]. Hence, cells in the biofilm are in a slow-growing or starved state. Slow growth, together with stress response, biofilm heterogeneity and slower compound penetration, increases biofilms resistance to antibiotics and biocides by 10-1000 fold compared with wild type, planktonic bacteria [57, 58]. As a result, biofilms cannot be easily destroyed with conventional antibiotics or without the use of intense mechanical cleaning processes [55]. Mature sessile biofilms can release active planktonic individuals that can rapidly multiply and disperse (see Figure 1.5). Studies have shown that nearly 80% of chronic bacterial infections in developed countries are attributable to microbes in biofilms [55, 59].

The planktonic-sessile transition and the initial steps of biofilm formation are complex mechanisms, with several cell-cell and cell-surface interactions involved. Environmental conditions usually trigger such transitions, but they are also deeply dependent of the bacteria itself; *P. Aeruginosa* will form biofilms under almost any growth conditions while *E. Coli* O517:H7 form biofilms only in low-nutrient media [54]. Among the multiple mechanisms, mechanical (via flagella and type-IV pili) interactions were shown to play a crucial role in the early events of biofilm development by *P. Aeruginosa* and *P. Fluorescens*, as was protein synthesis and subsequent adsorption on the surface [54, 60]. Similarly, Palmer observed that if the cell-surface composition is changed, by the modification of the surface chemistry for example, the bacteria biofilm forming ability was altered [61].

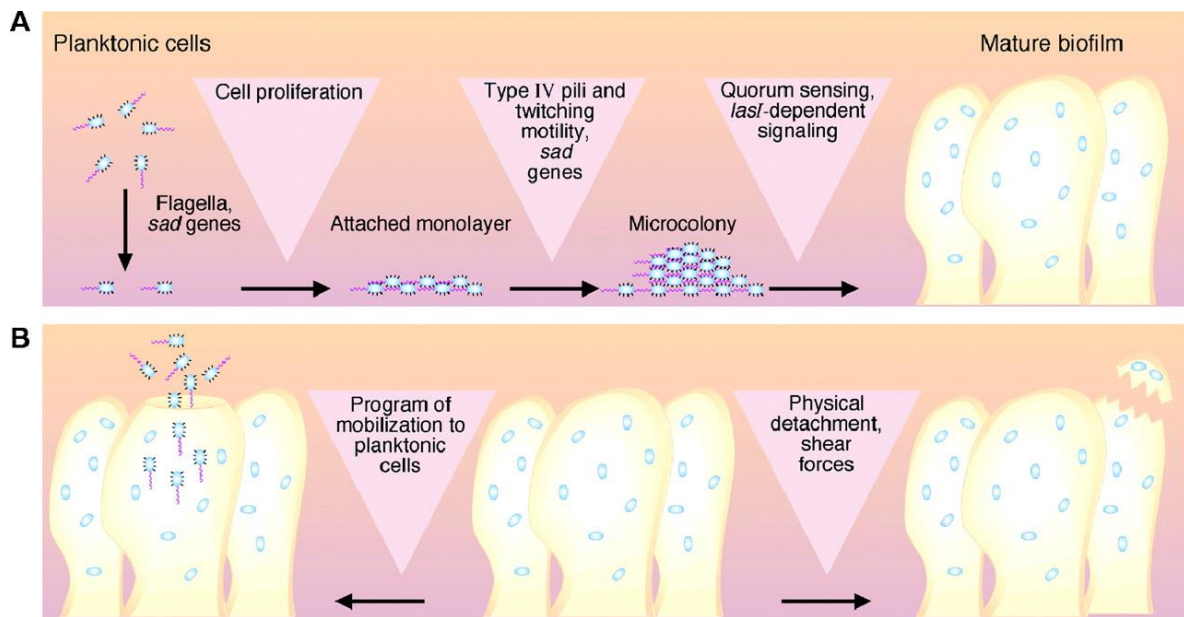


Figure 1.5 : Model of the development of biofilms from planktonic cells and dispersal of bacteria from a mature biofilm [55].

1.2.4.3 Resistance mechanisms

The increased resistance of bacteria to antibacterial agents constitutes arguably one of the greatest risk to human health [62]. Nowhere is the problem of resistant bacteria more apparent than in the medical field. Epidemic antibiotic resistance has been described for numerous pathogens, including several multidrug resistant species (e.g. *Clostridium Difficile*, *Acinetobacter*,

Pseudomonas Aeruginosa) and the well-known methicillin-resistant *Staphylococcus aureus* (MRSA), vancomycin resistant *enterococci* (VRE) and carbapenem-resistant *Enterobacteriaceae* (CRE) [63].

The basic mechanisms governing the development of bacterial resistance are now rather well understood. They essentially involve either reduction in the target access (impermeability and efflux), modification in specific antibiotic target sites by mutation, protection of target sites, or antibiotic degradation/inactivation (enzyme-catalysed modification or hydrolysis) [64-66]. For metallic elements that also fulfil certain cellular functions, other resistance mechanisms have been observed, such as sequestration and metabolic bypass (see Figure 1.6). However, thanks to the diversity in microbial targets of antibacterial metals, no single mechanism provides universal resistance to all toxic metals [65]. In the case of antibacterial metals with multiple mechanisms of actions, like silver, studies have shown that the development of resistant bacterial phenotype comes with high fitness costs, limiting the likelihood of resistance in the absence of constant selective pressure [67]. For high degrees of impairment, resistant bacterial strains present a severely reduced competitive fitness compared with parent strains and, therefore, a decreased likelihood to survive and proliferate in the environment. This explains why metallic nanomaterials (especially Ag and Cu) continue to have strong, broad spectrum antibacterial properties despite being used since antiquity.

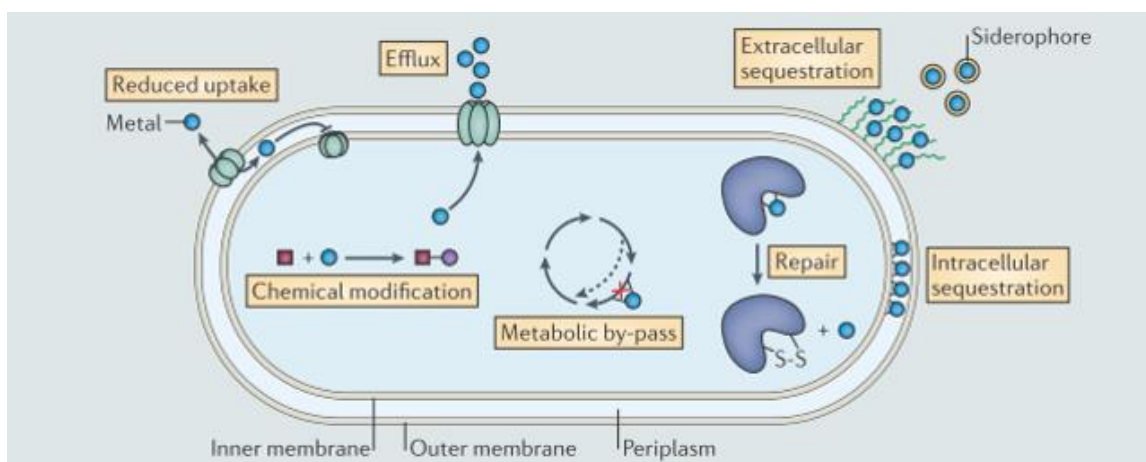


Figure 1.6: Genetic and biochemical mechanisms of the development of bacteria resistance to biocidal metals (from [65]).

1.2.5 Antimicrobial agents

The main mechanisms of action of antimicrobial agents are generally well documented. Antibiotics inhibit essential cellular functions by interacting with specific targets within the bacteria, inducing cell death (in most cases) or preventing cell growth. Known mechanisms associated with drug-target interactions include interference with protein synthesis (the mode of action for antibiotics such as aminoglycosides and tetracyclines), DNA synthesis (quinolones), RNA synthesis (rifamycins) or cell wall synthesis (glycopeptides, β -lactams) [68].

Antibiotics have been ubiquitous in hospitals since the discovery of penicillin in 1928, completely revolutionizing clinical practices and paving the way for the development of modern medicine. However, their high effectiveness and easy access prompted overuse in several areas, leading to the widespread problem of antibiotic resistance (see Section 1.2.4.3). The declining pipeline of potent antibiotics have spurred the investigation of a broad range of antibacterial compounds, including antimicrobial peptides, metals, enzymes, organic cationic compounds, etc. Their role and mechanisms of action will be reviewed in more details in Chapter 2. Amongst them, metals and especially silver, have been regarded as an interesting broad-spectrum alternative to antibiotics.

1.2.5.1 Silver

The understanding of the mechanisms by which silver inhibits bacterial growth is quite recent, despite the fact that the bactericidal properties of silver have been known for centuries. Although most studies on the antibacterial silver were made on colloidal nanoparticles solutions [67, 69-72] or ionic solutions (either from salts or silver electrodes) [73-77], there is valuable information to be taken from these experiences to guide the design of an effective silver-doped coating. In fact, silver interacts in a number of ways with the bacteria to disrupt vital functions, either under ionic form (Ag^+), metallic nanoparticles (Ag NPs) or as a catalyst for reactive oxygen species (ROS), so it might be convenient to distinguish the effects of each of them (Figure 1.7).

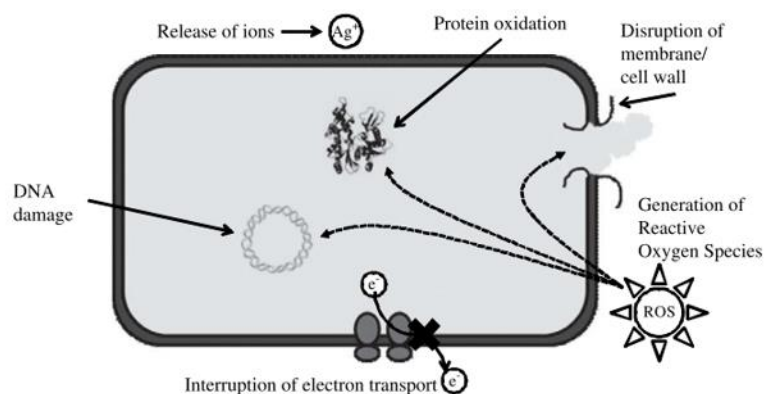


Figure 1.7: Mechanisms of action of silver against bacteria (from [78])

On one hand, silver ions can infiltrate the cytoplasmic membrane and either kill or prevent growth of bacteria by various mechanisms, such as creating agglomerate of condensed DNA [73], interacting with ribosomal subunits to suppress the production of proteins essential to ATP production [74, 79] or uncouple the respiratory control (electron transport) from ATP synthesis [77]. Although getting across the cellular membrane is necessary for these mechanisms to occur, silver-specific transporters are not needed since silver ions, as +1 charged particles, can access the interior of the cell through transmembrane proteins that normally function to transport other ions (K^+ , Na^+).

On the other hand, Ag ions can also interact with the membrane itself, disrupting the permeability to protons and phosphate and stopping further ionic exchanges [75, 79] and even cause the detachment of the cytoplasm membrane from the cell wall [73]. These specific interaction can be explained by the high affinity of ionic silver with thiol (-SH) groups. Silver ions can bind to thiol groups of essential enzymes [73, 75, 80] and catalyze the formation of disulfide bonds, changing the conformation of proteins [81]. Both interactions lead ultimately to the deactivation of enzymes crucial in the metabolism of the bacteria. Thereby, the major consequences of the interaction of Ag ions with the bacteria are the denaturation of the DNA, which prevent replication, and the inhibition of the respiratory chain, leading to the cell's death.

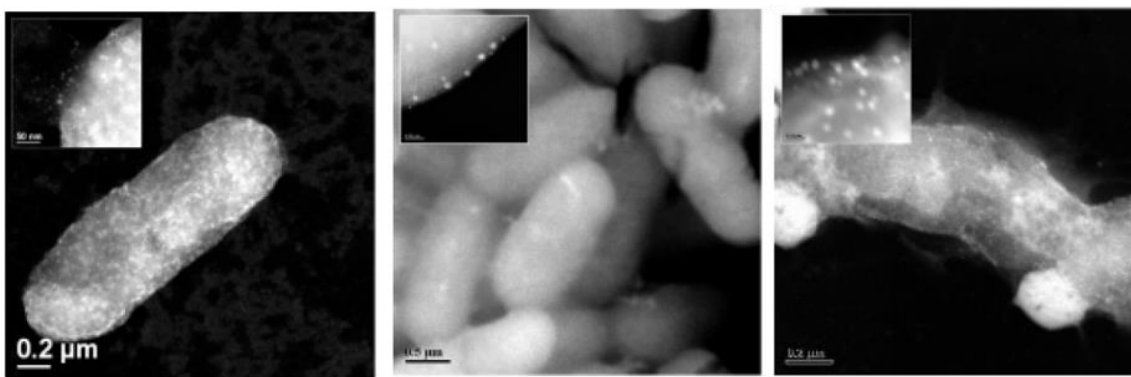


Figure 1.8: High-angle angular dark-field scanning TEM (HAADF STEM) images showing the interactions of silver nanoparticles with bacteria: (left) *E. coli*, (middle) *S. typhus*, (right) *P. aeruginosa* (adapted from [71])

Reported antibacterial mechanisms of silver NPs are similar to those of silver ions and include, among others, the inhibition of nucleic acids and essential proteins synthesis [67] and the disturbance of the membrane permeability and respiration [70, 71]. Even if silver NPs do produce ions, the nanoparticles themselves exhibit antibacterial properties when isolated from their ionic counterpart [71]. However, not all silver NPs are equally effective; smaller nanoparticles (between 1 and 10 nm) showed an increased antimicrobial activity [71, 82], probably due to their greater surface area to volume ratio. The shape of the NPs was also considered, with particles with more active, electron-dense facets having a more pronounced effect [83].

Moreover, silver also exhibits catalytic effects, forming reactive oxygen species, such as H_2O_2 , HO^\bullet and O^{2-} that can attack multiple sites on the bacteria. Conversely, non-aerated conditions drastically suppressed the bactericidal activity of silver [84, 85]. In all cases, the biocidal effect of silver, with its broad spectrum of activity including bacterial, fungal, and viral agents, could be achieved at submicromolar concentrations and the mechanisms were observed on both Gram-positive and Gram-negative bacteria [67, 70]. Interestingly, studies have demonstrated the ability of Ag^+ to potentiate antibiotics efficiency against a wide range of bacteria and biofilms [86]. Finally, no minimum exposition time was required for the observation of an inhibitory effect on bacteria, although the maximum effectiveness of silver was not instantaneous [67].

The number of products entering the market that incorporates silver nanoparticles have exploded in recent years, raising questions over the potential health, environmental and ecotoxicological issues [87-89]. The high stability of Ag nanoparticles (compared with ionic

Ag) contributes in bringing the source of Ag in close proximity to the sensitive biological targets, such as small aquatic invertebrates, algae and other small organisms. Although the concern and care over the use of silver nanoparticles is warranted, there is an important misconception regarding the respective risks associated with the different types of silver use in nanotechnology. Unlike silver nanoparticles, the potential environmental and human toxicity of ionic silver and ionic silver-based compounds remains very low [90, 91]. The presence of complexing agents (chloride, thiosulfate) and competing ions can bind Ag^+ or prevent Ag^+ binding with the surface of pluricellular organisms [90]. These important differences with Ag nanoparticles limit the concerns of bioaccumulation and potential harmful interactions with the environment.

1.3 Proposed platform

The search for new materials with specific combinations of properties has long guided research in several scientific and technological areas, leading to the development of novel alloys, composite, ceramics, polymers, and a number of other materials. However, developing such bulk materials is a rather long and arduous process and there is no guarantee that the desired properties can be obtained in bulk form. A valid solution to this problem is to use thin films or coatings in order to separate bulk and surface properties. In this way, it allows one to easily make ideal devices and appliances; the base bulk material can be selected for its mechanical properties, simplicity, and/or low-cost while the surface properties can be selectively modified to enhance the performance of the material. For instance, thin film deposition can be used to obtain the optimal surface physical, chemical, electrical, electronic, magnetic, mechanical, wear-resistant and corrosion-resistant properties on almost any type of material [92].

The principal objective of this research project is to develop a novel type of highly stable antibacterial coatings. Despite the importance of stability on long-term performances, there has been little discussion on the role of stability for antibacterial coatings and what it entails on design choices. In the current market, there are no surface treatments that can provide, at the same time, sufficient stability and antibacterial properties thus guaranteeing the long-term effectiveness of their synergy. Furthermore, the widespread problem caused by bacterial contamination of surfaces calls for the use of antibacterial coatings in several different settings within the healthcare system. In this regard, a deposition process offering flexibility and tunability would be greatly valued.

To this end, this doctoral project proposes to combine diamond-like carbon and silver nanomaterials in a single nanocomposite coating deposited by plasma techniques. The following paragraphs will introduce these aspects in more details.

1.3.1 Surface engineering by plasma

In several fields, plasma processes are rapidly taking the place of other, more traditional processing methods such as wet chemistry and spray coatings. This shift can be partly attributed to the flexibility of the process, which gives rise to a wide range of controllable properties and enables the production of unique materials not constrained by any phase diagrams, diffusion processes, or usual chemical pathways [93].

1.3.1.1 Plasma - Generalities

Plasmas, considered the fourth state of matter, are gases in which an important fraction of atoms are ionized [94]. Because plasmas are in a constant balance between collisional ionization and recombination events, they contain a mix of neutral atoms, molecules, ions, electrons, free radicals, and photons. However, plasmas are overall quasi-neutral, with both positively- and negatively-charged species in nearly perfect balance.

Plasmas are described by many characteristics such as temperature, density, or degree of ionization, leaving many possible classification systems [93]. One of the most popular is to classify plasmas based on their thermal equilibrium, as either in local thermodynamic equilibrium (LTE), also known as thermal or hot plasmas, or non-LTE (cold) plasmas. Thermal discharge applications lie mostly in fields where heat is beneficial, like welding, cutting, waste treatment, etc. [95]. In non-LTE plasmas, the energy coupling between electrons and heavier particles is weak (i.e. the electrons are not in thermal equilibrium with ions and neutrals, $T_n < T_i \ll T_e$). This non-equilibrium is only possible at low pressures, where collisions between particles are less frequent [95]. Cold plasmas are typically used for etching or coating applications and are the type most relevant to the current work.

1.3.1.2 Physical parameters

Although a complete description of physical characteristics of plasma is not within the scope of this thesis, it can be useful to introduce some parameters in addition to the temperature discussed above.

Debye length & Plasma Parameter

The Debye length (λ_D) represents the length at which perturbations in charge density or potential in the plasma tend to fall off. Conversely, it's also a measure of the length of a charge carrier's effect. When considering that the mobility of ions is negligible compared to that of electrons, the Debye length can be defined as:

$$\lambda_D = \left(\frac{\epsilon_0 k_B T_e}{n_e e^2} \right)$$

where ϵ_0 is the permittivity of free space, k_B is the Boltzmann constant, T_e is the temperature of the electrons, n_e is the density of electrons and e is the charge of an electron. An important feature of plasmas is the preponderance of collective effects over interactions between individual charged carriers. This stems from the characteristically short Debye length which is much shorter than the size of the plasma. In a plasma, charge carriers are effectively shielded by their surroundings, ensuring the precedence of collective effects. Typically, λ_D in gas discharges is in the range of 10^{-4} to 10^{-5} m [96]. A Debye sphere is a volume whose radius is the Debye length. The number of particles in the Debye sphere is called the "Plasma Parameter" (N_D) and is useful to define which type of effects (short range or long range) are dominant. If $N_D \gg 1$, then collective effects dominate over collisions in the plasma.

Electron energy distribution

Electrons in a plasma follow a distribution of energies (Figure 1.9). Consequently, despite T_e being less than the threshold energies for dissociation or ionization of precursor gas molecules, the high energy electrons in the tail end of the probability distribution possess sufficient energy to induce ionization or dissociation of feedgas molecules. However, because only a small fraction of electrons have a sufficient energy, the majority of precursors of cold plasmas are weakly ionized, with degree of ionization usually between 10^{-5} and 10^{-3} [93, 97]. The ionization potential and dissociation energy of important precursors are shown in Table 1.3.

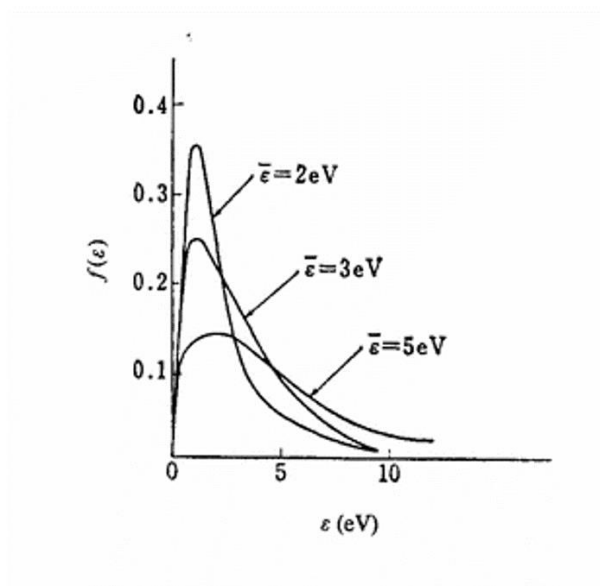


Figure 1.9: Maxwellian energy distribution of electrons in a weakly ionized plasma (from [98]). Another function that can be used to describe electron energy distribution is the Druyvesteyn function.

Table 1.3: Ionization potential and dissociation energy of relevant atoms and molecules. Data from [99-101]

Species	Bond	Ionization potential (eV)	Dissociation energy (eV)
H	-	13,6	-
He	-	24,6	-
O	-	13,6	-
F	-	17,4	-
Ar	-	15,7	-
H ₂	<i>H - H</i>	15,6	4,5
O ₂	<i>O = O</i>	12,5	5,1
N ₂	<i>N ≡ N</i>	15,6	9,8
CH ₄	<i>CH₃ - H</i>	12,6	4,5
Other organic precursors	<i>C - C</i>	-	6,3
	<i>C = C</i>	-	7,6
	<i>C ≡ C</i>	-	10,0
	<i>CHC - H</i>	-	5,7
	<i>C₂H₅ - H</i>	-	4,3

Plasma sheath

Due to differences in mass ($m_i / m_e > 1836$) and energy ($T_e \gg T_i$), electrons move much faster than ions in the plasma. As a result, electrons are more likely to escape the plasma towards surrounding “sinks” (i.e. surrounding surfaces or solids). The remaining ions create an accumulation of positive charges around the plasma, creating an electric field opposing further electron escape. Therefore, plasmas are positively charged with respect to the solids they can enter in contact with. The boundary region where potential variations occur is called “sheath”. In low pressure plasmas, the sheath can be considered collisionless, providing a way for ions to accelerate towards the substrate, reaching energies much exceeding T_e , a central requirement in all plasma processes [102]. The energy distribution of incident ions (Figure 1.10) strongly affects surface reactions, such as film deposition or etching processes [103].

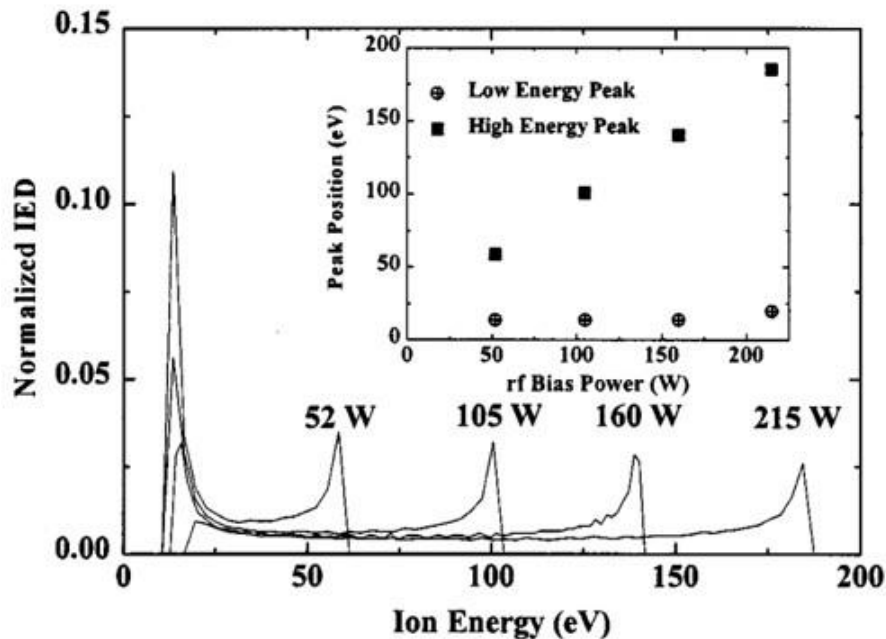


Figure 1.10: Ion energy distributions for an Ar plasma at different rf-bias power showing the characteristic double energy peak of ions [103].

The kinetic energy of impinging ions in cold plasma is determined by the voltage drop in the plasma sheath. In a collisionless sheath, the impinging ions will then have a kinetic energy corresponding to the total potential difference between the plasma and the surface. In the case of an RF discharge at low pressure, the kinetic energy corresponds to the DC self-bias (or applied bias, if a second generator is used) plus the plasma potential [102].

1.3.1.3 Plasma-surface interactions

Plasma surface interactions remain a significant field of studies, in part because of their importance in nuclear fusion. However, the physical and chemical surface processes are also central to plasma processing. Previous research have established that ions, photons and radicals all play a role of variable importance in energy transfer processes at the surface [96]. Since DLC coatings are produced primarily by an ion-mediated process, this section will focus mostly on ion-surface interactions [104-106].

The nature of interactions of heavy particles (ions and neutrals) is strongly related to the energy with which they impact the surface [96, 101, 107]. The fragmentation of molecules, which occur for energies above 10 eV, is a good illustration of this relationship. Other important ion-surface interactions include:

- Adsorption and desorption (0-10 eV, mostly at thermal energies)
- Etching and sputtering (>20-50 eV)
- Implantation (>1keV)

These interactions and how they relate to applications of plasma processes will be briefly discussed below.

Adsorption processes and film growth

Plasma processes are widely used for deposition and growth of thin layers with unique composition and properties. The adsorption of atoms and molecules can occur through weak van der Waals forces (physisorption) or from the formation of a chemical bond between molecule and surface (chemisorption) [93]. Growth rates in plasma thin films have been shown to be proportional to the flux of growth precursors to the surface, the cross section for chemisorption ($\sigma_{\text{adsorption}}$), and the total number of adsorption sites [102].

Macroscopic deposition rates are however the sum of total adsorption and desorption processes. For example, the thermally activated desorption of hydrocarbon species have been identified as the reason for the decrease in growth rate of a-C:H films with increasing temperature [102, 106]. Adsorption plays an important role in most plasma processing applications, such as functionalization of organic and inorganic surfaces, plasma-enhanced deposition of coatings, plasma oxidation, plasma nitridation, etc. [93, 96, 108-112]

Etching and sputtering

Etching and sputtering are two of the most straightforward applications of plasmas and can be conducted with a variety of sources. They are essentially used to remove material from a surface; etching processes include a chemical reaction at the surface while sputtering is strictly physical bombardment. Sputtering processes normally use noble or other non-reactive gases (He, N₂, Ar) as precursors and are heavily energy-mediated. For example, classic sputtering studies of noble gas on metals have shown that the sputtering yield of Ar and Ne increases linearly with ion energy above 50 eV [113]. In etching, atoms from the carrier gas (O₂, H₂) will react chemically with atoms from the surface to form volatile molecules that can be evacuated by the pumping system.

The main advantages of plasma etching and, to a lesser extent, sputtering, is that they offer etch rate uniformity, anisotropy and selectivity [114]. Applications include, but are not restricted to, surface cleaning [115], removal of surface layers [116], sputter deposition [117, 118], nanotexturing [119], and nanostructuring [120]. An example of this is the study carried out by Lewis et al. in which H₂ and C₂F₆ are used alternatively to remove the native oxide layer from stainless steel substrates, providing both chemical reactions with the surface and physical bombardment [109, 121].

Implantation

At a certain point (about 1keV), the sputtering yield of ions incoming on the surface goes down as the energy is dissipated too deep within the substrate. In this case, the ions are implanted within the material. This process can be used to modify the atomic composition, structure, and properties of the material surface layer [93]. Plasma implantation is heavily used in the semi-conductor industry for doping applications. The mechanical complexity and high cost needed to develop systems capable of imparting high energies to heavy atoms, a condition necessary for implantation, have prevented a more universal adoption of plasma implantation.

Implantation can also occur at lower energies, especially for lighter atoms. Shallow implantation of carbon ions gives rise to the sp³ bonding in DLC films, through a mechanism called subplantation [106, 122]. The energy penetration threshold at the surface being only 30 eV for carbon ions, these conditions can be easily reached in a classical plasma reactor.

One important consequence of all those interactions is the atomic interfacial mixing occurring at the interface, which account for the generally enhanced adhesion of plasma-deposited films to their substrate materials [123].

1.3.2 Deposition techniques

The wide variety of coating techniques and the overlap of deposition mechanisms of certain hybrid techniques makes it difficult to establish a unique classification. Plasma discharges may be grouped according to the heating mechanisms used to sustain the plasma, since they play essential roles in determining the plasma density, sheath voltages and the energy of bombarding ions. This system of classification includes capacitive discharges, inductive discharges, wave-heated discharges (electron cyclotron resonance, helicon), and direct current (DC) discharges (hollow cathode, magnetron) [96]. Alternatively, plasma processes can be based on the frequency of their power source: DC, Radio-frequency (0.1-100 MHz) or microwave (1-20 GHz). Rather than presenting a complete review of the different plasma-generating approaches, the next section will focus on the two deposition processes used in the doctoral project.

1.3.2.1 Plasma-enhanced chemical vapor deposition

PECVD will be used in this project to deposit the DLC coatings from a hydrocarbon precursor. The operating principle of PECVD is simple. The electron energy from a non-thermal plasma is used to activate the dissociation of the precursor gases and the ions and radicals formed can then interact with a substrate. During operation, gases are injected in a reactor chamber, pumped to a controlled vacuum/pressure, usually in the 1-50 mTorr range, and ignited. The plasma can be formed either by varying an electric field in the gas (capacitively coupled plasma or CCP) or by varying the magnetic field (inductively coupled plasma or ICP). The advantage of ICP is the higher plasma density, usually of one order of magnitude, in comparison to CCP reactors (Figure 1.11) [124]. Even in that case, the maximum degree of ionization in the deposition flux (toward the substrate) is inferior to 30%, the rest being neutrals [125].

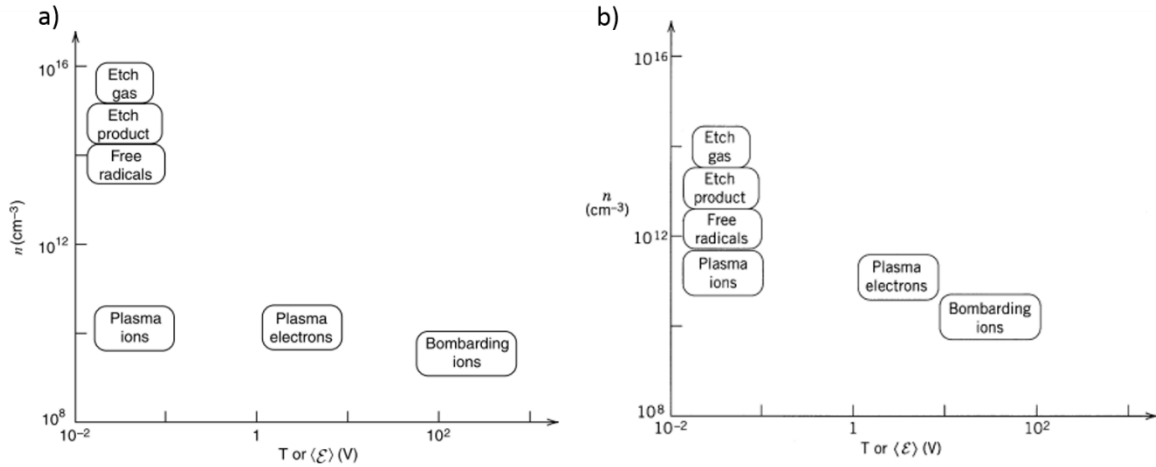


Figure 1.11: Range of energies and densities for various species found in CCP (left) and ICP (right) processing plasmas (low pressure, RF discharges). From [96]

In ICP discharges, an RF power supply, usually at 13.56 MHz, is connected to one of the electrodes of a parallel-plate reactor (see Figure 1.12). At this frequency, the mass of the ions makes them relatively immobile and only the electrons can follow the temporal variation of the applied potential. An RF current driven through a coil will produce an alternating magnetic field that can induce alternating currents in the gas [126]. Because of the orientation of the induced electrical currents, electrons follow a circular path normal to the reactor axis, limiting loss of electrons at the walls.

A typical PECVD system includes a gas distribution system, vacuum pumping and power source (usually RF) connected to the plates/coil via a matching network controller. The substrate holder, in the plasma, can be heated, cooled or biased by an external source depending on the reactor and the requirements.

The characteristics of plasma-deposited materials depend mainly on two factors. The choice of precursor defines the composition while the plasma-surface interactions are related to the film growth kinetics and, consequently, to the resulting microstructure, density, stability, stress, etc. [127]. Several parameters can be used to control in real-time the ion-surface interactions and the film deposition and are presented in Table 1.4.

Table 1.4: Important parameters of plasma discharges and their respective impact on the deposition process. The selected examples are taken from DLC literature.

Parameters	Role/Impact	Examples/refs
Bias voltage (energy)	Related to the sheath potential. Will dictate the energy of the ions incoming on the substrates. It is the most important parameter for the deposition of DLC.	[106, 128-130]
Precursors flows/ratio	Can change the stoichiometry and the final concentration of elements in the film.	[131, 132]
Pressure	Can change the mean free path of species in the plasma, influence their energy and energy distribution and modify the reactions in the gas phase.	[106, 133]
Power	Influence the rates ionisation and dissociation of particles in the plasma and overall degree of ionization.	[132, 134]
Temperature	Influences surface reaction in the materials and can promote certain mechanisms such as desorption of H ₂ from the surface	[135]

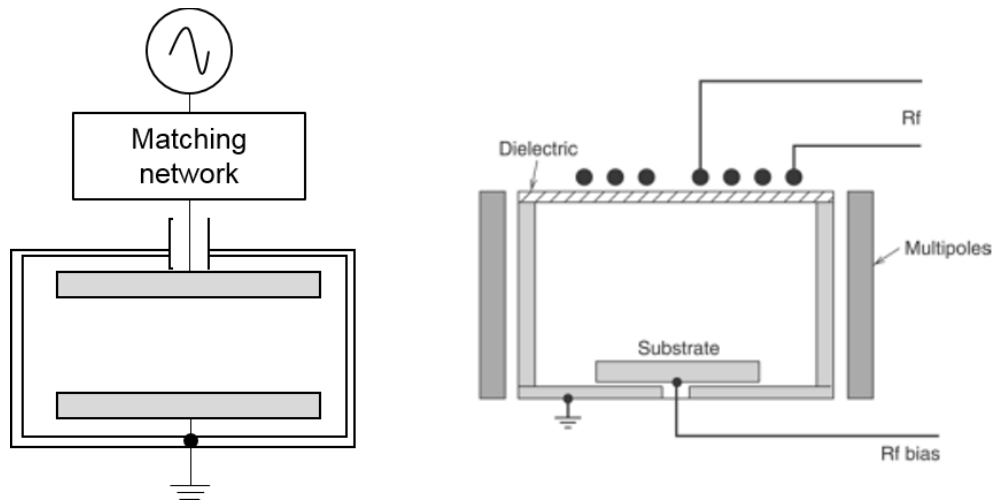


Figure 1.12 : (left) Parallel plate reactor (for CCP) and (right) inductively driven planar source (for ICP) [96, 124].

The advantages of using PECVD to deposit materials are multiple. It is less greedy, in terms of energy consumption, than other deposition processes such as cathodic arc. Compared with thermal chemical vapor deposition, PECVD enables deposition at much lower temperature [111]. Besides, it can deposit ultrathin films with a low roughness, in the nanometer range, on a

variety of substrates with a good adhesion compared bulk techniques deposition [92]. More importantly, it offers a good flexibility and control over the microstructure of the film. This allows unique film chemistry and high density films that are excellent permeation barriers with low level of leachables [92]. The process can also be easily scaled up to deposit on large areas, up to several meters [126]. Combined together, those characteristics allow the modification of the surface properties of a material without affecting its bulk. However, PECVD is a vacuum technique and the reactor needed to generate and contain the plasma can be quite sophisticated. There are also some difficulties to deposit high purity films. Desorption of by-products and neutral species can be integrated in the coating during the deposition process [111].

1.3.2.2 Physical vapor deposition (PVD)

PVD will be employed in the project to load the DLC coating with the silver dopant in a one-step process, simultaneously with the PECVD deposition. In short, physical vapor deposition relies on the condensation of a source material (silver in our case) from a vaporized form on the desired component. This is done under vacuum and the vaporized form is usually achieved via either evaporation or sputtering of the target material. This approach has been successfully used to deposit various composite coatings, such as carbon/carbide tungsten composites[136], Cr-doped DLC[137] and Si-doped DLC [138]. Sputter deposition is the easiest type of PVD to use in conjunction with a PECVD process. In this method, the desired element is obtained via a plasma bombardment of a target, sputtering atoms away, as a vapor, that can be subsequently condensed on a surface for deposition. The plasma can be localized around the target using magnet (magnetron sputtering) or by applying a bias.

1.3.3 Diamond-Like Carbon

DLC is a term attributed to a family of metastable amorphous materials. They are usually classified in four different subgroups related to their hydrogen content and their atomic bonding (Figure 1.13). Although no nomenclature has been officially established, films are usually grouped as either amorphous hydrogenated carbon (a-C:H, containing up to 50% hydrogen) or as amorphous carbon (a-C, with less than 1% hydrogen) as well as their

tetrahedral counterpart, ta-CH and ta-C, which contain a larger fraction of carbon atoms with sp^3 bonding. Among them, the broadest industrial use of DLC films is certainly of a-C:H films as protective coatings [139].

1.3.3.1 Structure

Carbon can form a variety of allotropic structures, both disordered and crystalline because it is tetravalent, having four electrons available from covalent bonds. Carbon atoms can exist in three different hybridisations, sp^1 , sp^2 , and sp^3 . For example, in diamond, the crystalline structure is composed exclusively of sp^3 carbon atoms, each atom's four valence electrons are assigned to a tetrahedrally directed sp^3 orbital, which make a strong σ bond with adjacent atoms. On the other hand, in graphite, three of the four valence electrons form trigonally directed sp^2 orbital, in the same plane. The fourth electron of the sp^2 atom lies in a $p\pi$ orbital, which is perpendicular to the σ bonding plane and forms a weaker π bond with a corresponding orbital of one neighbouring atom [106]. Similarly to diamond, DLC derives its impressive physical properties from its strong, directional σ bonds, but these are achieved in an isotropic amorphous thin film instead of a crystalline structure. Consequently, DLC films can be produced at room temperature. However, DLC is a metastable form of carbon. If sufficient energy is given through heating, it can return to the graphitic, more thermodynamically stable form. This typically happens at temperatures above 400°C [106].

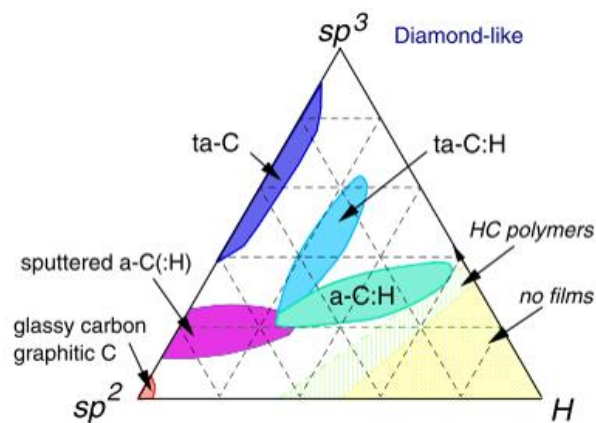


Figure 1.13: Ternary diagram of Diamond-Like Carbon. [140]

1.3.3.2 Deposition mechanism

The current accepted model for the formation of sp^3 during plasma deposition of diamond-like carbon is called subplantation [141, 142]. According to the model, atoms with energies exceeding the penetration threshold (>30 eV) will penetrate the outer layer of atoms (see Figure 1.14a). Penetration creates local quenched-in increases of density. Since diamond is denser than graphite, the densification converts sp^2 into sp^3 [125]. However, increasing the energy above a certain threshold will not lead to higher sp^3 content; high energy implanting ions induce relaxation via a thermal spike and provoke the decrease of sp^3 content into the more thermodynamically stable phase of graphite (see Figure 1.14b). Another phenomena leading to the formation of sp^3 in DLC is the preferential sputtering of hydrogen [143]. C-H bonds already present in the film will be broken more easily than C-C bonds and the displaced hydrogen can recombine into H_2 and desorb from the surface (see Figure 1.15c). In a:C-H materials, C-H bonds add no rigidity to the network.

DLC can be deposited in a PECVD process using various hydrocarbon precursors, the most popular being acetylene and methane. Growth rates are linked to the hydrocarbon feedstock; gases with lower ionization potential, like acetylene, will consequently have higher growth rates. Typical growth rate values range between 0.1 and 1 nm/s [125]. However, in methane (CH_4), the carbon atom is already in a sp^3 hybridisation. Methane usually produce higher sp^3/sp^2 ratio than other gases under similar operating conditions [106]. A combination of methane and hydrogen, usually around 25%/75%, is a popular precursor choice for DLC deposition with PECVD.

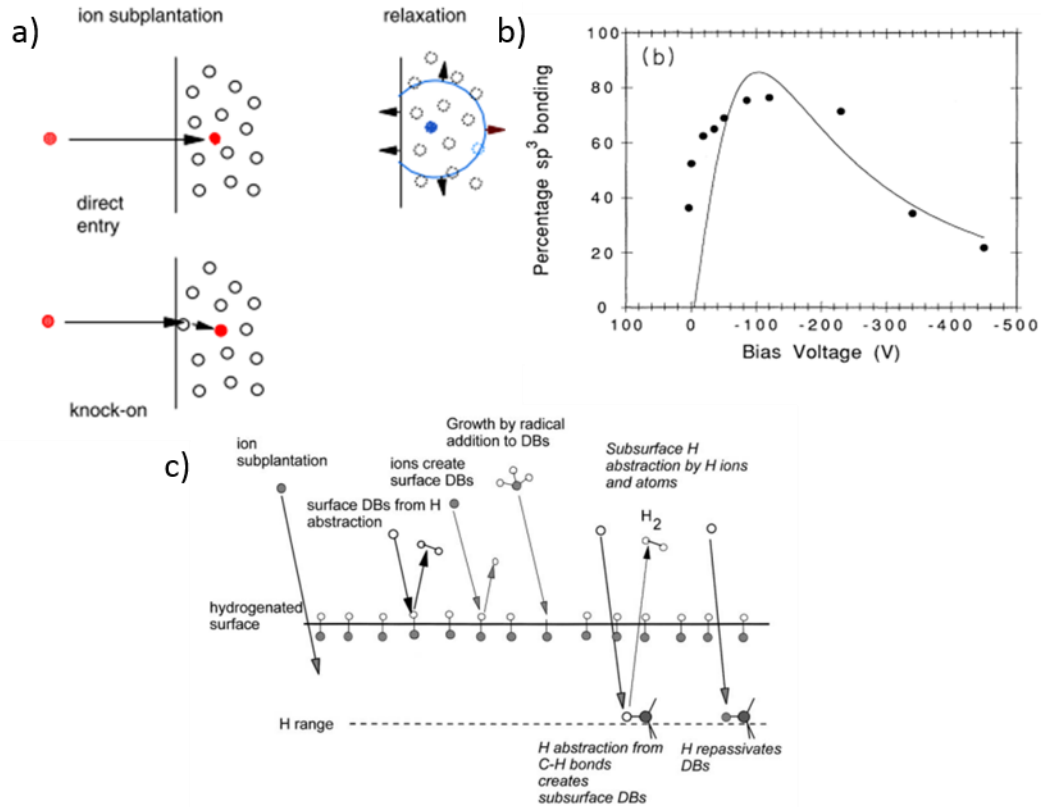


Figure 1.14: a) Subplantation and relaxation processes leading to the formation of sp^3 bonding in a:C-H film [125]; b) Sp^3 fraction as a function of the bias voltage/ion energy [144]; c) The various plasma-surface processes playing a role in the deposition of DLC [125].

1.3.3.3 Properties

DLC has always been reported as a 100% biocompatible material, thanks to its amorphous nature and carbon/hydrogen-based composition. Generally speaking, the mechanical properties depend on the microstructure of the film, highlighted by the ratio of sp^2 and sp^3 atoms and the hydrogen content (Figure 1.13). DLC films are characterized by high hardness and a high elastic modulus, but also by high internal compressive stresses. The properties are directly correlated to the fraction of sp^3 carbon atoms in the film; films with higher sp^3 content exhibit better mechanical properties. Amongst the other interesting characteristics of DLC for our applications: excellent abrasive wear resistance and corrosion resistance, low friction coefficient, nano-smoothness and chemical inertness [106, 125, 145-149]. Hence, DLC is a perfect choice for highly resistant, highly stable biocompatible coatings. However, one of the main drawbacks is the lack of adhesion to certain materials. Due to the high stress, delamination of the film can occur when the bonding strength with the substrate is not

sufficient, thereby limiting the thickness of the film [106, 139, 150, 151]. Several strategies have been proposed in the literature to maximize the adhesion of DLC coatings on a variety of substrates (see Table 5). Since the mechanical properties and the stress are both linked to the sp^3 fraction, it is important to find a compromise between the desired thickness, properties, and stability of the coatings.

Table 1.5: Interface modification strategies for the optimisation of adhesion strength.

Strategy	Principle	Rationale	Refs
Surface etching	Bombarding the metallic surface with high energy argon/hydrogen atoms	Elimination of surface layer contaminants Etching of oxide layer Creation of dangling bonds on the surface	[106, 115, 116]
Si-based interlayer	Deposition of a Si interlayer on the surface of stainless steel	Silicon is a carbide forming element, providing a good interface for DLC bonding.	[106, 152]
Metallic interlayer	Deposition of carbide-forming elements (W or Cr) on the interface in a separate reactor	Same as si-based interlayer.	[106, 150, 153]
Graded interface*	Creating a carbon composition gradient, throughout the coating	Diminution of the residual stress in the coating	[154-156]
Alloying via heterogeneous atom implantation*	Implantation of non-carbon atoms (metals/silicon/nitrogen) from a plasma	Create heterogeneous zones to achieve the relaxation of the compressive residual stress Thermal spike effect of implantation can also reduce stress	[151]

Techniques marked with an asterisk (*) are not interface treatments, but are frequently used approached for DLC films.

1.4 Summary of approach and research objectives

The proposed approach of this doctoral thesis is to combine the properties of diamond-like carbon and silver nanomaterials to form a stable, antibacterial nanocomposite coating. DLC coatings are amorphous, carbon-based materials well-known for their excellent biocompatibility, outstanding mechanical properties (such as hardness and wear-resistance), extremely low surface roughness and chemical inertness. As such, they can act as a stable matrix for the loaded antibacterial agents. Silver is a highly effective broad spectrum biocide with multiple mechanisms of action against bacteria. Silver-loaded coatings will be deposited using a hybrid PECVD-PVD system, a versatile low-cost technique that can provide extremely adherent and stable coatings on a number of surfaces (e.g. polymers, metals, fabrics, etc.). The combination of PECVD and PVD gives the unique possibility to deposit silver-DLC nanocomposite thin films in a one-step, continuous process with high controllability over the deposition parameters.

The existing body of research on antibacterial coatings suggests that they could be used in several applications, each in a different environment and with a complex set of requirements. These arguments clearly reflect the need for the development of a versatile material and deposition process. Therefore, this project also sets out to assess the potential to use the Ag-DLC coatings as a flexible material platform. To do so, this thesis explores four essential aspects of Ag-DLC coatings (Figure 1.15):

- The interface between the coating and substrate, especially in the case of passivated materials such as stainless steel;
- The mechanisms governing the growth and silver distribution of Ag-DLC coatings;
- The silver release and resulting antibacterial properties;
- The coatings' long-term stability.

Each theme was the subject of a published article and will be discussed in chapters 3, 4, 5, and 6, respectively. Before that, Chapter 2 will further present the context and review the latest progress in antibacterial coatings.

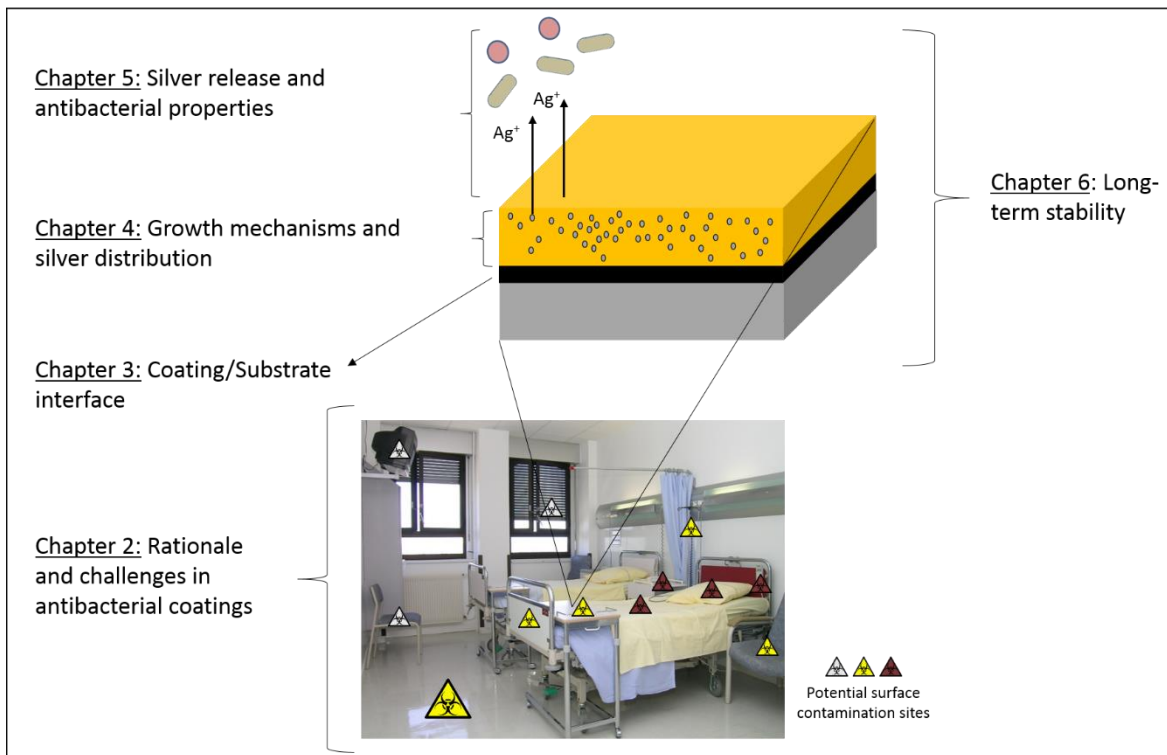


Figure 1.15: Graphical representation of the different topics addressed in this doctoral thesis.

2 Antibacterial coatings: challenges, perspectives and opportunities

M. Cloutier^{a,b,c}, D. Mantovani^{a*}, F. Rosei^{d,e*}

^aLaboratory for Biomaterials and Bioengineering, CRC-Tier I, Dept of Min-Met-Materials Engineering, & CHU de Québec Research Center, Laval University, Pavillon Pouliot, salle 1745-E, Québec, Québec G1V 0A6, Canada

^bChimie ParisTech, PSL Research University, Institut de Recherche de Chimie Paris (IRCP), 11 rue Pierre et Marie Curie, F-75005 Paris, France

^cSorbonne Universités, UPMC Univ Paris 06, F-75005, Paris, France

^dUNESCO Chair in Materials and Technologies for Energy Conversion, Saving and Storage, Centre for Energy, Materials and Telecommunications, INRS, 1650 Boul. Lionel Boulet, J3X 1S2 Varennes (QC) Canada

^eInstitute for Fundamental and Frontier Science, University of Electronic Science and Technology of China, Chengdu 610054, PR China

Trends

- Coatings releasing antibacterial agents have shown great potential to reduce nosocomial infections.
- The development of controlled release strategies is necessary to optimize therapeutic effects.
- Next generation coatings should be multifunctional and integrate multiple anti-bacterial effects.
- Standardized assessment of both stability and antibacterial properties still need to be addressed, especially for long-term applications.

Keywords

Antibacterial coatings, Antibacterial agent release, Controlled release, Multifunctional coatings, Stability

2.1 Résumé

Les revêtements antibactériens ont rapidement émergé comme l'une des composantes primaires de la stratégie globale de lutte contre les bactéries pathogènes. Grâce à des avancées récentes en science des matériaux, à l'amélioration des procédés biotechnologiques et à une compréhension croissante de notre environnement microbiologique, une importante variété d'options a pu être développée pour la conception de surfaces antibactériennes. Les progrès vers une utilisation plus répandue de ces surfaces en milieux cliniques demeurent toutefois fortement liés à notre capacité d'aborder certains problèmes clés. Dans cette étude, nous avons passé en revue les connaissances actuelles sur les revêtements antibactériens à libération, en soulignant plus particulièrement les défis et les opportunités présentées par la dernière génération de ces matériaux. Nous avons notamment souligné les approches récentes visant à contrôler la libération des agents antibactériens, à conférer un caractère multifonctionnel aux surfaces, et à accroître leur stabilité à long-terme.

2.2 Abstract

Antibacterial coatings are rapidly emerging as a primary component of the global mitigation strategy of bacterial pathogens. Thanks to recent concurrent advances in materials science, biotechnology methodologies and a growing understanding of environmental microbiology, an extensive variety of options is now available to design surfaces with antibacterial properties. However, progress towards a more widespread use in clinical settings critically depends on addressing the key outstanding issues. Here we review release-based antibacterial coatings and focus on the challenges and opportunities presented by the latest generation of these materials. In particular, we highlight recent approaches aimed at controlling the release of antibacterial agents, imparting multi-functionality and enhancing long term stability.

2.3 Antibacterial surfaces in health applications

2.3.1 Advances in biomedical engineering prompted by the development of new materials

Recent advances in materials science have brought about high performance, multifunctional materials with bioactive properties [157]. Materials bulk properties determine the general mechanical behavior, while bioactivity is linked to surface properties. The main driving force for developing biocompatible coatings is the increased performance of functionalized surfaces that cannot be achieved by bulk materials. Thin films can simultaneously satisfy multiple requirements with respect to stability in biological environments, e.g. mechanical (hardness, Young's modulus, stress), tribological (wear resistance, friction, adhesion), chemical (corrosion resistance) and others.

2.3.2 Nosocomial infections and the role of surfaces

So-called nosocomial (hospital acquired) infections result from hospital or healthcare service unit treatment, yet are secondary to the patient's original condition [158]. Such infections are considered a major health challenge in healthcare units worldwide. The prevalence rate of nosocomial infections, which are primarily caused by bacterial colonization of a broad range of biomedical surfaces, generally ranges from 4 to 10% (reaching up to 30% in intensive care units) in western-industrialized countries, making them the sixth leading cause of death [2, 6, 22, 159]. The proportion is typically higher (over 15%) in the developing world [21]. It is fortunate that the operating room is a sterile environment because it is filled with the largest number of potentially-infectious objects: instruments, the back table, the surgical table, monitoring/ anesthesia equipment and drapes. Although ventilation follows strict requirements during the design of an operating room, it is also considered as a major cause of bacterial contamination at the surgical area [160]. Consequences are catastrophic, especially in high risk operations (open heart, prosthesis implantation, etc.). In 2011, an estimated 722,000 nosocomial infections occurred in the U.S., resulting in nearly 75,000 deaths [1]. Estimates of the annual cost range from \$4.5 billion to over \$11 billion.

It is now widely accepted that bacteria survive by attaching to solid substrates, in sessile structured communities called biofilms, where they can persist for extended periods, acting as a reservoir of pathogens and multiplying their pathways of transmission [26, 55]. Bacteria in

biofilms are drastically more resistant to antibiotics and external forces and can withstand host immune responses [161]. In addition, most nosocomial infections can be attributed to Gram-negative bacterial pathogens, for which there is a dwindling supply of antibiotics [162]. There is also increasing epidemiological evidence that, besides indwelling devices and implants, surfaces in the near-patient environment play a major role in the spread of nosocomial infections [1, 11, 28].

2.3.3 Importance of antibacterial coatings

Preventing the bacterial colonization of biomedical surfaces is the key to limiting the spread of infections. Nowadays, the bulk properties (e.g. mechanical) of materials in health applications have been more or less fully optimized. On the other hand, thin films can impart desired surface functions without affecting bulk mechanical properties. Antibacterial coatings have become a very active field of research, strongly stimulated by the increasing urgency of identifying alternatives to the traditional administration of antibiotics.

There are three major strategies for designing antibacterial coatings: antibacterial agent release, contact-killing and anti-adhesion/bacteria-repelling (see Box 1). The last two non-release approaches will be only briefly described in this review; interested readers are directed to other reviews that have documented these approaches in detail [163-165]. On the other hand, the present review offers a critical overview of research on antibacterial agent release systems and will then discuss some recent and innovative strategies.

Box 1 : Main approaches to antibacterial surfaces

Antibacterial agent release

Release-based coatings exert their antibacterial activity by leaching loaded antibacterial compounds over time, which allows to kill both adhered and adjacent planktonic bacteria. The release of incorporated antibacterial agents is achieved by diffusion to the aqueous medium, erosion/degradation or hydrolysis of covalent bonds [166]. Compared with traditional antibiotic delivery methods, direct elution from the material surface offers the possibility to deliver a high antibacterial agent concentration locally, without exceeding systemic toxicity or ecotoxicity limits. It provides the antibacterial activity only where needed, thus minimizing the development of resistance and avoiding potentially harmful systemic repercussions. However, because coatings have inherently limited reservoirs of antibacterial agents, their action is ultimately only temporary.

Contact-killing

Contact-killing coatings have been developed to circumvent the reservoir exhaustion issue of release-based materials [167]. In this approach, antimicrobial compounds are covalently anchored to the material surface by flexible, hydrophobic polymeric chains. Adhered bacteria are believed to be killed due to the disruption of their cell membrane by the attached compounds, reaching across the microbial envelope thanks to the long tethering chains [168]. Because the main mechanisms of action are based on membrane interactions, such as physical lysing or charge disruption, the most effective compounds for contact-killing coatings have been either cationic compounds (QACs, chitosan, AMPs, etc.) or enzymes [164].

Anti-adhesion / Bacteria-repelling

Anti-adhesion coatings seek to prevent the earliest step of biofilm formation using non-cytotoxic mechanisms. Bacterial adhesion at biomaterial surfaces is generally described using a two-stage model; an initial, rapid and reversible stage (stage I) mediated by non-specific physico-chemical interactions followed by a secondary "locking" stage (stage II) involving, among others, species-specific bacterial adhesion proteins [169]. Surface immobilization of molecules that can resist protein adsorption, such as PEG and zwitterion, have demonstrated great anti-adhesion properties *in vitro* and, despite stability issues, are generally regarded as the standard approach for anti-adhesion coatings. However, the use of physical surface modifications (especially surface topography) as non-specific methods to modulate bacterial adhesion is most likely more complex than previously thought [170-172].

Table 2.1: Main antibacterial compounds in release-based coatings

AB type	Released compounds	Mechanisms of action	Comments ^a	Refs
Antibiotics	Aminoglycosides (Gentamicin, Tobramycin)	Inhibit protein synthesis by binding to the bacterial 30S ribosomal subunit		[166, 173]
	Quinolones (Ciproflaxin, Norfloxacin)	Inhibit DNA replication and transcription, targeting DNA topoisomerase II and IV.		
	Penicillins (Ampicillin)	Disrupt cell wall peptidoglycan synthesis through enzymatic inhibition.	Mainly Gram-positive and some Gram-negative bacteria	
	Glycopeptides (Vancomycin)	Disrupt cell wall peptidoglycan synthesis by binding to amino acids.	Effective against Gram-positive and mycobacteria.	
	Tetracyclines (Minocycline, Tetracycline)	Inhibit protein synthesis		
	Rifamycins (Rifampin)	Inhibit transcription by binding to RNA polymerase	Effective against mycobacteria and Gram-positive bacteria.	
Antimicrobial peptides (AMPs)	Over 2000 known AMPs, both anionic and cathodic (notable examples include magainin and nisin).	Depends on the type of AMP. Include transmembrane pore formation and several metabolic inhibition mechanisms.	Based on naturally occurring molecules, part of the host immune defense system.	[161, 174, 175]
Elements (metals and non-metals)	Silver	Complete description of modes of action remain unresolved. Known to deactivate enzymes by binding to thiol groups and inhibit the respiratory chain. Contributes to ROS formation	By far the most used antibacterial metal/nanomaterial. Along with other elements, have shown potential toxicity in human at high	[28, 176, 177]

			doses.	
	Copper	Generate ROS and deplete antioxidants. Induce lipid peroxidation in bacterial membranes.	Most heavy metals can induce several metal-catalyzed oxidation reactions that damage proteins, membranes or DNA.	[65]
	Zinc	Inhibit enzymatic activity.		[65, 178, 179]
	Gallium	Perturbs bacterial metabolism by acting as an iron mimetic.		[180]
	Selenium	Unclear, likely associated with oxidative stress to the bacterial cell wall.	Essential micronutrient in animals.	[181, 182]
	Halogens (Chlorine, iodine)	Penetrate the cell wall and disrupt proteins and nucleic acids structure and synthesis.		[183]
Enzyme	Lysozyme	Catalyze hydrolysis of glycosidic bonds in bacterial cell wall peptidoglycans.	Effective against Gram-positive strains	[184, 185]
	Acyase	Quorum quenching	Specific to Gram-negative bacteria	[186]
Organic cationic compounds	Quaternary ammonium compounds (QAC)	Disrupt intermolecular interactions in bacterial enzymes and membranes components.	Positively charged polyatomic ions of the structure NR_4^+	[187]
	Chlorhexidine	Bind to negatively charged bacterial walls, causing membrane disruption.	Often used in dental or topical applications.	[188]
	Octenidine	Similar to QAC		[189]
	Cationic surfactants (BAC, CTAB, DODAB)	Change the sign of the cell surface potential from negative to positive		[166, 187]
	Chitosan	Still unclear. Mostly centered on the disruption of cell membrane by	Antibacterial activity depends mainly on molecular	[190]

		positively charged chitosan molecules.	weight and cationic charge density.	
Organic non-cationic compounds	Furanones	Interfere with key bacterial quorum-sensing and swarming pathways	Derived from marine algae.	[191, 192]
	Triclosan	Bind to bacterial enzyme (ENR), which deactivates fatty acid synthesis	Recently banned in some countries for ecotoxicity issues. Endocrine disruptor.	[193, 194]
Other non-organic compounds	Nitric oxide	Exert nitrosative and oxidative stresses after diffusion across cellular membranes. Bacterial signaling disruptor.	Short half-life (seconds), requires good control over release parameters.	[195-197]
	TiO ₂ and TiO ₂ -based nanocomposites	Photocatalytically activate the production of ROS	Requires UV light. Very broad spectrum efficacy	[198]

^aAll listed compounds have exhibited broad spectrum activity unless otherwise indicated

2.4 Relevance of release-based antibacterial coatings

The 1st generation of release-based coatings mainly consisted of devices impregnated with antibiotics or silver compounds [199]. An in-depth analysis of the body of literature from the last decade offers contradictory findings on the performance of this first generation of coatings. On one hand, their introduction was associated with a significant decline in nosocomial infections [193, 200, 201]. On the other hand, several clinical trials revealed only limited success or reported complications [202, 203]. Frequent issues linked with release-based coatings are limited reservoirs/lack of long-term properties, cytotoxicity, inflammatory responses and increase in resistance of bacterial strains [161, 204]. These concerns have spurred recent major advances in antibacterial coatings towards non-release approaches [168].

2.4.1 Recent developments in antibacterial strategies

New evidence has emerged that could bring back release-based coatings at the forefront of the fight against nosocomial infections. For example, using a paradigm that originated from cancer treatment, researchers have identified hundreds of drugs that could be deployed cyclically in a sustainable process, so that the same antibiotics could be used continuously without the risk of developing resistance to bacteria [205]. This approach, called collateral sensitivity cycling, takes advantage of the hypersensitivity to other drugs of multidrug resistant pathogens. It could be particularly useful for Gram-negative bacterial pathogens, where multidrug resistance has increased rapidly. Similarly, newly discovered antibiotics, such as teixobactin, are likely to completely avoid the development of resistance. This was achieved by targeting less mutable components of the bacteria (lipid precursors of cell wall components), rather than relatively mutable proteins [206].

In addition, viable alternatives to biocidal antibacterial agents are being widely investigated. Bacteria secrete and detect signaling molecules (autoinducers), enabling cell to cell communication (quorum-sensing, QS) and the regulation of several bacterial processes, including gene expression, virulence factor production and biofilm formation [207]. Consequently, molecules that target and disrupt QS have garnered increasing interest as releasable antibacterial agents. Gram-positive bacteria typically use peptides for intercellular communication while this role is filled by acylhomoserine lactones (AHL) in Gram-negative bacteria [207]. By inducing less evolutionary stress on bacteria than biocidal compounds, QS inhibitors are less likely to induce development of resistance. Another key target for bacterial

signaling disruption is a small messenger molecule, bis-(3'-5')-cyclic dimeric guanosine monophosphate (c-di-GMP), known as a central regulator of biofilm formation and dispersal in a wide variety of bacteria by controlling the switch between motile planktonic and sedentary, biofilm-forming phenotypes [208]. Altering intracellular c-di-GMP concentrations, either through c-di-GMP analogs or inhibitors, could emerge as a new pathway to reduce biofilm formation and biofilm-related infections.

There are still major issues related to anti-adhesion and contact-killing surfaces. Surfaces become rapidly contaminated with materials that attach non-specifically or are buried under a layer of dead cells, resulting in their deactivation [166, 204, 209]. In addition, since their antibacterial action requires very close proximity with bacteria, both approaches require defect-free surfaces, thereby making large-scale production and subsequent handling even more challenging.

2.4.2 Key challenges

Antibacterial agent release and antibacterial coatings in general should not be viewed as a panacea, or universally effective strategy. Rather, they should be considered as part of a concerted effort to control known risk factors of nosocomial infections. Still, there are a number of key challenges that must be overcome for release-based coatings to become a truly useful tool in the fight against pathogens. We have identified these to be: (1) controlled release, (2) multi-functionality and (3) long-term stability.

2.5 Release-based coatings

Over the last decades, a broad range of antibacterial compounds have been developed for release-based systems (see Table 2.1). The oldest and still commonly used method to deliver these compounds consists in coating surfaces by simple impregnation, by soaking a porous material or coating with the desired antibacterial compound. The lack of a particular bonding mechanism to the coating leads to fast release [204]. Delivery systems have since evolved to include a wide variety of carrier materials (i.e. any material that an antibacterial compound can be loaded in) and deposition methods. The most frequently used carriers include poly(methacrylic acid) (PMMA), polyacrylic acid (PAA), poly(lactic-co-glycolic acid) (PLGA),

hydroxyapatite, polyurethane (PU), a hyaluronic acid and chitosan [166, 210]. A comprehensive review of antibacterial delivery systems can be found in [166].

A more recent approach to control the formation and release of antibacterial agents from coatings is to use polyelectrolyte multilayers (PEMs). PEMs are nanostructured polymeric systems and can be formed by layer-by-layer (LbL) deposition, which consist in the growth of alternating layers with opposite charges. This represents one of the most successful approaches to incorporate antibacterial compounds in coatings, due to its simplicity, versatility and low cost [209]. Antibacterial agents can be either trapped between layers or constitute an integral part of the coating, by substituting one of the charged species.

Hydrogels, ceramics and plasma-deposited polymers have also been widely reported as suitable carrier coatings for the delivery of antibacterial compounds [211-213]. The choice of coating materials ultimately depends on the chemical compatibility between the scaffold and the antibacterial agent, the required matrix functionalities (biointegration, wear-resistance, etc.) and the desired release modality. As each antibacterial agent/scaffold system has unique properties, a careful examination of the specific requirements for a targeted application is needed when designing release-based antibacterial coatings.

Beyond conventional biocide release, disruptors of bacterial signaling pathways have been widely explored, due to their ability to limit bacterial adhesion and biofilm formation. QS-inhibiting molecules incorporated in release-based coatings, including several furanones as well as enzymes, demonstrated great *in vitro* antibacterial properties [161, 186, 192]. For instance, the negatively charged acylase enzyme was immobilized on silicone catheters by LbL deposition without major loss of its enzymatic activity. The resulting coating showed a 50% reduction in biofilm formation over 7 days compared to untreated silicone and did not present any cytotoxicity against fibroblasts [186]. Peptides have also shown potential as QS inhibiting molecules in Gram-Positive bacteria. RNAIII-inhibiting peptide (RIP) prevented *S. Aureus* biofilm formation *in vivo* when released from PMMA beads [214]. Similarly, NO donors are important signaling molecules with wide-ranging functions, including biofilm dispersal due to their interaction with c-di-GMP [215]. Several NO release systems have been described in the literature, a few among them for antibacterial applications such as silica nanoparticles [216] and modified xerogels [217].

2.6 Control of release kinetics

The overall timeframe and kinetics of antibacterial delivery are highly application-dependent. Currently, typical release profiles follow first- or second-order kinetics, with an initial burst release followed by a decreasing tail distribution, usually ranging from hours to a few days. At first sight, a short-term, high dose release of antibacterial agent could appear as generally desirable. It provides antibacterial protection during the early post-operation period, which is considered the most critical stage for infection risk and limits the development of bacterial resistance. However, for implanted devices, surfaces should maintain their antibacterial properties until integration with the surrounding tissues, which can take up to several months, to prevent bacterial colonization from the hematogenous route [210, 218]. Long-term release is also regularly needed in case of revision or second surgery, where tissues surrounding the primary implant are often already infected, and for near-patient environmental surfaces [28, 218]. To date, designing coatings that maintain released antibacterial compounds levels within the therapeutic window, sufficient to kill bacteria but low enough to limit cytotoxicity toward eukaryotes, remains a significant challenge. Innovative approaches to control and extend release kinetics are therefore necessary to generate new solutions and products.

2.6.1 Passive approaches

Several variables have been shown to passively influence (without active triggers) release kinetics. Engineering strategies are being developed to tune the properties of the antibacterial agent itself (concentration, distribution, size, charge, etc.), the carrier matrix (porosity, surface roughness, functional groups, etc.) or the overall micro/nanostructure of the antibacterial coating (Figure 2.1) [166, 219, 220]. Alternatively, special architectures, which possess their own tunable parameters, can be incorporated in coatings to control release kinetics. These include nanotubes (e.g. carbon or TiO_2), nanowires, dendrimers and nanocapsules [220, 221].

Nevertheless, the sustained release of poorly charged (i.e. with no polar group or few polar groups compared to its size) or small molecules is very challenging. A recent study showed that using a large polyacid core in PEMs could lead to impressive sustained release [222]. The polymer coating released physiologically relevant drug concentrations over 14 months. Diclofenac (a nonsteroidal anti-inflammatory drug) was functionalized and conjugated to a

hydrophilic PGA polymer backbone via esterification and could be released by ester hydrolysis. The observed slow release kinetics were likely caused by the high negative charge along the PGA backbone (caused by a polar ester group within the short polymer backbone). Negative charges are known to slow down the rate of ester hydrolysis [223]. However, the polymer-drug conjugate itself is soluble in water and cannot be used to create a stable thin film coating. The PGA-bonded Diclofenac had to be immobilized in a PEM film, using PLL and chitosan as polycations.

The addition of a thin polymeric top layer can act as a rate-limiting barrier to extend the duration of sustained release from antibacterial coatings. The thickness [224], degree of crosslinking (inversely proportional to the porosity) [224] and hydrophobicity [225] of the top layer were shown to be the main factors influencing the release kinetics. These techniques efficiently prevented the initial burst release and displayed instead zero or near zero-order kinetics [224, 225]. A promising approach to deposit the top layer is plasma polymerization (see Box 2). Alternatively, for polymeric carrier coatings, plasma-post-treatments can also be used to directly induce additional cross-linking at the topmost surface of the polymer without affecting its bulk properties [226].

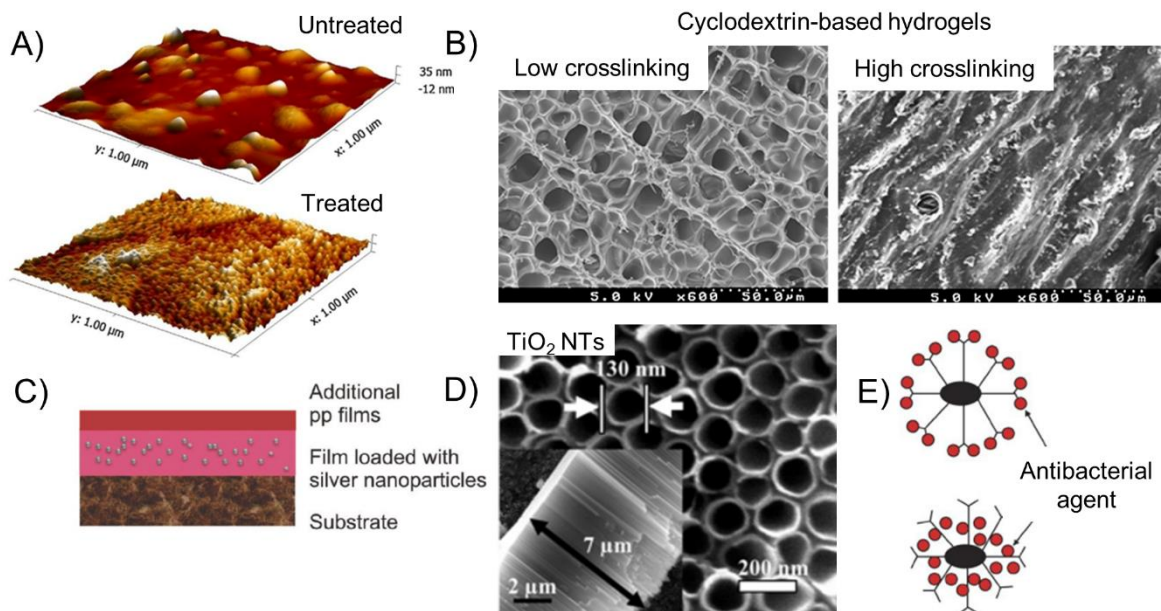


Figure 2.1: Schematics and images illustrating various passive strategies to control the release kinetics and antibacterial properties of coatings. a) AFM images showing the change of topography and nanotexture of Ti surfaces after an acid etching treatment [227]. b) SEM micrographs of cyclodextrin-based hydrogels with tunable porosity [228]. Porous coatings with a lower crosslinking density exhibit faster release kinetics than more crosslinked hydrogels. c) The deposition of a thin plasma polymer film can be used as a diffusion barrier for release-based antibacterial coating, enabling the control of the antibacterial agents rate of release by adjusting its thickness [229]. d) SEM images of TiO₂ nanotubes (NTs) used as tunable reservoirs for Ag NPs [230]. e) Other special architectures, such as dendrimers, can be used for loading and delivery of antibacterial compounds from a coating [221]. Figures reproduced with permission from Elsevier (a-b, d-e). ©2009 ACS (c)

2.6.2 Active approaches – stimuli-responsive materials

Stimuli-responsive materials have been investigated in the biomedical field for several decades, for applications such as self-healing coatings, micro/nano-sized sensors and actuators and drug release systems [231, 232]. Polymers and polymer-based hydrogels can undergo volume changes (swelling, shrinking or bending), structural transformations or bond cleavage in response to a particular trigger, causing subsequent elution of drugs from the matrix [231, 233]. These materials however are still seldom used as antibacterial coatings. Materials responsive to physical exogenous stimuli, which can be applied externally, offer great signal control and are not restricted by diffusion, hold great potential for use as bioactive coatings. They have the ability to (1) produce “on demand” antibacterial effects and (2) extend the useful lifetime of coatings. Antibacterial release systems based on electrical, ultrasonic, photothermal, magnetic and mechanical triggers have been reported [234-239]. The main challenges facing stimuli-triggered coatings are to achieve release of meaningful doses over multiple cycles and to minimize the non-triggered background leaching from surfaces.

A promising strategy to eliminate background leaching from a poly(2-hydroxyethyl methacrylate) (HEMA) involves the control of its swelling by co-polymerizing HEMA with a hydrophobic monomer, hydroxypropyl methacrylate (HPMA) and by adding a methylene-chain coating with tunable density and organization [237]. The added layer acted as a rate-limiting barrier for both water entry and antibiotic release from the underlying hydrogel. The ultrasound-triggered release of ciprofloxacin was found to be up to 14 times more intense than the background release rate and was repeatable multiple times, although at a decreasing dose with each pulse [237]. Ultimately, triggered-release doses and background release rates from hydrogel are interconnected since both are correlated with the polymer swelling. The choice between higher delivered doses or increased control over delivery should be dictated by the potential application.

In an alternative approach, the concept of including antibiotic-producing microorganisms within a sandwich structured coating was proposed [240]. A nanoporous top membrane controls the diffusion of molecules to and from the agar middle layer serving as a habitat for *Penicillium chrysogenum*. The production of penicillin is induced by providing nutrients to the fungus. While the choice of antibacterial agent and the range of applications of this approach are limited, it could constitute one of the only *truly* permanent antibacterial coatings.

A major avenue that remains largely unexplored in antibacterial coatings is the use of embedded metallic nanoparticles (NPs) as plasmon-resonators for light-trigger release. Silver NPs are already widely present in antibacterial coatings and could be employed to induce NIR-light triggered degradation of antibacterial agent-containing coatings, such as PEMs [241]. Alternatively, when used directly as the released compound, they may be conjugated with antibacterial-antibodies and act as cell-targeted plasmonic heaters, thus further damaging the bacteria cell membrane [242]. Nanocontainers-based smart coatings, an emerging field with great potential for controlled delivery, could also offer a versatile solution for *precise* and *timed* active release of antibacterial agents, although their development has been quite challenging so far [243, 244]. For example, since it is a feedback active system at the nanoscale level, our understanding of the physical phenomena involved and control of the processes are still limited. Introducing functions that survive the coating manufacture has also been a key problem.

2.6.3 Bacterial triggers approaches

Coatings that deliver antibacterial agents only when surrounded by or in contact with bacteria represent the ultimate form of controlled release. Bacteria metabolism produces acidic substances, such as lactic and acetic acid, leading to a pH drop in their immediate environment [245, 246]. Several pH-responsive antibacterial coatings were developed by taking advantage of this phenomenon (see Figure 2.3). Using LbL assembly, Zhuk et al. combined positively charged antibiotics, gentamicin, tobramycin and polymyxin B, with a polyanionic counterpart, tannic acid, to form antibacterial PEMs [246]. In acidic conditions, the coatings release bursts of antibiotics determined by the degree of pH lowering. The driving force behind the release was reported to be caused by charge balance within the PEM films. The protonation of tannic acid at lower pH creates an accumulation of positive amino groups within the film, leading to an imbalance and consequent release of the cationic antibiotics to maintain electroneutrality. The release kinetics from the coating was found to be mainly influenced by the strength of the molecular interactions.

Using similar design principles, gentamicin was combined with poly(methacrylic acid) (PMMA) and polyacrylic acid (PAA) to form hydrogel-like films with bacteria-triggered release capabilities [247, 248]. The addition of anionic clay-platelets to the hydrogel matrix provided pH-independent binding site for gentamicin, thus ensuring that a fraction of the antibiotic

remained bound within the coating [248]. In all cases, the drug remained sequestered within the coatings up to several months in the absence of pH decrease or bacteria stimuli. This suggests that pH-triggered coatings could be more successful at fighting the occurrence of delayed infections than traditional drug-eluting films. However, the coatings were not tested against repeated bacterial challenges, mostly because there is no standard protocol for such tests.

The pH-mediated cleavage of chemical bonds was also used to induce bacteria-triggered responses in coatings [249]. Gentamicin sulfate was bonded to NPs using pH-sensitive imine bonds while the NPs are attached on the titanium through uncleavable amide bonds. The use of NPs allowed to increase drug densities (2000 pmol/cm² with NPs vs 600 pmol/cm² for the standard Ti surface) and granted better versatility by facilitating modifications to include various drugs or changing the substrate material. [249]

Another interesting approach consists in using bacteria-generated enzymes to degrade or cleave bonded antibacterial agents from a coating. While the pH-trigger approach cannot discriminate between different strains of bacteria, the enzymatic pathway offers the possibility to develop specific triggers for particular species. Only a few examples of enzyme-triggered release have been reported to date and most involved the bonding of the antibacterial compound to the substrate by an enzymatically cleavable bond. These include a thrombin-sensitive peptide linker [250] and anhydride bonds that can be hydrolyzed by lipase [251]. A notable exception in the enzyme/cleavage pathway is the polysaccharide multilayer reported by Cado et al. [252]. In that case, the release of cateslytin, an antimicrobial peptide, is provided by the enzymatic degradation of hyaluronic acid/chitosan films by hyaluronidase, an enzyme secreted by pathogens. The coatings maintain their activity during 3 cycles of use against fresh *C. albicans* suspensions, yet failed to fully inhibit *S. Aureus* after the first cycle [252].

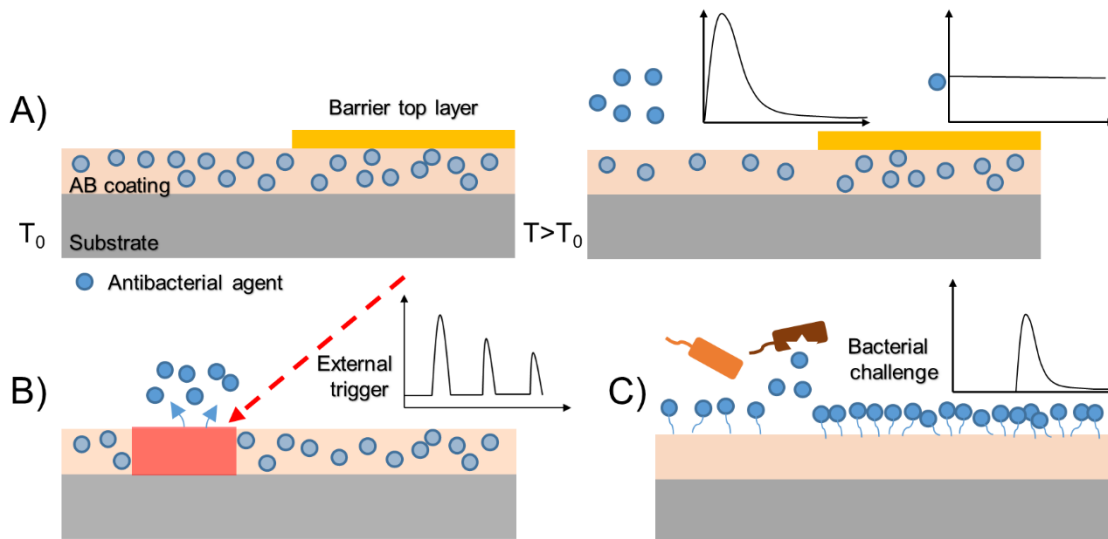


Figure 2.2: Designing antibacterial coatings within a 4D perspective. The design strategies to control the release of antibacterial agents over space and time can be grouped under three main categories. a) **Passive approaches.** By tuning the coating's properties, it is possible to impose specific preloaded release kinetics, giving the possibility to produce a variety a release profiles, including rapid bursts (left) or linear release (right) from AB coatings. b) **Active approaches.** External stimuli can be used to trigger the local release of embedded compounds. c) **Bacterial triggers approaches.** Bacteria-responsive coatings release antibacterial agents locally when challenged by bacteria. Inset: examples of representative release profiles for each approach, showing the release rate as a function of time.

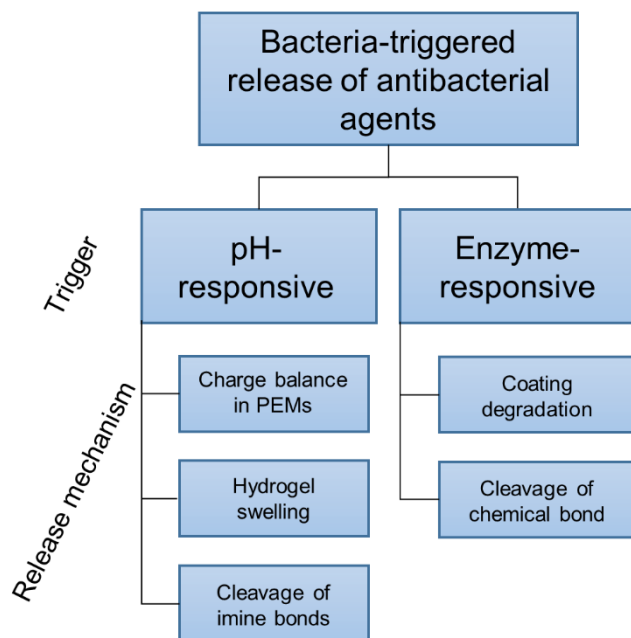


Figure 2.3: Control of release kinetics - Bacteria-triggered release. Coatings have been engineered to release antibacterial agents when subjected to two different bacterial triggers, the acidification of the local environment from bacterial metabolism and bacteria secreted enzymes. When challenged, the antibacterial compounds can be released by different mechanisms from simple bond cleavage to charge balance within the coating.

2.7 Multifunctional coatings

Because biological systems are inherently complex and hierarchically structured, coatings with multiple functions are required to achieve better performance in their environments. Recently, several multifunctional release-based antibacterial coatings have been developed and can generally be grouped into three categories: multi-release, multi-approach or multi-property.

2.7.1 Multi-release coatings

The co-release of antibacterial compounds with different mechanisms offers a dual advantage over single release coatings; a lower induction of bacterial resistance and, if adequately selected, a synergetic antibacterial action [253]. This paradigm has been successfully used over the years as design principle in antibiotics-impregnated catheters [254, 255]. While impregnation lacks control over release kinetics, degradable LbL assembled coatings may, on the other hand, offer a technically straightforward strategy for the pairing of controlled and combined release of antibacterial agents. Multiple antibacterial compounds can be embedded at different depths within the film and then released at different times [256]. Both the dosage and nature of the released compounds may be controlled by adjusting the chemistry of the degrading material. This scheme could be used to implement *in situ* cycling of antibacterial agents directly from biomaterial surfaces.

Silver has been successfully paired with several other antibacterial agents: antibiotics, metals, NO or ROS-generating compounds, etc. [86, 179, 195, 257, 258]. This could be attributed to the many modes of action of silver against bacteria, which increases the likelihood of synergetic effects. At this stage, however, direct comparisons of the effectiveness of paired antibacterial agents are not possible. Comparative effectiveness studies with a broader range of compounds will be required to develop and select more combinations with synergetic antibacterial properties and, ideally, no greater than additive cytotoxicity.

2.7.2 Multi-approach coatings

Unlike multi-release, multi-approach coatings do not rely solely on the release of biocides but rather seek to combine more than one antibacterial approach (see Box 1) against pathogens. Coupling approaches with complementary antibacterial mechanisms, acting as multiple lines of defense, represents a promising approach to overcome the inherent disadvantages associated with each strategy.

Li et al. were amongst the first teams to design coatings with both release and contact-killing capabilities [259]. They combined an LbL deposited reservoir of bilayers of PAH and PAA containing silver under a NP surface cap with immobilized QACs. The silver release from the coating provides a strong initial biocidal effect during the first few days while the QACs retained significant contact-killing activity after the depletion of the Ag reservoir [259]. This design has since been used in a variety of combinations [209, 260].

Coatings that include both biocide-release and anti-adhesion properties have also been reported [261-263]. The immobilization of PEG chains at the surface of a release-based coating represents an obvious and valid option to impart anti-fouling properties. Reduced adhesion can also be reached through non-grafting approaches, such as surface patterning and modifications of the surface chemistry. This opens up a wider range of materials and deposition techniques for the development of multi-approach coatings.

2.7.3 Multi-property (smart) coatings

The performance and functionality of biomedical devices depends on several parameters, including e.g. mechanical strength, resistance to corrosion and wear to avoid failure or even dangerous consequences [264, 265]. In addition, biocompatibility and resistance to corrosion and wear are two fundamental properties of implantable metals that are closely interconnected. In this framework, future generations of materials for health applications should have properties that exceed “functional”, effectively making them “smart” [266].

Several research teams have already undertaken the development of antibacterial agent releasing coatings with various added properties, including increased wear resistance, corrosion resistance, anticoagulation, enhanced bone-integration and improved overall tissue-integration, [178, 190, 230, 267, 268]. Co-delivery of other bioactive (therapeutic agents and growth factors) and signaling (quorum modulation) molecules have also been reported [251, 269, 270]. The various functions of nitric oxide (which plays an important role in cardiovascular systems, yet can also control biofilm formation) could make NO-releasing coatings attractive options as multi-property coatings for biomedical devices [196, 271]. The key difficulty in the design of such multifunctional coatings will likely be to implement functions that do not interact adversely and that can be maintained throughout the coating’s useful life [244].

2.8 Long-term stability

Stability, which is the capacity of a coating to maintain its properties over time, is one of the most critical factors determining the suitability of a surface for clinical applications. It remains, however, an often overlooked issue in the field of antibacterial coatings. Several studies have emphasized the lack of stability of some of the most popular approaches to antibacterial coatings, such as PEG-based antifouling surfaces [272, 273] and LbL/polyelectrolyte films [163, 209]. For example, investigations of the stability of PEG coatings in saliva, PBS and urine revealed a loss of their anti-fouling properties after only 0.5, 24 and 48h, respectively [274]. Drawbacks frequently identified in the literature to explain lackluster performances in long-term stability include chain cleavage, mechanical weakness, oxidative degradation, lack of adhesion to the substrate and high surface reactivity leading to surface conditioning [165, 171, 273-277].

As a result, recent efforts focused on the development and assessment of robust and stable coatings. Plasma-deposited coatings emerged as a viable option; while the coatings themselves rarely exhibit any antibacterial properties, they can act as robust carrier matrix or as platforms for immobilized bioactive molecules (see Box 2). They have been found to possess superior mechanical and chemical stability compared to dip, spray or spin coated materials [109, 212, 278]. Polymeric materials still make up the vast majority of plasma-deposited coatings [212], but several others have demonstrated excellent antibacterial properties. These include Ag/diamond-like carbon [267], TiO₂/Copper [198], AMPs/organosilicon [279] and Ag/hydroxyapatite [280] coatings.

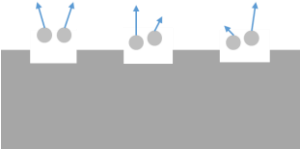
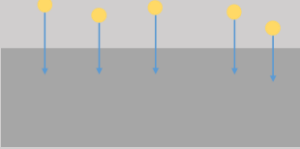
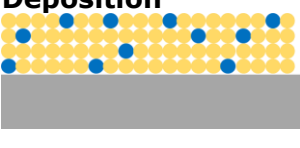
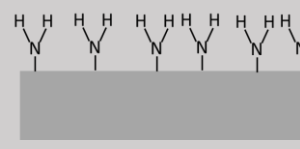
Although a wide spectrum of antibacterial coatings has been developed over the years and showed great potential in short term *in vitro* studies, investigations of this new generation of antibacterial coatings in controlled trials are still scarce [166, 194, 276]. There is no doubt that the absence of studies on the clinical stage is symptomatic of the lack of emphasis on long term stability studies in this field. At this stage, the widespread adoption of standard stability tests and the development of coherent guidelines are mandatory steps to accelerate progress towards a new generation of antibacterial coatings and their application.

Box 2: Engineering antibacterial surfaces using plasma-based tools.

Among antibacterial surface modification and coating approaches, plasma processes currently play a relatively minor role. However, this could change rapidly with the need for alternative deposition methods to solvent-based processes and the increasing requirements for robustness and long-term stability as design criteria in antibacterial applications. Plasmas, often called the fourth state of matter, are typically generated by the ionization (dissociation) of a gas by an electrical discharge. The charged particles formed, including ions, electrons and radicals, exhibit a strong collective response to applied electromagnetic fields and can interact with and modify surfaces in several ways (see Table 2.2). Plasma-based techniques are attractive processes for antibacterial surfaces design because they combine easy preparation, great versatility, economical and solvent-free processing, compositional control, conformal and pinhole free coverage, no thermodynamic constraints, sterility upon preparation and the possibility for commercial scale deposition [92, 281].

The most straightforward use of plasma in the antibacterial coating field consist in using a plasma deposited material as a reservoir for antibacterial compounds, which can be loaded either during the deposition itself or by an *ex situ* method [212]. The ion bombardment during deposition (effectively expanding the atomic intermixed zone) and graded interfaces of plasma coatings endow them with superior cohesion and adhesion compared with those deposited by wet chemistry methods. Alternatively, plasma processes can impart various functionalities at the materials surface, such as amino, hydroxyl and carboxyl groups. These can then be used to immobilize several biomolecules with antibacterial or other bioactive properties. Since plasma processes are compatible with masking techniques, enabling surface patterning, this could be an interesting option for the development of multi-release antibacterial coatings.

Table 2.2: Uses of plasma processes for antibacterial coatings and surfaces

Plasma processes	Uses for antibacterial surfaces	Examples (Refs)
<p>Sputtering/etching</p> 	<p>Surface cleaning Adhesion optimization Nanopatterning Nanostructuring</p>	<p>[267, 282].</p>
<p>Implantation</p> 	<p>Introduction of different elements into the materials, providing control over: Bioactive properties Corrosion resistance Mechanical properties Crosslinking and densification of polymers</p>	<p>[178, 283]</p>
<p>Deposition</p> 	<p>Thin films coatings with AB properties Reservoir or platform for AB compounds Diffusion barrier coatings</p>	<p>[197, 212, 267, 284]</p>
<p>Functionalization</p> 	<p>Surface activation Surface amination Formation of polar groups Immobilization of molecules</p>	<p>[212, 279, 285]</p>

Box 3: Outstanding questions

- What are the health and environmental impacts of the increased use of metallic nanoparticles in antibacterial coatings for short, medium and long term applications?
- What could justify the development of strain-specific antibacterial surfaces rather than broad spectrum ones?
- How can *in vitro* and *in vivo* testing methodologies be designed to both provide useful, standardized information and satisfy regulatory concerns?
- How could the regular clinical practice be changed/affected/influenced for the successful integration of new antibacterial products and solutions?

2.9 Conclusions and perspectives

The field of release-based antibacterial coatings has developed rapidly in recent years, to become one of the most widely studied areas of biotechnology, due to their potential importance in preventing nosocomial infections. With the significant burden from biomaterial associated infections (i.e. infections related to or caused by the presence of materials such as implants, catheters, near-patient surfaces, etc.), decreasing usefulness of traditional antibiotic therapies and growing concerns over bacterial resistance, they offer the much needed ability to limit pathogen's colonization of biomaterial surfaces by providing a local and defined delivery of antibacterial compounds.

In this review, we identified key features that must be imparted to antibacterial coatings to maximize their effectiveness and expand their area of application. Interesting questions have been raised along the way and are presented in Box 3. Strategies for controlled release, aimed at delivering precise doses within a proper timeframe, will ultimately govern the success of these coatings. As noted earlier, bacteria triggered release could provide the ultimate form of controlled delivery of antibacterial agents, yet future research should be devoted to testing those surfaces against repeated bacterial challenges as well as developing additional triggering pathways. Similarly, a multi-pronged approach, involving different mechanisms of action against bacteria as well as multiple integrated functions, have emerged as a critical requirement of the next generation of antibacterial coatings. In that regard, the release of quorum-disrupting molecules paired with a potent biocide may prove to be an interesting direction to follow.

However, despite the large amount of reported antibacterial approaches in the literature, to date there have been very few platforms that made their way to clinical studies, and even less to clinical practice. The lack of translational success can be attributed in part to the complexity the problem and the diversity of actors and professional cultures (researchers, physicians, regulatory agencies, etc.) [286]. An even more important factor remains that most current *in vitro* methodologies used to test antibacterial materials do not incorporate realistic *in vivo* conditions (biofouling, polymicrobial communities, relevant proteins, co-culture models, host immune response, etc.) [218, 287]. Objective evaluations of coatings stability, consistent with the intended application, have been similarly overlooked. A structured specific research is therefore needed to develop standardized and widely accepted validation methodologies for

antibacterial coatings in laboratories, from which we could effectively extrapolate clinical efficacy. These should be reliable, high throughput alternatives to clinical studies, able to withstand regulatory scrutiny, as the length and cost of testing potential antibacterial surfaces in controlled human trials are prohibitive [218]. Tackling these important challenges will require a collaborative effort from researchers across disciplines to provide real advancement in the biomedical field but should offer plenty of opportunities for innovation.

Acknowledgements

The ongoing work on antibacterial coatings in DM and FR laboratories was and is funded by the Natural Science and Engineering Research Council of Canada, the Canadian Foundation for Innovation, the *Fonds du Québec en Recherche sur les Natures et les Technologies*, and the Canadian Space Agency. DM is grateful to the Canada Research Chairs program for funding and partial salary support. FR acknowledges NSERC for an EWR Steacie Memorial Fellowship. MC acknowledges funding from a NSERC Vanier scholarship.

3 Adhesion enhancement of DLC coatings on 316L stainless steel surfaces by *in situ* plasma carburation

Authors and affiliations

M. Cloutier^{a,b,c}, S. Turgeon^a, P. Chevallier^a, M. Tatoulian^b, D. Mantovani^{a*,*}

^aLaboratory for Biomaterials and Bioengineering, CRC-Tier I, Dept of Min-Met-Materials Engineering, & CHU de Québec Research Center, Laval University, Pavillon Pouliot, salle 1745-E, Québec, Québec G1V 0A6, Canada

^bChimie ParisTech, PSL Research University, Institut de Recherche de Chimie Paris (IRCP), 11 rue Pierre et Marie Curie, F-75005 Paris, France

^cSorbonne Universités, UPMC Univ Paris 06, F-75005, Paris, France

Keywords

Plasma carburation, Diamond-like carbon, Interface, Adhesion, X-ray photoelectron spectroscopy

3.1 Résumé

L'intérêt soutenu dans l'utilisation de couches minces de carbone amorphe adamantin (Diamond-Like Carbon ou DLC) comme revêtements protecteurs réside dans leurs propriétés mécaniques et tribologiques exceptionnelles. Cependant, une importante limite à leur utilisation plus répandue est la faible adhérence du DLC sur plusieurs matériaux, qui provient des grandes contraintes de compression inhérentes à ces revêtements. La majorité des approches populaires utilisées pour contrer ce manque d'adhérence reposent sur le dépôt d'intercouches entre le revêtement DLC et le substrat. Ce type d'approches, en créant des interfaces additionnelles, s'expose toutefois à des problèmes potentiels de corrosion et de stabilité. Afin de prévenir ces problèmes à long terme, nous avons étudié l'utilisation d'un simple traitement plasma pour former des carbures métalliques, une excellente interface pour l'adhérence du DLC, directement sur la surface de l'acier inoxydable. Le traitement consiste à irradier la surface de l'acier inoxydable avec des ions d'un plasma de méthane avec une énergie croissante, en variant la tension appliquée sur le substrat. La formation de carbure a été observée à la surface de l'acier inoxydable par spectroscopie de photoélectrons X et était fortement corrélée avec la tension appliquée au substrat. La tension maximale étudiée (-650V) avait également le plus grand contenu en carbure. Des analyses approfondies de l'interface DLC/acier inoxydable ont révélé que les carbures détectés étaient principalement des carbures de chrome. Des essais de traction ont montré une amélioration de l'adhérence après le traitement plasma, avec une augmentation de l'adhérence du revêtement DLC de 116 ± 25 kg/cm² à 215 ± 35 kg/cm² après la carburation plasmas. La simplicité, la nature in situ du procédé et l'interface unique créée par la carburation plasma devrait répondre aux exigences de plusieurs domaines d'application des revêtements DLC.

3.2 Abstract

The recurrent interest in using diamond-like carbon (DLC) thin films as protective coatings has been driven by their exceptional mechanical and tribological properties. However, one of the limits to their broader application is the poor adhesion of DLC to several materials, which arises from their intrinsic high compressive stresses. Popular approaches to the adhesion problems rely on the deposition of interlayers between the DLC coating and the substrate. To prevent potential long-term issue caused by the creation of additional interfaces, we investigated the use of a simple plasma procedure to form metallic carbides, an excellent interface to promote DLC adhesion, directly on the surface of stainless steel. The treatment consisted in irradiating the stainless steel surface with ions from a methane plasma at increasing energy, by varying the substrate bias. Carbide formation was observed at the surface of stainless steel by X-ray photoelectron spectroscopy and was strongly correlated with the substrate bias applied, with the highest investigated bias (-650V) specimens having the largest carbide content. Further analyses of the DLC/stainless steel interface revealed the carbide compounds detected to be mostly chromium carbides. Pull-off tests showed an improved adhesion of DLC films with the plasma interfacial treatment, with the bonding strength increasing from 116 ± 25 kg/cm² to 215 ± 35 kg/cm² after plasma carburation. The straightforwardness, *in situ*, and “single interface” nature of plasma carburation should meet the requirements of several areas of application of DLC coatings.

3.3 Introduction

Carbon-based thin films-based coatings have emerged as powerful platforms and multipurpose materials in recent years, spurred by remarkable advances in processing techniques and surface engineering. The rich surface chemistry and polyvalence of these nanostructured materials lend themselves to numerous modifications, opening up countless opportunities for application in diverse, highly technical fields [288, 289]. A prime example of this widespread potential is given by diamond-like carbon (DLC), a metastable form of amorphous carbon with a significant fraction of sp^3 bonds. This confers to DLC many of the beneficial properties of diamond itself (e.g. superior mechanical and tribological properties, chemical inertness, stability, etc.) but in an isotropic conformal thin film [106, 278]. Moreover, the amorphous microstructure of DLC allows for the incorporation of other species such as hydrogen, nitrogen, silicon, titanium, silver, gold, or copper, which can be used to tailor the materials properties to the desired application [290-293]. In this respect, DLC is particularly attractive as a multifunctional protective coating in tribological and biomedical applications [294, 295]. Unfortunately, prospects of using DLC as a versatile protective coating have been long been hampered by low adhesion and delamination issues on several application-relevant substrates, including stainless steels. Bombardment by energetic ions and atoms occurring during the deposition process creates high density regions and important distortions in local bonding, producing high levels of compressive stress in the material [106, 296]. The high levels of stress create in turn a strong driving force for the coating to become detached, ultimately limiting the thickness and range of substrates that can be used with DLC coatings [297].

Several approaches have been proposed to get around the delamination problem. They may be classified according to whether they target the film itself or the film/substrate interface respectively into 1) stress reduction and 2) adhesion enhancement strategies. Coating stress reduction strategies include multilayering and gradation, incorporation of alloying elements, annealing, and the deposition of low sp^3 content films [298-300]. On the other hand, adhesion enhancement strategies target the DLC/substrate interface to increase adhesion through surface treatments (etching, roughening, etc.) of the substrates and deposition of interlayers (chromium, silicon, titanium, etc.) [106, 115, 153, 301-303]. The deposition of interlayers of carbide-forming elements remains the most popular and successful method to optimize DLC adhesion on a variety of coatings and has been used extensively both in laboratory and

industrial settings. However, recent investigations exposed important drawbacks associated with the use of such interlayers. The creation of additional interfaces: 1) multiply the possibilities for long-term adhesion problems and debonding and 2) create an environment prone to crevice corrosion [302]. The additional elements can also cause toxicity problems in biomedical applications. Furthermore, the interlayer deposition itself adds energy and resource consumption to the DLC coating process.

This study investigates the alternative possibility of improving the adhesion of DLC on 316L stainless steel (SS316L) through the use of a plasma interfacial treatment aimed at forming carbides directly on the surface, without deposition of an additional layer. The treatment, termed plasma carburation, consists in bombarding the stainless steel surface with relatively high energy hydrocarbon ions. X-Ray photoelectron spectroscopy (XPS) was used to thoroughly investigate the chemical bonding of the different elements at the interface. The resulting improvement of film adhesion was studied using a pull-off test and optical microscopy.

3.4 Materials & Methods

3.4.1 Sample preparation

The DLC coatings were grown on AISI 316L stainless steel (Fe/Cr18/Ni10/Mo3, from Goodfellow, Huntingdon, England) disks of 12.7 mm in diameter, punched from 0.5 mm thick sheets using a radio-frequency (13.56 MHz) inductively-coupled plasma PECVD reactor, which has been described in details previously [267]. The energy of the ions (essentially carbon and hydrogen) incoming on the substrate was independently adjusted by applying a low frequency (90 kHz) voltage to the sample holder, which was rectified by the plasma and resulted in an adjustable (between -100V and -650V) negative bias voltage (V_b).

The reactor was cleaned for 60 min with an argon/oxygen plasma prior to each deposition. Substrates were cleaned in an ultrasonic bath and subjected to an electrochemical polishing procedure to obtain a smooth, homogenous surface [304]. They were then loaded in the deposition chamber which was evacuated to a base pressure of 10^{-6} Torr. Before deposition, the SS316L substrates were etched with an Ar plasma and pre-treated with a high-energy hydrocarbon plasma. The bias voltages used in that step were -100V, -250V, -450V and -650V.

Specimens not treated with the hydrocarbon plasma step were used as a control group. Following pretreatment, DLC deposition was then carried out in the same reactor, which prevented contact with air. All plasma treatments were performed without heating, at room temperature. The details of the plasma treatments are summarized in Table 1.

Table 3.1 : Plasma treatment parameters

	Ar etching	Hydrocarbon plasma	DLC coating
Precursor (%)	Ar (100)	CH ₄ (100)	CH ₄ /H ₂ (20/80)
Pressure (mTorr)	50	10	10
Peak RF power (W)	100	100	100
Bias voltage (V)	-100	-100/ -250/ /-450/-650	-100
Treatment time (min)	15	1/5	15

3.4.2 Characterization

The surface and depth composition was investigated by X-ray photoelectron spectrometry (K-alpha spectrometer, Thermo Scientific) coupled with a 1 keV Ar⁺ sputtering beam, unless indicated otherwise. High resolution XPS spectra are acquired at regular sputtering time intervals using a monochromatic Al K α source (1486.68 eV) with a spot size of 250 μ m, and a pass energy of 200 eV for the survey scans and 50 eV for the elemental scans. An electron flood gun was used to prevent surface charging. Angle Resolved X-ray Photoelectron Spectroscopy (ARXPS) was obtained by collecting spectra from 5 takeoff angles, namely 15, 25, 40, 60 and 80°, which are defined as the angle between the surface and the detector. Peak fitting was performed with the Avantage© software (Thermo Scientific) after subtraction of a Shirley background. Samples were also studied by optical microscopy, with a BX41M microscope (Olympus). For each independent sample, data were acquired at three (XPS) or five (Optical microscopy and AFM) randomly selected positions on the specimen surface.

3.4.3 Adhesion tests

The pull-off adhesion strength of DLC coatings was measured in tension using an Instron 5944 mechanical testing system (Instron Corporation, Norwood, MA) equipped with a 2kN

load cell. A metallic stud of 7.85 mm diameter was attached perpendicularly to the DLC coated surface using a commercial epoxy (J.B Weld, Sulfur Springs, TX) which was allowed to cure for 24 h, reaching a guaranteed tensile strength of 27 MPa. A specially designed sample holder was used to ensure the complete alignment of the system. The stud was pulled upward at a constant speed (50 mm/min) while holding the sample stationary, resulting in the application of a gradually increasing tensile force on the sample. The instrument recorded the highest value of force applied before failure. At least five tests were carried out on each type of samples. After the pull-test, specimens were studied visually and with an optical microscope to determine the origin of the coating failure.

3.5 Results and discussions

3.5.1 Effect of interfacial treatment on composition

The energy dependent nature of plasma-surface interactions in hydrocarbon plasmas has been well documented [130, 305, 306]. Consequently, a range of energies, consistent with existing deposition systems, was selected and used to explore the effects of a plasma carburization pretreatment on the resulting DLC/SS316L interface properties, most notably on the local chemical bonding. Uncoated specimens treated at different bias voltages were initially analyzed by XPS. At this stage, treatment times were kept to a minimum (1 min) to facilitate the straightforward inspection of the film/substrate interface. The presence of bias-dependent features was observed on the carbon C1s spectra (Figure 3.1a). A clear contribution below the main C-C/C-H peak was detected for samples treated at -250V, with further increases in negative bias leading to a more pronounced peak. Only metal-bonded carbon atoms give rise to C1s XPS contributions below the main 285 eV C-C peak [307, 308]. Angle-resolved XPS investigations showed that in this case, carbide formation occurred concurrently with carbon deposition (Figure 3.2b). The relative contribution of the carbide peak increases with the take-off angle, suggesting that the carbides are located below a thin, likely amorphous, C-C rich overlayer. Because biased plasmas characteristically have a bimodal ion energy distributions (IED), the kinetic energy of ions from the lower end of the IED must be too low for implantation or subplantation process, sticking instead on the surface and creating growth of the amorphous carbon layer [103, 309]. Conversely, for the low bias interface treatment (-100V), only amorphous carbon deposition occurred, covering the surface and partially

extinguishing the signal from the underlying metallic substrate (Table 3.2). The absence of a carbide peak, even at the largest take-off angle, and the lack of evolution between different depths for the -100V samples (Figure 3.2a) confirm that the measured increase in carbon at the interface is due to amorphous carbon deposition.

To obtain a more quantitative assessment of the carbon bonding, the high resolution C(1s) spectra were decomposed in four peaks, assigned to C=O (BE = 288.0-288.4 eV), C-O (BE = 286.3 – 286.5 eV), C-C/C-H (BE = 284.8 eV) and C-metal (282.8 - 283 eV) (Figure 3.1b). The attribution of the carbon-metal component entails its own challenge, as there are several carbide-forming metallic elements (Fe, Cr, Mo, Ni) in the SS316L that could contribute to the signal. Furthermore, an ion deposition process cannot be expected to yield a pure material with only one bonding type. Therefore, we did not seek to precisely determine the stoichiometry of the metal carbides found at the interface, but rather to look for qualitative information on the bonding mechanisms.

Despite the expected mixture of different bonds at the interface, comparing the C-Me peak binding energy with the literature provides a simple way to identify its major contributors. Only $\text{Cr}_{1-x}\text{C}_x$ (282.8-282.9 eV) and $\text{Mo}_{1-x}\text{C}_x$ (282.8 eV) compounds binding energies reported in the literature match the one of the measured experimental C-Me peak [310, 311]. The limited presence of Mo at the interface (Table 3.2) makes it, however, unlikely that Mo-based compounds make up a significant portion of the observed carbide peak. The presence of nickel (283.3-283.8 eV) [312, 313] and especially iron (283.3-284.1 eV) [314, 315] carbide phases have also been considered. However, their small relative intensity and lack of separation with the main C-C peak makes further decomposition problematic.

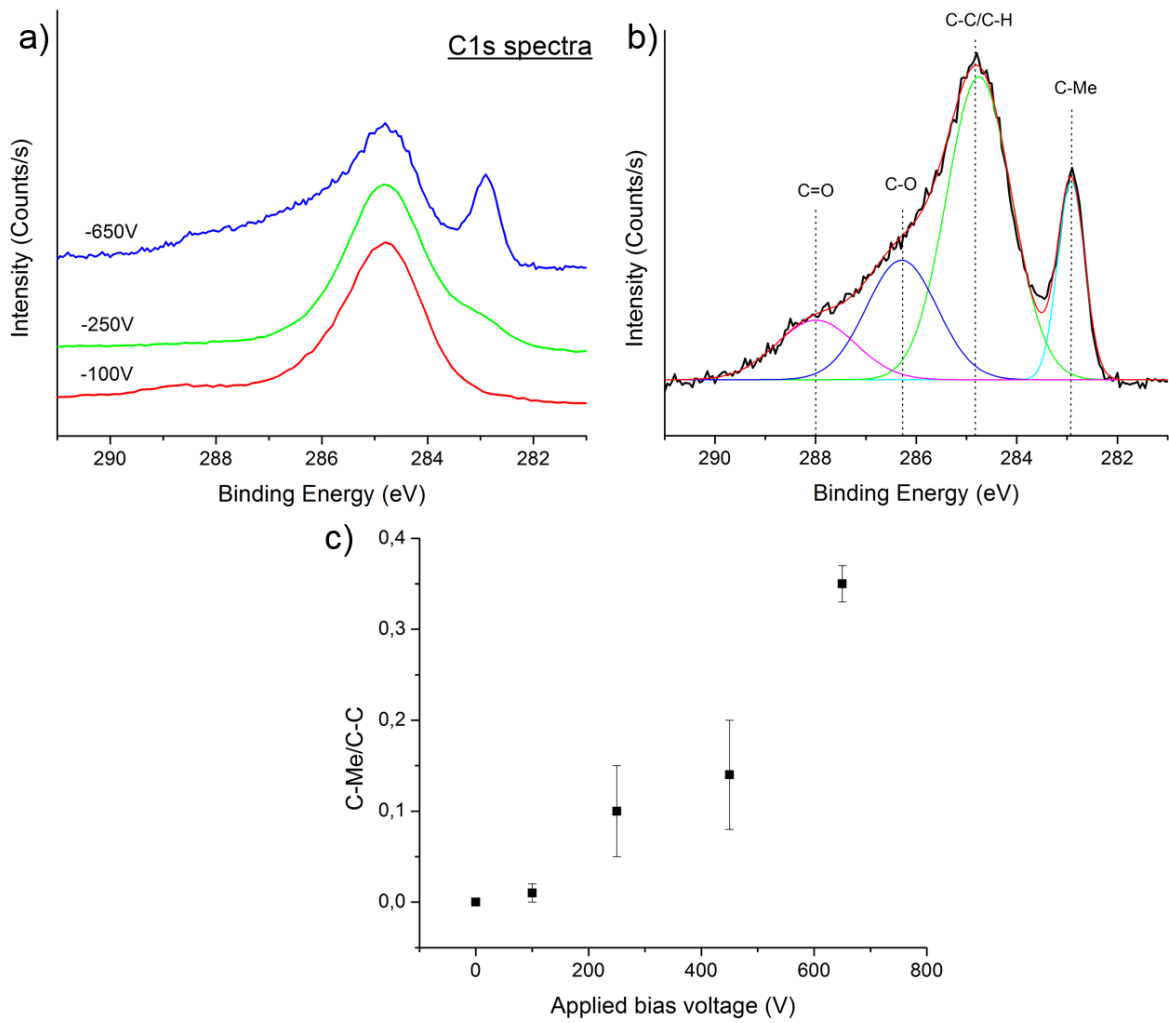


Figure 3.1 : a) XPS core-level spectra of C1s after plasma carburation treatment b) Example of decomposed spectrum. The c) Comparison of the C-Me/C-C ratio for the different treatment biases.

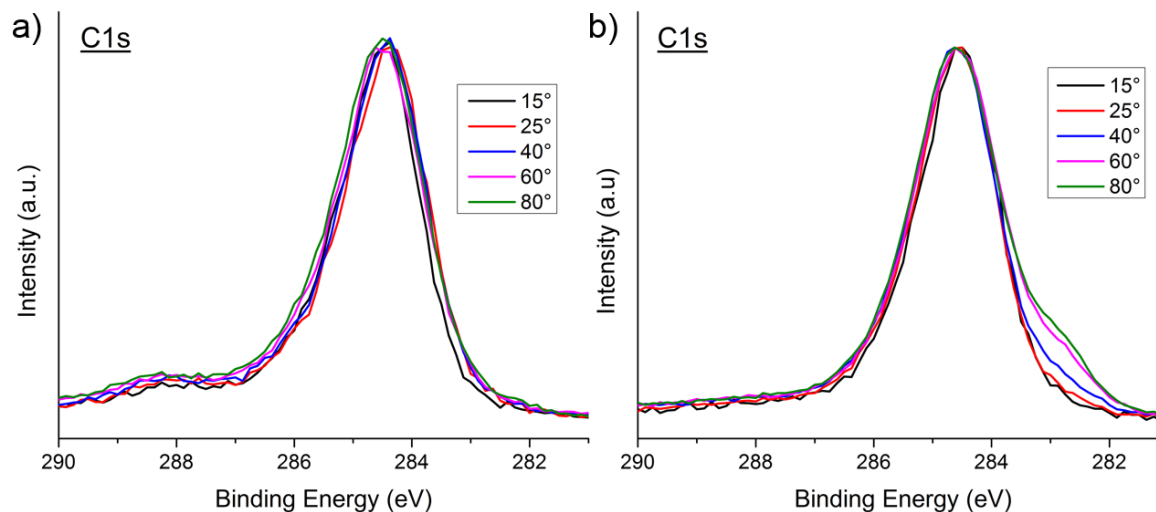


Figure 3.2 : XPS core level spectra of C1s at the interface of samples treated with (a)-100V and (b)-250V plasma carburation treatment recorded at take-off angles from 15° to 80°.

Table 3.2 : Chemical surface composition of untreated and treated samples measured by XPS.

Treatment type	ID	Atomic composition (at.%)					
		C	O	Fe	Cr	Mo	Ni
Control	SS316L	32±12	47±3	9±5	11±4	0.3±0.2	1.1±0.6
Carburation Interface treatment	100V	70±3	14±2	8±1	7±3	-	-
	250V	51±3	31±2	12±2	6±1	0.2±0.2	0.2±0.1
	450V	55±3	25±2	16±2	3.5±0.5	0.6±0.2	0.1±0.1
	650V	57±3	24±3	14±3	4.0±0.7	0.6±0.1	0.3±0.2
Coating	DLC	95±3	5±3	-	-	-	-

High resolution XPS analyses of the metallic components were performed to help corroborate any formation of metal-carbon species at the interface. A systematic peak deconvolution and fitting approach was not pursued in this case because of: 1) the large number of possible oxidation states for the investigated metals [307], 2) the complex multiplet splitting occurring for a few oxidation states (e.g. Cr(III) and Fe(III)), creating many possible compounds with overlapping binding energies and 3) the presence of carbon and oxygen at the interface, complicating the attribution of fitted peaks to either one of carbide or oxide compounds. For these reasons, we restricted our investigation to a qualitative analysis of the Cr2p and Fe2p

regions. Analyses of the Mo3d and Ni2p regions were not performed because of their low signal/noise ratios.

Figure 3.3 shows the Fe2p and Cr2p spectra of samples treated by plasma carburation at different bias voltages. In all cases, the detected total metal content was at least 15 at.%, guaranteeing that the SS316L interface was effectively reached. The most striking features are the very broad Cr2p peaks for the plasma-treated (-650V) samples, which are shifted to lower binding energies than those typically associated with chromium oxide/hydroxide compounds (575.7 eV – 579 eV) [307, 316]. Although a broad peak can be expected due to the presence of multiple overlapping components, the overall spectral shape suggests a contribution from one or multiple components between the metallic chromium (Cr(0) at 574.2 eV) and the oxide region. Similar binding energies have been previously measured in chromium carbide precipitates and carbon-chromium sputtered films [317, 318]. By contrast, the Fe2p peak had the typical asymmetric shape of metallic iron, with a trailing tail towards higher binding energies associated with the presence of iron oxide. Although the -650V presents an additional feature/shoulder centered around 710 eV, it is impossible to confirm whether it arises from Fe-C bonds or not.

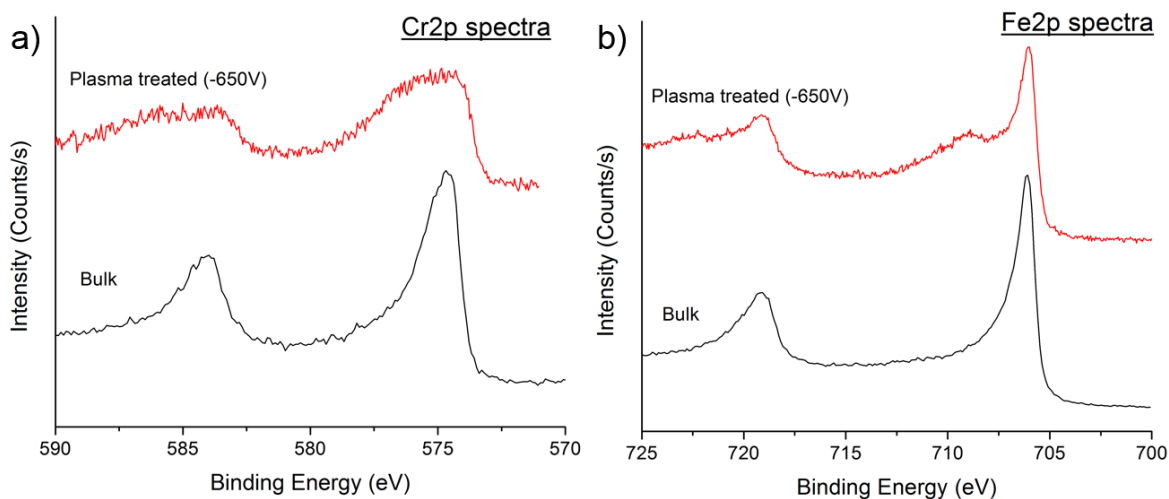


Figure 3.3 : XPS core-level spectra of (a) Cr2p and (b) Fe2p after plasma carburation treatment.

3.5.2 Depth profiling

A full profiling study was conducted on DLC coated samples treated by plasma carburation at -650V. The depth profiling experiment consisted of successive sequences of etching and XPS analyses (Figure 3.4). A moderate energy Ar^+ beam (1 KeV ions) was used to minimize damage, sputtering induced formation of carbides and ion beam mixing. Overall, the profile analysis was consistent with the XPS high resolution and survey experiments performed previously, with iron and chromium being the primary elements present at the interface. Decomposition of the C1s peak throughout the profile showed a local maximum of the C-Me component (~ 10 at.%), which is reached after between 525 and 550 seconds of sputtering. The location of this layer underneath the remaining metallic oxides indicates that carbide formation originates from high energy (i.e. higher penetration depth) implanting ions. This agrees well with our previous experimental results and confirms the importance of the carburation treatment bias.

Plotting the evolution of the C-Me atomic concentration alongside the other elements shows strong similarity between the C-Me and Cr profiles (Figure 3.4b). In general, therefore, taken together with the lower binding energy of the C-Me signal and the broadness of the chromium peak after plasma treatment discussed previously, this finding seems to reinforce the hypothesis that the main contributors to the C-Me signal are indeed $\text{Cr}_{1-x}\text{C}_x$ compounds. Looking back at Table 3.2, this results however indicates that from a stoichiometric standpoint, the carbides formed at the interface are richer in carbon than typical compounds with Me_3C_2 or Me_3C compositions. The concentration of chromium detected at the interface (4 at.% for the -650V sample) is not sufficient to produce by itself the C-Me peak observed on the C1s spectra if the compounds formed were indeed Cr_3C_2 or Cr_3C .

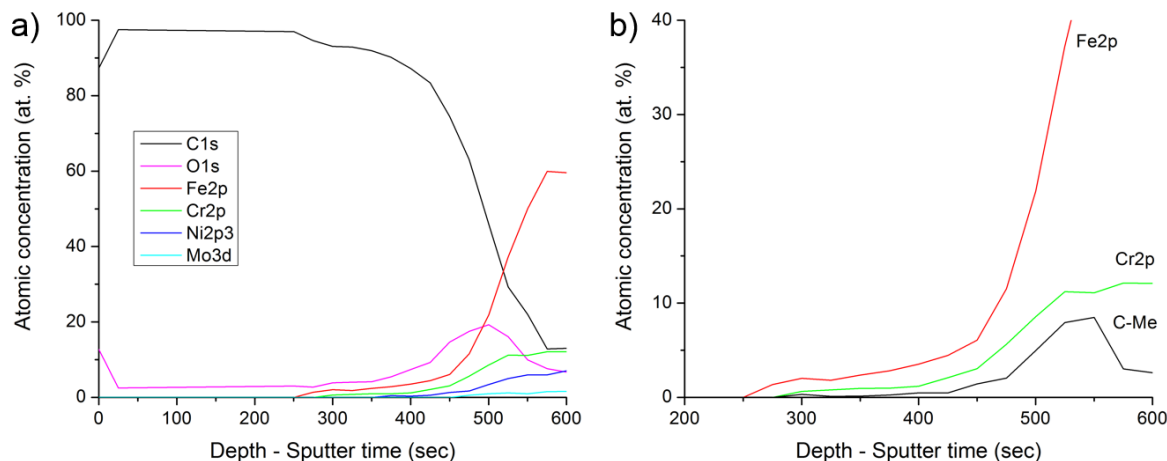


Figure 3.4 : a) XPS depth profile of a DLC coated, interface treated sample ($V_b = -650V$). b) Evolution of the atomic concentration of the main metals (Fe and Cr) with the C-Me contribution measured using the C1s peak.

3.5.3 Adhesion measurements

Pull-off tests were performed on plasma-etched and carburation-treated ($V_b = -650V$) samples to assess the effect of plasma carburation on interfacial adhesion of DLC coatings. Studs ($d = 0,5$ cm diameter) were fixed to the DLC surface using a high-strength epoxy glue. The pulling force that broke the bond was recorded. Results indicative of poor epoxy adhesion or cohesion were excluded. Figure 3.5 shows pull-off results for the two types of interface treatments. The interfacial adhesion strength between DLC and the 316L stainless steel substrates increased from 116 ± 25 kg/cm² to 215 ± 35 kg/cm² after the plasma carburation treatment. A visual and microscopic inspection of the studs was used to determine the cause of failure. Although the separation was caused by adhesive failure in the majority of cases, the failure in some of the carburation-treated samples was due to a combination of adhesive and DLC cohesive failure (Figure 3.6). As-received substrates (without interface treatment/etching) could not be tested because the coatings self-delaminated rapidly after exiting the reactor (Figure 3.7).

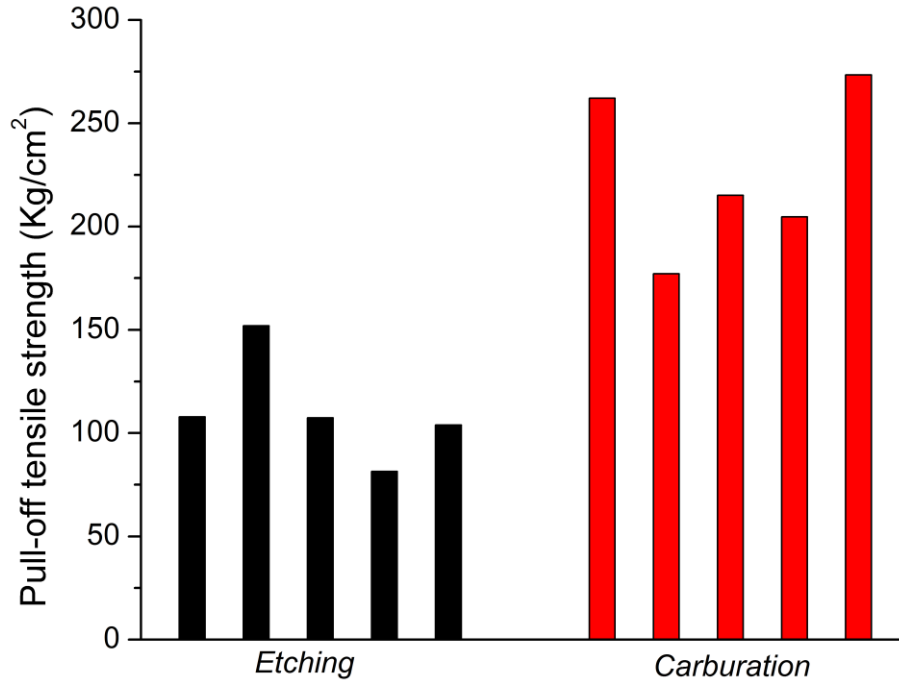


Figure 3.5 : Maximum tensile strength recorded during the pull-off experiment for specimens treated with etching (black, left) and plasma carburation at -650V (red, right). Each bar represents an individual DLC deposition and is the average of at least two pull-off tests.

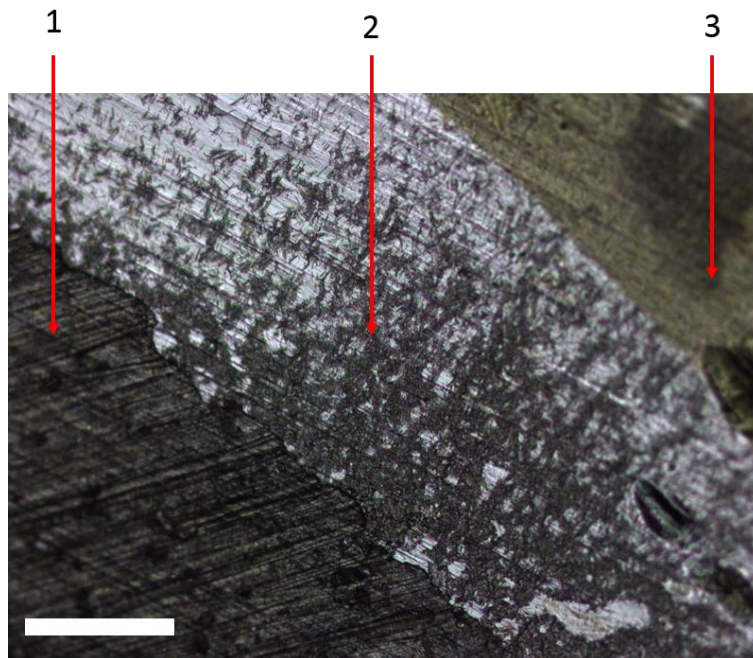


Figure 3.6 : Optical micrograph showing a combination of adhesive and cohesive failure of an interface-treated (-650V) DLC coating after a pull-off test. The different zones observed are 1) 316L substrate (adhesive failure), 2) damaged DLC film (cohesive failure), and 3) intact DLC film. The stud initially covered zone 1 and 2. Scale bar, 250 μ m

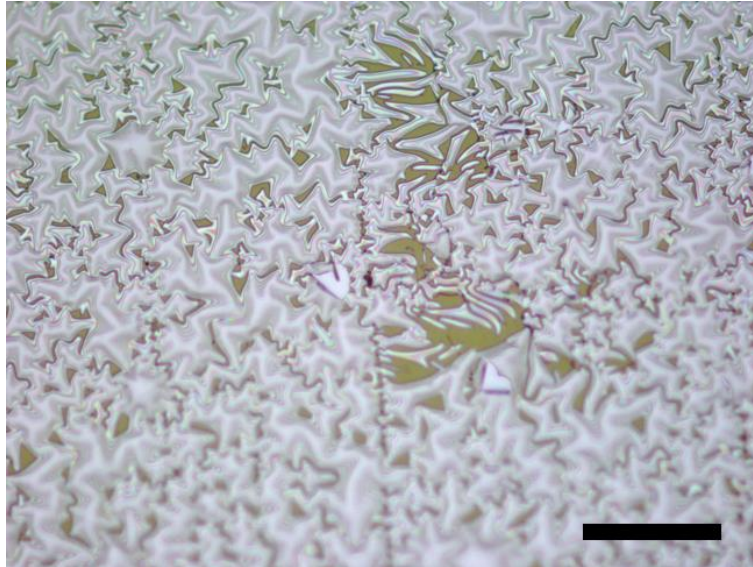


Figure 3.7 : Representative optical micrographs showing the self-delamination and peeling of DLC coatings occurring for non-treated interfaces. Scale bar, 100 μ m.

3.6 Conclusions

Irradiation of stainless steel surfaces with moderately high energy ions from a hydrocarbon plasma can be used to form metallic carbides. XPS studies confirmed that, despite the presence of multiple potential carbide-forming elements in 316L stainless steel, chromium carbide comprised the majority of the carbide compounds found at the surface after the plasma treatment. Pull-off test results confirmed that the plasma carburization treatment doubled the adhesion strength of DLC coatings to the metallic substrate, compared with plasma etching.

Interface engineering strategies, such as interlayer deposition, have already been applied to improve DLC adhesion to several metallic surfaces, often resulting in significant improvements in interfacial bonding strength. Although the adhesion gain from plasma carburization is more modest, our results demonstrated for the first time that bonding strength improvements can be obtained with a short *in situ* treatment and without the deposition of additional interlayers. The interface treatment and DLC deposition steps can be performed sequentially in the same reactor, limiting contamination issues and facilitating a potential transition to a larger scale production. Plasma carburization could prove to be an interesting

option to improve DLC adhesion for applications where corrosion resistance or long-term stability are important challenges.

Acknowledgements

This work was partially funded by the Natural Sciences and Engineering Council of Canada through the Strategic Project Grants program. MC acknowledges the support from a NSERC Vanier Scholarship. The authors wish to thank Dr Jean-Jacques Pireaux and Dr Yan Busby from the Laboratoire Interdisciplinaire de Spectroscopie Electronique for providing the equipment and help necessary to perform the XPS profiling experiments.

4 Controlled distribution and clustering of silver in Ag-DLC nanocomposite coatings using a hybrid plasma approach

Author names and affiliations

M Cloutier^{a,b,d}, S Turgeon^a, Y Busby^c, M Tatoulian^b, J J Pireaux^c and D Mantovani^a

^a Laboratory for Biomaterials and Bioengineering, CRC-Tier I, Dept of Min-Met-Materials Engineering, & CHU de Québec Research Center, Laval University, Pavillon Pouliot, salle 1745-E, Québec, Québec G1V 0A6, Canada

^b Chimie ParisTech, PSL Research University, Institut de Recherche de Chimie Paris (IRCP), 11 rue Pierre et Marie Curie, F-75005 Paris, France

^c Laboratoire Interdisciplinaire de Spectroscopie Electronique (LISE), University of Namur, 61 rue de Bruxelles, B-5000 Namur, Belgium.

^d Sorbonne Universités, UPMC Univ Paris 06, F-75005, Paris, France

Keywords

Silver, diamond-like carbon, X-Ray photoelectron spectroscopy, segregation, clustering, plasma deposition

4.1 Résumé

L'introduction d'éléments métalliques dans le carbone amorphe adamantin (Diamond-Like Carbon ou DLC) a émergé comme une approche innovatrice pour ajouter des propriétés uniques aux revêtements, ouvrant ainsi une gamme de nouvelles applications dans des domaines aussi divers que les capteurs, la tribologie et les biomatériaux. Le dépôt par technique plasma de revêtements DLC contenant avec des propriétés structurales et une distribution d'éléments métalliques bien définies est cependant entravé par une compréhension limitée de leurs mécanismes de croissance. Nous rapportons ici l'élaboration d'un revêtement composite argent-DLC (Ag-DLC) préparé dans un réacteur plasma hybride, permettant un contrôle indépendant de la teneur en métal, de la microstructure et de la morphologie du film. Des analyses de la morphologie et de l'état chimique des revêtements Ag-DLC ont été effectuées par microscopie à force atomique, microscopie électronique à balayage et par spectroscopie de photoélectrons X. La distribution verticale de l'argent, de la surface vers le cœur du revêtement, fut révélée comme étant très inhomogène, dû à des phénomènes de ségrégation en surface et de formation de grappes de particules d'argent. En se basant sur ces observations, un modèle permettant de décrire les mécanismes de croissance des revêtements Ag-DLC est proposé.

4.2 Abstract

The incorporation of selected metallic elements into diamond-like carbon (DLC) has emerged as an innovative approach to add unique functional properties to DLC coatings, thus opening up a range of new potential applications in fields as diverse as sensors, tribology and biomaterials. However, the deposition by plasma techniques of metal-containing DLC coatings with well-defined structural properties and metal distribution is currently hindered by the limited understanding of their growth mechanisms. We report here a silver-incorporated diamond-like carbon coating (Ag-DLC) prepared in a hybrid plasma reactor which allowed to independently control the metal content and the carbon film structure and morphology. Morphological and chemical analyses of Ag-DLC films were performed by atomic force microscopy, scanning electron microscopy and X-ray photoelectron spectroscopy. The vertical distribution of silver, from the surface towards the coating bulk, was found to be highly inhomogeneous due to top surface segregation and clustering of silver nanoparticles. Two plasma parameters, the sputtered Ag flux and the ion energy, were shown to influence the spatial distribution of silver particles. Based on these findings, a mechanism for Ag-DLC growth by plasma was proposed.

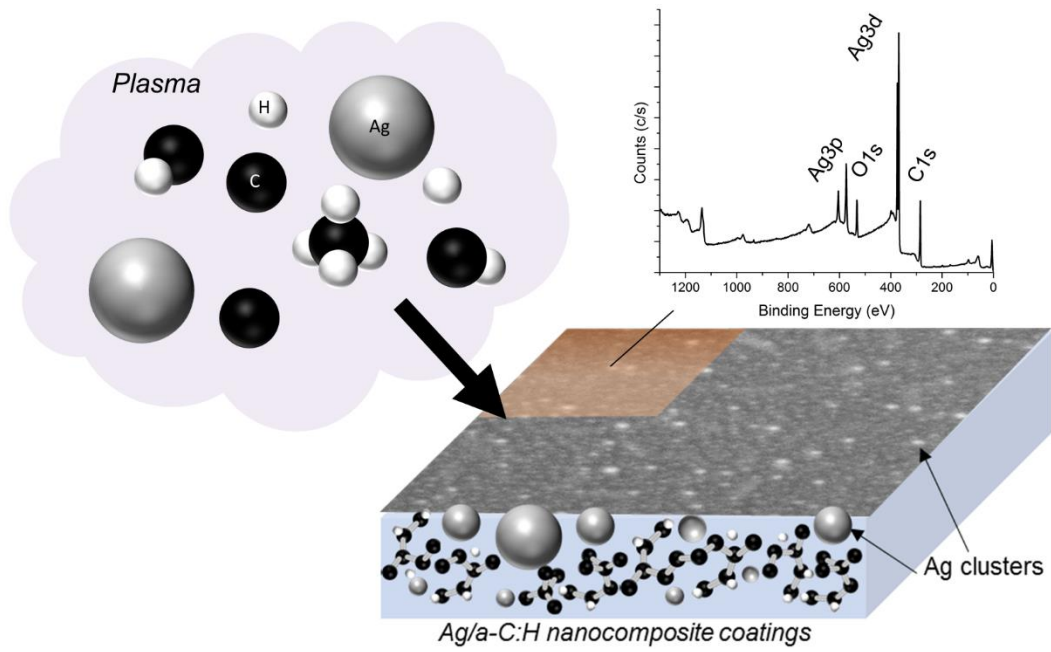


Figure 4.1 : Graphical abstract

4.3 Introduction

With the soaring complexity and performance requirements of advanced technological applications, many materials are nowadays tailored to perform a specific set of functions [319]. Emerging areas of nanotechnology hold the promise of opening new pathways for engineers and scientists to develop materials that combine multiple desirable properties. As the size of a material decreases to reach the nanometre range, unique physical properties (absent in macroscopic systems) emerge. Embedding such nanoscale structures within a bulk matrix creates a multiphase nanocomposite material that can exhibit a range of novel and tunable functionalities, from altered biological activity [320, 321] to enhanced mechanical [322] or electrical properties [323]. Although precisely tuning the desired properties remains an important challenge, their inherent flexibility makes nanocomposite materials uniquely well suited to meet the extreme requirements of modern applications.

Diamond like carbon (DLC) is a form of amorphous carbon with a significant fraction of sp^3 bonds which have been mainly used as protective coatings because of their unique combination of mechanical hardness, wear-resistance, chemical stability and atomic smoothness [106, 147, 278]. In order to expand their area of application, metallic elements have been recently incorporated into DLC, giving way to a new generation of DLC nanocomposite coatings. Examples include copper, molybdenum, silver, platinum, tungsten and chromium [324-329]. Among them, the unique optical, thermal and biological properties of silver nanomaterials have attracted the most interest and have prompted scientists to investigate potential synergies with DLC and other amorphous carbon coatings. Applications of Ag-DLC coatings have been proposed in fields ranging from biomaterials (e.g. bioactive coatings) to spectroscopy (e.g. substrates for surface-enhanced Raman spectroscopy) [28, 330]. For example, Ag-DLC nanocomposite coatings combining the great stability of DLC with silver's broad-spectrum activity against a wide range of bacteria have shown promising results in long-term antibacterial applications [267, 331]. Like other release-based systems, their translational success as an antibacterial platform hinges on the ability to control and tune the timeframe and kinetics of antibacterial agents' delivery (silver ions in this case) from the coatings [320].

While the growth of DLC by plasma-enhanced chemical vapour deposition (PECVD) is now well understood as being primarily due to the subplantation of carbon and/or hydrogen atoms

[122, 305], the deposition mechanism and properties of nanocomposites combining non-carbide forming metals and DLC have been poorly investigated. Several factors may influence the properties and silver ions release of the nanocomposite films, including the distribution, clustering and chemical bonding of the metallic element in the DLC matrix. To identify the growth mechanisms of this new material and their potential impact on the coatings properties, we have thoroughly investigated the influence of key plasma deposition parameters on the metal distribution within the silver-incorporated diamond-like carbon nanocomposite coatings (Ag-DLC).

The study was conducted on Ag-DLC coatings prepared in a continuous, single-step plasma process using a hybrid, inductively coupled radio frequency (RF) plasma reactor combined with a very-low-frequency (VLF) sputtering setup. The Ag-DLC film morphology and the distribution, clustering and chemical state of silver nanoparticles were assessed by surface and depth profile X-ray photoelectron spectroscopy (XPS), scanning electron microscopy (SEM) and atomic force microscopy (AFM). The film properties were studied as a function of key deposition parameters such as the metal ions flux and their impact energy. The results shine light on interesting features of the growth process of Ag-DLC coatings.

4.4 Experimental

Films were prepared on p-doped <100> silicon (Si) substrates (University Waffer, South Boston, MA, USA) cleaved into 10 x 10 mm squares. The coatings were deposited in a one-step continuous process using a RF (13.56 MHz) inductively couple plasma reactor (Plasmionique, Varennes, QC, Canada) coupled to a VLF sputtering setup. DLC is deposited by PECVD from a methane (CH₄) precursor while silver is simultaneously introduced by sputtering from a pure silver target (99.9%, Alfa Aesar, MA, U.S.A.). The deposition time (15 minutes), CH₄ flux (7 sccm), reactor pressure (15mTorr) and RF power (100W) were kept fixed throughout this experiment as they provided convenient deposition rate (~6 nm/min) and film thickness (~100 nm) for subsequent analyses. Substrates were cleaned by plasma etching prior to deposition to limit the occurrence of surface defects and optimize the coatings' adhesion [109, 332]. Silver incorporation was achieved through cathodic sputtering of a negatively biased (V_{Ag}) silver target from the application of a VLF (7.6 KHz) voltage which is

rectified by the plasma. The resulting voltage could be adjusted from 0 to -900V resulting in a direct control over the silver flux toward the sample. Similarly, the energy of the ions (essentially carbon and hydrogen) incoming on the substrate was independently adjusted by applying a low frequency (90 kHz) voltage to the sample holder, which was rectified by the plasma and resulted in an adjustable (between 0 and -150V) negative bias voltage (V_b). For simplicity, specimens deposited at non-zero biases ($V_b \neq 0$) will be referred to as Ag-DLC while the more general designation a-C:H:Ag will be used when describing both biased and unbiased specimens. Details of the PECVD-PVD system and a complete deposition procedure can be found in the article by Cloutier et al.[267].

The depth composition was investigated by X-ray photoelectron spectrometry (K-alpha spectrometer, Thermo Scientific) coupled with a 1 keV Ar^+ sputtering beam, unless indicated otherwise. High resolution XPS spectra are acquired at regular sputtering time intervals using a monochromatic Al $K\alpha$ source (1486.68 eV) with a spot size of 250 μm , and a pass energy of 200 eV for the survey scans and 50 eV for the elemental scans. An electron flood gun was used to prevent surface charging. The modified Auger parameter (α') of silver was calculated by adding the binding energy of the $Ag3d_{5/2}$ peak and the kinetic energy of the Auger transition ($\alpha' = E_k(M_4VV) + E_b(3d_{5/2})$). Peak fitting was performed with the *Avantage*© software (Thermo Scientific) after subtraction of a *Shirley* background.

Surface morphology was studied with a Dimension 3100 AFM (Veeco) operated in tapping mode and equipped with an ultra-sharp silicon tip. Images were acquired on 1 x 1 μm^2 area and analysed with the *Nanoscope* analysis software. Samples morphology was studied by scanning electron microscopy (JEOL 7500-F) with 15 kV accelerating voltage. ImageJ software [333] was used for particle size analysis. The size distribution histogram of silver clusters was built from N=1197 particles, with bin size of 1 nm. Clusters under 4.5 nm in diameter were difficult to distinguish from the background and were excluded from counting. The number of independent experiments (n) are noted in the figure legends. For each independent sample, data were acquired at three (XPS) or five (SEM and AFM) randomly selected positions on the specimen surface.

4.5 Results

4.5.1 General composition and morphology of Ag-DLC coatings

Because it is well established that DLC coatings with the highest sp^3 fraction are deposited in a relatively narrow ion energy range around 100 eV [106], we first investigated the chemical composition and morphology of nanocomposite coatings deposited at a constant ion energy ($V_b = -100$ V) and silver flux ($V_{Ag} = -750$ V). The XPS profile shown in Figure 4.2a reveals a highly inhomogeneous vertical distribution of silver, with a strong segregation towards the surface. A maximum concentration (atomic percentage of about 12 at%) of silver was detected at the film surface and then fell down within the first seconds of sputtering, quickly saturating to a stable value of 0.40 ± 0.04 at.% after 200s of sputtering which was maintained until the interface with the Si substrate was reached.

The study of the chemical state and oxidation of silver by high resolution analyses of the Ag3d peaks (Figure 4.2b, inset) is hindered by the small theoretical shift of a few tenths of eV between metallic silver peak (Ag^0) and its oxidized forms (AgO or Ag_2O) [334]. Still, interesting information can be derived from the variations in the Ag3d_{5/2} binding energy (BE) with depth. Core level BE shifts, proportional to the cluster size, have been previously reported for small supported metal clusters [335, 336]. Figure 4.2b shows the Ag3d_{5/2} BE as a function of sputtering time (depth). In order to precisely measure the BE shifts, a spectral calibration was performed by fixing the C1s peak BE at 284.6 eV. The increasing binding energy shift with the depth indicates that silver in the film is in the form of nm-sized clusters, and that their size decreases with the depth as observed during the first 60 seconds of ion beam sputtering.

Auger parameter analysis was used to determine the chemical state of silver particles without interference of surface charging effects. The modified Auger parameter (α') is derived from the photoelectron and Auger peaks positions. The reported value for metallic silver, disilver oxide (Ag_2O) and silver oxide (AgO) are 726.0 ± 0.1 eV, 724.4 ± 0.1 and 724.3 ± 0.3 , respectively [337]. Low energy monoatomic argon ions (200 eV) were used in this depth profile to prevent ion beam induced modification of the chemistry and provide a much slower and more controlled profile. Figure 4.2c shows the evolution of the silver modified Auger parameter (α_{Ag}') as a function of depth. At the topmost surface, silver was partly oxidized ($\alpha_{Ag}' = 724.9$ eV); but the Auger parameter then rapidly increased towards the value of metallic silver.

Taking into account the very low sputtering rate, these results suggest that only the topmost atomic layers are oxidized and that the large majority of the silver embedded in the coating is in a metallic state.

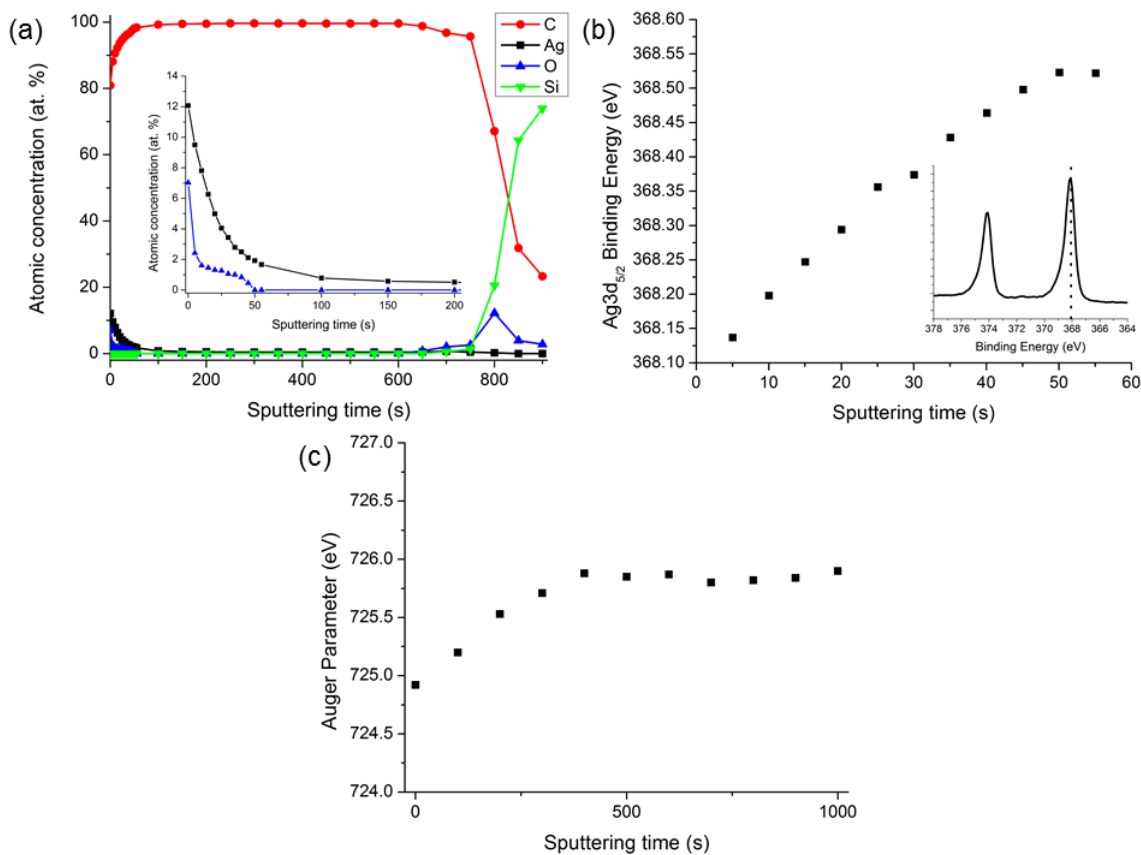


Figure 4.2: Example of XPS depth profile of Ag-DLC films ($V_b = -100V$, $V_{Ag} = -750V$) showing (a) the atomic percentages (at.%) of carbon, silver, oxygen and silicon with a zoom-in (inset) on the first 200s of sputtering, (b) the Ag_{3d_{5/2}} peak binding energy, and (c) the evolution of the silver modified Auger parameter as a function of the profiling time.

In order to clarify the surface segregation of silver, the morphology of Ag-DLC films was studied by SEM. The incorporated silver clearly formed circular, nanometre sized and uniformly dispersed clusters (Figure 4.3a and b). While bigger clusters approached 20 nm in diameter, the majority were much smaller. The size distribution is reported in the size histogram in Figure 4.3(c). Clusters below 4.5 nm could not be clearly distinguished and have

been discarded from the analysis. Despite the absence of small particles, a positive skew to the right typical of lognormal distributions (LND) and the presence of two modes can be clearly identified from the data. The analysis of the size histogram gives maximum diameter values (mode) of 3.6 ± 0.2 nm and 11.1 ± 0.2 nm for the smaller (M1) and larger (M2) clusters, respectively. The geometric standard deviation (shape parameter) of the silver clusters are $\sigma_{M1} = 1.60 \pm 0.05$ and $\sigma_{M2} = 1.21 \pm 0.04$. Metallic nanoparticles or clusters sizes are frequently described by LND in the literature [338, 339]. Bimodal distributions have also been observed for similar systems [340].

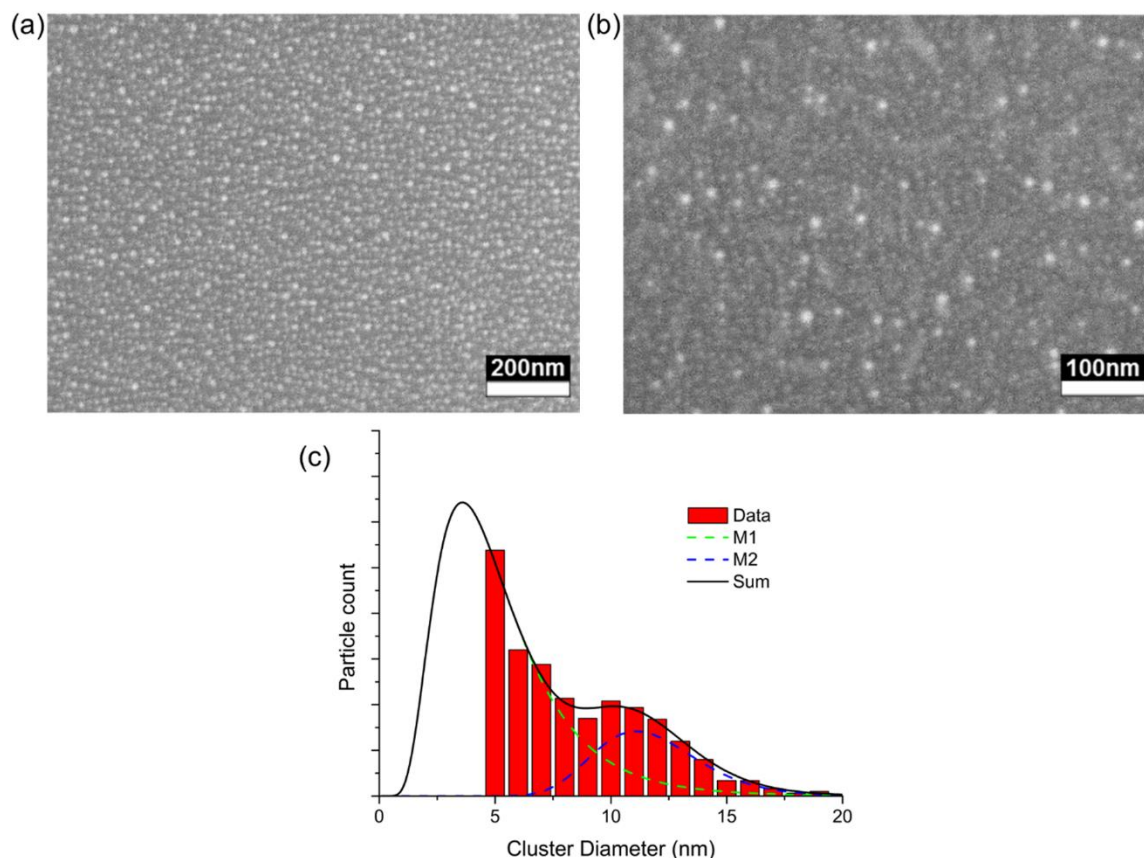


Figure 4.3: (a, b) Representative SEM images ($n=4$) of Ag-DLC coatings. ($V_{Ag} = -750V$, $V_b = -100V$). c) Size distribution histogram of silver clusters ($N=1197$, $\square d = 1$ nm). Dotted curves show the best fit simulated LND functions for each mode (M1 and M2) of the bimodal distribution. The solid curve is the sum of the two components. Counting was limited to particle diameter above 4.5 nm due to image resolution limits.

AFM studies were carried to further investigate the hybrid film morphology. As observed on Figure 4.4, (metal-free) DLC films were very flat ($R_{RMS} = 0.20 \pm 0.02$ nm), while Ag-DLC

nanocomposite films displayed densely packed clusters having a clear phase difference with the underlying film. Phase differences in AFM images are due to hardness/chemical contrast and can be used to distinguish the carbon matrix from the metallic clusters. The aspect ratio between the diameter and height of clusters was found to be about 10/3, suggesting that surface clusters were not spherical but rather grew in a more oblate shape.

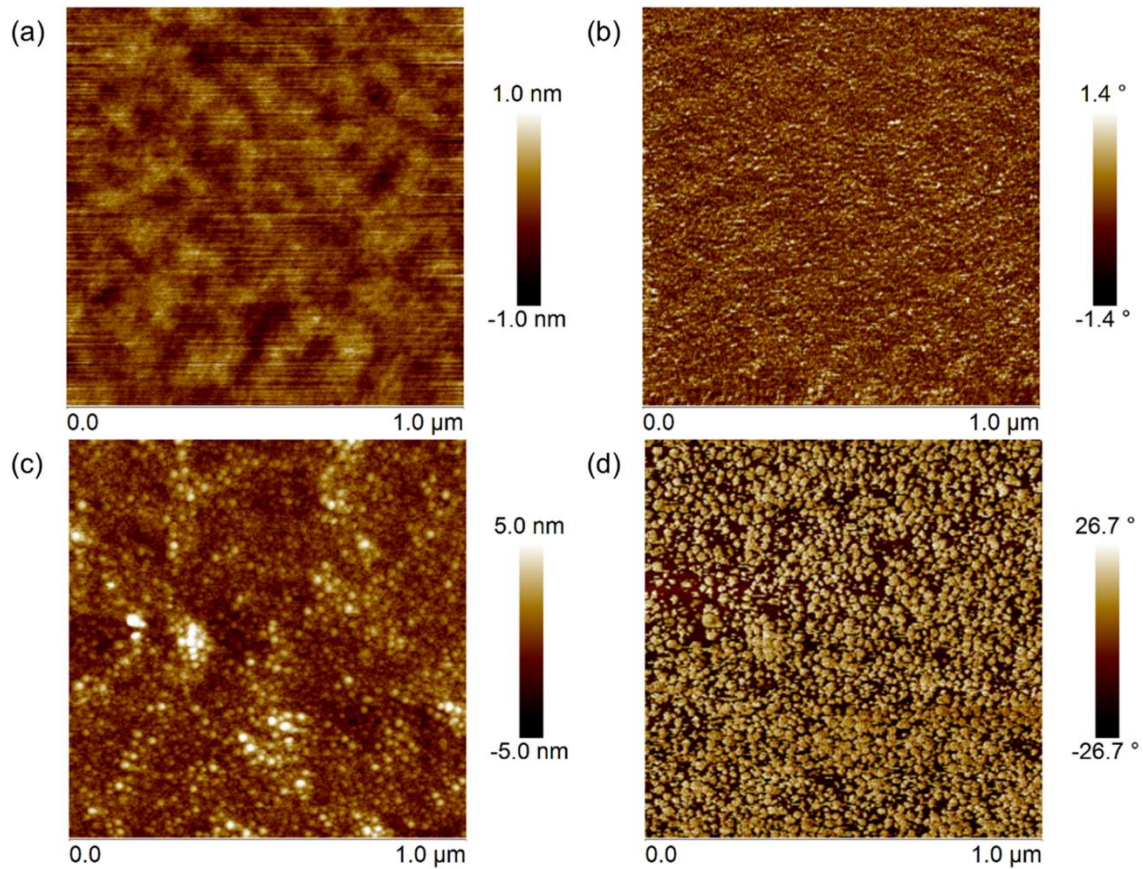


Figure 4.4 : AFM topography (left panels) and phase contrast (right panels) images of DLC (a, b) and Ag-DLC coatings (c, d). Representative images taken from $n = 5$. Please note the scale height/phase differences.

4.5.2 Effect of silver ion flux

The composition and morphology of Ag-DLC films deposited with different incoming silver flux (at a constant sample bias $V_B = -100V$) was investigated by XPS depth profiling (Figure 4.5). The silver flux was varied by changing the bias of the Ag target (V_{Ag}). For all tested V_{Ag} , the depth distribution of silver remained fairly similar, with a strong segregation of silver

towards the surface followed by a mostly constant concentration in the bulk of the film. The main effect of the increase of V_{Ag} was to induce a nearly linear increase of the silver surface concentration. Silver at.% in the nanocomposite film bulk also displayed a positive, although weaker, correlation with V_{Ag} . When increasing V_{Ag} from 400V to 900V, the Ag at.% in the bulk roughly doubled (from ~ 0.3 at.% to ~ 0.6 at.%), while the surface concentration of silver increased by a factor of 10 (from ~ 1.8 at.% to ~ 19 at.%). AFM characterization showed that Ag-DLC films deposited at lower silver flux (lower V_{Ag}) are characterized by smaller, sparse, oblate spheroidal clusters while at higher flux, densely packed silver nanoparticles are formed (Figure 4.6).

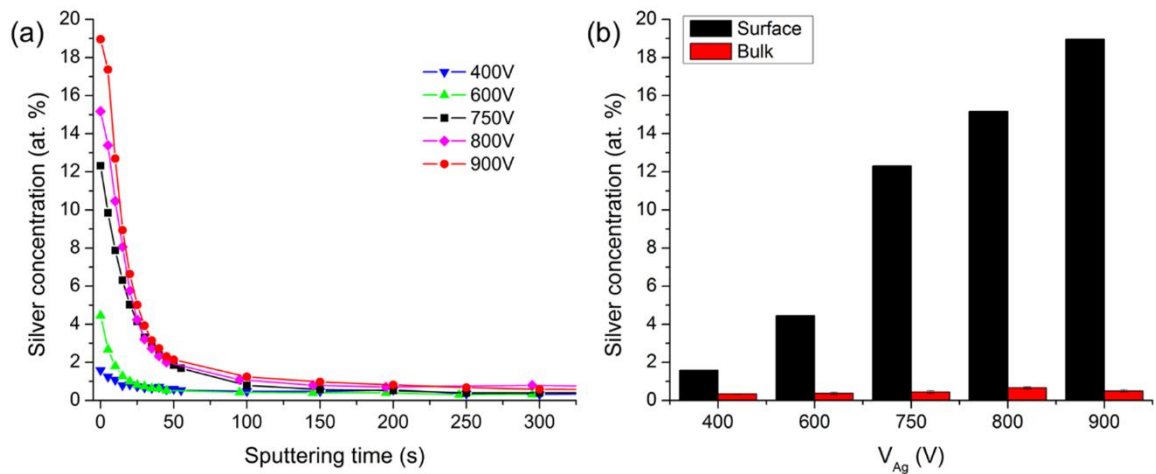


Figure 4.5 : Effect of the variation of the silver target bias /silver flux on silver distribution in Ag-DLC films. a) Representative silver concentration profiles (n=2) measured by XPS profiling. b) Surface and bulk concentrations for each condition. Bulk Ag concentration corresponds to the average value between 200 and 300 s sputtering time.

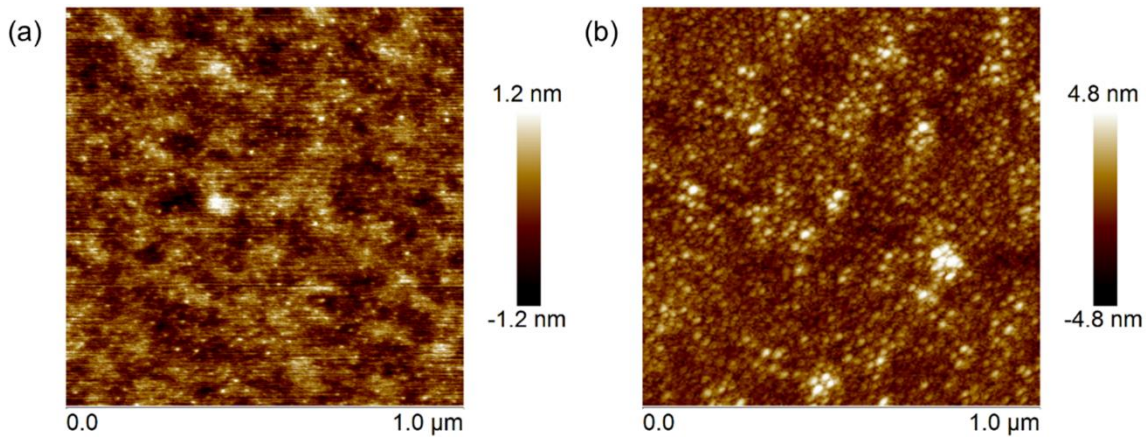


Figure 4.6 : Effect of Ag flux on silver clusters size and density in Ag-DLC. Representative AFM height images ($1 \times 1 \mu\text{m}$, $n=3$) of coatings deposited with (a) low (-400V) and (b) high (-750V) silver target bias (VAg).

4.5.3 Effect of ion energy

The influence of ion energy on Ag-DLC films was investigated by changing the substrate bias (V_b) during deposition. The ion energy is the primary deposition parameter that governs the sp^3 fraction and hardness of the deposited material, from soft, low sp^3 content, polymer-like films (0V bias) to hard, high sp^3 content, diamond-like coatings (50V bias or higher) [106, 132]. The highest sp^3 fraction was previously found at $V_b = 100\text{V}$ [267].

XPS depth profiles (Figure 4.7a) showed that polymer-like films deposited at $V_b = 0\text{V}$ displayed a much higher silver content in the film bulk compared with coatings deposited at higher sample biases. The unbiased samples were also the only ones where the maximum silver content was not recorded at the topmost surface, but slightly beneath it. Coatings deposited at $V_b = 50\text{V}$ and 100V exhibited similar profiles, with a strong surface segregation of silver followed by a mostly constant bulk concentration. However, the bulk concentration was three times higher for the 50V samples ($1.4 \pm 0.3 \text{ at.}\%$) compared with 100V ($0.44 \pm 0.07 \text{ at.}\%$). At 150V bias, both the surface and bulk silver concentration decreased, suggesting that increased sputtering occurred during deposition.

The analysis of the high resolution Ag $3d^{5/2}$ spectra provided further evidence of the differences in silver dispersion between the polymer-like and diamond-like carbon coatings. Lesser BE shift with sputtering depth and smaller peak FWHM were obtained for polymer-like 0V samples (Figure 4.7b and c) indicating that larger clusters were embedded in the film bulk.

On the other hand, the large BE shifts and widening of the Ag3d peak for 50V, 100V and 150V Ag-DLC samples revealed that, while clusters were relatively large at the surface, their size dropped rapidly with depth. As an indication, large BE shifts have been reported for supported Ag clusters for diameter size smaller than 3 nanometres [18].

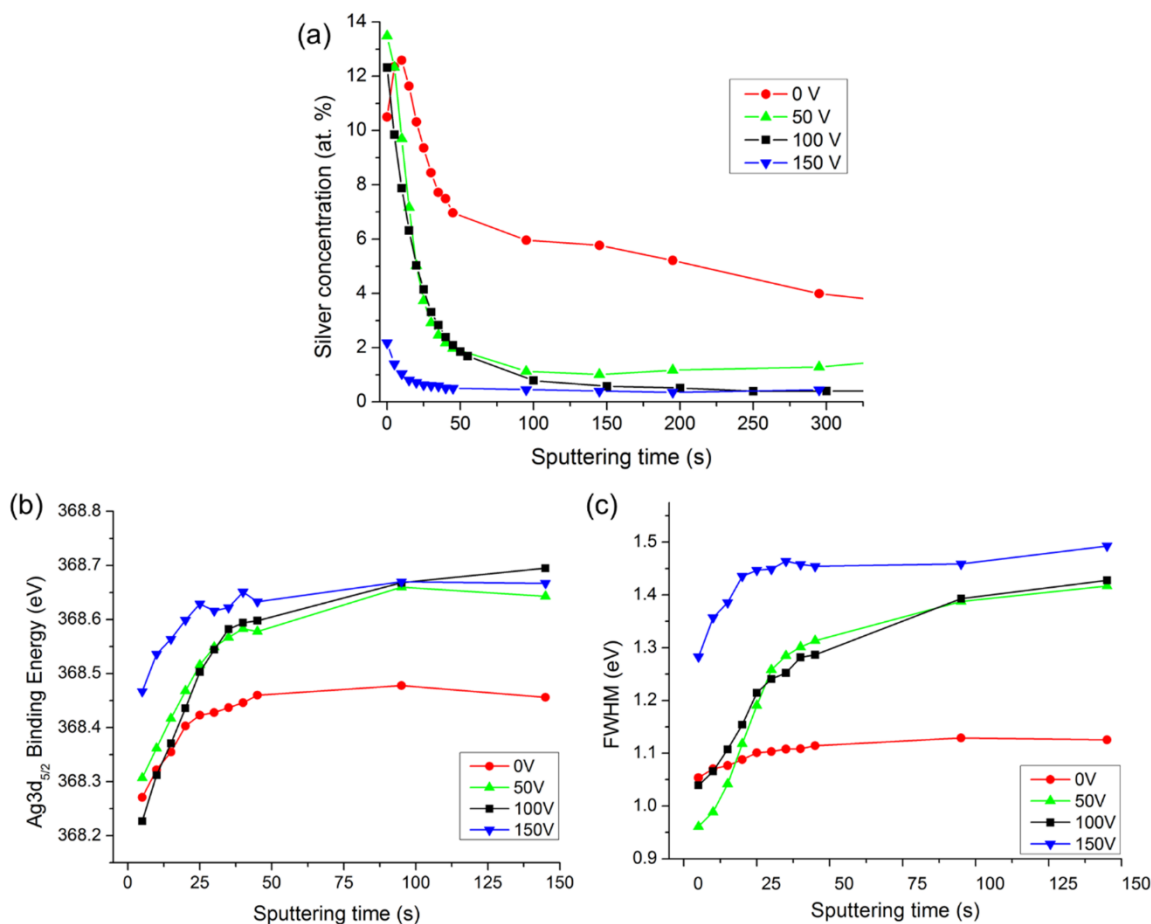


Figure 4.7: Representative XPS depth profile (n=3) analysis showing the effect of the ion energy (V_b) on silver dispersion and clustering in Ag-DLC samples. (a) Silver concentration (at.%) profiles, (b) Binding energy and (c) FWHM of the Ag3d_{5/2} peak for different substrate bias. Higher FWHM /BE shifts indicate the presence of smaller clusters.

Silver clusters morphology was further investigated by AFM (Figure 4.8). Polymer-like samples (V_b=0V) displayed a much rougher topography, with globular structures emerging from the surface. The topography being similar to that observed for metal-free a-C:H coatings and the absence of clear phase contrast in the phase image suggests that the observed features were not related to silver clusters, but were more likely linked to the different growth mechanism

occurring at $V_b=0V$. The most surprising result came from the characterization of the sample deposited at $V_b=50V$, which, unlike what could be expected from the XPS analysis displayed a very different surface topography than their 100V and 150V counterparts. For $V_b=50V$, silver clusters were more deeply embedded in the film in comparison to the well outlined, circular particles observed at higher deposition biases. Finally, the surface morphologies of the 100V and 150V samples were similar, but the latter had more isolated and smaller clusters, as evidenced by the lower Z scale. This confirmed the observations previously made by XPS suggesting the presence of smaller particles for high sample bias.

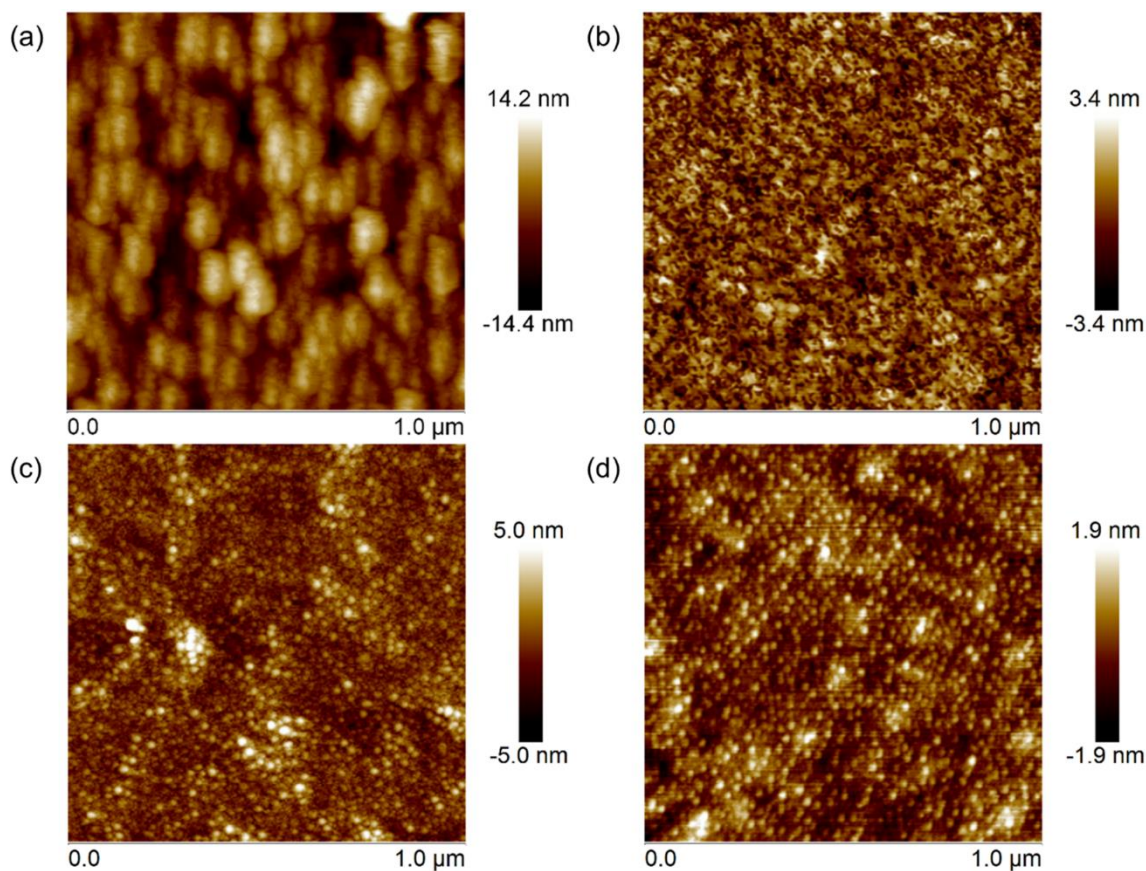


Figure 4.8: Effect of ion energy on silver surface distribution and cluster size in a-C:H:Ag films. Representative AFM height images (1 x 1 μm , n=3) of coatings deposited at a substrate bias (V_b) of (a) 0V (b) -50V (c) -100V and (d) -150V substrate bias (V_b). Please note the scale height differences.

4.6 Discussion

This work showed that silver distribution in a-C:H:Ag films was directly influenced by specific parameters of the plasma deposition but remained primarily governed by two dominant effects: surface segregation and metal clustering. The reactor design enabled to independently

tune the ion energy (through V_b) and the sputtered silver flux (through V_{Ag}). The influence of these key parameters on the film morphology, growth mode and composition have been characterized in details. The insight gained in this investigation can help to understand several aspects of the growth of silver-carbon nanocomposite coatings by plasma methods, such as:

A- The formation of metal clusters can be primarily attributed to the low affinity of silver with the carbon matrix and the high cohesive energy of silver [341]. Combined with the relatively energetic deposition method, this ensures high surface mobility to incoming Ag atoms, which diffuse on the surface until they coalesce with other Ag atoms/particles. The strong anisotropy in the clusters anisotropic shape (as observed by AFM), forming oblate spheroids (Figure 4.6), is indicative of a dominant in-plane diffusion (rather than cross-plane) ruling the cluster growth. LND are coherent with the size distribution of cluster/nanoparticles grown by coalescence [338]. However, the bimodal distribution identified in the cluster size analysis (see SEM images in Figure 4.3) indicates the existence of a second mechanism, Ostwald ripening, which appears to be involved in the Ag clusters growth [342, 343]. Both the location (only found at the surface) and the higher size uniformity in the distribution of large clusters ($\sigma_{M2} = 1.21 \pm 0.04 < \sigma_{M1}$) corroborate that their growth is governed by this second mechanism. Indeed, this process is thermodynamically favoured at the surface and produces particle size distributions with lower standard deviations (σ) than pure coalescence processes [338].

B- XPS profiles on biased nanocomposite coatings ($V_b=50, 100$ and $150V$) revealed a strong surface segregation of silver. While these results are consistent with the literature, other studies have mentioned the low solubility of non-carbide-forming metals in carbon-based matrices [292, 326, 344], no approach to explain or circumvent the segregation have been proposed so far. We suggest that this phenomenon is due to the particular, ion-dominated growth of DLC films, a process called ion subplantation [345]. The term is used to describe the shallow implantation of hyperthermal carbon species (C^+ ions or other ionized hydrocarbon molecules accelerated toward the surface) into subsurface sites, promoting local densification and increasing the sp^3 bonding of carbon atoms. The impacting ions are slowed down, losing much of their energy via thermal dissipation [106]. The local heating allows thermally activated diffusion of dense atoms (such as Ag) to the surface [125]. In addition, because of their size (108 amu for Ag vs 12 amu for C), the incoming silver particles are not expected to deeply penetrate the surface at the explored energy range. Therefore silver from the incoming

deposition flux remains confined at the surface and is kept segregated by the subsurface growth of implanting carbon species. The presence of a small amount of silver in the bulk of Ag-DLC coatings could originate from mechanisms such as knock-on collisions, trapping by depositing low energy carbon neutrals or diffusion of small particles, which was reported for metallized plasma polymer films [346].

C- For unbiased samples, low energy hydrocarbon species from the plasma can adhere directly at the top surface, effectively switching the growth mode from subplantation to conventional plasma polymerization (subsurface vs surface film growth). Additionally, in the absence of thermal spikes from high energy impacting ions, cross-plane Ag mobility is considerably reduced, limiting Ag diffusion and segregation to the top surface. Indeed, the XPS profiles obtained on the unbiased sample revealed a much higher silver concentration in the bulk (5 to 10 fold increase at 150 sec) compared with biased samples (Figure 4.7a). Moreover, the smaller BE shift observed in polymer-like unbiased coatings (Figure 4.7b-c) indicates that Ag clusters size is fairly the same at any depth, while it is strongly inhomogeneous in diamond-like (DLC) coatings. The growth mechanism of a-C:H:Ag coatings by plasma methods is thus represented schematically depicted in Figure 4.9, which shows how the modification in sample bias/ion energy affects the silver distribution and clustering into the carbon matrix.

D- The incoming ion energy appears to be the main parameter affecting silver distribution. Unbiased coatings present a homogeneous silver distribution however they do not possess the mechanical properties (high hardness and wear-resistance) of their diamond-like counterparts grown at higher biases. The addition of an interfacial element, such as a carbide-forming metal, could help to improve the mechanical properties of unbiased coatings without having to sacrifice control over the Ag depth distribution. This may be an alternative way to tune more independently the metal distribution and mechanical properties of a-C:H:Ag coatings for specific applications.

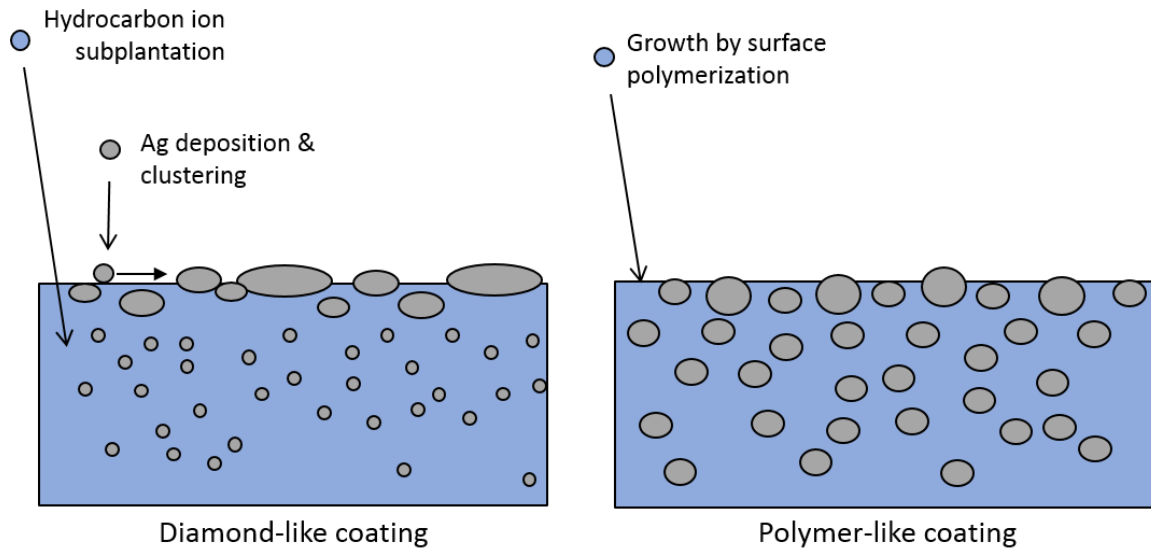


Figure 4.9: Schematics of silver distribution for two different growth modes of a-C:H:Ag. Hydrocarbon ions subplantation leads to subsurface film densification and growth. The process also induces a thermally activated diffusion of Ag which, combined with the inability of Ag atoms to implant in the film due to their size, ultimately causes Ag segregation at the surface of Ag-DLC coatings where it diffuses to form nanoclusters. Surface growth occurs at all deposition biases (V_b) but is the only mode of growth in polymer-like coatings. This leads to a more uniform distribution of Ag through the coatings depth, with less fluctuation in cluster size.

4.7 Conclusions

In this study, the incorporation of silver in plasma-deposited DLC coatings was shown to be dominated by surface energy, surface segregation and clustering. Two key deposition parameters, the sputtered Ag flux and the carbon ion energy, have been found to influence the silver distribution, with the latter demonstrating a considerable impact on the morphology, growth mode and amount of incorporated silver of the deposited coatings. The main driving forces behind the observed segregation and clustering are poor silver/carbon affinity and energetic subplantation growth from the plasma. Thus, we believe that our findings can be extended to PECVD-grown DLC nanocomposite coatings incorporating other non-carbide-forming metals. Results of such metal distribution studies help to improve our understanding of the growth mechanisms of metal-DLC films which, in turn, is expected to lead to the realization of high quality coatings with tunable composition and properties. As they offer a unique combination of properties using an economical and versatile processing method, those materials could be attractive candidates for sensor, biomedical and tribological applications.

4.8 Acknowledgements

This work was partially funded by the Natural Sciences and Engineering Council of Canada through the Strategic Project Grants program and was conducted with the support of Wallonie-Bruxelles International (WBI). MC acknowledges the support from a NSERC Vanier Scholarship. The authors wish to thank Dr Pierre Louette and Dr Alexandre Felten for their help and guidance, as well as Dr Laurent Houssiau and Dr Pascale Chevallier for fruitful discussions.

5 On the long term antibacterial features of silver-doped diamond-like carbon coatings deposited via a hybrid plasma process

M Cloutier^{a,b,c}, R Tolouei^a, O Lesage^{a,b}, L Lévesque^a, S Turgeon^a, M Tatoulian^b and D Mantovani^a

^aLaboratory for Biomaterials and Bioengineering, CRC-Tier I, Dept of Min-Met-Materials Engineering, & CHU de Québec Research Center, Laval University, Pavillon Pouliot, salle 1745-E, Québec, Québec G1V 0A6, Canada

^bChimie ParisTech, PSL Research University, Institut de Recherche de Chimie Paris (IRCP), 11 rue Pierre et Marie Curie, F-75005 Paris, France

^cSorbonne Universités, UPMC Univ Paris 06, F-75005, Paris, France

Keywords

Environmental hospital surfaces, hybrid plasma process, diamond-like carbon, antibacterial silver, long-term antibacterial effect

5.1 Résumé

Les différentes surfaces des milieux hospitaliers sont de plus en plus reconnues comme étant des sources importantes de transmission d'infections. L'utilisation de revêtements antibactériens pourrait s'avérer être une solution efficace pour réduire la propagation de la contamination bactériennes dans les milieux hospitaliers, à condition qu'ils démontrent une stabilité et une efficacité à long-terme suffisantes. Dans cette étude, des revêtements de carbone amorphe adamantin contenant de l'argent (Ag-DLC) ont été préparés par un procédé plasma continu, en une seule étape, à l'aide d'un réacteur hybride à plasma inductif combiné à un système de pulvérisation très basse fréquence. La concentration moyenne d'argent dans les films, entre et 0 et 2.4 at.%, était contrôlée en ajustant la tension de polarisation appliquée à la cible d'argent. L'activité d'*Escherichia Coli* a été réduite de 2.5 ordres de grandeur par rapport à une surface contrôle, après un contact de 4h sur les revêtements Ag-DLC contenant 2.4 at.% d'argent. Les revêtements ont démontré une cinétique de relargage lente, avec un relargage total des ions d'argent dans l'ordre du sous-ppb après 4h en solution, tel que mesuré par spectroscopie d'absorption atomique à four graphite. Ce résultat a été confirmé par des tests de diffusion Kirby-Bauer, qui ont montré une diffusion limitée de l'argent biocide et un effet antibactérien localisé. Comme un relargage lent et continu est obligatoire pour assure un effet antibactérien de longue durée, les revêtements Ag-DLC nouvellement développés apparaissent comme des matériaux prometteurs pour le recouvrement de surfaces en milieu hospitalier.

5.2 Abstract

Environmental surfaces are increasingly recognized as important sources of transmission of hospital-acquired infections (HAIs). The use of antibacterial surface coatings may constitute an effective solution to reduce the spread of contamination in healthcare settings, provided that they exhibit sufficient stability and a long-term antibacterial effect. In this study, silver-incorporated diamond-like carbon films (Ag-DLC) were prepared in a continuous, single-step plasma process using a hybrid, inductively coupled plasma reactor combined with a very-low-frequency sputtering setup. The average Ag concentration in the films, ranging from 0 to 2.4 at.%, was controlled by varying the sputtering bias on the silver target. We found that the activity of *E. coli* was reduced by 2.5 orders of magnitude, compared with the control surface, after a 4-hour contact with a 2.4 at.% Ag-DLC coating. The coatings displayed slow release kinetics, with a total silver ion release in the sub-ppb range after 4 hours in solution, as measured by GF-AAS. This was confirmed by Kirby-Bauer diffusion tests, which showed limited diffusion of biocidal silver with a localized antibacterial effect. As a slow and continuous release is mandatory to ensure a lasting antibacterial effect, the newly developed Ag-DLC coatings appears as promising materials for environmental hospital surfaces.

5.3 Background

Hospital-acquired infections (HAIs) continue to be a major public health concern in hospitals and healthcare units worldwide, with reported prevalence rates ranging from 5 to 10% in industrialized countries[2, 4, 30]. As a result, a considerable amount of literature has been published in recent years on the development of antibacterial biomaterials for implants and other medical devices[166, 209, 218]. However, far too little attention has been paid to the microbial contamination in the inanimate environment, despite mounting evidence linking contaminated environmental surfaces to HAIs[10, 11, 347]. Because of the ability of bacteria to survive in a range of environments[15], forming adhered sessile communities protected in biofilms[55, 348], common surfaces and articles may act as reservoirs of pathogenic microorganisms and establish additional pathways of transmission to susceptible patients[11, 26, 28]. Therefore, the development of antibacterial surfaces for near-patient clinical areas, acting in conjunction with cleaning and disinfection procedures, emerges as a necessary measure to reduce the spread of HAIs.

There is significant knowledge to be gained from the sizeable literature published on anti-infective implantable medical devices, which can be used to guide the design of environmental antibacterial surfaces. However, it is important to realize that the design of coatings for environmental surfaces represents a distinct challenge to the engineers and scientists (Table 5.1). For instance, one of the most obvious differences lies in the respective environment to which they are exposed. Implantable devices can be subjected to very low wear (catheters) or high, continuous friction between two moving bearing surfaces (knee or hip implants). On the other hand, environmental surfaces are not only exposed to abrasion and wear caused by patients and personnel everyday operations, but also to aggressive cleaning procedures involving strong detergents and/or high temperatures used in sanitation procedures[349]. Thus, superior mechanical and chemical stability become mandatory properties for such environment and need to be taken into consideration in the design.

There have been multiple surface modifications approaches targeted at the inhibition of bacterial colonization of surfaces, such as PEG-based antifouling coatings[165, 350], polycationic contact-killing surfaces[167, 351, 352], biocide-impregnated[353] and other biocide-releasing materials[354, 355]. However, in the current market, there is no surface treatment that can provide, at the same time, sufficient stability and antibacterial properties for

use as environmental surfaces in healthcare, as the surfaces are either mechanically or chemically unstable[277, 352], quickly lose their antibacterial agent by leaching[356] or cannot prevent cell adhesion[277, 357]. For example, contact-killing surfaces are often labeled as permanent[351]; their active element is covalently grafted to a substrate via anchoring polymer brushes, preventing leaching and gradual loss of antibacterial activity[191]. Nonetheless, one can question if such surfaces are robust enough for the harsh hospital operating conditions, given the mechanical and chemical fragility of tethered polymer surface layers[164, 272, 273, 358].

Alternatively, biocide-releasing coatings offer the advantage of embedding the bioactive element in a scaffold, which can be chosen, for example, for its mechanical and chemical stability. Therefore, the remaining challenge in this case is to control the release kinetics, which governs the duration and effectiveness of the antibacterial action[191]. For environmental surfaces, where a long-term antibacterial effect is required (Table 5.1), a slower release profile is required, to prevent the fast depletion of the antibacterial compound.

Building upon these observations, we present in the current study a preliminary antibacterial assessment of plasma-deposited silver-doped diamond-like carbon (Ag-DLC) coatings. Reports of the antibacterial action of silver-containing films, due to the strong bactericidal effect of silver ions, are readily available in the literature. Likewise, DLC is an amorphous, carbon-based material well-known for its outstanding mechanical properties (such as hardness and wear-resistance), extremely low roughness and chemical inertness[106, 295]. Its potential, both as an antibacterial scaffolding material and a surface coating able to reduce bacterial adhesion, has already been reported in the literature[28, 355, 359, 360]. Therefore, those properties were combined into a single film to develop a stable antibacterial coating for the inhibition of bacterial growth on environmental surfaces. In this work, a hybrid plasma method, combining physical vapor deposition (PVD) and plasma-enhanced chemical vapor deposition (PECVD), was developed in order to deposit the films in a continuous single-step plasma process. This paper reports a comprehensive investigation of the chemical composition and antibacterial activity of Ag-DLC coatings obtained using this technique.

Table 5.1: Critical properties to consider in the design of antibacterial coatings. Comparison between implantable devices and environmental surfaces.

Aspects	Design criteria/guidelines	
	Implantable devices	Environmental surfaces
Infection sources	Punctual, mostly peri- or early postoperative contamination, although delayed infection caused by planktonic bacteria might occur[191, 218].	Constant, multiple transmission pathways[28, 194, 361].
Antibacterial effect duration	High initial effectiveness, to prevent biofilm formation upon implantation [191, 361, 362], since infections generally begin within a few days post-operation[363].	Continuous, prolonged effect required as surfaces are constantly exposed to both patients and personnel[27, 28].
Cytotoxicity	Must generally favor host tissue integration over bacterial adhesion and biofilm growth[218, 363]. Localization of the device affects the risk of side effects for the host organism[361, 362].	Non-toxic when in contact with patient/personnel. Same requirements used for current biocides and germicides products[364].
Stability	Variable, depending on the function of the device. High wear resistance necessary for certain implants[147]. Chemical resistance to attacks by salts, chloride, dissolved oxygen and organic molecules contained in body fluids[275].	Resistant to mechanical abrasion from cleaning procedure[364] and chemical stability against common clinic cleaning agents (peracetic acid, H ₂ O ₂ , contact time from 30s up to 3h)[365, 366].
Surface accessibility (cleaning)	Limited: implants can stay 10-20 years in the body.	Highly accessible : Frequent cleaning (1+/day) and always in contact with the environment[349, 364].
Fate of antibacterial agents	Restricted to the human body. Must not exceed systemic toxicity level.	For biocide leaching surfaces, should demonstrate limited ecotoxicity as they can diffuse in the environment (soils, water, etc.)[87, 367].

5.4 Materials & Methods

5.4.1 Materials

Films were prepared on 100-oriented single crystal silicon (Si) substrates cut into 10×10 mm squares. Before plasma deposition, the samples were cleaned by using an ultrasonic bath (10 min) in three different solvents in the following order: (i) acetone, (ii) deionized water and (iii) methanol. Samples were dried after each step. Uncoated Si and pure DLC coated substrates served as control surfaces throughout the present work.

5.4.2 Plasma deposition of thin film

Ag-DLC coatings (thickness 80 ± 5 nm) were deposited in a 1-step continuous process with a modified FLARION series system (Plasmionique, Varennes, Qc, Canada) consisting of a radio frequency, inductively coupled plasma reactor coupled to a very-low-frequency (VLF) sputtering setup (Figure 5.1b). Before each experiment, the plasma reactor was cleaned for a minimum of 60 min with argon-oxygen plasma. After introduction of the Si substrates, the chamber was pumped down to a base pressure of 10^{-6} Torr. The specimens were then treated with a continuous plasma process composed of three successive sequences: Ar etching, H₂ activation and CH₄/H₂ deposition with simultaneous Ag sputtering (Figure 5.1a). The plasma parameters were determined experimentally to obtain the optimal properties for the coatings. However, the optimisation process and complete characterisation will not be presented here for brevity. Silver introduction in the film was achieved through cathodic sputtering of a heated silver target. During the deposition sequence, a negative bias voltage (V_b) is produced on the silver target from the applied VLF voltage and the rectifying effect of the plasma, leading to impacting ionic carbon fragments on the target surface and resulting in sputtering of silver atoms. The relatively high bias voltage (many hundred volts) and high temperature ($>800^\circ\text{C}$) of the target prevent the formation of a protective carbon layer. Experiments with different bias voltages were performed to obtain a range of silver contents in the DLC film.

5.4.3 X-Ray Photoelectron Spectroscopy

The surface composition was investigated using an X-ray Photoelectron Spectrometer (XPS - PHI5600-ci spectrometer, Physical Eletronics USA, Chanhassen, MN, USA). Survey and high resolution spectra were acquired at a detection angle of 45° using the $K\alpha$ line of a standard aluminum and magnesium X-ray source, respectively, operated at 300 W. The curve fittings for

the survey and high resolution Ag3d peaks were determined by means of least-squares using a Shirley background subtraction. All peak positions were normalized to that of the C1s peak, which was taken to be at 284.4 eV. Silver content results represent the average of three measurements on at least two different samples deposited under the same conditions.

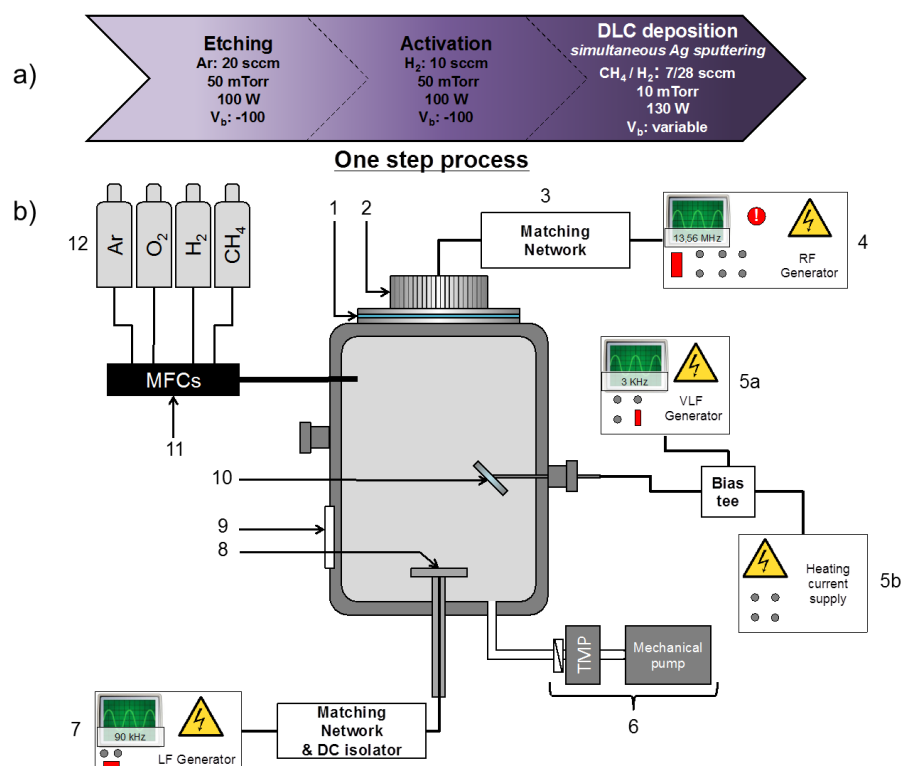


Figure 5.1 : a) Deposition procedure of the Ag-DLC films b) Schematic of the plasma reactor 1. Quartz window, 2. Spiral antenna, 3. Matching and tuning networks, 4. RF generator (13,56 MHz, Max: 1000 W) of the ICP plasma source, 5a. VLF generator (3 kHz) for biasing of the silver target, 5b. Heating current supply 6. Vacuum system (throttle valve + turbo mechanical pump + primary mechanical pump), 7. LF generator (90 kHz) for biasing of the sample holder, 8. Sample holder (4 inches diameter), 9. Reactor door and observation window, 10. Silver target (silver wire 99,99% purity, biased and heated), 11. Mass flow controllers, 12. Gas cylinders.

5.4.4 Silver release analysis

Ion release from Ag-DLC surfaces was monitored in static conditions in deionized (DI) millipore water (resistivity: 18 M Ω , *Barnstead™*, *Thermo Scientific*). Coated samples (10 x10 mm) were immersed in 3 ml DI water and kept at room temperature for a period varying between 30 min and two weeks. The fluids were then sampled and analyzed by graphite furnace-atomic absorption spectroscopy (GF-AAS, AAnalyst 800 AAS, model 3110, *Perkin Elmer*), with a detection limit of 0.15 $\mu\text{g/L}$. The presence of silver-based precipitates such as phosphate salts in the analyzed solutions was verified through nitric acid digestion. Digested and non-digested solutions were analyzed and showed no difference in terms of silver ion concentration, indicating that there was no formation of silver complex in the solutions.

5.4.5 Bacterial strain and culture preparation

Escherichia coli (ATCC 25922) was used in this study. The strain was maintained in Tryptic Soy Broth (TSB) with 10% glycerol and stored at -80°C . Prior to experiment, the stock culture was streak on Tryptic Soy Agar (TSA) and incubated at 37°C for 24 hours. A colony was then cultured under agitation in TSB at 37°C for 24 hours. The bacteria were, afterward, resuspended in TSB medium to a concentration of 10^6 cells/ml.

5.4.6 Antibacterial activity test

The antibacterial activity was determined using a modified version of the American Society for Testing and Materials International E2149 (ASTM E2149), where samples had a reduced surface area and longer bacteria contact time compared with the standard. Substrates of 10×10 mm were first sterilized in a standard autoclave cycle (120°C , 100 kPa, 20 min). Next, ten milliliters of the bacterial suspension was added to each substrate in a 50 ml tube and shaken incubated at 125 rpm for 4 hours at 37°C . Then, 100 μl serial 10-fold dilutions of the bacterial solution were spread on TSA plates and grown overnight at 37°C . Colony Forming Units (CFU) count was made afterward. For all antibacterial tests, the results represent the average of at least 3 independent experiments.

5.4.7 Live/dead bacterial viability assay

Bacterial cell viability was assessed after 4 hours contact with the tested surfaces using a two-color fluorescence live/dead assay according to the manufacturer's instructions (LIVE/DEAD® *BacLight™* bacterial viability kit (ref. L7012), *Molecular Probes®*, Burlington,

Ontario). The *E. coli* solution was centrifuged at 10 000 rpm for 15 minutes. The TSB was then removed and the pellets were resuspended in a 20 ml NaCl 0,85% solution for one hour. During the hour, the solution with bacteria was vortexed every 15 minutes. After one hour, the solution was centrifuged again at 10 000 rpm for 15 minutes. The NaCl 0,85% solution was removed and the pellets were resuspended in 5 ml NaCl 0,85% solution. Subsequently, 1 ml of all the bacteria solution were mixed thoroughly with 3 μ l of a combined equal amount of the fluorescent dyes SYTO 9 and propidium iodide stains and incubated for 15 minutes at room temperature in the dark. A fluorescence microscope (Olympus BX51, Olympus America Corp., Tokyo, Japan) was used to observe and take images of the surfaces after staining. The Live/Dead fluorescence images were analyzed with *ImageJ* (National Institutes of Health, USA)

5.4.8 Modified Kirby-Bauer diffusion test

Mueller Hinton agar plates were inoculated with 0.5 McFarland standardized *E. coli* culture. Coated samples were placed face down on the plate beside antibiotic disks of Penicillin (10 units), Streptomycin (10 μ g), Carbenicillin (100 μ g) and Gentamicin (10 μ g) and incubated for 24 hours at 37°C. The plates were afterward analyzed for clear zone around the antibiotic disks and the samples indicating diffusion of the antibacterial agent.

5.5 Results and discussion

5.5.1 Chemical composition

Ag-DLC films were first analyzed by XPS in order to determine their elemental surface composition, as shown in Figure 5.2. The XPS survey shows that the first nanometers of the film are strictly composed of carbon, oxygen and silver atoms (Figure 5.2a). As mentioned previously, control of the amount of implanted silver in the DLC film can be achieved through the modulation of the negative bias voltage (V_b) produced on the sputtering target. Average silver atomic concentrations between 0 and 2.4 at.% could be attained over the range of bias investigated (Figure 5.2b). At the maximum tested voltage, $V_b = -800V$, the average Ag content was 2.4 ± 0.6 at.%.

Depth profile analysis indicated that silver was present both at the surface and in the bulk of the DLC film. In the case of oxygen, its concentration on the top surface of the film was 10-12at.% and rapidly dropped to zero after few nanometers (Figure 5.2c). The presence of oxygen at the topmost surface can be caused by a post oxidation of the non-passive thin film exposed to ambient air. Oxidation has been known to shift the $Ag3d^{5/2}$ peak towards lower binding energy, as Ag_2O (BE = 367.8 eV) and AgO (BE = 367.4 eV) both have lower binding energy than metallic silver (BE = 368.4 eV)[334, 368]. As seen in Figure 5.2c, the depth profile revealed a weak shift of the $Ag3d^{5/2}$ peak from 368.13eV to 368.40eV, from the surface to the bulk respectively, indicating the presence of silver in oxide form at the surface. However, the weakness of the measured shift suggests that only a small fraction of the silver is oxidized and it is possible to conclude that the surface silver is mainly of metallic form. The oxidation state of silver, among other factors such as the aqueous solution pH and aerobic condition, plays an important role in the release kinetics of silver ions [369, 370] and should therefore influence the antibacterial activity of the surface.

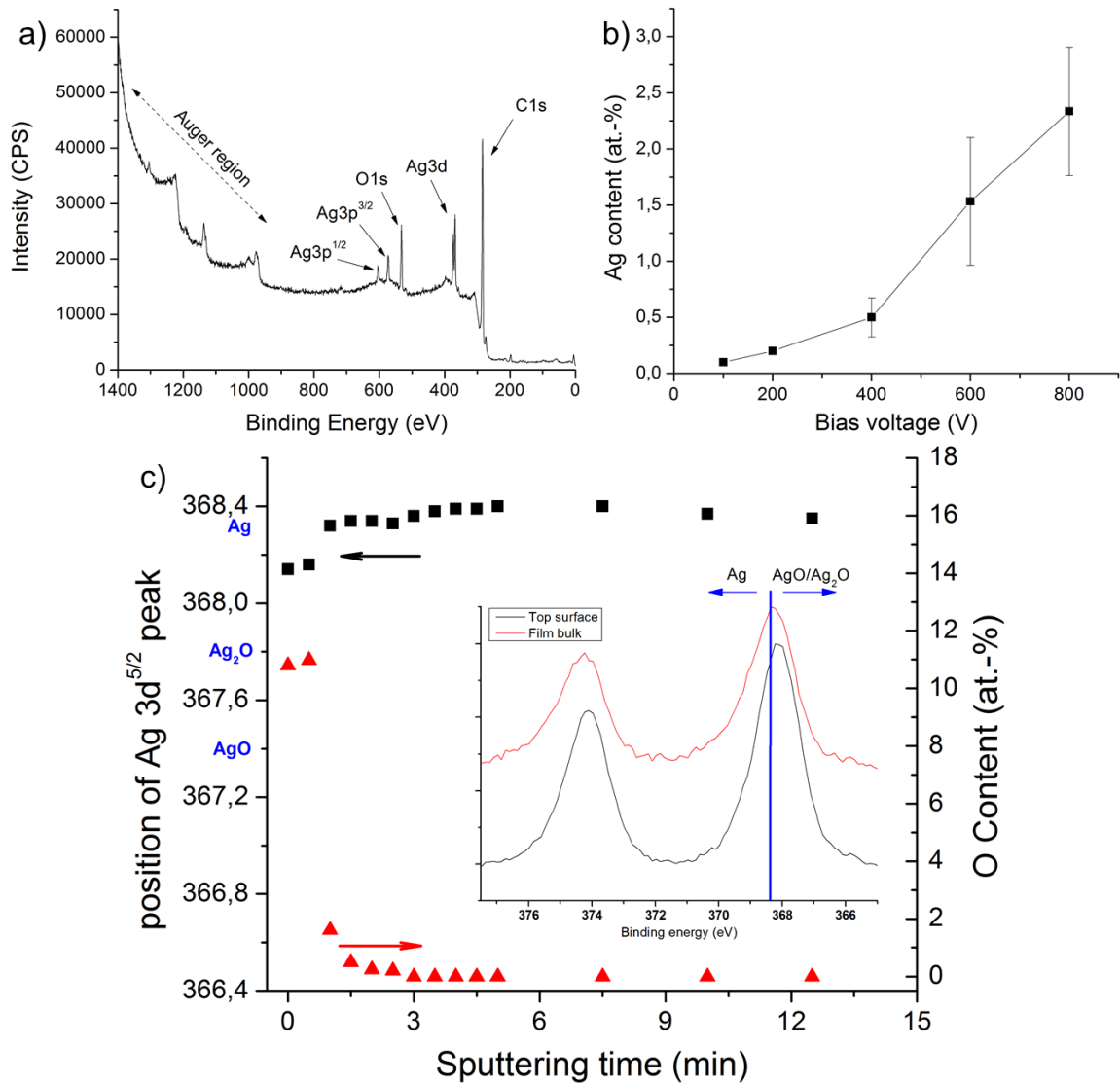


Figure 5.2: Results of XPS analyzes: a) typical XPS survey of Ag-DLC (Ag 2.4 at.%), b) Silver concentration (at.%) of Ag-DLC films for different negative bias on the silver cathode and c) Depth profile showing the position of Ag3d^{5/2} peak (black squares) and oxygen concentration (red triangles) . In inset, high resolution Ag3d peak showing the influence of the oxidation state on the peak position.

5.5.2 Antibacterial activity evaluation

The antibacterial activity of the prepared films was first evaluated with a qualitative live-dead assay (Figure 5.3a-b). In this experiment, *E. coli* viability was studied with membrane integrity (live-dead) staining for blank silicon and 2.4at.% Ag-DLC surfaces. The bacteria remained in contact with the samples for 4 hours, in order to get a preliminary qualitative assessment of the antibacterial activity of Ag-DLC coatings. It should be emphasized that live/dead marking test enables differentiation only between bacteria with intact and damaged cytoplasmic membranes, rather than between active and dead cells [371]. Given silver's multiple mechanisms of action against bacteria, not necessarily resulting in short-term cytoplasmic membrane damages [67, 73, 77], this may lead to an underestimation of the antibacterial activity of the films using this technique. As seen on Figure 5.3b, there is a significant increase in the number of inactivated, red-stained bacteria for the coated surfaces compared with the control silicon surface (Figure 5.3a). Interestingly, data also indicated that the coated surfaces also had the least amount of total bacteria after 4 hours. When combining both results, it can be concluded that Ag-DLC coatings can both kill existing *E. coli* bacteria and limit their growth.

Therefore, in order to obtain a more complete assessment of the antibacterial activity of the coatings, a quantitative test, based on ASTM E2149, was carried out on surfaces with different concentration of silver (Figure 5.3c). After a 4-hour contact, all silver-containing surfaces showed a significant ($p < 0.01$) decrease of their bacterial count compared with the control silver-free DLC surface. Results indicated that the decrease in bacterial count was modest for low silver content films (0.2 at.%) but reached 2.5 order of magnitude for 2.4 at.% Ag-DLC coatings. Indeed, the intensity of the antibacterial activity was proportional to the silver concentration in the film. There is a general consensus that the antibacterial properties of silver-containing films are due to its ionic Ag^+ form, which are released from elemental silver particles via oxidative dissolution[372, 373].

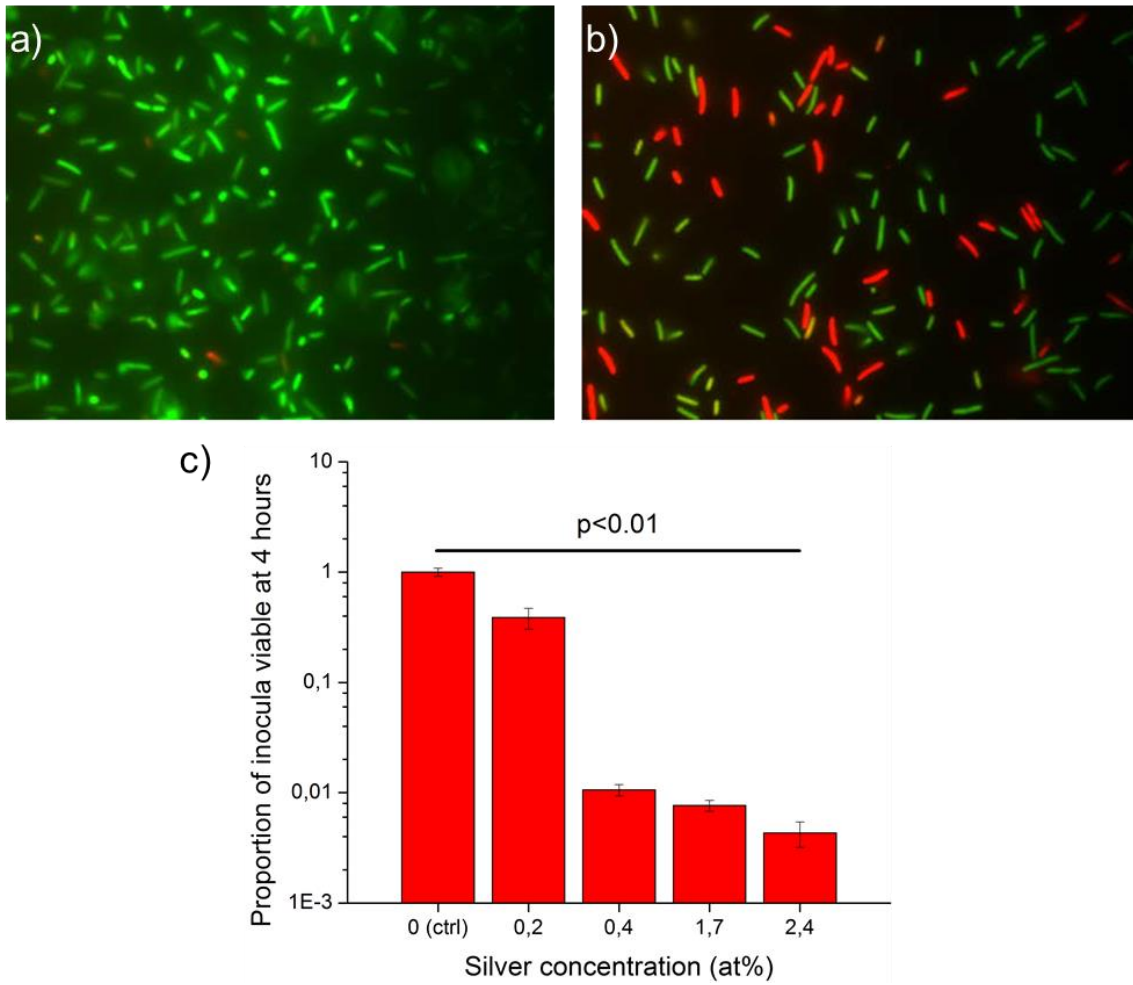


Figure 5.3 : Antibacterial activity of Ag-DLC coatings against *E. coli*. Fluorescent optical micrographs showing the distribution of Live (green)/Dead (red)-stained cells on a) uncoated silicon and b) 2.4at.% Ag-DLC coated silicon. c) Quantitative antibacterial activity test of Ag-DLC with different silver concentration.

E. coli was selected as the test organism for the antibacterial activity assessment since it is a common hospital pathogen and a source of HAIs[347, 374-376]. Besides, the selected strain is already well characterized and presents limited biosafety risks. Although an exhaustive antibacterial assessment would have also included a Gram-positive bacteria such as *Staphylococcus aureus*, the purpose of this work was rather to conduct a preliminary study of the antibacterial properties of Ag-DLC coatings. Furthermore, the active biocide in the coatings, silver ions, have shown similar antibacterial effectiveness on Gram-positive and Gram-negative bacteria[73]. For these reasons, only the Gram-negative *E. coli* was chosen in this experiment and was used to infer the overall antibacterial behavior of the coatings. The experimental results indicated that Ag-DLC coated surfaces showed excellent antibacterial properties, which could be directly controlled via the proportion of embedded silver in the film.

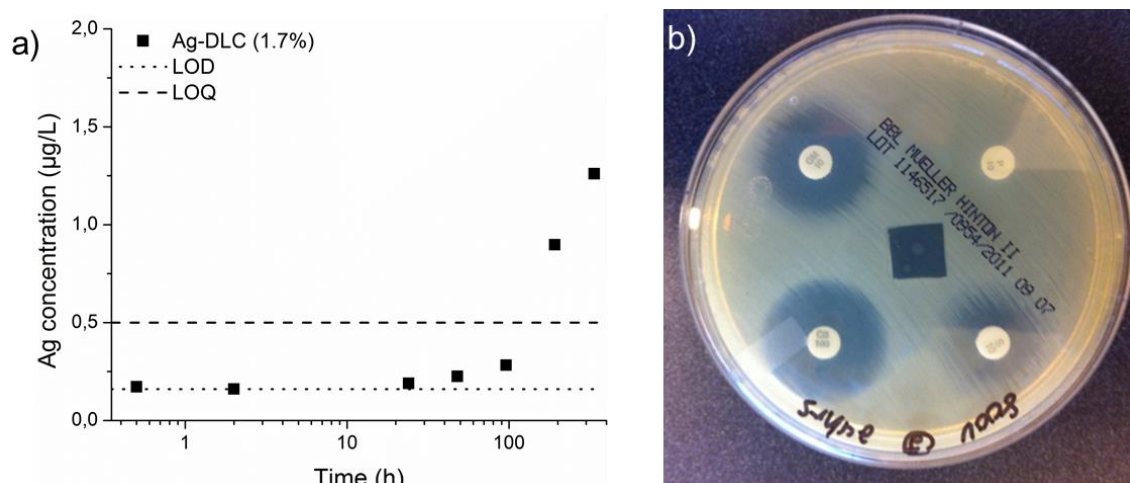


Figure 5.4: a) Silver release (in $\mu\text{g/L}$ or ppb) from Ag-DLC (1.7 at% silver) coatings in deionized water, for up to two weeks. b) Modified Kirby-Bauer diffusion test with a 2.4 at% Ag-DLC coating at the middle.

5.5.3 Release of silver ions from the coating

Sustained release of antibacterial agent is of paramount importance for maintaining the antibacterial activity for longer periods of time. To check whether the deposited films are suitable as long-term antibacterial coatings, the release of soluble silver into deionized water from Ag-DLC surfaces was investigated by GF-AAS. Figure 5.4 shows the cumulative measured concentration of silver in solution over two weeks, together with the limit of

detection (LOD) and the limit of quantification (LOQ) determined experimentally. The release profile showed a low initial detected concentration, inferior to the LOD for the first two hours, followed by a steady increase of the silver ions in solution throughout the immersion period. Furthermore, no concentration plateau was observed, even after two weeks, suggesting that the incorporated silver is not being merely washed away upon contact with the medium, but is rather strongly embedded in the carbon matrix and slowly producing silver ions via oxidative dissolution. This differs from the behaviour of several silver-based antibacterial surfaces reported in the literature, where the immersion is associated with an initial burst of silver ions followed by a rapidly decreasing silver release[361, 377, 378]. During the whole experiment, the soluble silver concentration remained in the ppb range. Silver concentrations as low as 0.1 ppb have been reported as having a bactericidal effect in water[378-380]. However, it should be pointed out that this method measures concentrations of silver eluted in the whole volume of the solution. Higher concentrations (10-100 fold) are present near the liquid-solid interface, in the “unstirred water layer” which prevents the colonisation of the surface, proliferation of adhering organisms and biofilm formation[356].

A modified Kirby-Bauer diffusion test was used as an additional qualitative assessment of the leaching from the antibacterial coating (Figure 5.4b). No zone of inhibition was detected beyond the specimen boundaries and only bacteria in contact with the coating or directly below it were killed. This result is consistent with the release rates measured by GF-AAS, since these leaching levels are expected to have a very limited diffusion into the Mueller Hinton agar. This suggests a slow silver release from the Ag-DLC surface and a localized antibacterial effect.

Rapid release of silver ions in the ppm range during the early stages of immersion can certainly be beneficial for the development of indwelling antibacterial devices or implants. However, as discussed previously, environmental surfaces must exert their antibacterial activity for much longer periods of time. They should exhibit a considerably slower release profile to prevent rapid silver depletion of the film. Furthermore, the design of such surface must take into account the environmental risks and ecotoxicity associated with leaching highly toxic heavy ions in the environment[90]. Hence, while the deposited coating should prevent bacterial contamination of the surface, it should do so without releasing large amounts of ions in their surroundings[381]. Based on this knowledge, the silver release of coatings for antibacterial environmental surfaces should be tailored to provide doses close to the minimum inhibitory

concentration. This seems to be the case for Ag-DLC films, as the sub-ppb silver release measured were enough to provide a clear antibacterial effect after 4 hours despite the very high level of contamination (10^6 cells/ml) used in the experiment.

5.6 Conclusions

In this study, Ag-DLC antibacterial coatings were produced by a 1-step hybrid plasma process. The proportion of silver embedded in the film was shown to be directly controllable via the voltage applied on the silver cathode, up to an average value of 2.4 at.%. XPS investigations showed that silver was present throughout the film under its metallic form, at the exception of a small fraction of oxidized silver at the surface. More importantly, the films showed a high antibacterial activity against *E. coli*, with a 2.5 orders of magnitude reduction in bacterial activity after 4 hours for the coatings with the highest silver content. The antibacterial effect was found to be directly related to the amount of silver embedded in the films and was attributed to the slow release of silver ions from the Ag-DLC coatings. The ion release from the films was shown to be quite slow, but continuous, with a silver concentration of $1,25 \mu\text{g.L}^{-1}$ after two weeks of immersion in distilled water. This slow release kinetics ensures a relatively slow depletion of silver in the film, minimizes the potential ecotoxicity of the surface and suggests the possibility of a long-term effectiveness of the coatings.

While the antibacterial activity might seem modest compared with other results reported in the literature, it is important to note this trade-off is necessary in order to ensure a longer effectiveness. Besides, because of the intended role of this coating, high antibacterial activity and total bacterial inactivation might not be necessary since environmental surfaces are subjected to regular cleaning procedures. In general, the results of this study suggest that Ag-DLC coatings display a good potential to reduce bacterial contamination of environmental surfaces in healthcare settings.

Further experimental investigations are, however, needed to estimate the mechanical and chemical stability of the coatings in realistic applications. Research is also needed to determine whether Ag-DLC films can exhibit a dual antibacterial effect, by also reducing bacterial adhesion on the surface.

5.7 Competing interests

The authors declare that there are no conflicts of interest.

5.8 Authors' contributions

All authors read and approved the final manuscript.

5.9 Acknowledgements

This work was supported by grants from the Canadian Space Agency (CSA) and the Natural Sciences and Engineering Research Council of Canada (NSERC). MC acknowledges funding from a NSERC Vanier scholarship. The authors are grateful to the people at Plasmionique Inc, and especially to Dr Andranik Sarkissian, for their participation, technical support and valuable discussions. We would also like to express our thanks to Dr Pascale Chevallier and Vicky Dodier for skilled assistance with the XPS and GF-AAS experiments, respectively.

6 Long-term stability of hydrogenated DLC coatings: Effects of ageing on the structural, chemical and mechanical properties

Author names and affiliations

M. Cloutier^{a,b,c}, C. Harnagea^d, P. Hale^d, O. Seddiki^d, F. Rosei^{d,e}, D. Mantovani^{a*}

^aLaboratory for Biomaterials and Bioengineering, CRC-Tier I, Dept of Min-Met-Materials Engineering, & CHU de Québec Research Center, Laval University, Pavillon Pouliot, salle 1745-E, Québec, Québec G1V 0A6, Canada

^bChimie ParisTech, PSL Research University, Institut de Recherche de Chimie Paris (IRCP), 11 rue Pierre et Marie Curie, F-75005 Paris, France

^cSorbonne Universités, UPMC Univ Paris 06, F-75005, Paris, France

^d Centre Énergie, Matériaux et Télécommunications, Institut National de la Recherche Scientifique, Université du Québec, Varennes, QC, J3X 1S2, Canada.

^e Center for Self-Assembled Chemical Structures, McGill University, H3A 2K6 Montreal, Quebec, Canada

Highlights

- Hydrogenated DLC films were analyzed before and after a three years ageing period
- The coatings exhibited significant structural stability over time
- Hardness and surface morphology remained unaffected
- Stress decreased due to ageing but was not associated with a sp^3 to sp^2 conversion
- Increased surface oxidation and loss of hydrophobicity were observed after ageing

Keywords

Diamond-like carbon, a-C:H, plasma enhanced CVD, ageing, long-term stability, surface characterization, microstructure, mechanical properties, coatings

6.1 Résumé

La stabilité à long terme est une condition essentielle pour l'utilisation des revêtements protecteurs à grande échelle. Néanmoins, c'est un aspect qui demeure souvent négligé dans la littérature. Nous rapportons dans cette étude les effets du vieillissement environnementale à long terme sur les propriétés de revêtements de carbone amorphe adamantin (DLC) hydrogénés. Une gamme de revêtements DLC produits par dépôt chimique en phase vapeur assisté par plasma ont tout d'abord été minutieusement analysés et ensuite rangés pendant trois ans avant une deuxième série d'analyses. Les analyses par spectroscopie Raman ont montré que les films possédaient une excellente stabilité structurale durant la période de vieillissement puisqu'ils n'ont montré aucun signe de conversion de carbone sp^3 à sp^2 . Pareillement, la dureté et la rugosité des revêtements DLC sont restées inchangées, malgré l'observation d'une relaxation du stress intrinsèque au film avec le temps. Toutefois, les analyses de spectroscopie de photoélectrons X ont révélé une certaine oxydation de la surface due au vieillissement, qui a été confirmée par une diminution du caractère hydrophobe de la surface (angle de contact avec l'eau a diminué à 65°). En général, les résultats suggèrent que le DLC possède une stabilité à long terme adéquate lorsqu'exposé à des conditions environnementales standards.

6.2 Abstract

Long-term stability is an essential condition for the commercial use of protective coatings, yet often remains overlooked in the literature. Here we report the effects of long-term environmental ageing on the properties of hydrogenated diamond-like carbon (DLC) films. A range of DLC coatings produced by plasma-enhanced chemical vapour deposition were first thoroughly characterized and then stored for three years before the second set of analysis. Raman spectroscopy showed that the films exhibited excellent structural stability during ageing, observing no sign of sp^3 to sp^2 conversion. Similarly, the hardness and smoothness of the DLC coatings remained unchanged, despite the observed relaxation of their intrinsic stress with time. However, X-ray photoelectron spectroscopy analyses provided evidence of ageing-induced surface oxidation, which was confirmed by reduced hydrophobicity (water contact angle dropped to 65°). Overall, these findings suggest that DLC possesses a suitable long-term stability when exposed to environmental conditions.

6.3 Introduction

The high stability of amorphous diamond-like carbon (DLC) films has been actively promoted in recent years and has encouraged its use in various applications as a durable protective coating, ranging from bioactive biomedical implants [146, 382-384] to magnetic data storage disks [106, 385]. This interest stems from the unique set of properties of DLC, which includes high hardness and elastic modulus, excellent wear resistance, low friction coefficient, high chemical inertness and atomic smoothness [106, 139, 386, 387]. Like diamond, several of their beneficial properties are conferred by the strong σ bonds of sp^3 hybridized carbon atoms. However, unlike diamond, they are achieved in an isotropic, amorphous thin film containing both sp^2 and sp^3 bonded carbon in nanometer-sized clusters and, in some cases, hydrogen [106]. This particular microstructure arises from the bombardment of energetic species during growth via a physical process termed sputter deposition [143, 305, 345]. Penetration of carbon or hydrocarbon ions creates local quenched-in increases in density, which causes the local bonding to convert to sp^3 , but also generates high compressive stresses in the film. The latter phenomenon can result in delamination, especially on non-optimized interfaces, and generally limits the thickness of deposited films, as stresses can act as a driving force for debonding from the substrate [388].

Although the importance of these intrinsic stresses in the formation of sp^3 bonds is still controversial (McKenzie et al. [296, 389] vs Robertson et al. [106, 390]), they remain a defining characteristic of DLC coatings, which brings forth questions about their long-term stability. The thermal stability of DLC coatings has been extensively studied [298, 391-393], but very little work has been reported on the effects of long-term environmental ageing (i.e. stability in environments that are not deliberately severe), either on stress-related degradation or on the stability of the aforementioned properties. However, this is of particular interest for applications such as protective and barrier coatings where DLC films are expected to maintain their protective behavior for several years [147, 394, 395]. Furthermore, it has been extensively reported that plasma-deposited coatings and other thin films materials are particularly prone to progressive surface alterations induced by environmental ageing [109, 396-398]. The study of the long-term stability and the occurrence of time-dependant degradation in DLC coatings is therefore necessary before they can be used in practical applications. The importance of

investigating the long-term stability of hard coatings at room temperature for periods up to three years has already been highlighted in an excellent review by Veprek et al. [399].

The aim of this experiment was to study the effects of long-term ageing on the stability of the structure and properties of hydrogenated DLC films to better assess their use as durable protective coatings. The few studies published on this subject until now usually tracked the evolution of a single property and studied one single type of film. On the other hand, this work presents a comprehensive analysis of the chemical, mechanical, morphological and microstructural properties of films with a range of different microstructures. The properties of DLC coatings were measured after deposition, and again after three years of environmental ageing in ambient air at room temperature. The choice of this time period was based on several considerations, including the expected lifetime of DLC coatings (from several months to several years depending on the application) and the reported timespan of time-dependent surface and structural changes in plasma deposited carbon coatings following deposition [399-402].

DLC coatings were produced at different deposition powers by plasma-enhanced chemical vapor deposition, to obtain films with different microstructures. While the term DLC encompasses a range of materials with different characteristics, from hydrogen-free tetrahedral amorphous carbon to their hydrogenated counterparts, it will be used in this text in a more specific sense to refer to hydrogenated amorphous carbon (a-C:H) films. The present investigation includes thorough characterization of the specimens by Raman Spectroscopy, X-Ray Photoelectron Spectroscopy (XPS), water contact angle, Atomic Force Microscopy (AFM), optical microscopy, Scanning Electron Microscopy (SEM), profilometry and nanoindentation.

6.4 Materials & Methods

6.4.1 Sample preparation and storage

The a-C:H films were deposited on 100-oriented single crystal Silicon substrates via a commercial RF (13.56 Mhz) capacitively-coupled plasma enhanced chemical vapor deposition system (Plasmalab system 100, Oxford Instruments, Abingdon, UK). Substrates were cut into pieces of 1x1 cm and 1x10 cm, loaded in the deposition chamber, which was then pumped

down to a base pressure below 1×10^{-4} Pa. Before deposition, the Si substrates were etched with an Ar plasma (50 sccm Ar, 40Pa, 150W) for 20 min. Deposition was performed using a pure methane plasma (50 sccm CH₄, 30Pa) at room temperature. Films between 100 and 250 nm were deposited by controlling and adjusting the deposition time, while preventing excessive heating of the substrate using a water cooling system. Different RF powers (50 W, 100 W, 150 W, 200 W, 250 W and 300 W) were used to vary the ion energy during the process and obtain a variety of microstructures. Specimens were first characterized post-deposition and then stored in tissue-culture polystyrene dishes at room temperature ($T=23 \pm 1^\circ\text{C}$), in contact with air and exposed to ambient humidity. They were kept in storage for three years before the second set of analysis.

6.4.2 Characterisation

The structural properties of the DLC films were analyzed by Raman spectroscopy (Renishaw inVia spectrometer, Renishaw, Wootton-under-Edge, UK) using an Ar laser at 488 nm operated at 20 mW. Spectra were collected with a 5x objective using an 1800g/mm grating. Each sample was scanned at three different positions to monitor the homogeneity of the coating. For the analysis, both characteristic peaks (G and D) were fitted with Gaussian functions, following the procedure established by Casiraghi et al. [403]. The photoluminescence (PL) background was taken between 1050 cm^{-1} and 1800 cm^{-1} .

The surface composition was investigated using an X-ray Photoelectron Spectrometer (XPS - PHI5600-ci spectrometer, Physical Electronics USA, Chanhassen, MN, USA). Survey and high resolution spectra were acquired at a detection angle of 45° using the K_α line of a standard aluminum and magnesium X-ray source, respectively, operated at 300 W. The curve fittings for the high resolution C(1s) peaks were determined by means of the least-squares method using Gauss-Lorentz functions with a Shirley background subtraction. Contact angles of the samples were measured by sessile drop method with the VCA optima XE (AST Products, Billerica, MA, USA) using distilled water.

Surface imaging was performed using an EnviroScope AFM (Veeco, Woodbury, NY, USA) operating in tapping mode and equipped with a T300R silicon tip (VISTAProbes, Nanoscience Instruments Inc., Phoenix, AZ, USA). The roughness was measured over $1 \times 1 \mu\text{m}^2$ areas. Samples were also studied by optical microscopy, with a BX41M microscope (Olympus, Center Valley, PA, USA) and scanning electron microscopy (SEM), using a JEOL 7500-F

scanning electron microscope (JEOL Ltd., Tokyo, Japan). For these measurements, prior to imaging, the aged specimens were thoroughly cleaned with deionized water and subsequently dried with nitrogen to minimize the presence of dust and other particles on the surface.

The film and substrate curvatures were measured with a microstylus profilometer (Dektak 150, Veeco) and the internal stresses of the deposited coatings were calculated using Stoney's equation [404]. The thickness was considered constant for aged samples. Hardness measurements were made using an atomic force microscope (Dimension 3100, Veeco) equipped with a corner cube diamond indenting tip (PDNISP model, Bruker, Billerica, MA, USA) working in nanoindentation mode [405]. The maximum indentation load used was 450 μN . Indented zones were imaged using the same setup, so as to directly measure the projected contact area.

The friction coefficient was estimated at nanoscale, using atomic force microscopy by scanning the AFM tip in contact mode, at a fast scan direction perpendicular to the cantilever axis (scan angle 90°), such that the friction force induces the torsional deformations of the cantilever [406, 407]. The speed of the tip was set at 2 $\mu\text{m/s}$, and the normal force was increased up to 4 μN . We used commercial doped diamond-coated silicon tips (DDESP-FM-10 model, Veeco) with a tip radius of approximately 250 nm. These tips were chosen because they are presumed to preserve their properties over long periods of sustained scanning in contact mode. The calibration of the cantilever was performed by measuring its resonance frequency, dimensions, and using the known relationships for the calculation of normal and torsional spring constants as described in [406].

6.5 Results and discussion

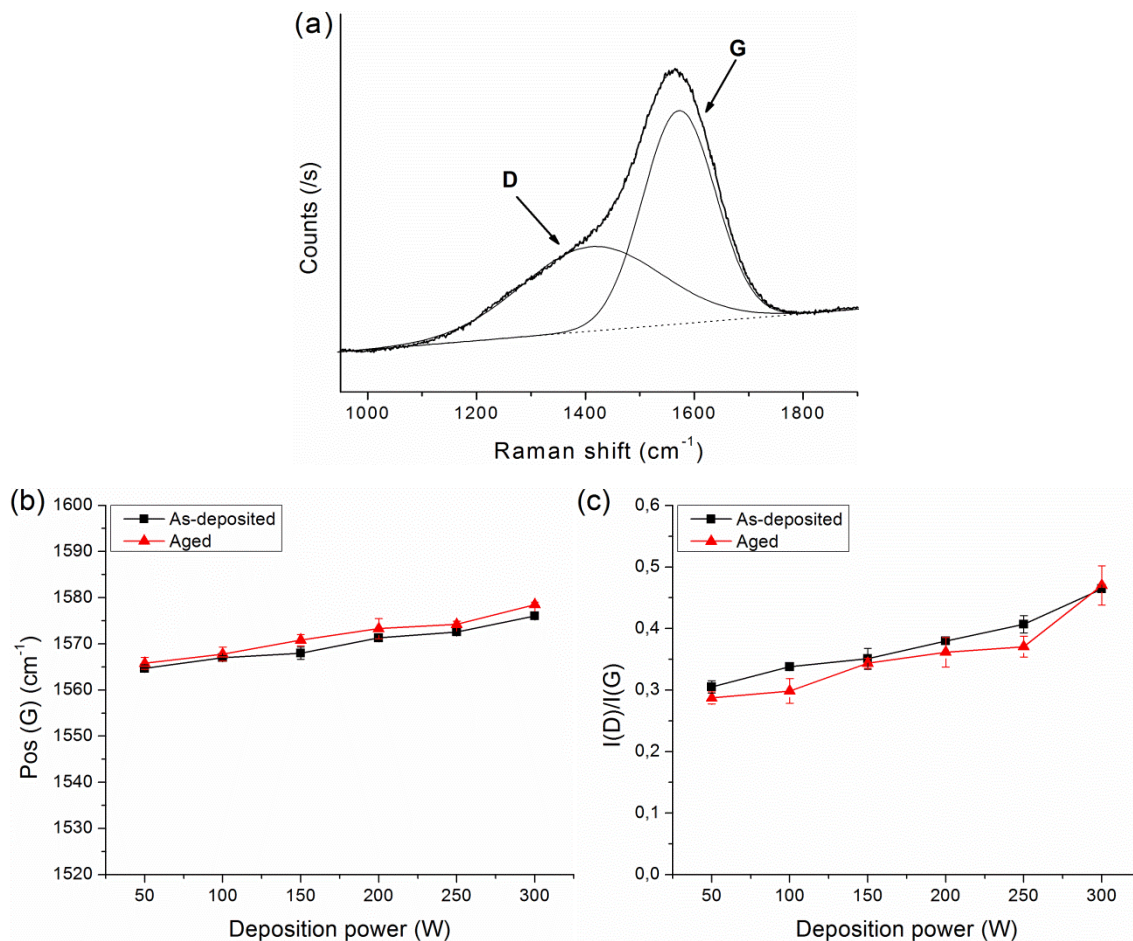
6.5.1 Structural properties

The Raman spectra of as-deposited samples (Figure 6.1a) showed the characteristic fingerprints of hydrogenated DLC films: the G peak (originating in the stretching vibration of pairs of sp^2 sites), the D peak (breathing mode of sp^2 sites within six-fold rings) and an increasing PL background [106, 408, 409]. Fitting and analysis of both peaks provided valuable information on the evolution of the bonding structure and the occurrence of structural changes with deposition and ageing conditions. The parameters of interest are the position and

full width at half maximum of the G peak, Pos(G) and FWHM(G) respectively, the intensity ratio of the peaks I(D)/I(G) and the hydrogen content deduced from the intensity of the PL background. These parameters are plotted against deposition power in Figure 6.1, for as-deposited and aged specimens. According to the three stage model introduced by Ferrari and Robertson [408], the Raman spectrum is primarily influenced by the clustering of the sp^2 phase. However, Pos(G) and I(D)/I(G) can offer an indirect evaluation of the sp^3 bonding in the film, since the presence of hydrogen in a-C:H films links the amount and configuration of the sp^2 phase with the overall sp^3 content (C-C & C-H sp^3) [106, 403, 408]. Similarly, for hydrogenated DLC films, FWHM(G) is influenced by the structural disorder, as it is mainly a probe of bond angle and length distortion. Both properties ultimately depend on the amount of C-C sp^3 bonds and FWHM(G) can hence be used to derive the structural and mechanical properties of the films [403]. Lastly, the hydrogen content can be empirically determined by using the ratio between the slope m of the PL background and the intensity of the G peak, $m/I(G)$ [403].

For as-deposited films, Pos(G) and I(D)/I(G) exhibit a roughly linear increase with deposition power (Figure 6.1b and c), indicating, as expected, an evolution of the structural order of the films with ion energy. It also suggests that films deposited at lower power/bias energy have a higher sp^3 content since they have lower Pos(G) and I(D)/I(G) values [408]. On the other hand, the FWHM(G) of as-deposited films exhibits a different trend, with a local maximum at 100 W surrounded by decreasing FWHM(G) values for other deposition powers (Figure 6.1d). This difference results from the fact that both Pos(G) and I(D)/I(G) probe the overall sp^3 content (C-C + C-H sp^3), while FWHM(G) is only influenced by the C-C sp^3 fraction. Hence, even if they do have a lower C-C sp^3 content, the higher sp^3 fraction for 50 W films calculated with Pos(G) and I(D)/I(G) could be indeed due to the higher hydrogen content measured in such films (see Figure 6.1e). The behaviour observed in Figure 6.1d with the presence of an optimum ion energy value for maximizing the C-C sp^3 content was also observed by several other authors for a-C and a-C:H coatings [132, 144, 410-412]. The observed increase in hydrogen content at low deposition power is consistent with the literature [409, 413] and could be attributed to incomplete methane dissociation at lower power, which may cause an increased incorporation of H-bonded carbon atoms into the film. Conversely, it was also suggested that this behaviour could be associated with the increased release of H in the collision cascades induced by higher energy atoms [414].

After ageing, Pos(G), I(D)/I(G) and FWHM(G) all show the same trends as their as-deposited counterparts, with highly similar values (Figure 6.1b, c, d). This suggests that there was no significant phase change, conversion of sp^3 into sp^2 carbon or other modification in the structural bonding of hydrogenated DLC films during ageing, regardless of the deposition power. An increase, between 18 and 27 % of the hydrogen concentration was noted for all samples (Figure 6.1e). Films of various thicknesses were subsequently analysed by Raman spectroscopy to assess the origin of the %H increase but no correlation was observed between thickness and increase in hydrogen content. Thus, this suggests that the %H increase was due to surface adsorbed water rather than bulk diffusion of hydrogen or other bulk structural modifications. This would also imply that the hydrogenated films did not undergo a graphitization process at room temperature, despite the long exposure time [415].



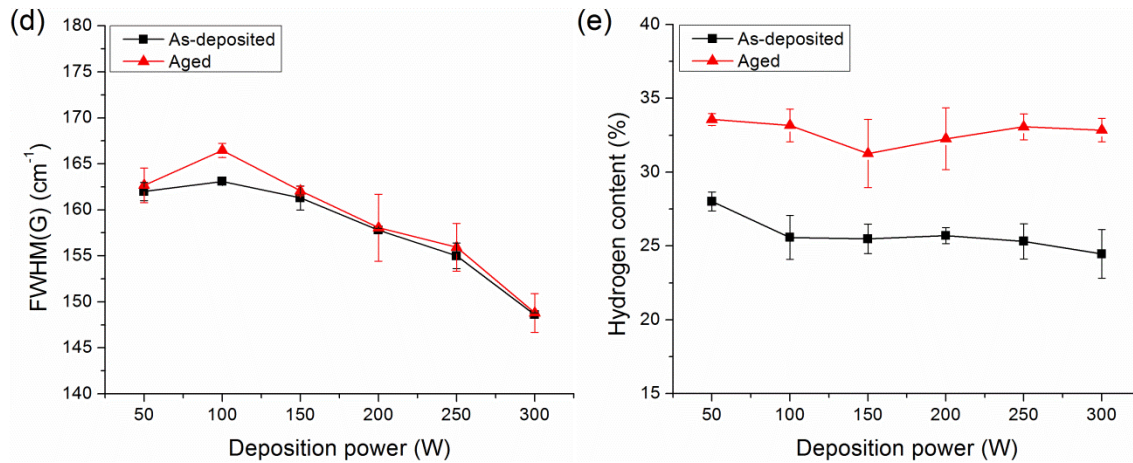


Figure 6.1: Single-wavelength Raman spectroscopy ($\lambda=488$ nm) analysis of DLC samples. a) Typical Raman spectra showing both deconvoluted peaks and the fitted linear background. b) Pos(G) c) I(D)/I(G) ratio d) FWHM(G) and e) hydrogen content of as-deposited (squares) and aged (triangles) DLC films as a function of deposition power.

6.5.2 Surface chemistry

The surface of DLC films was investigated with X-Ray Photoelectron Spectroscopy (XPS), so as to characterize the as-deposited surface chemistry and the changes induced by ageing. XPS survey analyses of as-deposited and aged specimens revealed the presence of both carbon (284.6 eV) and oxygen (532.5 eV) (Figure 6.2). Plasma-deposited carbonaceous materials are known to promptly oxidize upon air exposure, through the formation of surface oxygen functional groups [416, 417].

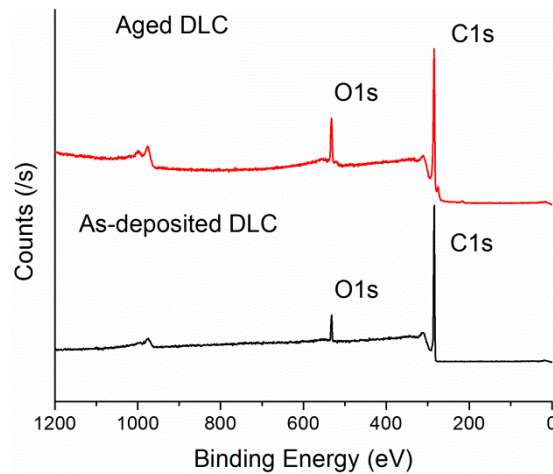


Figure 6.2: Representative XPS survey spectra of DLC films (deposition power 200 W) before and after ageing. Only carbon (C1s) and oxygen (O1s) were detected on both samples.

The influence of deposition power and ageing on the surface chemistry of the film was further investigated with high resolution XPS. An example of the C1s carbon region is depicted in Figure 6.3a, showing the characteristic asymmetric tailing due to the contribution of surface oxygen groups. The C1s high resolution spectrum of carbon was decomposed into four components, assigned to C-C and C-H (BE=284.6 eV), C-O (BE=286.4 eV), C=O (BE=287.8 eV) and O-C=O (BE=289.1 eV) [418-420]. Figure 6.3b compares the proportion of oxygen components of the C(1s) peak before and after ageing at different deposition powers. For as-deposited films, results show an increasing proportion of O groups with deposition power. A similar behaviour can be observed on aged films. Although it is impossible with the current data to pinpoint the exact mechanism involved in this phenomenon, this increase could be explained by the higher density of dangling bonds created at higher deposition power, caused by ions impacting the surface with more energy, thus enhancing the surface's reactivity to the highly reactive oxygen molecules [421]. Figure 6.3b also shows a clear increase in the proportion of all O groups in the C1s region due to ageing. The trend was confirmed with similar increases of the oxygen content measured from the survey spectra (Figure 6.2). This augmentation is not due to physisorbed molecules since increases in pumping time did not induce any change on the resulting spectra. While chemisorbed molecules may partially explain the oxygen increase due to ageing, they are unlikely to account for the whole variation (between 70% and 140%). For amorphous carbon, surface oxidation has rather been associated with UV-induced breaking of C-C and C-H bonds and subsequent formation of C-O bonds [139] and hydrolysis of carbon-carbon bonds [422].

Besides altering the surface composition of DLC, ageing also affected the wetting behavior of the films. The measured increase in oxygen was associated with an increase in surface energy, as revealed by contact angle measurements (Figure 6.4). We observed a drop of the water contact angle from $81\pm 3^\circ$ for as-deposited samples to $65\pm 3^\circ$ after ageing and we associated this with the slow, albeit significant, formation of hydrophilic functional groups such as carbonyl (O=C), carboxyl (O-C=O) and ether (O-C) and the consequent loss of hydrophobic hydrocarbon (CH₃ and CH₂) groups at the surface of DLC films.

This alteration of the surface chemistry could impact the long-term performance of DLC coatings in several fields, but especially in biomedical and tribological applications. For

instance, for biomedical coatings, the observed decrease in chemical inertness may result in additional, undesirable interactions with surrounding cells and body fluids.

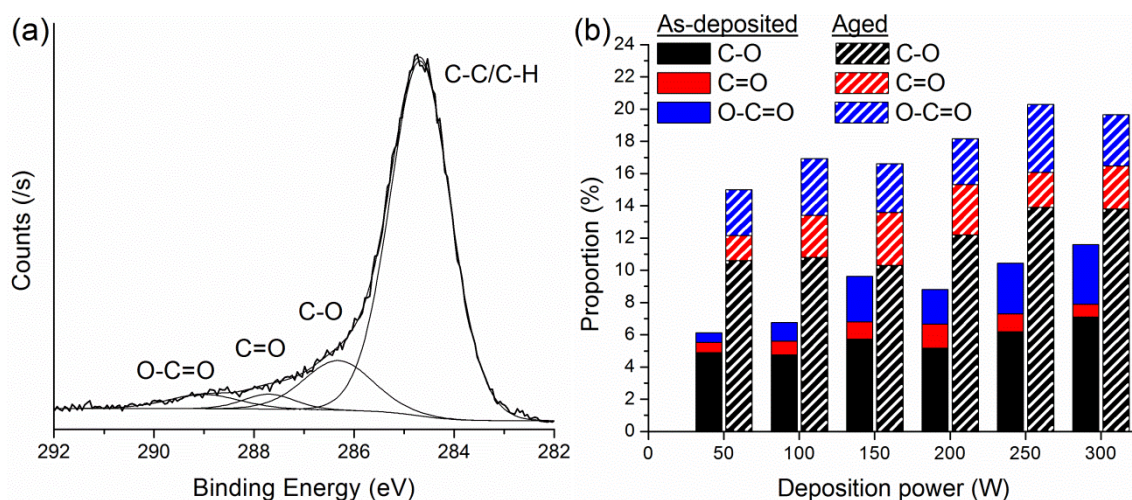


Figure 6.3: High resolution (HR) XPS analysis of the investigated films. a) HR XPS C(1s) spectrum of the DLC films with corresponding peak deconvolution (deposition power 150 W, post-ageing). b) Proportion of oxygen components of the C(1s) peak for the as-deposited and aged DLC films.

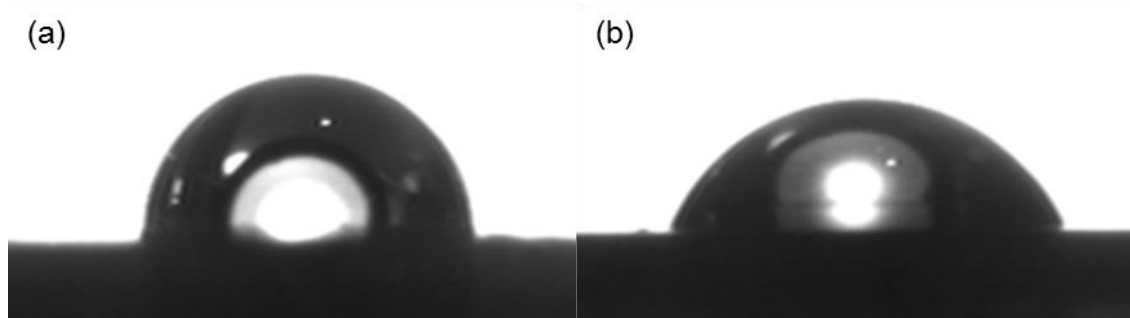


Figure 6.4: Representative water contact angle measurements of a) as-deposited ($81 \pm 3^\circ$) and b) aged DLC coatings ($65 \pm 3^\circ$)

6.5.3 Surface morphology

Both as-deposited and aged films revealed the typical nanosmooth topography of DLC coatings (see Figure 6.5) [386]. The measured R_{RMS} for as-deposited films was 0.11 ± 0.04 and 0.20 ± 0.03 , for 100-300 W and 50 W deposition power, respectively. This rougher topography obtained at lower deposition power is due to the inability of incoming ions to penetrate the surface, leading to the formation of ordered sp^2 -rich surface clusters which increases the roughness, as described by Peng et al. [423] The same pattern was observed after ageing, with R_{RMS} values of 0.10 ± 0.02 nm for films deposited between 100 W and 300 W and of

0.17±0.02 nm for films deposited at 50 W. This topological stability suggests the absence of any stress/strain-induced roughening mechanisms during the ageing process.

Optical microscopy and SEM were also used to assess the presence of defects at the surface of the films. DLC deposited on inadequate surfaces can undergo stress-relieving processes that lead to buckling, cracking or even complete delamination [147, 388, 424]. In our case, the analyses revealed the absence of such features; no stress-related surface defects were observed at the macro-, micro- and nano-scale levels for all samples before and after ageing. The aged films were very similar to as-deposited coatings, indicating that the coating adhesion and cohesion was sufficient to resist the high compressive stresses of DLC for extended periods of time.

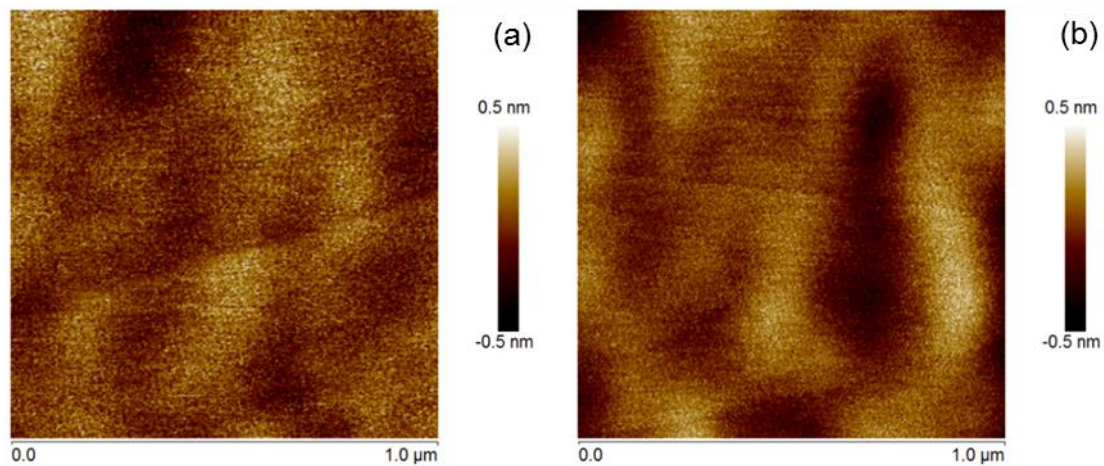


Figure 6.5: Characteristic tapping mode AFM height images (1 μm x 1 μm) of DLC films a) as-deposited and b) aged (deposition power 250 W). Please note that the vertical scale bars represents only 1 nm, for both images.

6.5.4 Mechanical properties

Figure 6.6 shows the measured stress of as-deposited and aged specimens as a function of deposition power. For as-deposited films, the stress curve is typical of DLC films. [143, 297]. The initial increase in compressive stress with increasing deposition power is the result of the intensification of implantation as the bombarding carbon ions have higher energy. However, the stress reaches a maximum at 100 W RF power, which is explained by the creation of local thermal spikes upon implantation with high energy ions. These local increases in temperature

promote a thermally activated relaxation of the bonding into sp^2 [305], resulting in the observed decrease in stress.

Although both as-deposited and aged samples exhibit a high level of stress in the GPa range, we observed a decrease of the compressive stress levels for all aged samples, with a more pronounced reduction for specimens deposited at lower power. A similar time-induced relaxation of residual stresses was observed by Bull and Hainsworth [400] in DLC coatings deposited by ion-beam-assisted deposition (IBAD). The origin of this relaxation is, however, problematic to pinpoint. It may not be attributable to an important sp^3 to sp^2 conversion [425], since such a transformation was not detected in the Raman analysis (Figure 6.1b-d). Another possibility would be a time and strain-induced roughening, that would allow a partial relaxation through the formation of grooves and pits at the surface [426]. Other common stress relief mechanisms observed at the surface of amorphous carbon films with high intrinsic stresses are buckling and cracking [388]. However, as revealed previously by AFM and optical microscopy analyses, the surface morphology of the films did not show any sign that these stress relief mechanisms took place.

Bonds length and angle distortions (i.e. deviations from their equilibrium value) are the primary contributions to the high residual compressive stress of DLC films [296, 427, 428]. Accordingly, Ferrari et al. pointed out that the stress could be relieved by a tiny strain relaxation [390]. Due to the high Young's modulus of the DLC coatings (125-200 GPa), the strain relaxation necessary to produce a large stress reduction would be minimal and thus not necessarily perceptible with Raman analysis. As a result, the observed relaxation of the film could be due to the release of bonds' length and orientation distortions created during the deposition process. A similarly slow relaxation process was also noted by Bouzerar et al. in plasma deposited hydrogenated DLC films [401]. In our case, the relaxation phenomenon appears more pronounced for specimens deposited at lower power, and we attribute this to the fact that these films have not already undergone the thermal spike relaxation associated with implantation of high energy ions.

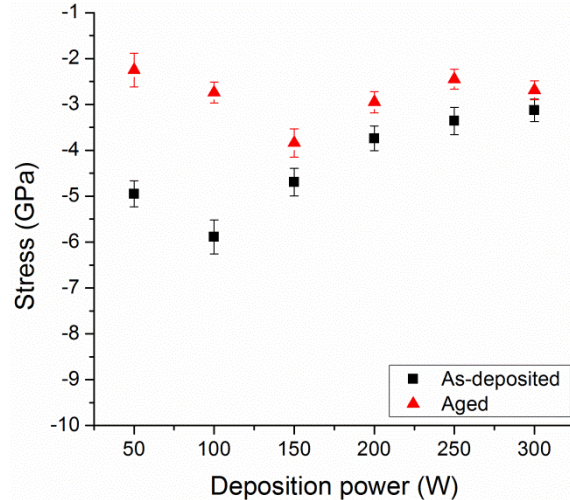


Figure 6.6: Compressive stress measured experimentally in as-deposited (square, black) and aged (triangle, red) DLC coatings, as a function of deposition power.

The hardness was measured using an AFM equipped with a diamond indenter. The results are shown in Table 6.1. While this technique is useful for investigating mechanical properties of films at the nanometer scale, nanoindentation is best suited for making relative hardness measurements and the results should not be used to make absolute comparisons with data from the literature. Both tested ageing conditions showed the same tendency, with a clear hardness maximum at 100 W, confirming the trend observed previously with the Raman and stress experiments for as-deposited samples. Samples deposited at other powers exhibited roughly similar hardness levels of ~ 11 GPa. After ageing, there was no significant decrease of the measured hardness as the observed differences were within the experimental error. This confirms our previous finding that the films did not undergo a significant sp^3 conversion, since their C-C sp^3 content, governing the mechanical properties, appears to be unchanged after ageing.

Table 6.1: Hardness of DLC films measured by nanoindentation

Deposition power (W)	Hardness (GPa)					
	As-deposited			Aged		
50	10,6	±	0,5	9,8	±	0,4
100	14,5	±	0,6	12,8	±	0,5
150	11,6	±	0,6	10,6	±	0,4
200	11,3	±	0,7	11,0	±	1,3
250	11,9	±	0,8	10,8	±	0,5
300	11,8	±	0,6	10,3	±	1,0

6.5.5 Tribological properties

To assess the effect of ageing on the tribological properties of DLC, nanoscale friction studies were performed using a diamond AFM tip in contact mode as the counterface (Figure 6.7). The initial friction coefficient was found to be 0.24, which is coherent with other studies performed in normal atmosphere [429, 430]. The measurements were repeated after ageing and we observed an increase of the friction coefficient to 0.37.

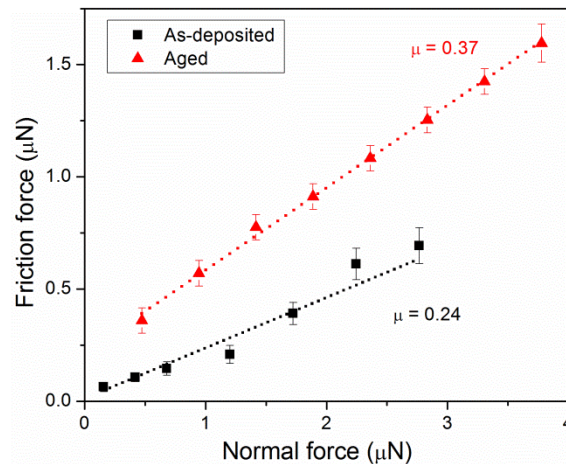


Figure 6.7 : Representative nanoscale friction measurements (deposition power 150 W) of as-deposited (square, black) and aged (triangle, red)

The increase in the friction coefficient can be attributed to several factors. First, the observed stress relaxation that we interpreted as being due to the release of bond's length may also influence the film's Young modulus, making it more compliant. As a result, the real contact area between tip and film would increase, and, according to the theory of Bowden and Tabor [431], lead to an increase of the (effective) friction coefficient.

A second effect on the friction coefficient may come from the increase in the surface energy. It is well-known from the adhesive contact theory [431] that the surface energy between the two bodies in contact causes an additional attraction force (adhesion) which affects the friction coefficient. Therefore, any increase in the surface energy of the film, is expected to increase the friction coefficient.

Finally, the third and we believe the major contribution to the increase in friction coefficient is the change in surface chemistry. Tribochemical interactions play a critical role on adhesion and friction at the sliding interface. Hence, in the case of the aged samples, the increase in bonded oxygen at the surface leads to an increased chemical activity of the DLC coating, giving rise to stronger adhesive friction and a higher friction coefficient [432]. Moreover, surface oxidation may lead to the generation of abrasive, non-lubricating wear debris which can considerably affect the friction coefficient and overall tribological behavior of the films [432, 433]. These polymer-like, oxidized hydrocarbon particles have been found to form during tribological testing of DLC films in high oxygen or high humidity environments, causing increases in friction coefficient. However, in the case of aged samples, these particles can be expected to form under any environment since the coating's surface is already oxidized.

6.6 Conclusion

In this work we investigated the effect of extended ageing on the properties of hydrogenated DLC films. The coatings exhibited great structural stability, showing no sign of microstructural changes or graphitization with time. There was however an important decrease in compressive stress associated with the ageing process, especially for films deposited at low deposition power. This was associated with the release of bonds' length and orientation distortions rather than to an sp^3 conversion. Consequently, the relaxation did not have a negative effect on the surface and mechanical properties of the film, as the surface topology and hardness remained unchanged after ageing. The results from this study suggest that DLC films retain their microstructure and mechanical properties throughout their useful life. However, an increase in surface oxygen and oxygen functional groups was observed for all deposited samples and accompanied by a loss of hydrophobicity. This suggests that DLC, despite being only subjected to ageing in environmental conditions, may undergo significant alterations in surface

chemistry. This could potentially affect the long-term performance of DLC films in applications such as protective tribological and biomedical coatings.

6.7 Acknowledgment

This work was supported by grants from the Natural Sciences and Engineering Research Council of Canada through the Strategic Project Grants program (in partnership with Plasmionique Inc. and the Discovery Grants program). D.M. and F.R. thank FRQNT for funding through the team grants program and are grateful to the Canada Research Chairs program for partial salary support. MC acknowledges funding from a NSERC Vanier scholarship. The authors are grateful to Dr Andranik Sarkissian and Dr Stéphane Turgeon for valuable discussions. The authors would also like to acknowledge the contribution of Dr Pascale Chevallier and Dr Ranna Tolouei for their assistance with the XPS analysis and AFM imaging respectively.

7 General discussion

This thesis set out with the aim of developing a new type of stable antibacterial coating and assessing whether the chosen platform offered the flexibility and tunability needed to adapt the process to different applications. Due to the inherent complexity and novelty of the project, a multipronged approach was adopted, combining technical, exploratory and fundamental work within an evolving framework steered by the rapid progress in the field. This chapter first provides a brief overview of the findings and discusses their **pertinence, originality** and likely **impact** in the field of surface engineering and antibacterial surfaces. Then, it will address the potential of Ag-DLC coatings as a material platform, discuss their performance in certain investigated applications and examine the limitations of this project.

7.1 Summary and significance of contribution

Because the concept of antibacterial coatings is in itself rather new, a comprehensive literature review was undertaken and presented in **Chapter 2**. It showed that, despite a wide variety of existing approaches and tools, three main areas of improvements were needed to progress towards a more widespread adoption of antibacterial coatings. These challenges were the controlled release of antibacterial agents, the development of multi-functional and flexible coatings and the improvement of long-term stability. Both the timing and focus of the work could significantly boost the impact of this contribution. With the recent explosion in antibacterial coating literature, thorough reviews of the field such as this one can help gear current research towards more promising avenues, ultimately resulting in faster and better translation of academic development projects into clinically or industrially applied materials.

The platform proposed in this work falls directly within this endeavour. However, although promising in theory, the combination of diamond-like carbon and silver nanomaterials within a single nanocomposite coating entails its own challenges, which were examined in chapters 3 through 6. A novel strategy to enhance the adhesion of DLC was proposed in **Chapter 3**. The bonding strength of DLC coatings on stainless steel was nearly doubled with the use of an *in situ* plasma carburation interfacial treatment. Although the adhesion gain is modest compared to the ones obtained by other techniques, the interest of this approach stems from its ease of implementation (interface treatment in the same reactor as DLC deposition), limited chance of

contamination between treatment steps, and single interface approach. Indeed, creating additional interfaces, through the deposition of interlayers, have been linked with long-term corrosion and adhesion problems. Still, the most interesting and original finding from this work was that it provided evidence that micrometre-thick layers are not unavoidable for improving the adhesion of DLC or other high-stress coatings. Shallow surface modifications can be used to effectively treat the topmost surface of materials. From a global perspective, this could open the door for the development of more time-, energy-, and cost-saving approaches to adhesion improvement.

One of the obvious downside of working on the development of novel materials is the significant gap in knowledge concerning fundamental aspects of their growth and properties. This topic was tackled in **Chapter 4**, which presented an investigation of the growth mechanisms and distribution of silver in Ag-DLC. In a clear contrast with standard material optimisation studies, who typically simply link deposition conditions with final properties, this work focused on extracting trends and patterns from the exhaustive spectroscopy and microscopy investigations undertaken. As a result, this study identified segregation and clustering of silver as the main mechanisms governing the growth of Ag-DLC coatings and singled out two plasma parameters (sputtered Ag flux and ion energy) which had the most influence over the coating's final structure. One of the issues that emerged from these findings was that a uniform silver distribution and a high hardness were mutually exclusive properties under those growth conditions. The films could be either deposited at 1) high energy and have a high hardness but important silver segregation at the surface or 2) be deposited at lower energy, which formed softer coatings with well disperse silver throughout their bulk. The preferred choice of energy and corresponding film properties then become strategic and must be adjusted based on each specific application. Because the driving forces (i.e. the poor silver/carbon affinity and the energetic subplantation process) are not specific to silver, these finding can be extended to other metal-DLC nanocomposite coatings grown by the same method. Thus, this work not only filled an important theoretical gap in the growth of metal-containing DLC, but also provided practical, application-oriented input for the deposition of nanocomposite coatings.

The evaluation of the antibacterial effectiveness remains the crux of the matter of all investigations in the field of antibacterial coatings. In that regard, the study presented in

Chapter 5 is both significant and necessary to gauge the potential of Ag-DLC coatings as an antibacterial material. The data must be interpreted with caution because the amount of incorporated silver in the samples tested was far inferior to the concentrations achieved in the latter stages of the project (maximum surface concentration of 2.4 at.% for this study compared with close to 20 at.% afterwards). Still, despite this hindrance, the results remain very encouraging: a 2.5 orders of magnitude reduction in the activity of *E. Coli* after 4h achieved with a slow and continuous Ag⁺ release. The latter result is especially interesting when considering the challenges previously identified in Chapter 2. It is essential to develop coatings with slow release kinetics (while maintaining concentrations in the therapeutic window) to hope to achieve any long-term potency in release-based antibacterial coatings. Another distinctive aspect of the contribution presented in Chapter 5 is the comprehensive discussion surrounding design criteria of antibacterial coatings for environmental surfaces. While most of the literature have so far been focused on developing antibacterial solutions for implantable devices, environmental surfaces constitute a uniquely different challenge in several aspects, most importantly in the local environment in which the coatings evolve, the optimal duration of the antibacterial effect and the required additional stability.

Finally, an important aspect of stability was investigated and presented in **Chapter 6**. Stability to aging is an essential condition for potentially reactive, plasma-deposited materials, yet remains overlooked in the literature. Compositional changes, oxidation and even topographic changes have been known to occur in plasma-deposited coatings during aging. Such modifications are bound to influence the properties and functions of the deposited material and should therefore be studied in detail. Moreover, the high intrinsic stress in DLC can act as an additional driving force for aging-related modification in the film, further highlighting the need for an investigation in their long-term stability. A 3-year investigation was undertaken with coatings first deposited by colleagues from INRS. It revealed the excellent structural stability of the specimens, despite stress-relaxation occurring over time. DLC coatings retained their mechanical properties (hardness, stiffness, etc.) and nanosmooth surface morphology, but suffered aging-induced surface oxidation and consequent loss of their hydrophobic character. This could negatively impact the performances of DLC coatings in applications where surface energy is an important factor. Although this investigation covered only one of the several aspect of long-term stability, it was the first study to underline its importance for DLC

coatings. As it has been well received so far by the scientific community, this could lead to similar investigations being performed on DLC and other plasma-deposited coatings.

7.2 Ag-DLC as a tunable platform

As discussed previously, one of the main objective of this thesis was to assess the potential of Ag-DLC coatings as a tunable material platform. The recent prevalent idea that there exist a specific, ideal material for each application have generated significant interest for such material platform. Instead of starting from scratch when targeting a new area of application, which can incur important cost and time investments, a good material platform offers enough flexibility to be easily adapted to fit the new application's requirements. Notable examples of this concept include hydrogels and metal-organic frameworks [434-436]. This section will further explore this facet of Ag-DLC coatings using the insights gathered over the previous chapters.

7.2.1 Choice of substrates

Two types of substrates, silicon and 316L stainless steel, have been used in all the investigations presented above. The reasoning behind these choices was based on both practical and realistic considerations. On one hand, silicon was used as a “best case” substrate. The flat surface and carbide-forming chemistry of silicon wafers offer an ideal surface for deposition of DLC, but also for the easy characterisation of the deposited coatings. On the other hand, stainless steel was a more application-oriented substrate, they have become ubiquitous in industrial and hospital settings, but could also be considered at the “worst case” scenario. The thin passivation layer at the surface of stainless steel produces a naturally poor bonding strength with deposited DLC coatings, leading to rapid delamination. The challenge presented by stainless steel have been recognized for a long time by the scientific community and have spurred the development of several surface engineering approaches to promote DLC adhesion (see Chapter 3). Besides, although their deposition was not characterized as thoroughly as with the two mentioned above, several other materials were used as substrates during this project, including metals (aluminum, copper, and titanium alloys) and polymers (PTFE, PET, COC). Overall, the properties of the deposited thin films were not substrate-dependent, suggesting that this deposition process could be applied to a broad range of materials, but only if an interface treatment can provide adequate adhesion between the coating and substrate.

7.2.2 Structure and mechanical properties

Because the deposition of DLC coatings is a heavily ion-dominated process, their mechanical properties can be controlled directly through the ion energy and the applied substrate bias. In contrast, other plasma parameters such as the pressure, plasma power, and gas composition had little influence on the deposited coating's properties and were therefore of limited use in assessing the adjustability of the process.

The investigated bias range for Ag-DLC deposition in this project (from 0 to -200V) produced coatings with widely different mechanical properties and structures. They may be divided into four main sub-groups:

- Low bias (0-30V): Soft, polymer-like coating with low intrinsic stress. However, they had the highest concentration of incorporated silver as well as the most uniform silver distribution. Typical hardness around 1 GPa.
- Intermediate bias (30-75V): Hard, diamond-like coatings. Significant silver segregation, but with higher bulk Ag concentrations (1.5-2 at.%).
- High bias (75-125V): Hardest, dense, diamond-like coatings with high intrinsic stresses and, consequently, important delamination issues. Optimal bias range for sp^3 formation. Hardness could reach up to 20 GPa. Superior wear-resistance. Significant silver segregation towards the surface, limiting the amount of silver in the bulk to below 1 at.%.
- Highest bias (>125V): Hard diamond-like coating. Limited introduction of silver at the surface or within the bulk due to increased sputtering.

Despite the range of possible structures (segregated vs well-dispersed Ag component) and mechanical properties (from polymer-like to diamond-like), the tunability of the coatings was limited in the sense that all combinations of the properties are not possible. For example, a very hard coating with a well distributed silver phase could not be deposited with the current technique, because the two properties are inversely correlated to a single deposition parameter.

The wear-resistance was positively correlated with the hardness of the coatings. However, the chemical stability, the ability of the material to resist change or decomposition when in contact with another medium, was independent from the deposition bias. Coatings deposited at all substrate biases showed good stability when in contact with detergents and liquids in general.

An implication of this is the possibility to use softer nanocomposite coatings deposited at low biases when a high hardness or wear-resistance are not necessary.

7.2.3 Silver ions release

Silver ions are released by oxidative dissolution from the surface and are the primary element responsible for the antibacterial properties of Ag-DLC coatings. Because the incorporated silver must react with water or another solution in order for the ion release to occur, silver release from Ag-DLC coatings can be controlled by changing the amount of silver exposed at its surface. Therefore, direct approaches to achieve controlled Ag^+ release include changing the silver concentration at the surface (by adjusting the silver flux within the plasma), varying the size and distribution of silver clusters (by adjusting the ion energy) or changing the porosity, density or surface energy of the coating. Using this nanocomposite approach, the silver ions release could be adjusted over a two orders of magnitude range, between 0.005 and 0.5 $\mu\text{g}/\text{cm}^2$ day.

Additional plasma approaches were investigated to try to maximize the range of silver ions release attainable. Using a combination of techniques available at the 2PM and LBB laboratories, several approaches that could be used to tune the release from silver-containing coatings were identified. These approaches targeted modifications in the oxidation state of silver (plasma oxidation, reactive sputtering), changes in the active surface area (nano-roughening, surface patterning), control over diffusion and silver's contact with leaching solutions (barrier coating, nanocomposite approach) or even promoted increased corrosion by the co-deposition of additional metals (galvanic coupling). Altogether, the control of Ag^+ release was extended to a 5 orders of magnitude range (see Figure 7.1). Although the investigation of these different approaches remained at a preliminary stage in the context of this thesis, we have shown the possibility to increase or decrease Ag^+ release, in a repeatable and controllable way, using strictly plasma-based methods.

This result has important implications for developing coatings with long-lasting antibacterial action, to reduce excessive leaching of silver ions in the environment or to create surfaces with controlled burst-release of biocides. For instance, coatings used on healthcare environmental surfaces which are expected to have long-lasting antibacterial properties should have a slow but sufficient Ag^+ release (within the low end of the therapeutic window) combined with a

large reservoir of silver. In that case, a precise control over the release kinetics of silver ions, achieved through the approaches proposed in this thesis, will be a crucial element to consider.

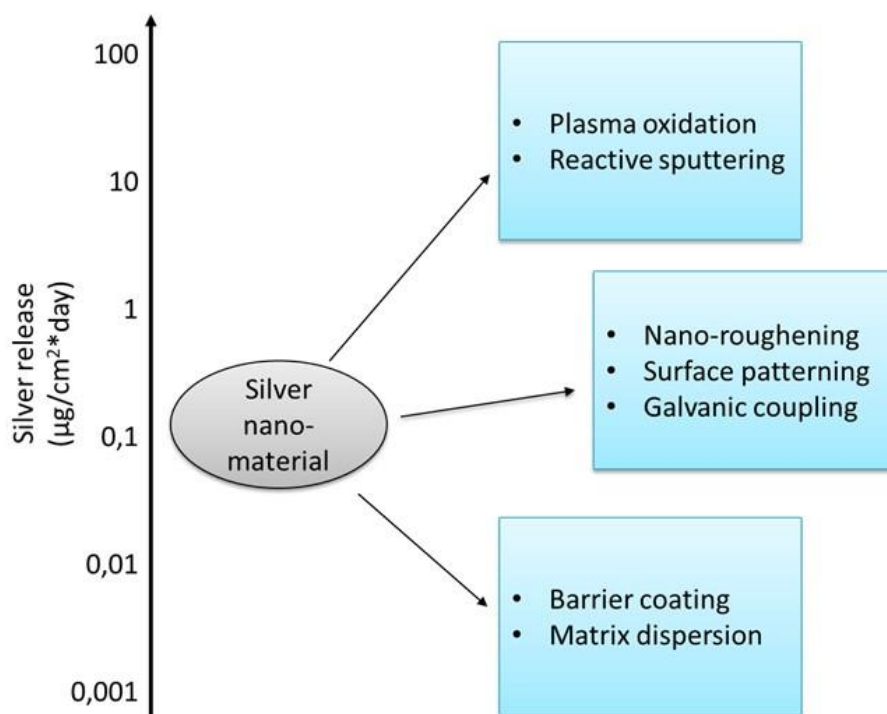


Figure 7.1: The different investigated strategies for the controlled release of Ag⁺ ions from silver-based plasma coatings.

7.2.4 Antibacterial properties

The biocidal properties of Ag-DLC coatings are directly linked to the release of Ag⁺ ions and strategies to control it have already been discussed in the previous paragraphs. However, one of the initial purpose behind the use of DLC was that its low roughness and low surface energy would be detrimental to bacterial adhesion. Analyses performed at the LBB showed that no significant reduction in bacterial adhesion was observed on DLC coatings compared with a control stainless steel surface (data not shown). A possible explanation for this result may be that the surface energy of Ag-DLC was not low enough (the water contact angle of DLC coated specimens was close to 90°) to act as a truly hydrophobic surface. Furthermore, the relationship between common surface properties such as topography, surface charge, or energy, and bacteria adhesion is much more complex than previously thought, partly due to the diversity of adhesion mechanisms use by microorganism [170]. It can be therefore be

assumed that the Ag-DLC coatings investigated did not demonstrate any anti-adhesion properties, but this remain an important issue for future research.

7.3 Investigated areas of applications of Ag-DLC coatings

The inherent flexibility of nanocomposite coatings offers tremendous possibilities to apply them in many different fields. The following section discusses how the findings presented in this thesis impact the potential applications of Ag-DLC coatings. Insights gained from additional investigations that are not included in the main chapters of this thesis will also be used when relevant.

7.3.1 Healthcare environmental surfaces

The most obvious application for Ag-DLC coatings and the one discussed throughout this thesis is as antibacterial coatings for healthcare environmental surfaces. Chiefly from a conjectural standpoint, the results presented in the previous chapters indicates that Ag-DLC coatings indeed possessed the required combination of properties to be efficient as antibacterial surfaces. Still, despite their combination of good adhesion, high hardness, and structural stability, it is difficult to extrapolate from this data how the coatings would fare in a healthcare facility, where they must maintain their functions in harsh operating conditions. Hence, the stability of Ag-DLC coatings to realistic abrasion and chemical stresses was investigated in more details (see Annex A). The tests were designed to mimic common surface sterilization procedures found in healthcare environments: repeated back and forth scrubbing with a scouring pad sponge (abrasion test) and prolonged contact with a hydrogen peroxide (H_2O_2) cleaning detergent (chemical stability test).

As expected, the harder DLC coatings performed better in the abrasion test, showing very limited surface damage even after 1000 wear cycles. However, the softer coatings maintained higher silver concentrations during the chemical cleaning cycles than their harder counterparts (see figure A.2 of annex A). These results are likely related to the energy-correlated segregation of Ag identified in Chapter 4. The more uniform Ag distribution in soft a-C:H coatings offered better protection from the oxidizing solution (i.e. less Ag clusters were exposed at the surface), limiting the rapid loss of Ag to the cleaning solution. The segregation occurring in the harder

coating (deposited at -100V) left the majority of the silver exposed as clusters at the surface of the film.

This results exemplifies the crossroad at which Ag-DLC coatings currently stands in its application in healthcare. On one hand, the interest of very hard thin films such as DLC is their superior wear-resistance, which help them thrive as environmental surface coatings. On the other hand, the silver segregation towards the surface occurring in harder coatings is detrimental to the full retention of their bioactive properties over time. This outcome has important implications regarding the range of applications of Ag-DLC coatings in their current form. Softer coatings could be used in low-wear applications. Similarly, hard Ag-DLC coatings could potentially be employed on surfaces where their exposure to chemicals and solutions in general is limited.

7.3.2 Catalytic coating for depollution

Worldwide concern over water contamination and the importance of water as vehicle for pathogen transmission made water depollution an appealing option as an area of application for Ag-DLC coatings. Furthermore, the potential of silver as a catalyst in catalytic ozonation processes has already been underlined in the literature [437]. This have prompted the 2PM laboratory to investigate the efficiency of several plasma-deposited coatings, including Ag-DLC thin films, as catalysts in an advanced ozonation process. The ideal role of the coating would be twofold here: 1) release Ag^+ to prevent surface colonization by bacteria and 2) act as a catalyst in the ozone-mediated formation of reactive oxygen species and other reactive species (e.g. OH^\cdot , H_2O_2 , OH^\cdot).

The effectiveness of Ag-DLC coating as a catalyst for an ozonation process was investigated by following the degradation of a model pollutant, pyruvic acid (see Annex B for more details on this study). Silver did have a major effect as a catalyst, significantly increasing the rate of decomposition of ozone in solution. Compared with straightforward ozonation (without catalyst), it more than quadrupled the degradation rate of pyruvic acid. However, it did so by damaging heavily the coating, dissolving most of it after only 1 hour in contact with the ozone-saturated solution. The ozone rapidly oxidized the silver at the surface of the coating and the resulting silver oxide would then be dissolved quickly in the acidic environment generated by the ozone. These findings suggests that Ag-DLC or other silver-based coatings are not sufficiently stable in ozone-rich solutions to be used as catalysts.

7.4 Limitations

7.4.1 Limitations of this study

Firstly, an important aspect that was not addressed so far in this manuscript is the process reproducibility, a crucial element in any large-scale production and a particularly complex issue for plasma-deposited materials. Some reproducibility issues plagued the first year of development of the Ag-DLC coatings, with substrates sometimes emerging from the reactor with no trace of coatings. It was hypothesised that this phenomenon was due to a temperature-induced shift of the deposition-etch equilibrium towards the etch region [438]. A higher temperature at the surface, from the bombarding ions, could lower the sticking coefficient of hydrocarbon species and increase the hydrogen etching rate, leading to overall negative growth. A lack of control over the temperature of the topmost region of the substrates, where the heat from the bombarding plasma was deposited and the temperatures were highest, and the absence of water-cooling on the substrate holder (the metal plate was only air-cooled) complicated any systematic study of the effect of temperature on DLC deposition. Various temporary *in situ* cooling setups were tested, the most successful one being a Peltier cooler, which confirmed the role of temperature in the deposition/etch equilibrium of our deposition system. To permanently circumvent this issue, an “on and off” cycle plasma approach was adopted. A 1 minute cooling period with the discharge turned off was added after each minute of deposition in order to limit surface warming. This was successful in providing reproducible and constant DLC growth rates. However, the range of energies and deposition rates that could be investigated with this method remained limited.

Secondly, several properties, such as the mechanical properties or surface chemistry, were studied over long periods in this project, forming a robust set of data from which some long-term performances could be extrapolated. However, neither the antibacterial properties (maximum study period of 1 day) nor the silver release (maximum study period of 2 weeks) were studied over periods matching the projected lifecycle of the Ag-DLC coatings in their applications. The complexity and gross amount of time required to test the antibacterial properties prevented a more comprehensive long term investigation in the context of this thesis. This limitation suggests that easier and faster methodologies are needed to provide

useful, standardized information on the antibacterial properties that could be used to study materials over longer periods of time and, ideally, satisfy any regulatory concerns.

Finally, this study was not designed to develop Ag-DLC coatings specifically for the investigated applications. Hence, the Ag-DLC coatings properties were certainly not fully optimized whenever they were tested (see section 7.3). Any conclusions emerging from such test therefore needs to be interpreted with caution in regards to trying to analyse or predict any performances of the coatings.

7.4.2 Limitations of Ag-DLC coatings

Despite the interesting potential of Ag-DLC coatings, which was made obvious in the previous chapters, there are important limitations to their application which must be addressed. First and foremost, the segregation occurring in Ag-DLC coatings limits the amount of silver that can be incorporated in the Ag-DLC coatings, especially in the subsurface layers. This is highly problematic since the antibacterial action of Ag-DLC surfaces is mostly based on the release of Ag^+ ions, which, in our case, would be restricted in time due to the limited reservoir in the coatings.

In addition, there are no possibilities to truly regenerate the antibacterial effect of Ag-DLC coatings. Though not a deal-breaker in itself, when combined with the limited reservoir of silver in the current form of the coatings, this becomes much more problematic when considering the potential lifetime of Ag-DLC coatings.

A note of caution is also due here concerning the need of using hard, high- sp^3 DLC coatings as a matrix for the silver nanomaterials. The advantages of using DLC as a matrix for antibacterial coatings might not make up for their disadvantages. The impressive hardness and wear-resistance are not mandatory for all applications discussed in this thesis. Their disadvantages, including the high stress and silver segregation discussed previously, could be easily bypassed simply by using a softer amorphous carbon material as a matrix, with slightly inferior mechanical properties but the same chemical stability, instead of diamond-like carbon. Generally, it seems that exploring the whole range of amorphous carbon coatings and even other carbon-based coatings deposited by plasma, instead of focusing solely on diamond-like carbon, would provide more flexibility and, potentially, more optimal performances.

8 Conclusions and perspectives

The constant threat posed by bacterial colonization of surfaces has led to the emergence of a new paradigm in infection control, with antibacterial coatings taking a central role. This project was undertaken to develop silver-containing diamond-like carbon nanocomposite coatings and assessing their capability as a stable, versatile and tunable material platform for antibacterial applications. Throughout extensive literature review and experimental investigations, I successfully established the potential of Ag-DLC coatings via the following original contributions:

1. Identified and highlighted the design challenges specific to the development of antibacterial coatings for healthcare environmental surfaces;
2. Successfully engineered an *in situ* plasma treatment to promote interfacial adhesion of DLC coating with stainless steel substrates;
3. Devised a model for the growth of Ag-DLC coatings and identified the main mechanisms and plasma parameters governing it;
4. Provided the first evidence of *in vitro* antibacterial efficacy of Ag-DLC coating and investigated potential strategies to modulate the release of Ag⁺ ions;
5. Demonstrated the long-term stability of Ag-DLC coatings through the study of the evolution of its important properties over time.

The challenge now is to design coatings with a better control over the delivery of Ag⁺ ions, while keeping the central idea of high stability in mind. To this end, plasma surface engineering tools, many of which have been already identified in this thesis, still have a lot to offer and should be explored more systematically. Moreover, future investigations could expand the silver-carbon nanocomposite approach to integrate amorphous carbon materials other than DLC, as this would offer more polyvalence and, hopefully better performances in a wider range of applications.

9 References

1. Magill, S.S., J.R. Edwards, W. Bamberg, Z.G. Beldavs, G. Dumyati, M.A. Kainer, R. Lynfield, M. Maloney, L. McAllister-Hollod, J. Nadle, S.M. Ray, D.L. Thompson, L.E. Wilson, and S.K. Fridkin, *Multistate point-prevalence survey of health care-associated infections*. New England Journal of Medicine, 2014. **370**(13): p. 1198-1208.
2. Klevens, R.M., J.R. Edwards, C.L. Richards, Jr., T.C. Horan, R.P. Gaynes, D.A. Pollock, and D.M. Cardo, *Estimating health care-associated infections and deaths in u.S. Hospitals, 2002*. Public Health Reports, 2007. **122**(2): p. 160-6.
3. Coignard, B., L. Lacavé, S. Maugat, J.-M. Thiolet, and A. Firscher, *Enquête nationale de prévalence des infections nosocomiales 2006*, l.d.v. sanitaire, Editor. 2006, France: Paris.
4. Gravel, D., A. Matlow, M. Ofner-Agostini, M. Loeb, L. Johnston, E. Bryce, M.L. Sample, V.R. Roth, C. Goldman, and G. Taylor, *A point prevalence survey of health care-associated infections in pediatric populations in major canadian acute care hospitals*. American journal of infection control, 2007. **35**(3): p. 157-162.
5. Allegranzi, B., S. Nejad Bagheri, G. Garcia Castillejos, C. Kilpatrick, E. Kelley, E. Mathai, and D. Pittet, *Report on the burden of endemic health care-associated infection worldwide*. 2011, World Health Organization.
6. Rutledge-Taylor, K., A. Matlow, D. Gravel, J. Embree, N. Le Saux, L. Johnston, K. Suh, J. Embil, E. Henderson, M. John, V. Roth, A. Wong, J. Shurgold, and G. Taylor, *A point prevalence survey of health care-associated infections in canadian pediatric inpatients*. American Journal of Infection Control, 2012. **40**(6): p. 491-496.
7. Umscheid, C.A., M. Rajender Agarwal MD, M. Kendal Williams MD, and P.J. Brennan, *Estimating the proportion of healthcare-associated infections that are reasonably preventable and the related mortality and costs*. infection control and hospital epidemiology, 2011. **32**(2): p. 101-114.
8. Scott, R.D., *The direct medical costs of healthcare-associated infections in u.S. Hospitals and the benefits of prevention*, D.o.H.Q. Promotion, Editor. 2009.
9. Cole, M., *The true cost of health care associated infection*. Journal of Orthopaedic Nursing, 2008. **12**(3-4): p. 136-138.
10. Dancer, S.J., *Importance of the environment in meticillin-resistant staphylococcus aureus acquisition: The case for hospital cleaning*. The Lancet infectious diseases, 2008. **8**(2): p. 101-113.
11. Bartley, J.M. and R.N. Olmsted, *Reservoirs of pathogens causing health care-associated infections in the 21st century: Is renewed attention to inanimate surfaces warranted?* Clinical Microbiology Newsletter, 2008. **30**(15): p. 113-117.
12. Boyce, J.M., *Environmental contamination makes an important contribution to hospital infection*. Journal of Hospital Infection, 2007. **65**: p. 50-54.
13. Huskins, W.C., C.M. Huckabee, N.P. O'Grady, P. Murray, H. Kopetskie, L. Zimmer, M.E. Walker, R.L. Sinkowitz-Cochran, J.A. Jernigan, M. Samore, D. Wallace, D.A. Goldmann, and S.I.T. Investigators, *Intervention to reduce transmission of resistant bacteria in intensive care*. New England Journal of Medicine, 2011. **364**(15): p. 1407-1418.
14. Gerba, C.P., *Environmentally transmitted pathogens*, in *Environmental microbiology*. 2009, Academic Press. p. 445-484.
15. Wilks, S.A., H. Michels, and C.W. Keevil, *The survival of escherichia coli o157 on a range of metal surfaces*. International Journal of Food Microbiology, 2005. **105**(3): p. 445-454.
16. Curtis, V.A., *Dirt, disgust and disease: A natural history of hygiene*. Journal of Epidemiology and Community Health, 2007. **61**(8): p. 660-664.

17. Horan, T.C., M. Andrus, and M.A. Dudeck, *Cdc/nhsn surveillance definition of health care–associated infection and criteria for specific types of infections in the acute care setting*. American Journal of Infection Control, 2008. **36**(5): p. 309-332.
18. Kambhampati, A., M. Koopmans, and B.A. Lopman, *Burden of norovirus in healthcare facilities and strategies for outbreak control*. Journal of Hospital Infection, 2015. **89**(4): p. 296-301.
19. Sievert, D.M., P. Ricks, J.R. Edwards, A. Schneider, J. Patel, A. Srinivasan, A. Kallen, B. Limbago, and S. Fridkin, *Antimicrobial-resistant pathogens associated with healthcare-associated infections summary of data reported to the national healthcare safety network at the centers for disease control and prevention, 2009–2010*. Infection Control & Hospital Epidemiology, 2013. **34**(01): p. 1-14.
20. Gaynes, R., J.R. Edwards, R.A. Weinstein, and N.N.I.S. System, *Overview of nosocomial infections caused by gram-negative bacilli*. Clinical infectious diseases, 2005. **41**(6): p. 848-854.
21. Allegranzi, B., S.B. Nejad, C. Combescure, W. Graafmans, H. Attar, L. Donaldson, and D. Pittet, *Burden of endemic health-care-associated infection in developing countries: Systematic review and meta-analysis*. The Lancet, 2011. **377**(9761): p. 228-241.
22. Peleg, A.Y. and D.C. Hooper, *Hospital-acquired infections due to gram-negative bacteria*. New England Journal of Medicine, 2010. **362**(19): p. 1804-1813.
23. Siegel, J.D., E. Rhinehart, M. Jackson, and L. Chiarello, *2007 guideline for isolation precautions: Preventing transmission of infectious agents in health care settings*. American journal of infection control, 2007. **35**(10): p. S65-S164.
24. Eyre, D.W., D. Griffiths, A. Vaughan, T. Golubchik, M. Acharya, L. O'Connor, D.W. Crook, A.S. Walker, and T.E. Peto, *Asymptomatic clostridium difficile colonisation and onward transmission*. PloS one, 2013. **8**(11): p. e78445.
25. Boyce, J.M., G. Potter-Bynoe, C. Chenevert, and T. King, *Environmental contamination due to methicillin-resistant staphylococcus aureus possible infection control implications*. Infection Control & Hospital Epidemiology, 1997. **18**(09): p. 622-627.
26. Kramer, A., I. Schwebke, and G. Kampf, *How long do nosocomial pathogens persist on inanimate surfaces? A systematic review*. BMC Infectious Diseases, 2006. **6**(1): p. 130.
27. Otter, J.A., S. Yezli, and G.L. French, *The role played by contaminated surfaces in the transmission of nosocomial pathogens*. Infection Control and Hospital Epidemiology, 2011. **32**(7): p. 687-699.
28. Page, K., M. Wilson, and I.P. Parkin, *Antimicrobial surfaces and their potential in reducing the role of the inanimate environment in the incidence of hospital-acquired infections*. Journal of Materials Chemistry, 2009. **19**(23): p. 3819-3831.
29. Allegranzi, B. and D. Pittet, *Role of hand hygiene in healthcare-associated infection prevention*. Journal of Hospital Infection, 2009. **73**(4): p. 305-315.
30. Pittet, D., S. Hugonnet, S. Harbarth, P. Mourouga, V. Sauvan, S. Touveneau, and T.V. Perneger, *Effectiveness of a hospital-wide programme to improve compliance with hand hygiene*. The Lancet, 2000. **356**(9238): p. 1307-1312.
31. Garner, J.S., *Guideline for isolation precautions in hospitals*. Infection Control & Hospital Epidemiology, 1996. **17**(01): p. 54-80.
32. Emori, T.G. and R.P. Gaynes, *An overview of nosocomial infections, including the role of the microbiology laboratory*. Clinical microbiology reviews, 1993. **6**(4): p. 428-442.
33. Weber, D.J., E.E. Sickbert-Bennett, C.V. Gould, V.M. Brown, K. Huslage, and W.A. Rutala, *Incidence of catheter-associated and non-catheter-associated urinary tract infections in a healthcare system*. Infection Control & Hospital Epidemiology, 2011. **32**(08): p. 822-823.

34. Joseph, N.M., S. Sistla, T.K. Dutta, A.S. Badhe, and S.C. Parija, *Ventilator-associated pneumonia: A review*. European Journal of Internal Medicine, 2010. **21**(5): p. 360-368.
35. Control, C.f.D. and Prevention, *Vital signs: Central line-associated blood stream infections—united states, 2001, 2008, and 2009*. Annals of Emergency Medicine, 2011. **58**(5): p. 447-450.
36. Weber, D.J., W.A. Rutala, M.B. Miller, K. Huslage, and E. Sickbert-Bennett, *Role of hospital surfaces in the transmission of emerging health care-associated pathogens: Norovirus, clostridium difficile, and acinetobacter species*. American journal of infection control, 2010. **38**(5): p. S25-S33.
37. Boyce, J.M., N.L. Havill, J.A. Otter, L.C. McDonald, N.M. Adams, T. Cooper, A. Thompson, L. Wiggs, G. Killgore, and A. Tauman, *Impact of hydrogen peroxide vapor room decontamination on clostridium difficile environmental contamination and transmission in a healthcare setting*. Infection Control & Hospital Epidemiology, 2008. **29**(08): p. 723-729.
38. Wilcox, M., W. Fawley, N. Wigglesworth, P. Parnell, P. Verity, and J. Freeman, *Comparison of the effect of detergent versus hypochlorite cleaning on environmental contamination and incidence of clostridium difficile infection*. Journal of Hospital Infection, 2003. **54**(2): p. 109-114.
39. Dancer, S., *The role of environmental cleaning in the control of hospital-acquired infection*. Journal of hospital Infection, 2009. **73**(4): p. 378-385.
40. Lemmen, S.W., H. Häfner, D. Zolldann, S. Stanzel, and R. Lütticken, *Distribution of multi-resistant gram-negative versus gram-positive bacteria in the hospital inanimate environment*. Journal of Hospital Infection, 2004. **56**(3): p. 191-197.
41. Sigler, V. and S. Hensley, *Persistence of mixed staphylococci assemblages following disinfection of hospital room surfaces*. Journal of Hospital Infection, 2013. **83**(3): p. 253-256.
42. Duckro, A.N., D.W. Blom, E.A. Lyle, R.A. Weinstein, and M.K. Hayden, *Transfer of vancomycin-resistant enterococci via health care worker hands*. Archives of internal medicine, 2005. **165**(3): p. 302-307.
43. Bhalla, A., N.J. Pultz, D.M. Gries, A.J. Ray, E.C. Eckstein, D.C. Aron, and C.J. Donskey, *Acquisition of nosocomial pathogens on hands after contact with environmental surfaces near hospitalized patients*. Infection Control and Hospital Epidemiology, 2004. **25**(2): p. 164-167.
44. Munoz-Price, L.S., D.J. Birnbach, D.A. Lubarsky, K.L. Arheart, Y. Fajardo-Aquino, M. Rosalsky, T. Cleary, D. DePascale, G. Coro, and N. Namias, *Decreasing operating room environmental pathogen contamination through improved cleaning practice*. Infection Control & Hospital Epidemiology, 2012. **33**(09): p. 897-904.
45. Wenzel, R.P. and M.B. Edmond, *Infection control: The case for horizontal rather than vertical interventional programs*. International Journal of Infectious Diseases, 2010. **14**: p. S3-S5.
46. Dancer, S., *Mopping up hospital infection*. Journal of hospital infection, 1999. **43**(2): p. 85-100.
47. Donskey, C.J., *Does improving surface cleaning and disinfection reduce health care-associated infections?* American journal of infection control, 2013. **41**(5): p. S12-S19.
48. Alfa, M.J., E. Lo, N. Olson, M. MacRae, and L. Buelow-Smith, *Use of a daily disinfectant cleaner instead of a daily cleaner reduced hospital-acquired infection rates*. American journal of infection control, 2015. **43**(2): p. 141-146.

49. Rutala, W.A. and D.J. Weber, *Are room decontamination units needed to prevent transmission of environmental pathogens?* Infection Control & Hospital Epidemiology, 2011. **32**(08): p. 743-747.
50. Dettenkofer, M. and C. Block, *Hospital disinfection: Efficacy and safety issues.* Current Opinion in Infectious Diseases, 2005. **18**(4): p. 320-325.
51. Jelden, K.C., S.G. Gibbs, P.W. Smith, A.L. Hewlett, P.C. Iwen, K.K. Schmid, and J.J. Lowe, *Comparison of hospital room surface disinfection using a novel ultraviolet germicidal irradiation (uvgi) generator.* Journal of Occupational and Environmental Hygiene, 2016. **13**(9): p. 690-698.
52. Todar, K., *Todar's online textbook of bacteriology.* 2006: University of Wisconsin-Madison Department of Bacteriology.
53. Brown, L., J.M. Wolf, R. Prados-Rosales, and A. Casadevall, *Through the wall: Extracellular vesicles in gram-positive bacteria, mycobacteria and fungi.* Nature Reviews Microbiology, 2015. **13**(10): p. 620-630.
54. O'Toole, G., H.B. Kaplan, and R. Kolter, *Biofilm formation as microbial development.* Annual Review of Microbiology, 2000. **54**: p. 49-79.
55. Costerton, J.W., P.S. Stewart, and E.P. Greenberg, *Bacterial biofilms: A common cause of persistent infections.* Science, 1999. **284**(5418): p. 1318-22.
56. Potera, C., *Biofilms invade microbiology.* Science, 1996. **273**(5283): p. 1795-7.
57. Mah, T.-F.C. and G.A. O'Toole, *Mechanisms of biofilm resistance to antimicrobial agents.* Trends in Microbiology, 2001. **9**(1): p. 34-39.
58. Stewart, P.S. and J.W. Costerton, *Antibiotic resistance of bacteria in biofilms.* The Lancet, 2001. **358**(9276): p. 135-138.
59. Phillips, K.S., D. Patwardhan, and G. Jayan, *Biofilms, medical devices, and antibiofilm technology: Key messages from a recent public workshop.* American journal of infection control, 2015. **43**(1): p. 2-3.
60. O'Toole, G.A. and R. Kolter, *Initiation of biofilm formation in pseudomonas fluorescens wcs365 proceeds via multiple, convergent signalling pathways: A genetic analysis.* Molecular Microbiology, 1998. **28**(3): p. 449-461.
61. Palmer Jr, R.J. and D.C. White, *Developmental biology of biofilms: Implications for treatment and control.* Trends in Microbiology, 1997. **5**(11): p. 435-440.
62. Spellberg, B., J.G. Bartlett, and D.N. Gilbert *The future of antibiotics and resistance.* New England Journal of Medicine, 2013. **368**(4): p. 299-302.
63. Spellberg, B., R. Guidos, D. Gilbert, J. Bradley, H.W. Boucher, W.M. Scheld, J.G. Bartlett, J. Edwards, and I.D.S.o. America, *The epidemic of antibiotic-resistant infections: A call to action for the medical community from the infectious diseases society of america.* Clinical Infectious Diseases, 2008. **46**(2): p. 155-164.
64. Blair, J.M.A., M.A. Webber, A.J. Baylay, D.O. Ogbolu, and L.J.V. Piddock, *Molecular mechanisms of antibiotic resistance.* Nature Reviews Microbiology, 2015. **13**(1): p. 42-51.
65. Lemire, J.A., J.J. Harrison, and R.J. Turner, *Antimicrobial activity of metals: Mechanisms, molecular targets and applications.* Nature Reviews Microbiology, 2013. **11**(6): p. 371-384.
66. Russell, A., *Antibiotic and biocide resistance in bacteria: Introduction.* Journal of Applied Microbiology, 2002. **92**(s1): p. 1S-3S.
67. Lara, H.H., N.V. Ayala-Nunez, L.D.I. Turrent, and C.R. Padilla, *Bactericidal effect of silver nanoparticles against multidrug-resistant bacteria.* World Journal of Microbiology & Biotechnology, 2010. **26**(4): p. 615-621.
68. Kohanski, M.A., D.J. Dwyer, and J.J. Collins, *How antibiotics kill bacteria: From targets to networks.* Nature Reviews Microbiology, 2010. **8**(6): p. 423-435.

69. Lok, C.N., C.M. Ho, R. Chen, Q.Y. He, W.Y. Yu, H. Sun, P.K.H. Tam, J.F. Chiu, and C.M. Che, *Silver nanoparticles: Partial oxidation and antibacterial activities*. Journal of Biological Inorganic Chemistry, 2007. **12**(4): p. 527-534.
70. Lok, C.N., C.M. Ho, R. Chen, Q.Y. He, W.Y. Yu, H.Z. Sun, P.K.H. Tam, J.F. Chiu, and C.M. Che, *Proteomic analysis of the mode of antibacterial action of silver nanoparticles*. Journal of Proteome Research, 2006. **5**(4): p. 916-924.
71. Morones, J.R., J.L. Elechiguerra, A. Camacho, K. Holt, J.B. Kouri, J.T. Ramirez, and M.J. Yacaman, *The bactericidal effect of silver nanoparticles*. Nanotechnology, 2005. **16**(10): p. 2346-2353.
72. Lee, D., R.E. Cohen, and M.F. Rubner, *Antibacterial properties of ag nanoparticle loaded multilayers and formation of magnetically directed antibacterial microparticles*. Langmuir, 2005. **21**(21): p. 9651-9659.
73. Feng, Q.L., J. Wu, G.Q. Chen, F.Z. Cui, T.N. Kim, and J.O. Kim, *A mechanistic study of the antibacterial effect of silver ions on escherichia coli and staphylococcus aureus*. Journal of biomedical materials research, 2000. **52**(4): p. 662-668.
74. Yamanaka, M., K. Hara, and J. Kudo, *Bactericidal actions of a silver ion solution on escherichia coli, studied by energy-filtering transmission electron microscopy and proteomic analysis*. Applied and Environmental Microbiology, 2005. **71**(11): p. 7589-7593.
75. Liao, S.Y., D.C. Read, W.J. Pugh, J.R. Furr, and A.D. Russell, *Interaction of silver nitrate with readily identifiable groups: Relationship to the antibacterial action of silver ions*. Letters in Applied Microbiology, 1997. **25**(4): p. 279-283.
76. Clement, J.L. and P.S. Jarrett, *Antibacterial silver*. Met Based Drugs, 1994. **1**(5-6): p. 467-82.
77. Holt, K.B. and A.J. Bard, *Interaction of silver(i) ions with the respiratory chain of escherichia coli: An electrochemical and scanning electrochemical microscopy study of the antimicrobial mechanism of micromolar ag*. Biochemistry, 2005. **44**(39): p. 13214-13223.
78. Emamifar, A., *Applications of antimicrobial polymer nanocomposites in food packaging*. Advances in nanocomposite technology. 2011.
79. Schreurs, W.J. and H. Rosenberg, *Effect of silver ions on transport and retention of phosphate by escherichia coli*. Journal of Bacteriology, 1982. **152**(1): p. 7-13.
80. Gupta, A., M. Maynes, and S. Silver, *Effects of halides on plasmid-mediated silver resistance in escherichia coli*. Applied and Environmental Microbiology, 1998. **64**(12): p. 5042-5045.
81. Davies, R.L. and S.F. Etris, *The development and functions of silver in water purification and disease control*. Catalysis Today, 1997. **36**(1): p. 107-114.
82. Martinez-Castanon, G.A., N. Nino-Martinez, F. Martinez-Gutierrez, J.R. Martinez-Mendoza, and F. Ruiz, *Synthesis and antibacterial activity of silver nanoparticles with different sizes*. Journal of Nanoparticle Research, 2008. **10**(8): p. 1343-1348.
83. Pal, S., Y.K. Tak, and J.M. Song, *Does the antibacterial activity of silver nanoparticles depend on the shape of the nanoparticle? A study of the gram-negative bacterium escherichia coli*. Applied and Environmental Microbiology, 2007. **73**(6): p. 1712-1720.
84. Le Pape, H., F. Solano-Serena, P. Contini, C. Devillers, A. Maftah, and P. Leprat, *Evaluation of the anti-microbial properties of an activated carbon fibre supporting silver using a dynamic method*. Carbon, 2002. **40**(15): p. 2947-2954.
85. Le Pape, H., F. Solano-Serena, P. Contini, C. Devillers, A. Maftah, and P. Leprat, *Involvement of reactive oxygen species in the bactericidal activity of activated carbon fibre supporting silver bactericidal activity of acf(ag) mediated by ros*. Journal of Inorganic Biochemistry, 2004. **98**(6): p. 1054-1060.

86. Morones-Ramirez, J.R., J.A. Winkler, C.S. Spina, and J.J. Collins, *Silver enhances antibiotic activity against gram-negative bacteria*. *Science Translational Medicine*, 2013. **5**(190): p. 190ra81.
87. Kaegi, R., A. Voegelin, C. Ort, B. Sinnet, B. Thalmann, J. Krismer, H. Hagendorfer, M. Elumelu, and E. Mueller, *Fate and transformation of silver nanoparticles in urban wastewater systems*. *Water Research*, 2013. **47**(12): p. 3866–3877.
88. Gottschalk, F. and B. Nowack, *The release of engineered nanomaterials to the environment*. *Journal of Environmental Monitoring*, 2011. **13**(5): p. 1145-1155.
89. Nel, A., T. Xia, L. Madler, and N. Li, *Toxic potential of materials at the nanolevel*. *Science*, 2006. **311**(5761): p. 622-7.
90. Ratte, H.T., *Bioaccumulation and toxicity of silver compounds: A review*. *Environmental Toxicology and Chemistry*, 1999. **18**(1): p. 89-108.
91. Wijnhoven, S.W., W.J. Peijnenburg, C.A. Herberths, W.I. Hagens, A.G. Oomen, E.H. Heugens, B. Roszek, J. Bisschops, I. Gosens, and D. Van De Meent, *Nano-silver—a review of available data and knowledge gaps in human and environmental risk assessment*. *Nanotoxicology*, 2009. **3**(2): p. 109-138.
92. Chu, P.K., J.Y. Chen, L.P. Wang, and N. Huang, *Plasma-surface modification of biomaterials*. *Materials Science & Engineering R-Reports*, 2002. **36**(5-6): p. 143-206.
93. Bogaerts, A., E. Neyts, R. Gijbels, and J. van der Mullen, *Gas discharge plasmas and their applications*. *Spectrochimica Acta Part B: Atomic Spectroscopy*, 2002. **57**(4): p. 609-658.
94. Mott-Smith, H.M., *History of "plasmas"*. *Nature*, 1971. **233**: p. 219.
95. Boulos, M.I., P. Fauchais, and E. Pfender, *Thermal plasmas: Fundamentals and applications*. 2013: Springer Science & Business Media.
96. Lieberman, M.A. and A.J. Lichtenberg, *Principles of plasma discharges and materials processing*. 2005: John Wiley & Sons.
97. Hayakawa, S., *Handbook of sputter deposition technology: Principles, technology, and applications*. 1992: William Andrew Publishing.
98. Konuma, M., *Reactions in plasmas*, in *Film deposition by plasma techniques*. 1992, Springer. p. 11-48.
99. Lide, D.R., *Crc handbook of chemistry and physics*. Vol. 85. 2004: CRC press.
100. Berkowitz, J., J. Greene, H. Cho, and B. Ruscić, *The ionization potentials of ch4 and cd4*. *The Journal of chemical physics*, 1987. **86**(2): p. 674-676.
101. Harry, J.E., *Introduction to plasma technology: Science, engineering, and applications*. 2013: John Wiley & Sons.
102. Von Keudell, A., *Surface processes during thin-film growth*. *Plasma Sources Science and Technology*, 2000. **9**(4): p. 455.
103. Edelberg, E.A. and E.S. Aydil, *Modeling of the sheath and the energy distribution of ions bombarding rf-biased substrates in high density plasma reactors and comparison to experimental measurements*. *Journal of Applied Physics*, 1999. **86**(9): p. 4799-4812.
104. Robertson, J., *Deposition mechanism of diamond-like carbon and cubic boron nitride*. *Radiation Effects and Defects in Solids*, 1997. **142**(1-4): p. 63-90.
105. Wild, C. and P. Koidl, *Ion and electron dynamics in the sheath of radiofrequency glow-discharges*. *Journal of Applied Physics*, 1991. **69**(5): p. 2909-2922.
106. Robertson, J., *Diamond-like amorphous carbon*. *Materials Science & Engineering R-Reports*, 2002. **37**(4-6): p. 129-281.
107. Takagi, T., *Ion-surface interactions during thin film deposition*. *Journal of Vacuum Science & Technology A*, 1984. **2**(2): p. 382-388.

108. Denes, F.S. and S. Manolache, *Macromolecular plasma-chemistry: An emerging field of polymer science*. Progress in Polymer Science, 2004. **29**(8): p. 815-885.
109. Lewis, F., M. Cloutier, P. Chevallier, S. Turgeon, J.J. Pireaux, M. Tatoulian, and D. Mantovani, *Influence of the 316 l stainless steel interface on the stability and barrier properties of plasma fluorocarbon films*. ACS Applied Materials & Interfaces, 2011. **3**(7): p. 2323-2331.
110. Cloutier, M., S. Turgeon, P. Chevallier, and D. Mantovani, *On the interface between plasma fluorocarbon films and 316l stainless steel substrates for advanced coated stents*. Advanced Materials Research, 2011. **409**: p. 117-122.
111. Choy, K.L., *Chemical vapour deposition of coatings*. Progress in Materials Science, 2003. **48**(2): p. 57-170.
112. Maya, P.N., U. von Toussaint, and W. Jacob, *What makes a dangling bond a binding site for thermal ch3 radicals? — a combined molecular dynamics and potential energy analysis study on amorphous hydrocarbon films*. Diamond and Related Materials, 2013. **40**(0): p. 41-50.
113. Laegreid, N. and G. Wehner, *Sputtering yields of metals for ar+ and ne+ ions with energies from 50 to 600 ev*. Journal of Applied Physics, 1961. **32**(3): p. 365-369.
114. Donnelly, V.M. and A. Kornblit, *Plasma etching: Yesterday, today, and tomorrow*. Journal of Vacuum Science & Technology A, 2013. **31**(5): p. 050825.
115. Morshed, M.M., D.C. Cameron, B.P. McNamara, and M.S.J. Hashmi, *Pre-treatment of substrates for improved adhesion of diamond-like carbon films on surgically implantable metals deposited by saddle field neutral beam source*. Surface & Coatings Technology, 2003. **174**: p. 579-583.
116. Lewis, F., P. Horny, P. Hale, S. Turgeon, M. Tatoulian, and D. Mantovani, *Study of the adhesion of thin plasma fluorocarbon coatings resisting plastic deformation for stent applications*. Journal of Physics D-Applied Physics, 2008. **41**(4): p. 045310.
117. Pierson, J.F., D. Wiederkehr, and A. Billard, *Reactive magnetron sputtering of copper, silver, and gold*. Thin Solid Films, 2005. **478**(1–2): p. 196-205.
118. Kelly, P. and R. Arnell, *Magnetron sputtering: A review of recent developments and applications*. Vacuum, 2000. **56**(3): p. 159-172.
119. Gogolides, E., V. Constantoudis, G. Kokkoris, D. Kontziampasis, K. Tsougeni, G. Boulousis, M. Vlachopoulou, and A. Tserepi, *Controlling roughness: From etching to nanotexturing and plasma-directed organization on organic and inorganic materials*. Journal of Physics D: Applied Physics, 2011. **44**(17): p. 174021.
120. Valbusa, U., C. Boragno, and F.B. de Mongeot, *Nanostructuring surfaces by ion sputtering*. Journal of Physics: Condensed Matter, 2002. **14**(35): p. 8153.
121. Lewis, F., S. Turgeon, P. Chevallier, J.J. Pireaux, M. Tatoulian, and D. Mantovani, *On the growth of fluorocarbon thin films deposited on plasma-etched 316l stainless steel*. Plasma Processes and Polymers, 2010. **7**(3-4): p. 309-317.
122. Lifshitz, Y., G.D. Lempert, and E. Grossman, *Substantiation of subplantation model for diamondlike film growth by atomic force microscopy*. Physical Review Letters, 1994. **72**(17): p. 2753-2756.
123. Yasuda, H., A.K. Sharma, E.B. Hale, and W.J. James, *Atomic interfacial mixing to create water insensitive adhesion*. The Journal of Adhesion, 1982. **13**(3-4): p. 269-283.
124. Walton, S.G. and J.E. Greene, *Chapter 2 - plasmas in deposition processes*, in *Handbook of deposition technologies for films and coatings (third edition)*, M.M. Peter, Editor. 2010, William Andrew Publishing: Boston. p. 32-92.

125. Robertson, J., *Plasma deposition of diamond-like carbon*. Japanese Journal of Applied Physics, 2011. **50**(1): p. 01AF01.
126. Martinu, L., O. Zabeida, and J.E. Klemberg-Sapieha, *Chapter 9 - plasma-enhanced chemical vapor deposition of functional coatings*, in *Handbook of deposition technologies for films and coatings (third edition)*, M.M. Peter, Editor. 2010, William Andrew Publishing: Boston. p. 392-465.
127. Martinu, L. and D. Poitras, *Plasma deposition of optical films and coatings: A review*. Journal of Vacuum Science & Technology A, 2000. **18**(6): p. 2619-2645.
128. Zhou, J., I.T. Martin, R. Ayers, E. Adams, D.P. Liu, and E.R. Fisher, *Investigation of inductively coupled ar and ch₄/ar plasmas and the effect of ion energy on dlc film properties*. Plasma Sources Science & Technology, 2006. **15**(4): p. 714-726.
129. Li, H., T. Xu, J. Chen, H. Zhou, and H. Liu, *The effect of applied dc bias voltage on the properties of ac: H films prepared in a dual dc-rf plasma system*. Applied surface science, 2004. **227**(1): p. 364-372.
130. Maître, N., T. Girardeau, S. Camelio, A. Barranco, D. Vouagner, and E. Breille, *Effects of negative low self-bias on hydrogenated amorphous carbon films deposited by pecvd technique*. Diamond and Related Materials, 2003. **12**(3-7): p. 988-992.
131. Caschera, D., P. Cossari, F. Federici, S. Kaciulis, A. Mezzi, G. Padeletti, and D.M. Trucchi, *Influence of pecvd parameters on the properties of diamond-like carbon films*. Thin Solid Films, 2011. **519**(12): p. 4087-4091.
132. Lifshitz, Y., *Hydrogen-free amorphous carbon films: Correlation between growth conditions and properties*. Diamond and Related Materials, 1996. **5**(3-5): p. 388-400.
133. Kim, Y., S. Cho, W. Choi, B. Hong, and D. Yoon, *Dependence of the bonding structure of dlc thin films on the deposition conditions of pecvd method*. Surface and Coatings Technology, 2003. **169**: p. 291-294.
134. Sun, Z., S. Xu, and K.N. Ostrikov, *E and h regimes of plasma enhanced chemical vapor deposition of diamond-like carbon film in low frequency inductively coupled plasma reactor*. Diamond and Related Materials, 2002. **11**(1): p. 92-97.
135. Sattel, S., J. Robertson, and H. Ehrhardt, *Effects of deposition temperature on the properties of hydrogenated tetrahedral amorphous carbon*. Journal of Applied Physics, 1997. **82**(9): p. 4566-4576.
136. Wänstrand, O., M. Larsson, and P. Hedenqvist, *Mechanical and tribological evaluation of pvd wc/c coatings*. Surface and Coatings Technology, 1999. **111**(2-3): p. 247-254.
137. Wang, D.-Y., K.-W. Weng, and S.-Y. Hwang, *Study on metal-doped diamond-like carbon films synthesized by cathodic arc evaporation*. Diamond and Related Materials, 2000. **9**(9-10): p. 1762-1766.
138. Ronkainen, H., S. Varjus, and K. Holmberg, *Tribological performance of different dlc coatings in water-lubricated conditions*. Wear, 2001. **249**(3-4): p. 267-271.
139. Grill, A., *Diamond-like carbon: State of the art*. Diamond and Related Materials, 1999. **8**(2-5): p. 428-434.
140. Casiraghi, C., J. Robertson, and A.C. Ferrari, *Diamond-like carbon for data and beer storage*. Materials Today, 2007. **10**(1-2): p. 44-53.
141. Robertson, J., *The deposition mechanism of diamond-like ac and ac: H*. Diamond and Related Materials, 1994. **3**(4): p. 361-368.
142. Lifshitz, Y., S.R. Kasi, and J.W. Rabalais, *Subplantation model for film growth from hyperthermal species - application to diamond*. Physical Review Letters, 1989. **62**(11): p. 1290-1293.

143. Robertson, J., *Diamond-like carbon*. Pure and Applied Chemistry, 1994. **66**(9): p. 1789-1796.
144. Fallon, P.J., V.S. Veerasamy, C.A. Davis, J. Robertson, G.A.J. Amaratunga, W.I. Milne, and J. Koskinen, *Properties of filtered-ion-beam-deposited diamond-like carbon as a function of ion energy*. Physical Review B, 1993. **48**(7): p. 4777-4782.
145. Erdemir, A., I.B. Nilufer, O.L. Eryilmaz, M. Beschliesser, and G.R. Fenske, *Friction and wear performance of diamond-like carbon films grown in various source gas plasmas*. Surface & Coatings Technology, 1999. **121**: p. 589-593.
146. Grill, A., *Diamond-like carbon coatings as biocompatible materials - an overview*. Diamond and Related Materials, 2003. **12**(2): p. 166-170.
147. Roy, R.K. and K.R. Lee, *Biomedical applications of diamond-like carbon coatings: A review*. Journal of Biomedical Materials Research Part B-Applied Biomaterials, 2007. **83B**(1): p. 72-84.
148. Thorwarth, G., B. Saldamli, F. Schwarz, P. Jurgens, C. Leiggner, R. Sader, M. Haeberlen, W. Assmann, and B. Stritzker, *Biocompatibility of doped diamond-like carbon coatings for medical implants*. Plasma Processes and Polymers, 2007. **4**: p. S364-S368.
149. Tillmann, W., E. Vogli, and F. Hoffmann, *Wear-resistant and low-friction diamond-like-carbon (dlc)-layers for industrial tribological applications under humid conditions*. Surface & Coatings Technology, 2009. **204**(6-7): p. 1040-1045.
150. Bentzon, M.D., K. Mogensen, J.B. Hansen, C. Barholmansen, C. Traeholt, P. Holiday, and S.S. Eskildsen, *Metallic interlayers between steel and diamond-like carbon*. Surface & Coatings Technology, 1994. **68**: p. 651-655.
151. Franceschini, D.F., C.A. Achete, and F.L. Freire, *Internal-stress reduction by nitrogen incorporation in hard amorphous-carbon thin-films*. Applied Physics Letters, 1992. **60**(26): p. 3229-3231.
152. Ugolini, D., J. Eitle, and P. Oelhafen, *Influence of process gas and deposition energy on the atomic and electronic-structure of diamond-like (a-c-h) films*. Vacuum, 1990. **41**(4-6): p. 1374-1377.
153. Segura-Giraldo, B., E. Restrepo-Parra, and P.J. Arango-Arango, *On the influence of a tin interlayer on dlc coatings produced by pulsed vacuum arc discharge: Compositional and morphological study*. Applied Surface Science, 2009. **256**(1): p. 136-141.
154. Kirinuki, M., A. Tomita, M. Kusuda, Y. Oka, A. Murakami, and M. Yatsuzuka, *Enhancement of adhesive strength of dlc film by plasma-based ion implantation*. New Frontiers of Processing and Engineering in Advanced Materials, 2005. **502**: p. 315-320.
155. Walter, K.C., M. Nastasi, and C. Munson, *Adherent diamond-like carbon coatings on metals via plasma source ion implantation*. Surface and Coatings Technology, 1997. **93**(2-3): p. 287-291.
156. Yatsuzuka, M., Y. Oka, M. Nishijima, and K. Hiraga, *Microstructure of interface for high-adhesion dlc film on metal substrates by plasma-based ion implantation*. Vacuum, 2008. **83**(1): p. 190-197.
157. Chilkoti, A. and J.A.E. Hubbell, *Biointerface science [special issue]*. MRS Bulletin, 2005. **30**(03): p. 175-210.
158. McBryde, E., L. Bradley, M. Whitby, and D. McElwain, *An investigation of contact transmission of methicillin-resistant staphylococcus aureus*. Journal of Hospital Infection, 2004. **58**(2): p. 104-108.
159. Zarb, P., B. Coignard, J. Griskeviciene, A. Muller, V. Vankerckhoven, K. Weist, M. Goossens, S. Vaerenberg, S. Hopkins, B. Catry, D. Monnet, H. Goossens, and C. Suetens, *The european centre for disease prevention and control (ecdc) pilot point prevalence survey of*

- healthcare-associated infections and antimicrobial use*. Euro surveillance: bulletin europeen sur les maladies transmissibles = European communicable disease bulletin, 2012. **17**(46): p. 20316.
160. Pasquarella, C., G.E. Sansebastiano, S. Ferretti, E. Sacconi, M. Fanti, U. Moscato, G. Giannetti, S. Fornia, P. Cortellini, P. Vitali, and C. Signorelli, *A mobile laminar airflow unit to reduce air bacterial contamination at surgical area in a conventionally ventilated operating theatre*. The Journal of hospital infection, 2007. **66**(4): p. 313-319.
 161. Glinel, K., P. Thebault, V. Humblot, C.M. Pradier, and T. Jouenne, *Antibacterial surfaces developed from bio-inspired approaches*. Acta Biomaterialia, 2012. **8**(5): p. 1670-1684.
 162. Fox, J.L., *Antimicrobial peptides stage a comeback*. Nature Biotechnology, 2013. **31**(5): p. 379-382.
 163. Salwiczek, M., Y. Qu, J. Gardiner, R.A. Strugnell, T. Lithgow, K.M. McLean, and H. Thissen, *Emerging rules for effective antimicrobial coatings*. Trends in Biotechnology, 2014. **32**(2): p. 82-90.
 164. Green, J.-B.D., T. Fulghum, and M.A. Nordhaus, *A review of immobilized antimicrobial agents and methods for testing*. Biointerphases, 2011. **6**(4): p. MR13-MR28.
 165. Banerjee, I., R.C. Pangule, and R.S. Kane, *Antifouling coatings: Recent developments in the design of surfaces that prevent fouling by proteins, bacteria, and marine organisms*. Advanced Materials, 2011. **23**(6): p. 690-718.
 166. Campoccia, D., L. Montanaro, and C.R. Arciola, *A review of the biomaterials technologies for infection-resistant surfaces*. Biomaterials, 2013. **34**(34): p. 8533-8554.
 167. Tiller, J.C., C.J. Liao, K. Lewis, and A.M. Klibanov, *Designing surfaces that kill bacteria on contact*. Proceedings of the National Academy of Sciences of the United States of America, 2001. **98**(11): p. 5981-5985.
 168. Lewis, K. and A.M. Klibanov, *Surpassing nature: Rational design of sterile-surface materials*. Trends in Biotechnology, 2005. **23**(7): p. 343-348.
 169. Dunne, W.M., *Bacterial adhesion: Seen any good biofilms lately?* Clinical microbiology reviews, 2002. **15**(2): p. 155-166.
 170. Friedlander, R.S., H. Vlamakis, P. Kim, M. Khan, R. Kolter, and J. Aizenberg, *Bacterial flagella explore microscale hummocks and hollows to increase adhesion*. Proceedings of the National Academy of Sciences of the United States of America, 2013. **110**(14): p. 5624-5629.
 171. Hasan, J., R.J. Crawford, and E.P. Ivanova, *Antibacterial surfaces: The quest for a new generation of biomaterials*. Trends in Biotechnology, 2013. **31**(5): p. 295-304.
 172. Variola, F., S.F. Zalzal, A. Leduc, J. Barbeau, and A. Nanci, *Oxidative nanopatterning of titanium generates mesoporous surfaces with antimicrobial properties*. International journal of nanomedicine, 2014. **9**: p. 2319-25.
 173. Zilberman, M. and J.J. Elsner, *Antibiotic-eluting medical devices for various applications*. Journal of Controlled Release, 2008. **130**(3): p. 202-215.
 174. Kazemzadeh-Narbat, M., B.F.L. Lai, C. Ding, J.N. Kizhakkedathu, R.E.W. Hancock, and R. Wang, *Multilayered coating on titanium for controlled release of antimicrobial peptides for the prevention of implant-associated infections*. Biomaterials, 2013. **34**(24): p. 5969-5977.
 175. Brogden, K.A., *Antimicrobial peptides: Pore formers or metabolic inhibitors in bacteria?* Nature Reviews Microbiology, 2005. **3**(3): p. 238-250.
 176. Chaloupka, K., Y. Malam, and A.M. Seifalian, *Nanosilver as a new generation of nanoparticle in biomedical applications*. Trends in Biotechnology, 2010. **28**(11): p. 580-588.

177. Eckhardt, S., P.S. Brunetto, J. Gagnon, M. Priebe, B. Giese, and K.M. Fromm, *Nanobio silver: Its interactions with peptides and bacteria, and its uses in medicine*. Chemical Reviews, 2013. **113**(7): p. 4708-4754.
178. Jin, G., H. Qin, H. Cao, S. Qian, Y. Zhao, X. Peng, X. Zhang, X. Liu, and P.K. Chu, *Synergistic effects of dual zn/ag ion implantation in osteogenic activity and antibacterial ability of titanium*. Biomaterials, 2014. **35**(27): p. 7699-7713.
179. Samani, S., S.M. Hossainipour, M. Tamizifar, and H.R. Rezaie, *In vitro antibacterial evaluation of sol-gel-derived zn-, ag-, and (zn + ag)-doped hydroxyapatite coatings against methicillin-resistant staphylococcus aureus*. Journal of Biomedical Materials Research Part A, 2013. **101**(1): p. 222-230.
180. Kelson, A.B., M. Carnevali, and V. Truong-Le, *Gallium-based anti-infectives: Targeting microbial iron-uptake mechanisms*. Current opinion in pharmacology, 2013. **13**(5): p. 707-716.
181. Tran, P.A. and T.J. Webster, *Antimicrobial selenium nanoparticle coatings on polymeric medical devices*. Nanotechnology, 2013. **24**(15): p. 155101.
182. Rodríguez-Valencia, C., M. López-Álvarez, B. Cochón-Cores, I. Pereiro, J. Serra, and P. González, *Novel selenium-doped hydroxyapatite coatings for biomedical applications*. Journal of Biomedical Materials Research Part A, 2013. **101**(3): p. 853-861.
183. Shirai, T., T. Shimizu, K. Ohtani, Y. Zen, M. Takaya, and H. Tsuchiya, *Antibacterial iodine-supported titanium implants*. Acta Biomaterialia, 2011. **7**(4): p. 1928-1933.
184. Eby, D.M., H.R. Luckarift, and G.R. Johnson, *Hybrid antimicrobial enzyme and silver nanoparticle coatings for medical instruments*. ACS Applied Materials & Interfaces, 2009. **1**(7): p. 1553-1560.
185. Zhou, B., Y. Li, H. Deng, Y. Hu, and B. Li, *Antibacterial multilayer films fabricated by layer-by-layer immobilizing lysozyme and gold nanoparticles on nanofibers*. Colloids and Surfaces B: Biointerfaces, 2014. **116**(0): p. 432-438.
186. Ivanova, K., M.M. Fernandes, E. Mendoza, and T. Tzanov, *Enzyme multilayer coatings inhibit pseudomonas aeruginosa biofilm formation on urinary catheters*. Applied microbiology and biotechnology, 2015. **99**(10): p. 4373-4385.
187. Carmona-Ribeiro, A.M. and L.D. de Melo Carrasco, *Cationic antimicrobial polymers and their assemblies*. International journal of molecular sciences, 2013. **14**(5): p. 9906-9946.
188. Zhao, L., P.K. Chu, Y. Zhang, and Z. Wu, *Antibacterial coatings on titanium implants*. Journal of Biomedical Materials Research Part B: Applied Biomaterials, 2009. **91B**(1): p. 470-480.
189. Baier, G., A. Cavallaro, K. Friedemann, B. Müller, G. Glasser, K. Vasilev, and K. Landfester, *Enzymatic degradation of poly(l-lactide) nanoparticles followed by the release of octenidine and their bactericidal effects*. Nanomedicine: Nanotechnology, Biology and Medicine, 2014. **10**(1): p. 131-139.
190. Chua, P.-H., K.-G. Neoh, E.-T. Kang, and W. Wang, *Surface functionalization of titanium with hyaluronic acid/chitosan polyelectrolyte multilayers and rgd for promoting osteoblast functions and inhibiting bacterial adhesion*. Biomaterials, 2008. **29**(10): p. 1412-1421.
191. Vasilev, K., J. Cook, and H.J. Griesser, *Antibacterial surfaces for biomedical devices*. Expert Review of Medical Devices, 2009. **6**(5): p. 553-567.
192. Baveja, J.K., M.D.P. Willcox, E.B.H. Hume, N. Kumar, R. Odell, and L.A. Poole-Warren, *Furanones as potential anti-bacterial coatings on biomaterials*. Biomaterials, 2004. **25**(20): p. 5003-5012.

193. Wang, Z., C. Jiang, Y. Cao, and Y. Ding, *Systematic review and meta-analysis of triclosan-coated sutures for the prevention of surgical-site infection*. British Journal of Surgery, 2013. **100**(4): p. 465-473.
194. Weber, D.J. and W.A. Rutala, *Self-disinfecting surfaces: Review of current methodologies and future prospects*. American Journal of Infection Control, 2013. **41**(5): p. S31-S35.
195. Storm, W.L., J.A. Johnson, B.V. Worley, D.L. Slomberg, and M.H. Schoenfisch, *Dual action antimicrobial surfaces via combined nitric oxide and silver release*. Journal of biomedical materials research. Part A, 2015. **103**(6): p. 1974-1984.
196. Carpenter, A.W. and M.H. Schoenfisch, *Nitric oxide release: Part ii. Therapeutic applications*. Chemical Society Reviews, 2012. **41**(10): p. 3742-3752.
197. Michl, T.D., B.R. Coad, M. Doran, M. Osiecki, M.H. Kafshgari, N.H. Voelcker, A. Hüsler, K. Vasilev, and H.J. Griesser, *Nitric oxide releasing plasma polymer coating with bacteriostatic properties and no cytotoxic side effects*. Chemical Communications, 2015. **51**(32): p. 7058-7060.
198. Rtimi, S., O. Baghriche, C. Pulgarin, J.-C. Lavanchy, and J. Kiwi, *Growth of tio₂/cu films by hipims for accelerated bacterial loss of viability*. Surface and Coatings Technology, 2013. **232**: p. 804-813.
199. Darouiche, R.O., I.I. Raad, S.O. Heard, J.I. Thornby, O.C. Wenker, A. Gabrielli, J. Berg, N. Khardori, H. Hanna, R. Hachem, R.L. Harris, and G. Mayhall, *A comparison of two antimicrobial-impregnated central venous catheters*. New England Journal of Medicine, 1999. **340**(1): p. 1-8.
200. Rupp, M.E., T. Fitzgerald, N. Marion, V. Helget, S. Puumala, J.R. Anderson, and P.D. Fey, *Effect of silver-coated urinary catheters: Efficacy, cost-effectiveness, and antimicrobial resistance*. American Journal of Infection Control, 2004. **32**(8): p. 445-450.
201. Casey, A.L., L.A. Mermel, P. Nightingale, and T.S. Elliott, *Antimicrobial central venous catheters in adults: A systematic review and meta-analysis*. The Lancet infectious diseases, 2008. **8**(12): p. 763-776.
202. Williams, D.L., K.D. Sinclair, S. Jeyapalina, and R.D. Bloebaum, *Characterization of a novel active release coating to prevent biofilm implant-related infections*. Journal of Biomedical Materials Research Part B: Applied Biomaterials, 2013. **101**(6): p. 1078-1089.
203. Arvaniti, K., D. Lathyris, P. Clouva-Molyvdas, A.B. Haidich, E. Mouloudi, E. Synnefaki, V. Koulourida, D. Georgopoulos, N. Gerogianni, G. Nakos, and D. Matamis, *Comparison of oligon catheters and chlorhexidine-impregnated sponges with standard multilumen central venous catheters for prevention of associated colonization and infections in intensive care unit patients: A multicenter, randomized, controlled study*. Critical care medicine, 2012. **40**(2): p. 420-429.
204. Tiller, J.C., *Antimicrobial surfaces*, in *Bioactive surfaces*, H.G. Börner and J.-F. Lutz, Editors. 2011, Springer Berlin Heidelberg. p. 193-217.
205. Imamovic, L. and M.O.A. Sommer, *Use of collateral sensitivity networks to design drug cycling protocols that avoid resistance development*. Science Translational Medicine, 2013. **5**(204): p. 204ra132.
206. Ling, L.L., T. Schneider, A.J. Peoples, A.L. Spoering, I. Engels, B.P. Conlon, A. Mueller, T.F. Schaberle, D.E. Hughes, S. Epstein, M. Jones, L. Lazarides, V.A. Steadman, D.R. Cohen, C.R. Felix, K.A. Fetterman, W.P. Millett, A.G. Nitti, A.M. Zullo, C. Chen, and K. Lewis, *A new antibiotic kills pathogens without detectable resistance*. Nature, 2015. **517**(7535): p. 455-459.
207. Sintim, H.O., J.A. Smith, J. Wang, S. Nakayama, and L. Yan, *Paradigm shift in discovering next-generation anti-infective agents: Targeting quorum sensing, c-di-gmp signaling and*

- biofilm formation in bacteria with small molecules*. Future medicinal chemistry, 2010. **2**(6): p. 1005-1035.
208. Chua, S.L., Y. Liu, J.K.H. Yam, Y. Chen, R.M. Vejborg, B.G.C. Tan, S. Kjelleberg, T. Tolker-Nielsen, M. Givskov, and L. Yang, *Dispersed cells represent a distinct stage in the transition from bacterial biofilm to planktonic lifestyles*. Nature Communications, 2014. **5**: p. 1-12.
 209. Lichter, J.A., K.J. Van Vliet, and M.F. Rubner, *Design of antibacterial surfaces and interfaces: Polyelectrolyte multilayers as a multifunctional platform*. Macromolecules, 2009. **42**(22): p. 8573-8586.
 210. Hetrick, E.M. and M.H. Schoenfisch, *Reducing implant-related infections: Active release strategies*. Chemical Society Reviews, 2006. **35**(9): p. 780-789.
 211. Ng, V.W.L., J.M.W. Chan, H. Sardon, R.J. Ono, J.M. García, Y.Y. Yang, and J.L. Hedrick, *Antimicrobial hydrogels: A new weapon in the arsenal against multidrug-resistant infections*. Advanced Drug Delivery Reviews, 2014. **78**(0): p. 46-62.
 212. Vasilev, K., S.S. Griesser, and H.J. Griesser, *Antibacterial surfaces and coatings produced by plasma techniques*. Plasma Processes and Polymers, 2011. **8**(11): p. 1010-1023.
 213. Bai, X., K. More, C.M. Rouleau, and A. Rabiei, *Functionally graded hydroxyapatite coatings doped with antibacterial components*. Acta Biomaterialia, 2010. **6**(6): p. 2264-2273.
 214. Anguita-Alonso, P., A. Giacometti, O. Cirioni, R. Ghiselli, F. Orlando, V. Saba, G. Scalise, M. Sevo, M. Tuzova, and R. Patel, *Rniii-inhibiting-peptide-loaded polymethylmethacrylate prevents in vivo staphylococcus aureus biofilm formation*. Antimicrobial agents and chemotherapy, 2007. **51**(7): p. 2594-2596.
 215. Barraud, N., D. Schleheck, J. Klebensberger, J.S. Webb, D.J. Hassett, S.A. Rice, and S. Kjelleberg, *Nitric oxide signaling in pseudomonas aeruginosa biofilms mediates phosphodiesterase activity, decreased cyclic di-gmp levels, and enhanced dispersal*. Journal of Bacteriology, 2009. **191**(23): p. 7333-7342.
 216. Hetrick, E.M., J.H. Shin, H.S. Paul, and M.H. Schoenfisch, *Anti-biofilm efficacy of nitric oxide-releasing silica nanoparticles*. Biomaterials, 2009. **30**(14): p. 2782-2789.
 217. Charville, G.W., E.M. Hetrick, C.B. Geer, and M.H. Schoenfisch, *Reduced bacterial adhesion to fibrinogen-coated substrates via nitric oxide release*. Biomaterials, 2008. **29**(30): p. 4039-4044.
 218. Busscher, H.J., H.C. van der Mei, G. Subbiahdoss, P.C. Jutte, J.J.A.M. van den Dungen, S.A.J. Zaat, M.J. Schultz, and D.W. Grainger, *Biomaterial-associated infection: Locating the finish line in the race for the surface*. Science Translational Medicine, 2012. **4**(153): p. 153rv10.
 219. Zarie, E.S., V. Kaidas, D. Gedamu, Y.K. Mishra, R. Adelung, F.H. Furkert, R. Scherließ, H. Steckel, and B. Groessner-Schreiber, *Solvent free fabrication of micro and nanostructured drug coatings by thermal evaporation for controlled release and increased effects*. PloS one, 2012. **7**(8): p. e40746.
 220. Cheng, H., Y. Li, K. Huo, B. Gao, and W. Xiong, *Long-lasting in vivo and in vitro antibacterial ability of nanostructured titania coating incorporated with silver nanoparticles*. Journal of Biomedical Materials Research Part A, 2014. **102**(10): p. 3488-3499.
 221. Hughes, G.A., *Nanostructure-mediated drug delivery*. Nanomedicine: Nanotechnology, Biology and Medicine, 2005. **1**(1): p. 22-30.
 222. Hsu, B.B., M.-H. Park, S.R. Hagerman, and P.T. Hammond, *Multimonth controlled small molecule release from biodegradable thin films*. Proceedings of the National Academy of Sciences, 2014. **111**(33): p. 12175-12180.
 223. Jo, Y.S., J. Gantz, J.A. Hubbell, and M.P. Lutolf, *Tailoring hydrogel degradation and drug release via neighboring amino acid controlled ester hydrolysis*. Soft Matter, 2009. **5**(2): p. 440-446.

224. Kwok, C.S., T.A. Horbett, and B.D. Ratner, *Design of infection-resistant antibiotic-releasing polymers: II. Controlled release of antibiotics through a plasma-deposited thin film barrier*. Journal of Controlled Release, 1999. **62**(3): p. 301-311.
225. Yin, B., T. Liu, and Y. Yin, *Prolonging the duration of preventing bacterial adhesion of nanosilver-containing polymer films through hydrophobicity*. Langmuir, 2012. **28**(49): p. 17019-17025.
226. Hagiwara, K., T. Hasebe, and A. Hotta, *Effects of plasma treatments on the controlled drug release from poly(ethylene-co-vinyl acetate)*. Surface and Coatings Technology, 2013. **216**(0): p. 318-323.
227. Seddiki, O., C. Harnagea, L. Levesque, D. Mantovani, and F. Rosei, *Evidence of antibacterial activity on titanium surfaces through nanotextures*. Applied Surface Science, 2014. **308**(0): p. 275-284.
228. Thatiparti, T.R., A.J. Shoffstall, and H.A. von Recum, *Cyclodextrin-based device coatings for affinity-based release of antibiotics*. Biomaterials, 2010. **31**(8): p. 2335-2347.
229. Vasilev, K., V. Sah, K. Anselme, C. Ndi, M. Mateescu, B. Dollmann, P. Martinek, H. Ys, L. Ploux, and H.J. Griesser, *Tunable antibacterial coatings that support mammalian cell growth*. Nano Letters, 2009. **10**(1): p. 202-207.
230. Zhao, L., H. Wang, K. Huo, L. Cui, W. Zhang, H. Ni, Y. Zhang, Z. Wu, and P.K. Chu, *Antibacterial nano-structured titania coating incorporated with silver nanoparticles*. Biomaterials, 2011. **32**(24): p. 5706-5716.
231. Alarcon, C.d.I.H., S. Pennadam, and C. Alexander, *Stimuli responsive polymers for biomedical applications*. Chemical Society Reviews, 2005. **34**(3): p. 276-285.
232. Stuart, M.A.C., W.T.S. Huck, J. Genzer, M. Muller, C. Ober, M. Stamm, G.B. Sukhorukov, I. Szleifer, V.V. Tsukruk, M. Urban, F. Winnik, S. Zauscher, I. Luzinov, and S. Minko, *Emerging applications of stimuli-responsive polymer materials*. Nature Materials, 2010. **9**(2): p. 101-113.
233. Roy, D., J.N. Cambre, and B.S. Sumerlin, *Future perspectives and recent advances in stimuli-responsive materials*. Progress in Polymer Science, 2010. **35**(1-2): p. 278-301.
234. Esrafilzadeh, D., J.M. Razal, S.E. Moulton, E.M. Stewart, and G.G. Wallace, *Multifunctional conducting fibres with electrically controlled release of ciprofloxacin*. Journal of Controlled Release, 2013. **169**(3): p. 313-320.
235. Hu, B., N. Wang, L. Han, M.-L. Chen, and J.-H. Wang, *Core-shell-shell nanorods for controlled release of silver that can serve as a nanoheater for photothermal treatment on bacteria*. Acta Biomaterialia, 2015. **11**(0): p. 511-519.
236. Norris, P., M. Noble, I. Francolini, A.M. Vinogradov, P.S. Stewart, B.D. Ratner, J.W. Costerton, and P. Stoodley, *Ultrasonically controlled release of ciprofloxacin from self-assembled coatings on poly(2-hydroxyethyl methacrylate) hydrogels for pseudomonas aeruginosa biofilm prevention*. Antimicrobial Agents and Chemotherapy, 2005. **49**(10): p. 4272-4279.
237. Noble, M.L., P.D. Mourad, and B.D. Ratner, *Digital drug delivery: On-off ultrasound controlled antibiotic release from coated matrices with negligible background leaching*. Biomaterials Science, 2014. **2**(6): p. 893-902.
238. Wang, H., J. Yi, S. Mukherjee, P. Banerjee, and S. Zhou, *Magnetic/nir-thermally responsive hybrid nanogels for optical temperature sensing, tumor cell imaging and triggered drug release*. Nanoscale, 2014. **6**(21): p. 13001-13011.
239. Shchukin, D.G. and H. Möhwald, *Self-repairing coatings containing active nanoreservoirs*. Small, 2007. **3**(6): p. 926-943.

240. Gerber, L.C., F.M. Koehler, R.N. Grass, and W.J. Stark, *Incorporation of penicillin-producing fungi into living materials to provide chemically active and antibiotic-releasing surfaces*. *Angewandte Chemie*, 2012. **124**(45): p. 11455-11458.
241. Borges, J., L.C. Rodrigues, R.L. Reis, and J.F. Mano, *Layer-by-layer assembly of light-responsive polymeric multilayer systems*. *Advanced Functional Materials*, 2014. **24**(36): p. 5624-5648.
242. Black, K.C.L., T.S. Sileika, J. Yi, R. Zhang, J.G. Rivera, and P.B. Messersmith, *Bacterial killing by light-triggered release of silver from biomimetic metal nanorods*. *Small*, 2014. **10**(1): p. 169-178.
243. Gallo, J., M. Holinka, and C.S. Moucha, *Antibacterial surface treatment for orthopaedic implants*. *International journal of molecular sciences*, 2014. **15**(8): p. 13849-13880.
244. Shchukin, D. and H. Möhwald, *A coat of many functions*. *Science*, 2013. **341**(6153): p. 1458-1459.
245. Traba, C. and J.F. Liang, *Bacteria responsive antibacterial surfaces for indwelling device infections*. *Journal of Controlled Release*, 2015. **198**(0): p. 18-25.
246. Zhuk, I., F. Jariwala, A.B. Attygalle, Y. Wu, M.R. Libera, and S.A. Sukhishvili, *Self-defensive layer-by-layer films with bacteria-triggered antibiotic release*. *ACS Nano*, 2014. **8**(8): p. 7733-7745.
247. Pavluchina, S., Y. Lu, A. Patimetha, M. Libera, and S. Sukhishvili, *Polymer multilayers with ph-triggered release of antibacterial agents*. *Biomacromolecules*, 2010. **11**(12): p. 3448-3456.
248. Pavluchina, S., I. Zhuk, A. Mentbayeva, E. Rautenberg, W. Chang, X. Yu, B. van de Belt-Gritter, H.J. Busscher, H.C. van der Mei, and S.A. Sukhishvili, *Small-molecule-hosting nanocomposite films with multiple bacteria-triggered responses*. *NPG Asia Materials*, 2014. **6**: p. e121.
249. Pichavant, L., G. Amador, C. Jacqueline, B. Brouillaud, V. Héroguez, and M.-C. Durrieu, *Ph-controlled delivery of gentamicin sulfate from orthopedic devices preventing nosocomial infections*. *Journal of Controlled Release*, 2012. **162**(2): p. 373-381.
250. Tanihara, M., Y. Suzuki, Y. Nishimura, K. Suzuki, Y. Kakimaru, and Y. Fukunishi, *A novel microbial infection-responsive drug release system*. *Journal of Pharmaceutical Sciences*, 1999. **88**(5): p. 510-514.
251. Komnatnyy, V.V., W.-C. Chiang, T. Tolker-Nielsen, M. Givskov, and T.E. Nielsen, *Bacteria-triggered release of antimicrobial agents*. *Angewandte Chemie*, 2014. **126**(2): p. 449-451.
252. Cado, G., R. Aslam, L. Séon, T. Garnier, R. Fabre, A. Parat, A. Chassepot, J.C. Voegel, B. Senger, F. Schneider, Y. Frère, L. Jierry, P. Schaaf, H. Kerdjoudj, M.H. Metz-Boutigue, and F. Boulmedais, *Self-defensive biomaterial coating against bacteria and yeasts: Polysaccharide multilayer film with embedded antimicrobial peptide*. *Advanced Functional Materials*, 2013. **23**(38): p. 4801-4809.
253. Cottarel, G. and J. Wierzbowski, *Combination drugs, an emerging option for antibacterial therapy*. *Trends in Biotechnology*, 2007. **25**(12): p. 547-555.
254. Raad, I., R. Darouiche, R. Hachem, M. Mansouri, and G.P. Bodey, *The broad-spectrum activity and efficacy of catheters coated with minocycline and rifampin*. *Journal of Infectious Diseases*, 1996. **173**(2): p. 418-424.
255. Kohnen, W., C. Kolbensschlag, S. Teske-Keiser, and B. Jansen, *Development of a long-lasting ventricular catheter impregnated with a combination of antibiotics*. *Biomaterials*, 2003. **24**(26): p. 4865-4869.
256. Holzapfel, B.M., J.C. Reichert, J.-T. Schantz, U. Gbureck, L. Rackwitz, U. Nöth, F. Jakob, M. Rudert, J. Groll, and D.W. Hutmacher, *How smart do biomaterials need to be? A*

- translational science and clinical point of view*. *Advanced Drug Delivery Reviews*, 2013. **65**(4): p. 581-603.
257. Fayaz, A.M., K. Balaji, M. Girilal, R. Yadav, P.T. Kalaichelvan, and R. Venketesan, *Biogenic synthesis of silver nanoparticles and their synergistic effect with antibiotics: A study against gram-positive and gram-negative bacteria*. *Nanomedicine: Nanotechnology, Biology and Medicine*, 2010. **6**(1): p. 103-109.
 258. Varisco, M., N. Khanna, P.S. Brunetto, and K.M. Fromm, *New antimicrobial and biocompatible implant coating with synergic silver–vancomycin conjugate action*. *ChemMedChem*, 2014. **9**(6): p. 1221-1230.
 259. Li, Z., D. Lee, X.X. Sheng, R.E. Cohen, and M.F. Rubner, *Two-level antibacterial coating with both release-killing and contact-killing capabilities*. *Langmuir*, 2006. **22**(24): p. 9820-9823.
 260. Worley, B.V., D.L. Slomberg, and M.H. Schoenfisch, *Nitric oxide-releasing quaternary ammonium-modified poly(amidoamine) dendrimers as dual action antibacterial agents*. *Bioconjugate Chemistry*, 2014. **25**(5): p. 918-927.
 261. Ho, C.H., J. Tobis, C. Sprich, R. Thomann, and J.C. Tiller, *Nanoseparated polymeric networks with multiple antimicrobial properties*. *Advanced Materials*, 2004. **16**(12): p. 957-961.
 262. Hu, R., G. Li, Y. Jiang, Y. Zhang, J.-J. Zou, L. Wang, and X. Zhang, *Silver–zwitterion organic–inorganic nanocomposite with antimicrobial and antiadhesive capabilities*. *Langmuir*, 2013. **29**(11): p. 3773-3779.
 263. Yu, Q., Z. Wu, and H. Chen, *Dual-function antibacterial surfaces for biomedical applications*. *Acta Biomaterialia*, 2015. **16**(0): p. 1-13.
 264. Jia, W.Y., M.W. Beatty, R.A. Reinhardt, T.M. Petro, D.M. Cohen, C.R. Maze, E.A. Strom, and M. Hoffman, *Nickel release from orthodontic arch wires and cellular immune response to various nickel concentrations*. *Journal of Biomedical Materials Research*, 1999. **48**(4): p. 488-495.
 265. Poitout, D.G., K.G. Thorngren, and R. Kotz, *Biomechanics and biomaterials in orthopedics*. 2004, London, UK: Springer.
 266. Variola, F., F. Vetrone, L. Richert, P. Jedrzejowski, J.-H. Yi, S. Zalzal, S. Clair, A. Sarkissian, D.F. Perepichka, J.D. Wuest, F. Rosei, and A. Nanci, *Improving biocompatibility of implantable metals by nanoscale modification of surfaces: An overview of strategies, fabrication methods, and challenges*. *Small*, 2009. **5**(9): p. 996-1006.
 267. Cloutier, M., R. Tolouei, O. Lesage, L. Lévesque, S. Turgeon, M. Tatoulian, and D. Mantovani, *On the long term antibacterial features of silver-doped diamondlike carbon coatings deposited via a hybrid plasma process*. *Biointerphases*, 2014. **9**(2): p. 029013.
 268. Goodman, S.B., Z. Yao, M. Keeney, and F. Yang, *The future of biologic coatings for orthopaedic implants*. *Biomaterials*, 2013. **34**(13): p. 3174-3183.
 269. Chen, D., M. Wu, J. Chen, C. Zhang, T. Pan, B. Zhang, H. Tian, X. Chen, and J. Sun, *Robust, flexible, and bioadhesive free-standing films for the co-delivery of antibiotics and growth factors*. *Langmuir*, 2014. **30**(46): p. 13898-13906.
 270. Wong, S.Y., J.S. Moskowitz, J. Veselinovic, R.A. Rosario, K. Timachova, M.R. Blaisse, R.C. Fuller, A.M. Klibanov, and P.T. Hammond, *Dual functional polyelectrolyte multilayer coatings for implants: Permanent microbicidal base with controlled release of therapeutic agents*. *Journal of the American Chemical Society*, 2010. **132**(50): p. 17840-17848.
 271. Frost, M.C., M.M. Reynolds, and M.E. Meyerhoff, *Polymers incorporating nitric oxide releasing/generating substances for improved biocompatibility of blood-contacting medical devices*. *Biomaterials*, 2005. **26**(14): p. 1685-1693.

272. Tugulu, S. and H.-A. Klok, *Stability and nonfouling properties of poly(poly(ethylene glycol) methacrylate) brushes under cell culture conditions*. *Biomacromolecules*, 2008. **9**(3): p. 906-912.
273. Pidhatika, B., M. Rodenstein, Y. Chen, E. Rakhmatullina, A. Mühlebach, C. Acikgöz, M. Textor, and R. Konradi, *Comparative stability studies of poly(2-methyl-2-oxazoline) and poly(ethylene glycol) brush coatings*. *Biointerphases*, 2012. **7**(1-4): p. 1-15.
274. Roosjen, A., J. de Vries, H.C. van der Mei, W. Norde, and H.J. Busscher, *Stability and effectiveness against bacterial adhesion of poly(ethylene oxide) coatings in biological fluids*. *Journal of Biomedical Materials Research Part B: Applied Biomaterials*, 2005. **73**(2): p. 347-354.
275. Ramsden, J.J., D.M. Allen, D.J. Stephenson, J.R. Alcock, G. Peggs, G. Fuller, and G. Goch, *The design and manufacture of biomedical surfaces*. *CIRP Annals-Manufacturing Technology*, 2007. **56**(2): p. 687-711.
276. Thom, K.A., H.C. Standiford, J.K. Johnson, N. Hanna, and J.P. Furuno, *Effectiveness of an antimicrobial polymer to decrease contamination of environmental surfaces in the clinical setting*. *Infection Control & Hospital Epidemiology*, 2014. **35**(08): p. 1060-1062.
277. Airey, P. and J. Verran, *Potential use of copper as a hygienic surface; problems associated with cumulative soiling and cleaning*. *Journal of Hospital Infection*, 2007. **67**(3): p. 271-277.
278. Cloutier, M., C. Harnagea, P. Hale, O. Seddiki, F. Rosei, and D. Mantovani, *Long-term stability of hydrogenated dlc coatings: Effects of aging on the structural, chemical and mechanical properties*. *Diamond and Related Materials*, 2014. **48**: p. 65-72.
279. Duday, D., C. Vreuls, M. Moreno, G. Frache, N.D. Boscher, G. Zocchi, C. Archambeau, C. Van De Weerd, J. Martial, and P. Choquet, *Atmospheric pressure plasma modified surfaces for immobilization of antimicrobial nisin peptides*. *Surface and Coatings Technology*, 2013. **218**(0): p. 152-161.
280. Roy, M., G.A. Fielding, H. Beyenal, A. Bandyopadhyay, and S. Bose, *Mechanical, in vitro antimicrobial, and biological properties of plasma-sprayed silver-doped hydroxyapatite coating*. *ACS Applied Materials & Interfaces*, 2012. **4**(3): p. 1341-1349.
281. Martin, P.M., *Handbook of deposition technologies for films and coatings: Science, technology and applications (3rd edition)*. 3rd ed, ed. P.M. Martin. 2010, Boston: William Andrew Publishing.
282. Serrano, C., L. García-Fernández, J.P. Fernández-Blázquez, M. Barbeck, S. Ghanaati, R. Unger, J. Kirkpatrick, E. Arzt, L. Funk, P. Turón, and A. del Campo, *Nanostructured medical sutures with antibacterial properties*. *Biomaterials*, 2015. **52**(0): p. 291-300.
283. Zhao, Y., M.I. James, W.K. Li, G. Wu, C. Wang, Y. Zheng, K.W. Yeung, and P.K. Chu, *Enhanced antimicrobial properties, cytocompatibility, and corrosion resistance of plasma-modified biodegradable magnesium alloys*. *Acta biomaterialia*, 2014. **10**(1): p. 544-556.
284. Zimmermann, R., A. Pfuch, K. Horn, J. Weisser, A. Heft, M. Röder, R. Linke, M. Schnabelrauch, and A. Schimanski, *An approach to create silver containing antibacterial coatings by use of atmospheric pressure plasma chemical vapour deposition (apcVD) and combustion chemical vapour deposition (ccVD) in an economic way*. *Plasma Processes and Polymers*, 2011. **8**(4): p. 295-304.
285. Vaz, J.M., E.C. Michel, P. Chevallier, M.M. Beppu, and D. Mantovani, *Covalent grafting of chitosan on plasma-treated polytetrafluoroethylene surfaces for biomedical applications*. *Journal of Biomaterials and Tissue Engineering*, 2014. **4**(11): p. 915-924.
286. Grainger, D.W., H.C. van der Mei, P.C. Jutte, J.J.A.M. van den Dungen, M.J. Schultz, B.F.A.M. van der Laan, S.A.J. Zaat, and H.J. Busscher, *Critical factors in the translation of*

- improved antimicrobial strategies for medical implants and devices*. *Biomaterials*, 2013. **34**(37): p. 9237-9243.
287. Moriarty, T., D. Grainger, and R. Richards, *Challenges in linking preclinical anti-microbial research strategies with clinical outcomes for device-associated infections*. *European Cells & Materials*, 2014. **28**: p. 112-128.
 288. Zhang, M., R.R. Naik, and L. Dai, *Carbon nanomaterials for biomedical applications*. Vol. 5. 2015: Springer.
 289. Jariwala, D., V.K. Sangwan, L.J. Lauhon, T.J. Marks, and M.C. Hersam, *Carbon nanomaterials for electronics, optoelectronics, photovoltaics, and sensing*. *Chemical Society Reviews*, 2013. **42**(7): p. 2824-2860.
 290. Cloutier, M., S. Turgeon, Y. Busby, M. Tatoulian, J.J. Pireaux, and D. Mantovani, *Controlled distribution and clustering of silver in ag-dlc nanocomposite coatings using a hybrid plasma approach*. *ACS Applied Materials & Interfaces*, 2016. **8**(32): p. 21020-21027.
 291. Khun, N.W. and E. Liu, *Investigation of structure, adhesion strength, wear performance and corrosion behavior of platinum/ruthenium/nitrogen doped diamond-like carbon thin films with respect to film thickness*. *Materials Chemistry and Physics*, 2011. **126**(1-2): p. 220-226.
 292. Paul, R., S. Hussain, and A.K. Pal, *Characterization of nanocrystalline gold/dlc composite films synthesized by plasma cvd technique*. *Applied Surface Science*, 2009. **255**(18): p. 8076-8083.
 293. Zhao, Q., Y. Liu, C. Wang, and S. Wang, *Evaluation of bacterial adhesion on si-doped diamond-like carbon films*. *Applied Surface Science*, 2007. **253**(17): p. 7254-7259.
 294. Hauert, R., K. Thorwarth, and G. Thorwarth, *An overview on diamond-like carbon coatings in medical applications*. *Surface and Coatings Technology*, 2013.
 295. Dearnaley, G. and J.H. Arps, *Biomedical applications of diamond-like carbon (dlc) coatings: A review*. *Surface & Coatings Technology*, 2005. **200**(7): p. 2518-2524.
 296. McKenzie, D.R., D. Muller, and B.A. Pailthorpe, *Compressive-stress-induced formation of thin-film tetrahedral amorphous carbon*. *Physical Review Letters*, 1991. **67**(6): p. 773-776.
 297. Peng, X.L. and T.W. Clyne, *Residual stress and debonding of dlc films on metallic substrates*. *Diamond and Related Materials*, 1998. **7**(7): p. 944-950.
 298. Ferrari, A., B. Kleinsorge, N. Morrison, A. Hart, V. Stolojan, and J. Robertson, *Stress reduction and bond stability during thermal annealing of tetrahedral amorphous carbon*. *Journal of Applied Physics*, 1999. **85**(10): p. 7191-7197.
 299. Li, X., P. Guo, L. Sun, A. Wang, and P. Ke, *Ab initio investigation on cu/cr codoped amorphous carbon nanocomposite films with giant residual stress reduction*. *ACS applied materials & interfaces*, 2015. **7**(50): p. 27878-27884.
 300. Ding, Q., L. Wang, Y. Wang, S. Wang, L. Hu, and Q. Xue, *Improved tribological behavior of dlc films under water lubrication by surface texturing*. *Tribology letters*, 2011. **41**(2): p. 439-449.
 301. Bonetti, L., G. Capote, L. Santos, E. Corat, and V. Trava-Airoldi, *Adhesion studies of diamond-like carbon films deposited on ti6al4v substrate with a silicon interlayer*. *Thin Solid Films*, 2006. **515**(1): p. 375-379.
 302. Hauert, R., G. Thorwarth, U. Müller, M. Stiefel, C.V. Falub, K. Thorwarth, and T.J. Joyce, *Analysis of the in-vivo failure of the adhesive interlayer for a dlc coated articulating metatarsophalangeal joint*. *Diamond and Related Materials*, 2012. **25**(0): p. 34-39.
 303. Chen, C.-C. and F.C.-N. Hong, *Interfacial studies for improving the adhesion of diamond-like carbon films on steel*. *Applied Surface Science*, 2005. **243**(1-4): p. 296-303.

304. Haidopoulos, M., S. Turgeon, C. Sarra-Bournet, G. Laroche, and D. Mantovani, *Development of an optimized electrochemical process for subsequent coating of 316 stainless steel for stent applications*. Journal of Materials Science-Materials in Medicine, 2006. **17**(7): p. 647-657.
305. Robertson, J., *Mechanism of sp(3) bond formation in the growth of diamond-like carbon*. Diamond and Related Materials, 2005. **14**(3-7): p. 942-948.
306. Von Keudell, A. and W. Möller, *A combined plasma-surface model for the deposition of c: H films from a methane plasma*. Journal of applied physics, 1994. **75**(12): p. 7718-7727.
307. Biesinger, M.C., B.P. Payne, A.P. Grosvenor, L.W.M. Lau, A.R. Gerson, and R.S.C. Smart, *Resolving surface chemical states in xps analysis of first row transition metals, oxides and hydroxides: Cr, mn, fe, co and ni*. Applied Surface Science, 2011. **257**(7): p. 2717-2730.
308. Müller, U., C.V. Falub, G. Thorwarth, C. Voisard, and R. Hauert, *Diamond-like carbon coatings on a cocrmo implant alloy: A detailed xps analysis of the chemical states at the interface*. Acta Materialia, 2011. **59**(3): p. 1150-1161.
309. Kawamura, E., V. Vahedi, M. Lieberman, and C. Birdsall, *Ion energy distributions in rf sheaths; review, analysis and simulation*. Plasma Sources Science and Technology, 1999. **8**(3): p. R45.
310. Goretzki, H., P.v. Rosenstiel, and S. Mandziej, *Small area mxps-and tem-measurements on temper-embrittled 12% cr steel*. Fresenius' Journal of Analytical Chemistry, 1989. **333**(4): p. 451-452.
311. Andersson, M., J. Högström, S. Urbonaitė, A. Furlan, L. Nyholm, and U. Jansson, *Deposition and characterization of magnetron sputtered amorphous cr-c films*. Vacuum, 2012. **86**(9): p. 1408-1416.
312. Sinharoy, S. and L.L. Levenson, *The formation and decomposition of nickel carbide in evaporated nickel films on graphite*. Thin Solid Films, 1978. **53**(1): p. 31-36.
313. Kovács, G.J., I. Bertóti, and G. Radnóczy, *X-ray photoelectron spectroscopic study of magnetron sputtered carbon-nickel composite films*. Thin Solid Films, 2008. **516**(21): p. 7942-7946.
314. Furlan, A., U. Jansson, J. Lu, L. Hultman, and M. Magnuson, *Structure and bonding in amorphous iron carbide thin films*. Journal of Physics: Condensed Matter, 2015. **27**(4): p. 045002.
315. Shabanova, I. and V. Trapeznikov, *A study of the electronic structure of fe 3 c, fe 3 al and fe 3 si by x-ray photoelectron spectroscopy*. Journal of Electron Spectroscopy and Related Phenomena, 1975. **6**(4): p. 297-307.
316. Salvi, A.M., J.E. Castle, J.F. Watts, and E. Desimoni, *Peak fitting of the chromium 2p xps spectrum*. Applied Surface Science, 1995. **90**(3): p. 333-341.
317. Detroye, M., F. Reniers, C. Buess-Herman, and J. Vereecken, *Aes-xps study of chromium carbides and chromium iron carbides*. Applied Surface Science, 1999. **144-145**(0): p. 78-82.
318. Agarwal, V., V.D. Vankar, and K.L. Chopra, *Reactive-magnetron-sputtered chromium carbide films*. Thin Solid Films, 1989. **169**(2): p. 281-288.
319. Zhou, M., *Exceptional properties by design*. Science, 2013. **339**(6124): p. 1161-1162.
320. Cloutier, M., D. Mantovani, and F. Rosei, *Antibacterial coatings: Challenges, perspectives, and opportunities*. Trends in Biotechnology, 2015. **33**(11): p. 637-652.
321. Bogdanović, U., V. Vodnik, M. Mitrić, S. Dimitrijević, S.D. Škapin, V. Žunič, M. Budimir, and M. Stoiljković, *Nanomaterial with high antimicrobial efficacy—copper/polyaniline nanocomposite*. ACS Applied Materials & Interfaces, 2015. **7**(3): p. 1955-1966.

322. Coleman, J.N., U. Khan, W.J. Blau, and Y.K. Gun'ko, *Small but strong: A review of the mechanical properties of carbon nanotube–polymer composites*. Carbon, 2006. **44**(9): p. 1624-1652.
323. Dwivedi, N., S. Kumar, J.D. Carey, R.K. Tripathi, H.K. Malik, and M.K. Dalai, *Influence of silver incorporation on the structural and electrical properties of diamond-like carbon thin films*. ACS Applied Materials & Interfaces, 2013. **5**(7): p. 2725-2732.
324. Wu, S., X. Liu, A. Yeung, K.W.K. Yeung, R.Y.T. Kao, G. Wu, T. Hu, Z. Xu, and P.K. Chu, *Plasma-modified biomaterials for self-antimicrobial applications*. ACS Applied Materials & Interfaces, 2011. **3**(8): p. 2851-2860.
325. Schiffmann, K.I., M. Fryda, G. Goerigk, R. Lauer, P. Hinze, and A. Bulack, *Sizes and distances of metal clusters in au-, pt-, w- and fe-containing diamond-like carbon hard coatings: A comparative study by small angle x-ray scattering, wide angle x-ray diffraction, transmission electron microscopy and scanning tunnelling microscopy*. Thin Solid Films, 1999. **347**(1–2): p. 60-71.
326. Gerhards, I., C. Ronning, H. Hofsäss, M. Seibt, and H. Gibhardt, *Ion beam synthesis of diamond-like carbon thin films containing copper nanocrystals*. Journal of Applied Physics, 2003. **93**(2): p. 1203-1207.
327. Endrino, J.L., R. Escobar Galindo, H.S. Zhang, M. Allen, R. Gago, A. Espinosa, and A. Anders, *Structure and properties of silver-containing a-c(h) films deposited by plasma immersion ion implantation*. Surface and Coatings Technology, 2008. **202**(15): p. 3675-3682.
328. Pardo, A., C. Gómez-Aleixandre, J.P. Celis, and J.G. Buijnsters, *Friction and wear behavior of plasma assisted chemical vapor deposited nanocomposites made of metal nanoparticles embedded in a hydrogenated amorphous carbon matrix*. Surface and Coatings Technology, 2012. **206**(13): p. 3116-3124.
329. Tang, X.S., H.J. Wang, L. Feng, L.X. Shao, and C.W. Zou, *Mo doped dlc nanocomposite coatings with improved mechanical and blood compatibility properties*. Applied Surface Science, 2014. **311**: p. 758-762.
330. Liu, F., Z. Cao, C. Tang, L. Chen, and Z. Wang, *Ultrathin diamond-like carbon film coated silver nanoparticles-based substrates for surface-enhanced raman spectroscopy*. ACS Nano, 2010. **4**(5): p. 2643-2648.
331. Marciano, F.R., L.F. Bonetti, L.V. Santos, N.S. Da-Silva, E.J. Corat, and V.J. Trava-Airoldi, *Antibacterial activity of dlc and ag-dlc films produced by pecvd technique*. Diamond and Related Materials, 2009. **18**(5-8): p. 1010-1014.
332. Wasy, A., G. Balakrishnan, S. Lee, J. Kim, D. Kim, T. Kim, and J. Song, *Argon plasma treatment on metal substrates and effects on diamond-like carbon (dlc) coating properties*. Crystal Research and Technology, 2014. **49**(1): p. 55-62.
333. Schneider, C.A., W.S. Rasband, and K.W. Eliceiri, *Nih image to imagej: 25 years of image analysis*. Nature methods, 2012. **9**(7): p. 671-675.
334. Hoflund, G.B., Z.F. Hazos, and G.N. Salaita, *Surface characterization study of ag, ago, and ag₂o using x-ray photoelectron spectroscopy and electron energy-loss spectroscopy*. Physical Review B, 2000. **62**(16): p. 11126-11133.
335. Busby, Y. and J.J. Pireaux, *Metal nanoparticle size distribution in hybrid organic/inorganic films determined by high resolution x-ray photoelectron spectroscopy*. Journal of Electron Spectroscopy and Related Phenomena, 2014. **192**: p. 13-18.
336. Citrin, P.H. and G.K. Wertheim, *Photoemission from surface-atom core levels, surface densities of states, and metal-atom clusters: A unified picture*. Physical Review B, 1983. **27**(6): p. 3176-3200.

337. Naumkin, A.V., A. Kraut-Vass, S.W. Gaarenstroom, and C.J. Powell, *Nist x-ray photoelectron spectroscopy database, version 4.1 (web version)*. 2012, National Institute of Standards and Technology: Gaithersburg.
338. Granqvist, C. and R. Buhrman, *Ultrafine metal particles*. *Journal of Applied Physics*, 1976. **47**(5): p. 2200-2219.
339. Galindo, R.E., N. Manninen, C. Palacio, and S. Carvalho, *Advanced surface characterization of silver nanocluster segregation in ag–t1cn bioactive coatings by rbs, gdoes, and arxps*. *Analytical and bioanalytical chemistry*, 2013. **405**(19): p. 6259-6269.
340. de los Arcos, T., P. Oelhafen, U. Aebi, A. Hefti, M. Düggelin, D. Mathys, and R. Guggenheim, *Preparation and characterization of tin–ag nanocomposite films*. *Vacuum*, 2002. **67**(3–4): p. 463-470.
341. Chakravadhanula, V.S.K., C. Kübel, T. Hrkac, V. Zaporozhtchenko, T. Strunskus, F. Faupel, and L. Kienle, *Surface segregation in tio2-based nanocomposite thin films*. *Nanotechnology*, 2012. **23**(49): p. 495701.
342. Antad, V., L. Simonot, and D. Babonneau, *Tuning the surface plasmon resonance of silver nanoclusters by oxygen exposure and low-energy plasma annealing*. *Nanotechnology*, 2013. **24**(4): p. 045606.
343. Tang, J., P. Photopoulos, A. Tserepi, and D. Tsoukalas, *Two-dimensional nanoparticle self-assembly using plasma-induced ostwald ripening*. *Nanotechnology*, 2011. **22**(23): p. 235306.
344. Hatada, R., S. Flege, A. Bobrich, W. Ensinger, C. Dietz, K. Baba, T. Sawase, T. Watamoto, and T. Matsutani, *Preparation of ag-containing diamond-like carbon films on the interior surface of tubes by a combined method of plasma source ion implantation and dc sputtering*. *Applied Surface Science*, 2014. **310**: p. 257-261.
345. Lifshitz, Y., S.R. Kasi, J.W. Rabalais, and W. Eckstein, *Subplantation model for film growth from hyperthermal species*. *Physical Review B*, 1990. **41**(15): p. 10468-10480.
346. Busby, Y., N. Crespo-Monteiro, M. Girleanu, M. Brinkmann, O. Ersen, and J.-J. Pireaux, *3d imaging of filaments in organic resistive memory devices*. *Organic Electronics*, 2015. **16**: p. 40-45.
347. Song, L., J. Wu, and C. Xi, *Biofilms on environmental surfaces: Evaluation of the disinfection efficacy of a novel steam vapor system*. *American Journal of Infection Control*, 2012. **40**(10): p. 926-930.
348. Arciola, C.R., D. Campoccia, P. Speziale, L. Montanaro, and J.W. Costerton, *Biofilm formation in staphylococcus implant infections. A review of molecular mechanisms and implications for biofilm-resistant materials*. *Biomaterials*, 2012. **33**(26): p. 5967-5982.
349. Sehulster, L., R.Y. Chinn, M. Arduino, J. Carpenter, R. Donlan, D. Ashford, R. Besser, B. Fields, M. McNeil, and C. Whitney, *Guidelines for environmental infection control in health-care facilities*. *Morbidity and Mortality Weekly Report Recommendations and Reports RR*, 2003. **52**(10): p. 1-42.
350. Chapman, R.G., E. Ostuni, M.N. Liang, G. Meluleni, E. Kim, L. Yan, G. Pier, H.S. Warren, and G.M. Whitesides, *Polymeric thin films that resist the adsorption of proteins and the adhesion of bacteria*. *Langmuir*, 2001. **17**(4): p. 1225-1233.
351. Murata, H., R.R. Koepsel, K. Matyjaszewski, and A.J. Russell, *Permanent, non-leaching antibacterial surfaces—2: How high density cationic surfaces kill bacterial cells*. *Biomaterials*, 2007. **28**(32): p. 4870-4879.
352. Lee, S.B., R.R. Koepsel, S.W. Morley, K. Matyjaszewski, Y.J. Sun, and A.J. Russell, *Permanent, nonleaching antibacterial surfaces. 1. Synthesis by atom transfer radical polymerization*. *Biomacromolecules*, 2004. **5**(3): p. 877-882.

353. Bright, K., C. Gerba, and P. Rusin, *Rapid reduction of staphylococcus aureus populations on stainless steel surfaces by zeolite ceramic coatings containing silver and zinc ions*. Journal of Hospital Infection, 2002. **52**(4): p. 307-309.
354. Varghese, S., S. Elfakhri, D. Sheel, P. Sheel, F. Bolton, and H. Foster, *Novel antibacterial silver-silica surface coatings prepared by chemical vapour deposition for infection control*. Journal of applied microbiology, 2013. **115**(5): p. 1107-1116.
355. Kwok, S.C.H., W. Zhang, G.J. Wan, D.R. McKenzie, M.M.M. Bilek, and P.K. Chu, *Hemocompatibility and anti-bacterial properties of silver doped diamond-like carbon prepared by pulsed filtered cathodic vacuum arc deposition*. Diamond and Related Materials, 2007. **16**(4-7): p. 1353-1360.
356. Samuel, U. and J.P. Guggenbichler, *Prevention of catheter-related infections: The potential of a new nano-silver impregnated catheter*. International Journal of Antimicrobial Agents, 2004. **23**, Supplement **1**(0): p. 75-78.
357. Katsikogianni, M., I. Spiliopoulou, D.P. Dowling, and Y.F. Missirlis, *Adhesion of slime producing staphylococcus epidermidis strains to pvc and diamond-like carbon/silver/fluorinated coatings*. Journal of Materials Science-Materials in Medicine, 2006. **17**(8): p. 679-689.
358. Tsukruk, V.V., I. Luzinov, and D. Julthongpiput, *Sticky molecular surfaces: Epoxysilane self-assembled monolayers*. Langmuir, 1999. **15**(9): p. 3029-3032.
359. Chen, G., Z. Wang, H. Wang, X. Zhao, J. Hu, S. Wang, and S. Zhang, *Effects of tetrahedral amorphous carbon film deposited on dental cobalt-chromium alloys on bacterial adhesion*. Surface and Coatings Technology, 2012. **206**(15): p. 3386-3392.
360. Liu, C., Q. Zhao, Y. Liu, S. Wang, and E.W. Abel, *Reduction of bacterial adhesion on modified dlc coatings*. Colloids and Surfaces B: Biointerfaces, 2008. **61**(2): p. 182-187.
361. Stobie, N., B. Duffy, J. Colreavy, P. McHale, S.J. Hinder, and D.E. McCormack, *Dual-action hygienic coatings: Benefits of hydrophobicity and silver ion release for protection of environmental and clinical surfaces*. Journal of Colloid and Interface Science, 2010. **345**(2): p. 286-292.
362. Gollwitzer, H., K. Ibrahim, H. Meyer, W. Mittelmeier, R. Busch, and A. Stemberger, *Antibacterial poly (d, l-lactic acid) coating of medical implants using a biodegradable drug delivery technology*. Journal of Antimicrobial Chemotherapy, 2003. **51**(3): p. 585-591.
363. Bratzler, D.W. and P.M. Houck, *Antimicrobial prophylaxis for surgery: An advisory statement from the national surgical infection prevention project*. Clinical Infectious Diseases, 2004. **38**(12): p. 1706-1715.
364. Havill, N.L., *Best practices in disinfection of noncritical surfaces in the health care setting: Creating a bundle for success*. American journal of infection control, 2013. **41**(5): p. S26-S30.
365. Rutala, W.A. and D.J. Weber, *Guideline for disinfection and sterilization in healthcare facilities, 2008*. 2008, Centers for Disease Control (US).
366. Schneider, P.M., *New technologies and trends in sterilization and disinfection*. American journal of infection control, 2013. **41**(5): p. S81-S86.
367. Whiteley, C.M., M. Dalla Valle, K.C. Jones, and A. Sweetman, J., *Challenges in assessing release, exposure and fate of silver nanoparticles within the uk environment*. Environmental Science: Processes & Impacts, 2013. **15**(11): p. 2050-2058.
368. Gao, X.-Y., S.-Y. Wang, J. Li, Y.-X. Zheng, R.-J. Zhang, P. Zhou, Y.-M. Yang, and L.-Y. Chen, *Study of structure and optical properties of silver oxide films by ellipsometry, xrd and xps methods*. Thin Solid Films, 2004. **455-456**(0): p. 438-442.

369. Liu, J. and R.H. Hurt, *Ion release kinetics and particle persistence in aqueous nano-silver colloids*. Environmental Science & Technology, 2010. **44**(6): p. 2169-2175.
370. Xiu, Z.-m., Q.-b. Zhang, H.L. Puppala, V.L. Colvin, and P.J.J. Alvarez, *Negligible particle-specific antibacterial activity of silver nanoparticles*. Nano Letters, 2012. **12**(8): p. 4271-4275.
371. Berney, M., F. Hammes, F. Bosshard, H.U. Weilenmann, and T. Egli, *Assessment and interpretation of bacterial viability by using the live/dead baclight kit in combination with flow cytometry*. Applied and Environmental Microbiology, 2007. **73**(10): p. 3283-3290.
372. Liu, J., D.A. Sonshine, S. Shervani, and R.H. Hurt, *Controlled release of biologically active silver from nanosilver surfaces*. ACS Nano, 2010. **4**(11): p. 6903-6913.
373. Damm, C. and H. Münstedt, *Kinetic aspects of the silver ion release from antimicrobial polyamide/silver nanocomposites*. Applied Physics A, 2008. **91**(3): p. 479-486.
374. Weinstein, R.A., R. Gaynes, J.R. Edwards, and N.N.I.S. System, *Overview of nosocomial infections caused by gram-negative bacilli*. Clinical Infectious Diseases, 2005. **41**(6): p. 848-854.
375. Zhanel, G.G., M. DeCorby, H. Adam, M.R. Mulvey, M. McCracken, P. Lagacé-Wiens, K.A. Nichol, A. Wierzbowski, P.J. Baudry, F. Taylor, J.A. Karlowsky, A. Walkty, F. Schweizer, J. Johnson, and D.J. Hoban, *Prevalence of antimicrobial-resistant pathogens in canadian hospitals: Results of the canadian ward surveillance study (canward 2008)*. Antimicrobial Agents and Chemotherapy, 2010. **54**(11): p. 4684-4693.
376. Lowe, J.J., S.G. Gibbs, P.C. Iwen, P.W. Smith, and A.L. Hewlett, *Impact of chlorine dioxide gas sterilization on nosocomial organism viability in a hospital room*. International Journal Of Environmental Research And Public Health, 2013. **10**(6): p. 2596-2605.
377. Pallavicini, P., A. Taglietti, G. Dacarro, Y. Antonio Diaz-Fernandez, M. Galli, P. Grisoli, M. Patrini, G. Santucci De Magistris, and R. Zaroni, *Self-assembled monolayers of silver nanoparticles firmly grafted on glass surfaces: Low ag+ release for an efficient antibacterial activity*. Journal of Colloid and Interface Science, 2010. **350**(1): p. 110-116.
378. Jamuna-Thevi, K., S.A. Bakar, S. Ibrahim, N. Shahab, and M.R.M. Toff, *Quantification of silver ion release, in vitro cytotoxicity and antibacterial properties of nanostructured ag doped tio2 coatings on stainless steel deposited by rf magnetron sputtering*. Vacuum, 2011. **86**(3): p. 235-241.
379. Joyce-Wöhrmann, R. and H. Münstedt, *Determination of the silver ion release from polyurethanes enriched with silver*. Infection, 1999. **27**(1): p. S46-S48.
380. Santoro, C.M., N.L. Duchsherer, and D.W. Grainger, *Antimicrobial efficacy and ocular cell toxicity from silver nanoparticles*. Nanobiotechnology, 2007. **3**(2): p. 55-65.
381. Arpa Sancet, M., M. Hanke, Z. Wang, S. Bauer, C. Azucena, H. Arslan, M. Heinle, H. Gliemann, C. Woll, and A. Rosenhahn, *Surface anchored metal-organic frameworks as stimulus responsive antifouling coatings*. Biointerphases, 2013. **8**(1): p. 29.
382. Hauert, R., *A review of modified dlc coatings for biological applications*. Diamond and Related Materials, 2003. **12**(3-7): p. 583-589.
383. Narayan, R., H. Abernathy, L. Riester, C. Berry, and R. Brigmon, *Antimicrobial properties of diamond-like carbon-silver-platinum nanocomposite thin films*. Journal of Materials Engineering and Performance, 2005. **14**(4): p. 435-440.
384. Maguire, P.D., J.A. McLaughlin, T.I.T. Okpalugo, P. Lemoine, P. Papakonstantinou, E.T. McAdams, M. Needham, A.A. Ogwu, M. Ball, and G.A. Abbas, *Mechanical stability, corrosion performance and bioresponse of amorphous diamond-like carbon for medical stents and guidewires*. Diamond and Related Materials, 2005. **14**(8): p. 1277-1288.

385. Ferrari, A.C., *Diamond-like carbon for magnetic storage disks*. Surface and Coatings Technology, 2004. **180**: p. 190-206.
386. Moseler, M., P. Gumbsch, C. Casiraghi, A.C. Ferrari, and J. Robertson, *The ultrasoothness of diamond-like carbon surfaces*. Science, 2005. **309**(5740): p. 1545-1548.
387. Lifshitz, Y., *Diamond-like carbon — present status*. Diamond and Related Materials, 1999. **8**(8–9): p. 1659-1676.
388. Lee, K.-R., Y.-J. Baik, and K.-Y. Eun, *Stress relief behaviour of diamond-like carbon films on glasses*. Diamond and Related Materials, 1993. **2**(2): p. 218-224.
389. Lau, D.W.M., D.G. McCulloch, M.B. Taylor, J.G. Partridge, D.R. McKenzie, N.A. Marks, E.H.T. Teo, and B.K. Tay, *Abrupt stress induced transformation in amorphous carbon films with a highly conductive transition phase*. Physical Review Letters, 2008. **100**(17): p. 176101.
390. Ferrari, A.C., S.E. Rodil, J. Robertson, and W.I. Milne, *Is stress necessary to stabilise sp(3) bonding in diamond-like carbon?* Diamond and Related Materials, 2002. **11**(3-6): p. 994-999.
391. Kalish, R., Y. Lifshitz, K. Nugent, and S. Prawer, *Thermal stability and relaxation in diamond-like-carbon. A raman study of films with different sp3 fractions (ta-c to a-c)*. Applied Physics Letters, 1999. **74**(20): p. 2936-2938.
392. Fu, R.K., Y. Mei, M. Fu, X. Liu, and P.K. Chu, *Thermal stability of metal-doped diamond-like carbon fabricated by dual plasma deposition*. Diamond and Related Materials, 2005. **14**(9): p. 1489-1493.
393. Hopf, C., T. Angot, E. Aréou, T. Dürbeck, W. Jacob, C. Martin, C. Pardanaud, P. Roubin, and T. Schwarz-Selinger, *Characterization of temperature-induced changes in amorphous hydrogenated carbon thin films*. Diamond and Related Materials, 2013. **37**(0): p. 97-103.
394. Shirakura, A., M. Nakaya, Y. Koga, H. Kodama, T. Hasebe, and T. Suzuki, *Diamond-like carbon films for pet bottles and medical applications*. Thin Solid Films, 2006. **494**(1–2): p. 84-91.
395. Johnston, S. and S.V. Hainsworth, *Effect of dlc coatings on wear in automotive applications*. Surface Engineering, 2005. **21**(1): p. 67-71.
396. Touzin, M., P. Chevallier, F. Lewis, S. Turgeon, S. Holvoet, G. Laroche, and D. Mantovani, *Study on the stability of plasma-polymerized fluorocarbon ultra-thin coatings on stainless steel in water*. Surface & Coatings Technology, 2008. **202**(19): p. 4884-4891.
397. Clair, S., F. Variola, M. Kondratenko, P. Jedrzejowski, A. Nanci, F. Rosei, and D.F. Perepichka, *Self-assembled monolayer of alkanephosphoric acid on nanotextured ti*. The Journal of chemical physics, 2008. **128**: p. 144705.
398. Truica-Marasescu, F., P. Jedrzejowski, and M.R. Wertheimer, *Hydrophobic recovery of vacuum ultraviolet irradiated polyolefin surfaces*. Plasma Processes and Polymers, 2004. **1**(2): p. 153-163.
399. Veprek, S., M.G.J. Veprek-Heijman, P. Karvankova, and J. Prochazka, *Different approaches to superhard coatings and nanocomposites*. Thin Solid Films, 2005. **476**(1): p. 1-29.
400. Bull, S.J. and S.V. Hainsworth, *Time-dependent changes in the mechanical properties of diamond-like carbon films*. Surface and Coatings Technology, 1999. **122**(2–3): p. 225-229.
401. Bouzerar, R., M. Benlahsen, and J.C. Picot, *Microstructural relaxation of hydrogenated amorphous carbon thin films*. Thin Solid Films, 2005. **482**(1–2): p. 90-93.
402. Hauert, R., C.V. Falub, G. Thorwarth, K. Thorwarth, C. Affolter, M. Stiefel, L.E. Podleska, and G. Taeger, *Retrospective lifetime estimation of failed and explanted diamond-like carbon coated hip joint balls*. Acta Biomaterialia, 2012. **8**(8): p. 3170-3176.
403. Casiraghi, C., A.C. Ferrari, and J. Robertson, *Raman spectroscopy of hydrogenated amorphous carbons*. Physical Review B, 2005. **72**(8): p. 085401.

404. Stoney, G.G., *The tension of metallic films deposited by electrolysis*. Proceedings of the Royal Society of London. Series A, 1909. **82**(553): p. 172-175.
405. Bhushan, B. and V.N. Koinkar, *Nanoindentation hardness measurements using atomic force microscopy*. Applied Physics Letters, 1994. **64**(13): p. 1653-1655.
406. Meyer, E., K. Dransfeld, T. Gyalog, and R. Overney, *Nanoscience: Friction and rheology on the nanometer scale*. 1998, Singapore: World Scientific.
407. Sarid, D., *Scanning force microscopy*. 1991: Oxford University Press.
408. Ferrari, A.C. and J. Robertson, *Interpretation of raman spectra of disordered and amorphous carbon*. Physical Review B, 2000. **61**(20): p. 14095-14107.
409. Tamor, M.A. and W.C. Vassell, *Raman "fingerprinting" of amorphous carbon films*. Journal of Applied Physics, 1994. **76**(6): p. 3823-3830.
410. Weiler, M., S. Sattel, K. Jung, H. Ehrhardt, V.S. Veerasamy, and J. Robertson, *Highly tetrahedral, diamond-like amorphous hydrogenated carbon prepared from a plasma beam source*. Applied Physics Letters, 1994. **64**(21): p. 2797-2799.
411. Chu, P.K. and L. Li, *Characterization of amorphous and nanocrystalline carbon films*. Materials Chemistry and Physics, 2006. **96**(2-3): p. 253-277.
412. Merkulov, V.I., J.S. Lannin, C.H. Munro, S.A. Asher, V.S. Veerasamy, and W.I. Milne, *Uv studies of tetrahedral bonding in diamondlike amorphous carbon*. Physical Review Letters, 1997. **78**(25): p. 4869-4872.
413. Hirai, H., O. Fukunaga, and O. Odawara, *Effect of microwave power on hydrogen content in chemically vapor deposited diamond films*. Journal of the American Ceramic Society, 1991. **74**(7): p. 1715-1718.
414. Miyagawa, Y., H. Nakadate, M. Ikeyama, S. Nakao, and S. Miyagawa, *Dynamic mc simulation for a-c : H deposition in methane plasma based on subplantation model*. Diamond and Related Materials, 2003. **12**(3-7): p. 927-930.
415. Tallant, D.R., J.E. Parmeter, M.P. Siegal, and R.L. Simpson, *The thermal stability of diamond-like carbon*. Diamond and Related Materials, 1995. **4**(3): p. 191-199.
416. Yang, M., M.J. Marino, V.J. Bojan, O.L. Eryilmaz, A. Erdemir, and S.H. Kim, *Quantification of oxygenated species on a diamond-like carbon (dlc) surface*. Applied Surface Science, 2011. **257**(17): p. 7633-7638.
417. Okpalugo, T.I.T., P. Papakonstantinou, H. Murphy, J. McLaughlin, and N.M.D. Brown, *High resolution xps characterization of chemical functionalised mwcnts and swcnts*. Carbon, 2005. **43**(1): p. 153-161.
418. Bourgoïn, D., S. Turgeon, and G.G. Ross, *Characterization of hydrogenated amorphous carbon films produced by plasma-enhanced chemical vapour deposition with various chemical hybridizations*. Thin Solid Films, 1999. **357**(2): p. 246-253.
419. Rybachuk, M. and J.M. Bell, *The effect of sp(2) fraction and bonding disorder on micro-mechanical and electronic properties of a-c : H films*. Thin Solid Films, 2007. **515**(20-21): p. 7855-7860.
420. Boehm, H., *Surface oxides on carbon and their analysis: A critical assessment*. Carbon, 2002. **40**(2): p. 145-149.
421. Gengenbach, T.R. and H.J. Griesser, *Compositional changes in plasma-deposited fluorocarbon films during ageing*. Surface and Interface Analysis, 1998. **26**(7): p. 498-511.
422. Clergereaux, R., D. Escaich, S. Martin, F. Gaillard, and P. Raynaud, *Aging of plasma-deposited carbon layers: Effect of their thickness and material structure*. Thin Solid Films, 2005. **482**(1-2): p. 216-220.
423. Peng, X., Z. Barber, and T. Clyne, *Surface roughness of diamond-like carbon films prepared using various techniques*. Surface and Coatings Technology, 2001. **138**(1): p. 23-32.

424. Hu, A., S. Griesing, M. Rybachuk, Q.B. Lu, and W.W. Duley, *Nanobuckling and x-ray photoelectron spectra of carbyne-rich tetrahedral carbon films deposited by femtosecond laser ablation at cryogenic temperatures*. Journal of Applied Physics, 2007. **102**(7): p. 074311.
425. Sullivan, J., T. Friedmann, and A. Baca, *Stress relaxation and thermal evolution of film properties in amorphous carbon*. Journal of Electronic Materials, 1997. **26**(9): p. 1021-1029.
426. Tersoff, J. and F.K. LeGoues, *Competing relaxation mechanisms in strained layers*. Physical Review Letters, 1994. **72**(22): p. 3570-3573.
427. Choi, J.-H., H. Ahn, S. Lee, and K. Lee. *Stress reduction behavior in metal-incorporated amorphous carbon films: First-principles approach*. in *Journal of Physics: Conference Series*. 2006. IOP Publishing.
428. Li, X.-W., M.-W. Joe, A.-Y. Wang, and K.-R. Lee, *Stress reduction of diamond-like carbon by si incorporation: A molecular dynamics study*. Surface and Coatings Technology, 2013. **228**, **Supplement 1**(0): p. S190-S193.
429. Donnet, C. and A. Erdemir, *Tribology of diamond-like carbon films: Fundamentals and applications*. 2008: Springer New York.
430. Choi, W.S., Y.-H. Joung, J. Heo, and B. Hong, *Friction force microscopy study of annealed diamond-like carbon film*. Materials Research Bulletin, 2012. **47**(10): p. 2780-2783.
431. Popov, V.L., *Contact mechanics and friction*. 2010: Springer.
432. Ronkainen, H. and K. Holmberg, *Environmental and thermal effects on the tribological performance of dlc coatings*, in *Tribology of diamond-like carbon films*. 2008, Springer. p. 155-200.
433. Donnet, C. and A. Erdemir, *Historical developments and new trends in tribological and solid lubricant coatings*. Surface and Coatings Technology, 2004. **180–181**(0): p. 76-84.
434. Wang, C., D. Liu, and W. Lin, *Metal–organic frameworks as a tunable platform for designing functional molecular materials*. Journal of the American Chemical Society, 2013. **135**(36): p. 13222-13234.
435. Xue, D.-X., A.J. Cairns, Y. Belmabkhout, L. Wojtas, Y. Liu, M.H. Alkordi, and M. Eddaoudi, *Tunable rare-earth fcu-mofs: A platform for systematic enhancement of co2 adsorption energetics and uptake*. Journal of the American Chemical Society, 2013. **135**(20): p. 7660-7667.
436. Herrick, W.G., T.V. Nguyen, M. Sleiman, S. McRae, T.S. Emrick, and S.R. Peyton, *Peg-phosphorylcholine hydrogels as tunable and versatile platforms for mechanobiology*. Biomacromolecules, 2013. **14**(7): p. 2294-2304.
437. Imamura, S., M. Ikebata, T. Ito, and T. Ogita, *Decomposition of ozone on a silver catalyst*. Industrial & Engineering Chemistry Research, 1991. **30**(1): p. 217-221.
438. Clay, K., S. Speakman, N. Morrison, N. Tomozeiu, W. Milne, and A. Kapoor, *Material properties and tribological performance of rf-pecvd deposited dlc coatings*. Diamond and related materials, 1998. **7**(8): p. 1100-1107.
439. Burke, J.P., *Infection control - a problem for patient safety*. The New England journal of medicine, 2003. **348**(7): p. 651-6.
440. French, G.L., J.A. Otter, K.P. Shannon, N.M. Adams, D. Watling, and M.J. Parks, *Tackling contamination of the hospital environment by methicillin-resistant staphylococcus aureus (mrsa): A comparison between conventional terminal cleaning and hydrogen peroxide vapour decontamination*. J Hosp Infect, 2004. **57**(1): p. 31-7.
441. Christopher, P., H. Xin, and S. Linic, *Visible-light-enhanced catalytic oxidation reactions on plasmonic silver nanostructures*. Nature chemistry, 2011. **3**(6): p. 467-472.

Annexes

A. Stability and robustness assessment of Ag-DLC coatings

Original title of contribution

Plasma deposition of silver-DLC as robust antibacterial coatings for health applications

Presented at ESCAMPIG 2016, July 12-16, 2016, Bratislava, Slovakia by D. Mantovani

Authors names and affiliations

M. Cloutier^{a,b,c}, F. Anooshehpour^{a,d}, S. Turgeon^a, D. Mantovani^a

^a Laboratory for Biomaterials and Bioengineering, CRC-Tier I, Dept of Min-Met-Materials Engineering, & CHU de Québec Research Center, Laval University, Pavillon Pouliot, salle 1745-E, Québec, Québec G1V 0A6, Canada

^b Chimie ParisTech, PSL Research University, Institut de Recherche de Chimie Paris (IRCP), 11 rue Pierre et Marie Curie, F-75005 Paris, France

^c Sorbonne Universités, UPMC Univ Paris 06, F-75005, Paris, France

^d Laboratoire d'Ingénierie de Surface (LIS), Dept of Min-Met-Materials Engineering, & CHU de Québec Research Center, Laval University, Pavillon Pouliot, salle 1718-D, Québec, Québec G1V 0A6, Canada

***** Parts of the experimental and results sections of the original contribution were removed since they were performed by F. Anooshehpour and are not related to the current thesis *****

Abstract

The development of antibacterial surfaces for near-patient clinical areas, acting in conjunction with cleaning and disinfection procedures, are needed to reduce the spread of nosocomial infections. The suitability of engineered materials for such task typically depends on their stability and general ability to withstand harsh operating conditions. Plasma technologies have been proposed as interesting options since they offer the possibility to deposit strongly adherent and cohesive coatings with a tunable set of properties. Herein, we present the development of silver-containing diamond-like carbon coatings as robust antibacterial surfaces and investigate their deposition, properties and operational stability.

Introduction

With high prevalence rates in healthcare centers in both developed and developing countries, nosocomial infections are amongst the most significant public health concerns worldwide [21, 439]. In this context, the development of robust antibacterial surfaces, acting in conjunction with cleaning and disinfection procedures, have emerged as a necessary measure to reduce the spread of nosocomial infections [166, 320]. Plasma-based coatings can impart the desired surface functions (e.g. antibacterial properties) without affecting bulk mechanical properties. Thanks to their superior robustness, long-term stability, compositional control and conformal and pinhole-free coverage, plasma coatings offer an interesting alternative to solvent-based coating methods [320].

Here, we report the development of a plasma deposition process for the one-step deposition of silver-incorporated diamond-like carbon coatings (Ag-DLC) as robust antibacterial surfaces. DLC coatings are known for their excellent mechanical properties and high stability granted by a high fraction of carbon sp^3 sites [106]. Likewise, silver have been the subject of renewed attention in the nanotechnology and biomedical communities as an effective, broad spectrum antibacterial compound. This paper first presents a plasma diagnostic study performed to establish a predictive model for DLC properties, based on data derived from diagnostic tools instead of process parameters. It then provides a characterization of the structure and properties of the resulting Ag-DLC coatings before reporting on the investigation of their performance in realistic mechanical and chemical stability tests.

Experimental

While the term DLC encompasses a range of materials with different characteristics, it will be used in this text in a more specific sense to refer to hydrogenated amorphous carbon (a-C:H) films. Ag-DLC coatings were prepared single crystal silicon substrates cut into 10mm x 10 mm squares. The film were deposited in a one-step continuous process with a modified FLARION series system (Plasmionique, Varennes. QC, Canada) consisting of a radio frequency, inductively coupled plasma reactor coupled to a very-low frequency sputtering setup (see [267] for details). The specimens were treated with a continuous plasma process composed of three successive sequences: 1) Argon etching, 2) H₂ activation and 3) DLC deposition from CH₄. Silver introduction in the film was achieved through cathodic sputtering of a silver target.

The resulting coatings structure and morphology were studied through a combination of techniques including x-ray photoelectron spectroscopy (XPS), scanning electron microscopy (SEM) and Dektak profilometry (for stress and film thickness measurements). Silver ions release from coating was measured in water over 24h using microwave plasma - atomic emission spectrometry. The wear resistance test consisted in a commercial scouring pad sponge scrubbing the surface at a constant force (20N) in a linear, back and forth motion performed by a mechanical testing system (MACH-1 from Biomomentum). The coatings were removed and analyzed by SEM after 20, 200 and 1000 cycles. The coatings chemical stability was assessed by exposing the surfaces to successive cycles (up to 5) of a 2 wt.% H₂O₂ solution for 5 minutes. After each cycle, the coating surface was inspected by SEM and the concentration of silver at the surface was measured by XPS.

Ag-DLC coatings deposition

The process monitoring tool previously developed was used to deposit Ag-DLC coatings with a range of properties in order to assess their potential as highly stable antibacterial surface. Silver incorporation was achieved through cathodic sputtering of a negatively biased silver target. The applied voltage could be adjusted from 0 to -900V, resulting in a direct control over the silver concentration in the film (from 0 up to 20 at. %). As shown in the previous section, V_b had the strongest influence on the Ag-DLC coatings, impacting the silver segregation, coating hardness and silver ion release (see Figure A.1). Due to the nature of the deposition

process, silver segregation towards the surface occurred in all investigated coatings, but was more pronounced for coatings deposited at higher V_b . Because the antibacterial activity of silver is primarily attributed to the biological activity of silver cations (Ag^+), silver release was also measured for both types of coatings. The higher release from 0V coatings could be partly attributed to higher surface porosity.

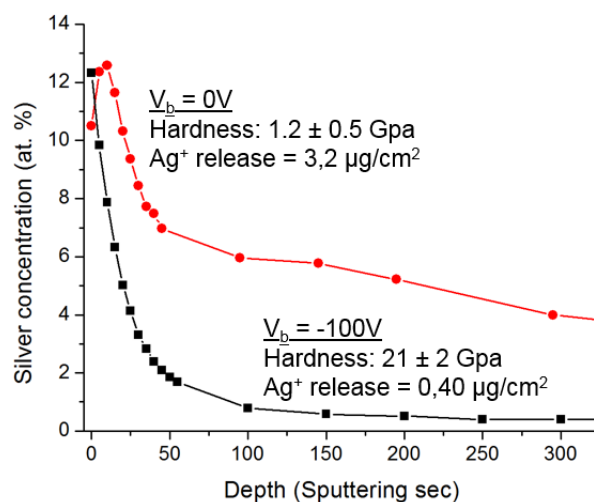


Figure A.1: Silver concentration (measured by XPS) as a function of sputtering depth for coatings deposited at 0V (red circles) and -100V (black square) bias voltage. The hardness and silver ion release values for each conditions are also shown. Both coatings were deposited at the same silver flux, [H] and [CH] concentrations.

Stability and robustness assessment

Poor wear resistance and insufficient stability to cleaning products have been identified as frequent pitfalls of antibacterial surfaces in hospital settings [209]. Consequently, an exploratory study was undertaken to assess the stability of the deposited coatings in realistic operating conditions. Coatings deposited at different V_b (0, -50V and -100V) were first subjected to increasing numbers of wear cycles. Their surfaces were then analyzed by scanning electron microscopy for signs of wear, delamination and other defects. Important qualitative differences could be observed in the wear resistance of the different coatings. On one hand, for 0V coatings, deep scratches and traces of delamination were observed as early as after 20 wear cycles (Figure A.2a). On the other hand, coatings deposited at $V_b = -100V$ could withstand important wear stress conditions, as illustrated by the shallow wear tracks and the absence of visible delamination after 1000 wear cycles (Figure A.2b). The wear resistance of

coatings deposited at -50V was deemed acceptable in that coating delamination was mostly absent after 1000 cycles, although deep wear marks were visible at the surface.

In addition, the coatings chemical stability was assessed by successive cleaning cycles with a hydrogen peroxide solution. Methods using H₂O₂ vapour have been proposed recently as alternatives to deep cleaning procedures in healthcare centers [440]. For all tested deposition condition, an important drop (between 60% and 75%) in the silver content at the surface was measured after the first cleaning cycle (Figure A.2c). Still, even after the maximum number of investigated cycles, all the surfaces maintained a sufficiently high silver content to exhibit antibacterial properties. Coatings deposited at V_b=0V consistently showed the highest remaining silver content after each cleaning cycle.

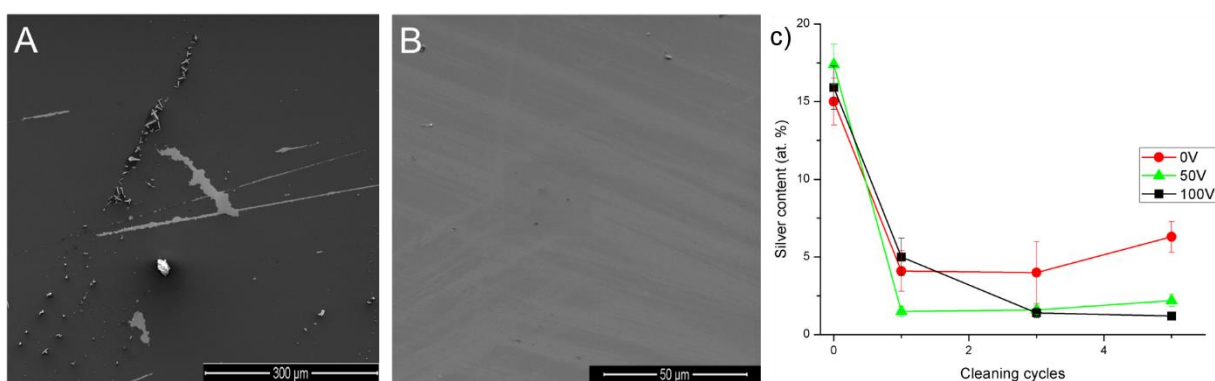


Figure A.2 Representative SEM images of a) V_b=0V coating after 20 wear cycles and b) V_b=-100V coating after 1000 wear cycles. c) Silver content at the surface of 0V, 50 and 100V Ag-DLC coatings for an increasing number of cleaning cycles.

Conclusions

A plasma deposition process was developed to coat surfaces with a silver-carbon composite coating with antibacterial properties. The deposition process could be monitored by simple optical emission spectroscopy, ensuring high reproducibility across deposition systems. The resulting Ag-DLC coatings exhibited superior stability to both mechanical and chemical stresses, suggesting a great potential to be used as robust antibacterial surfaces.

Acknowledgements

This work was partially funded by NSERC-Canada, FRQ-NT-Québec, CFI-Canada, the Canadian Space Agency and MRI-Québec. MC was awarded a prestigious NSERC Vanier Scholarship and also

acknowledges support from a FRQ-NT Frontenac scholarship. The authors are grateful to A. Lefebvre for help in the stability tests.

B. Report on the performances of Ag-DLC as catalytic coatings in an ozonation process

Original contribution presented to members of the Laboratoire Procédés, Plasmas, Microsystèmes (2PM, previously known as LGPPTS).

Context

Silver's unique chemical properties make him an ideal catalyst for several reactions, especially when they are related to an oxidation process [441]. Combined with the antibacterial properties of silver ions, it opens the possibility to design multi-functional coatings with catalytic and bioactive properties. One area where such coating would provide incredible benefits is water decontamination. Drinking water is often contaminated by microorganisms and organic pollutants simultaneously, requiring complex procedures in order to make it potable.

Therefore, we explored in this study the potential application of Ag-DLC and other silver-containing coatings as catalysts in a catalytic ozonation process. We investigated whether silver-based coatings could be used as a heterogeneous catalyst to accelerate the generation of hydroxyl radicals and other highly oxidative compounds from a solution of ozone (O_3). This efficiency as a catalyst was tested both through ability to accelerate the decomposition of ozone and in the ability to degrade a model pollutant, pyruvic acid.

Furthermore, because this study involved the prolonged contact of Ag-DLC coatings with different aqueous solutions (some of them highly oxidative), the stability of Ag-DLC coatings in liquids was also investigated and is reported herein.

Materials & Methods

Two different types of coatings were used in this studies: Ag-DLC films (silver content from 2 to 10 at.%) and Ag sputtered coatings. The deposition of Ag-DLC coatings has been already described in details [267]. The other Ag coatings were deposited by magnetron sputtering of a pure silver target (100W, 6 min) on substrates on a rotating substrate holder to guarantee a uniform deposition. Argon (30 sccm) was used as a sputtering gas during deposition, at a constant pressure of 9 mTorr. The substrates were previously cleaned *in situ* by an argon/oxygen plasma (20 sccm Ar, 10 sccm O₂, at 6 mTorr) at a constant RF power of 75W giving a -200V bias. The films were deposited on 2cm x 2cm cyclic olefin copolymer (COC) substrates

For the ozone degradation studies, the catalyst plate (COC substrate coated with either an Ag-DLC film or a sputtered Ag film) was fixed on the side of a UV-transparent quartz cell (see Figure B.1). A deuterium lamp (light source), optical fibers and a collecting lens were used and provided a direct measurement of the ozone concentration in the solution.

Four different conditions were investigated, 3 using substrates attached to the side of the glass cell and one using catalyst directly in the solution. These conditions were:

1. No catalyst/Bare COC (simple ozonation)
2. Ag-sputtered coatings
3. Ag-DLC coatings
4. Silver nanoparticles (used directly in the solution, not as a coating)

Before the start of the degradation experiment, an ozone saturated solution was prepared by bubbling ozone into 50 ml of deionized water for 30 min. The O₃ saturated solution was then poured in the glass cell, where the degradation of ozone was directly measured in real-time *in situ* using the UV-VIS spectrometer. A maximum of 30 sec occurred between the end of the bubbling and the start of the UV-VIS data acquisition, ensuring a constant saturation in O₃ for all independent experiments.

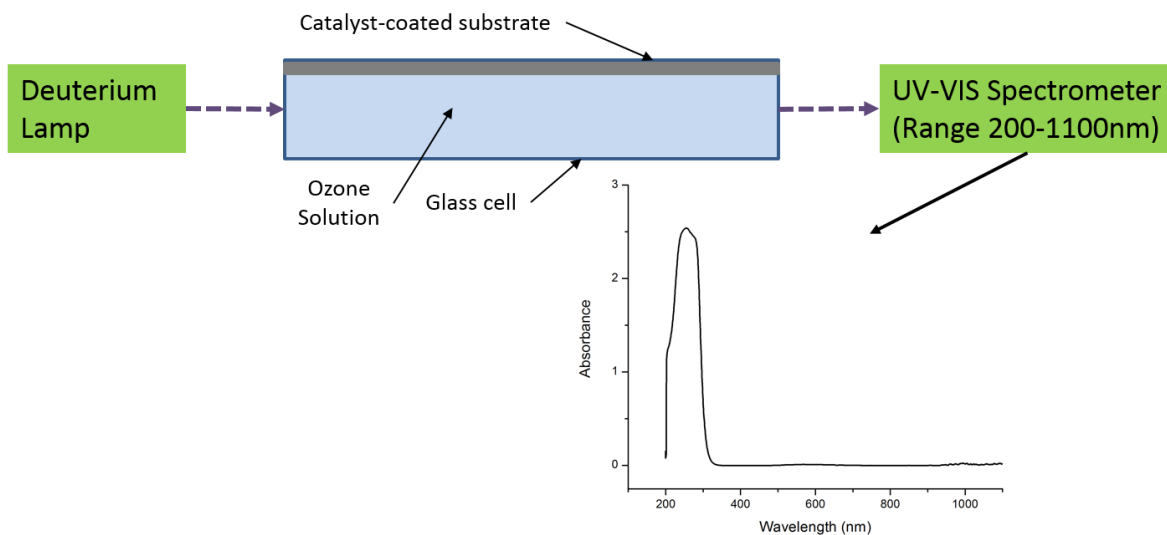


Figure B.1 Schematic of the setup used in the ozone degradation experiment.

For the model pollutant degradation experiment, the same setup (Figure B.1) was used, but only the effect of the Ag-sputtered specimens were investigated. A solution of 0.3 Mol of pyruvic acid was added into the glass cell, in which O_3 was bubbled for 1 hour. After the experiment, the bubbling was stopped and 1ml of the solution was taken in order to measure the final concentration of pyruvic acid by high-performance liquid chromatography (HPLC). HPLC analyses were typically performed between 2 and 3 days after the course of the experiment to prevent any interference from dissolved ozone.

The stability of the Ag-DLC coatings used throughout this experiment was also investigated. Coatings were inspected visually and by optical and scanning electron microscopy after contact with water and the different solutions. Finally, throughout this study, spectroscopic and degradation experiments were performed at least in triplicate.

Catalysis of ozone degradation

Figure B.2 shows a typical degradation profile of ozone, with the concentration of ozone (UV-VIS signal at 259 nm) plotted against time. Two distinct stages can be readily identified on the curve; 1) a slow initial, nearly zero-order decrease in concentration and 2) a much-faster decrease until full depletion of the ozone. The first phase, termed over-saturation stage, was due to a signal saturation of the UV-VIS detector and was not related to the ozone degradation kinetics themselves. Therefore, the only relevant information from this stage is its length.

Because the initial ozone concentration is similar for all experiments, the time it takes to get from that initial concentration to the limit of linearity of the UV-VIS system should be directly related to the overall, constant rate of ozone degradation.

In the second stage, the signal sits squarely in the limit of linearity (LOL) of the system, allowing a direct assessment of the ozone degradation kinetics. The reaction observed followed a typical first-order exponential decay profile and therefore can be described with

$$C(t) = C_0 e^{-t/\tau} \quad (\text{B.1})$$

Where $C(t)$ is the concentration of ozone over time, C_0 is the initial concentration, and τ is the time constant of the system.

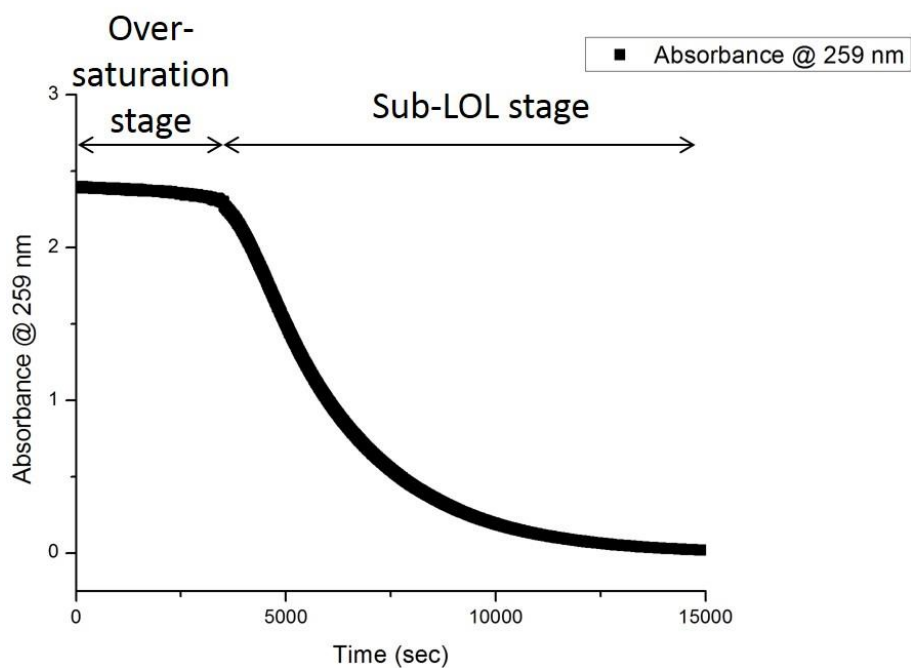


Figure B.2 : Typical reaction kinetics of ozone in solution, measured by UV-Spectroscopy. Because of the upper sensitivity detection limit of the setup, the initial stage of the decomposition kinetics could not be observed and were labeled over-saturation stage.

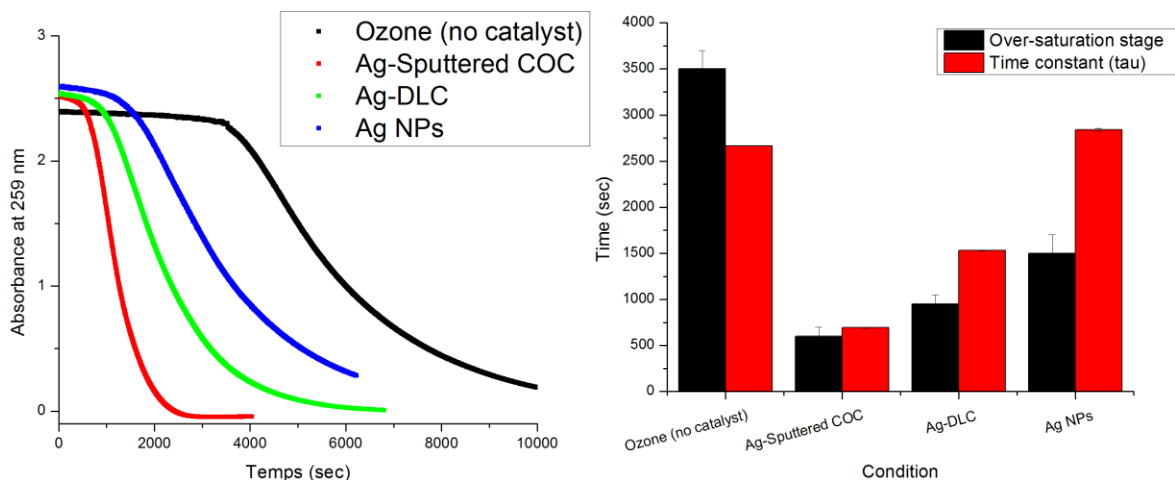


Figure B.3: Ozone decomposition curves when in contact the different silver-based catalyst investigated. The time constants presented on the right figure are associated with the first-order decomposition kinetics measured in the second stage (decomposition stage) of the experiment.

The degradation profile of ozone was measured with the four different conditions (Figure B.3). Both the length of the over-saturation stage, related to the degradation speed, and the time constants measured varied with the presence and type of catalysts used. Pure sputtered silver coatings (Ag-sputtered COC) had the lowest values for both parameters, with Ag-DLC coatings being a close second. Because these conditions were also the ones with the most (Ag-sputtered COC) and second-most (Ag-DLC) available silver, it suggests that silver can indeed catalyse the degradation of ozone. Therefore, their effectiveness in the degradation of a model pollutant, pyruvic acid, was investigated and is presented in the next section.

Catalyst in the degradation of a model pollutant

The efficiency of silver as a catalyst in catalytic ozonation was investigated with pyruvic acid as a model pollutant. The degradation after 1 hour for simple ozonation (no catalyst) and Ag-catalyzed ozonation is shown in Figure B.4. The degradation of pyruvic acid increase by nearly a factor of 5 (0.8% to 3.8%), confirming our previous results that silver did play a role in the degradation rate of ozone and the consequent formation of highly reactive species. We confirmed that this higher efficiency was not due to any adsorption processes, but strictly due to reactions with the ozone and its byproducts.

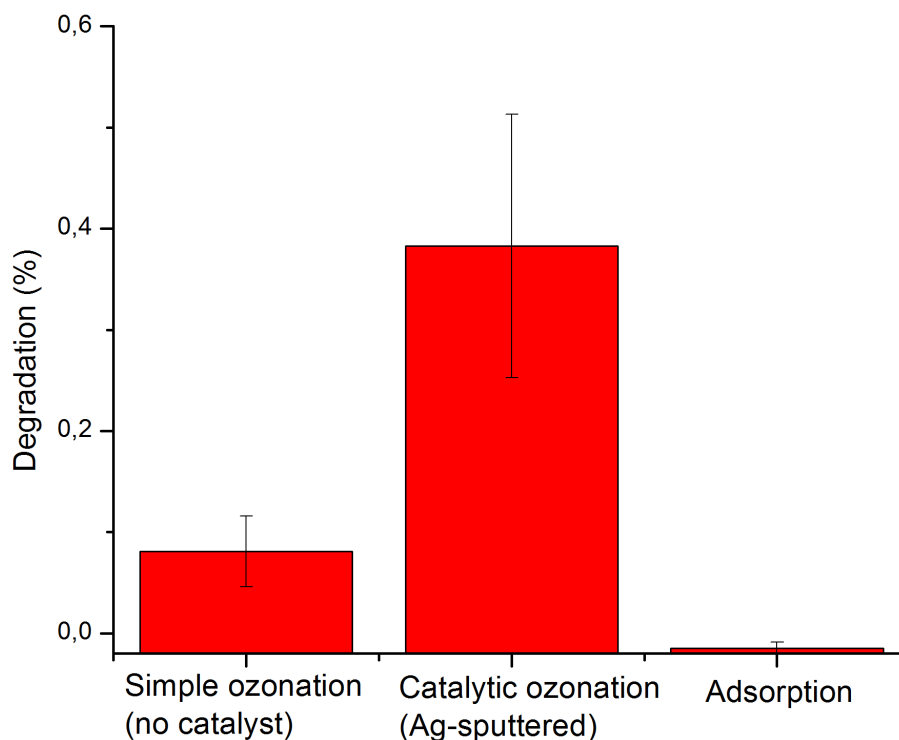


Figure B.4 : Degradation of pyruvic acid after 1 hour.

Stability of silver as a catalyst

Although silver-based coatings did accelerate the decomposition rate of ozone and the degradation of pyruvic acid, they unfortunately showed clear signs of degradation themselves (Figure B.5). Ag-sputtered coatings would be nearly completely dissolved after only 1 cycle of ozonation. We hypothesized that this was due to oxidative dissolution of silver from contact with the ozone solution. Silver oxides are readily dissolved into silver ions in acidic media (see reaction B.3), but oxidation of silver under normal conditions is usually a slow process. However, ozone (or one of its byproducts) seems to be a strong oxidizer of metallic silver, resulting in a rapid dissolution of the Ag-sputtered film into silver ions.



Reaction B.2 is usually much slower than reaction B.3 [369, 370].

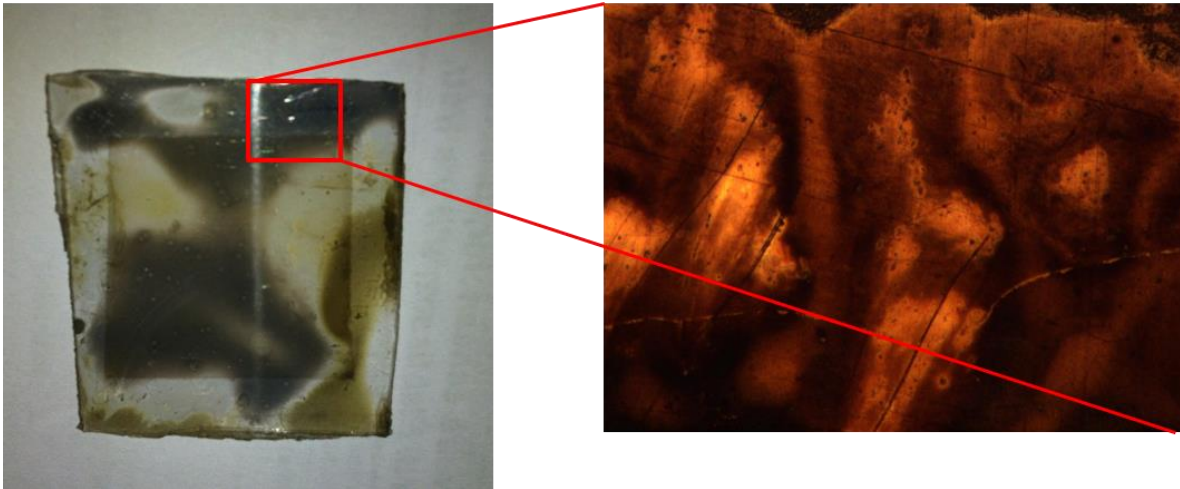


Figure B.5 : Representative images of sputtered silver coatings (on COC substrates) after 1 cycle of ozonation experiment.

Compared with Ag-sputtered film, Ag-DLC coatings fared much better and could resist full ozonation cycles without delamination or dissolution issues. This could be due to the stability provided by the DLC matrix, which can resist the oxidant environment of the ozone solution and therefore protect the silver incorporated in the coating. Although this was not tested, the silver clusters at the surface of the Ag-DLC coating likely underwent a fate similar to that of Ag-sputtered coatings.

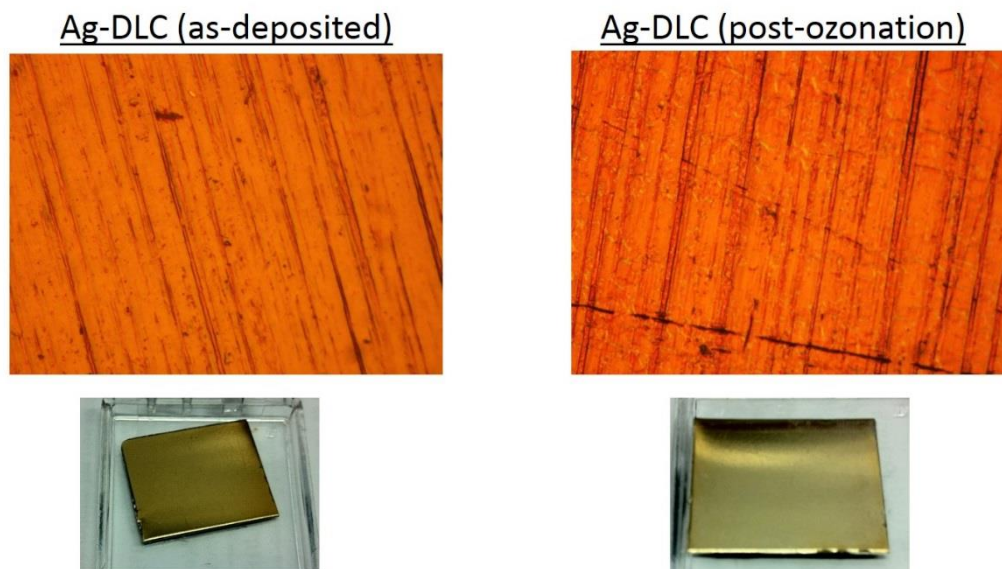


Figure B.6 : Representative images of Ag-DLC coatings on stainless steel before (as-deposited) and after ozonation. Top pictures are optical microscopy (zoomed X20).

Stability of Ag-DLC coatings under water flow

Additional experiments were carried out on the Ag-DLC samples in order to study the degradation of the coatings when exposed to a dynamic flow. Coated microsystems (ALD plate coated with Ag-DLC) were exposed to a deionized water flow of 100 ml / min for 24 hours.

In general, the films have demonstrated a very high stability; traces of delamination were very uncommon and only visible on the edges of the flow plate (Figure B.7). Furthermore, the coatings did not exhibit any swelling or important chemical modification of their surface that could be attributed to the water exposure, since the contact angle remained constant before and after the flow test (Table B.1).

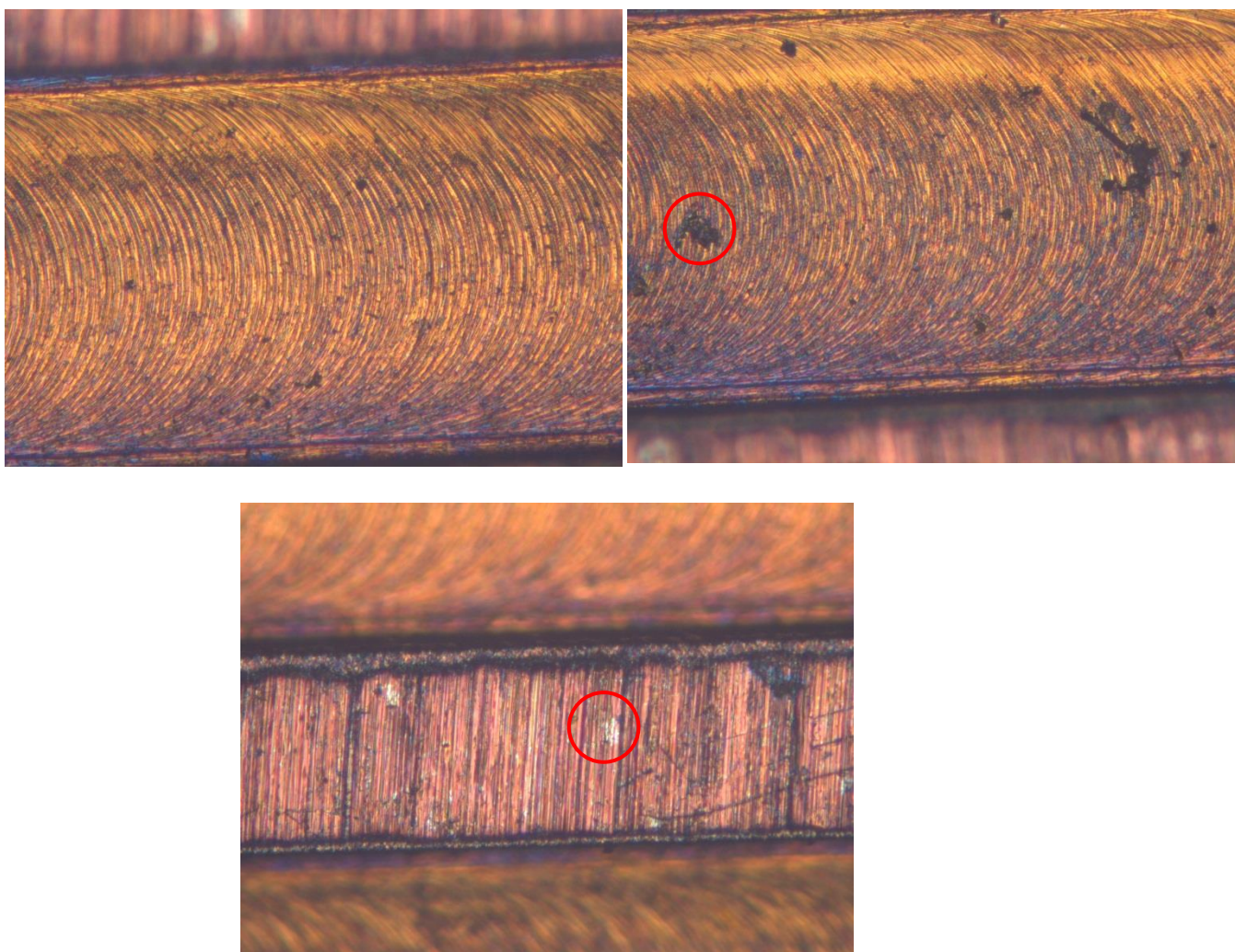


Figure B.7 : Optical microscopy images (50X) of Ag-DLC coated microchannels after 24h under a dynamic water flow. (Top) Inside of microchannels (Bottom) Ridge between pairs of microchannels.

Table B.1: Contact angle (water) of stainless steel and Ag-DLC coatings before and after 24h exposure to water flow

Surface	Stainless steel	Ag-DLC coating pre-immersion	Ag-DLC coating post-immersion (24h)
Contact angle (°)	68±3	81±2	82±3

Conclusions

Although silver-based coatings did increase the decomposition of ozone and the degradation of a model pollutant, it was consumed in the process due to the highly oxidative nature of ozonation. Therefore, it cannot be used in a heterogeneous catalyst in an ozonation process. This investigation however showed the superior stability of Ag-DLC coatings compared with pure sputtered silver thin films. Ag-DLC coatings were more resistant to highly oxidative environments and also showed great chemical and mechanical stability under a continuous water flow.

C. List of publications

Submitted contributions in peer-reviewed journal related to thesis

M. Cloutier, S. Turgeon, M. Tatoulian, D. Mantovani (2017) *Adhesion enhancement of DLC coatings on 316L stainless steel surfaces by in situ plasma carburation*. Submitted January 2017

Published contributions in peer-reviewed journal related to thesis

M. Cloutier, S. Turgeon, Y. Busby, M. Tatoulian, J.J. Pireaux, D. Mantovani (2016) *Controlled distribution and clustering of silver in Ag-DLC nanocomposite coatings using a hybrid plasma approach*. ACS Applied Materials & Interfaces, vol 8 (32), p. 21020-21027.

M. Cloutier, D. Mantovani, F. Rosei (2015) *Antibacterial Coatings: Challenges, Perspectives, and Opportunities*. Trends in Biotechnology, vol 33 (11), p. 637-652.

M. Cloutier, R. Tolouei, O. Lesage, L. Lévesque, S. Turgeon, M. Tatoulian, D. Mantovani (2014) *On the long term antibacterial features of silver-doped diamondlike carbon coatings deposited via a hybrid plasma process*. Biointerphases, vol 9 (2), p. 029013.

M. Cloutier, C. Harnagea, P. Hale, O. Seddiki, F. Rosei, D. Mantovani (2014) *Long-term stability of hydrogenated DLC coatings: Effects of aging on the structural, chemical and mechanical properties*. Diamond and Related Materials, vol 48, p. 65-72.

Other published contributions in peer-reviewed journals (non-thesis related)

M. Dorri, S. Turgeon, N. Brodusch, M. Cloutier, P. Chevallier, R. Gauvin, D. Mantovani (2016) *Characterization of Amorphous Oxide Nano-Thick Layers on 316L Stainless Steel by Electron Channeling Contrast Imaging and Electron Backscatter Diffraction*. Microscopy and Microanalysis vol 22 (5), p. 997-1006.

B. Çelebi, M. Cloutier, R.B. Rabelo, D. Mantovani, A. Bandiera (2012) *Human Elastin-Based Recombinant Biopolymers Improve Mesenchymal Stem Cell Differentiation*. Macromolecular bioscience vol 12 (11), p. 1546-1554.

Other published contributions

G. Sabbatier, L. Lévesque, M. Leroy, Vanessa Montañó-Machado, M. Cloutier, C. Loy, I. Bilem, M. Byad, R. Tolouei, C. Paternoster, D.G. Seifu, C.A. Hoesli, B. Drouin, D. Mantovani, G. Laroche (2014) *Advanced materials for biomedical applications* In book: Functional Materials For Energy, Sustainable Development and Biomedical Sciences, Chapter: 12. Publisher: De gruyter, Editors: Mario Leclerc, Robert Gauvin, pp.277-326

D. List of scientific communications

Oral presentations

International conferences

M. Cloutier, M. Tatoulian, D. Mantovani. *Plasma approaches for the controlled release of silver ions from antibacterial nanocoatings*. NANO 2016, Québec, Canada, August 7-12 2016.

M. Cloutier, S. Turgeon, P. Chevallier, M. Tatoulian, D. Mantovani. *Silver-doped diamond-like carbon: towards highly stable antibacterial coatings*. 10th World Biomaterials Congress, Montréal, Canada May 17-22 2016.

M. Cloutier, V. Montaña-Machado, M. Dorri, L. Angeloni, F. Anooshehpour, S. Díaz-Rodríguez, L. Hugoni, E. Michel, R. Tolouei, C. Paternoster, P. Chevallier, S. Turgeon, D. Mantovani. *The importance of the interface for improving adhesion and stability of substrate/ nanocoating systems*. 10th World Biomaterials Congress, Montréal, Canada May 17-22 2016.

M. Cloutier, S. Turgeon, P. Chevallier, M. Tatoulian, D. Mantovani. *Silver-Containing Diamond-Like Carbon as Highly Stable Antibacterial Coatings*. MRS Spring meeting, Phoenix, USA, March 28 – April 1 2016.

M. Cloutier, S. Turgeon, J-J. Pireaux, D. Mantovani. *Silver-doped diamond-like carbon coatings as highly stable antibacterial surfaces : XPS investigation of silver clustering*. International Conference on Diamond and Carbon Materials, Madrid, Spain, 7-11 September 2014.

M. Cloutier, R. Tolouei, S. Turgeon, L. Lévesque, O. Lesage, M. Tatoulian, D. Mantovani. *Highly stable, dual effect antibacterial coatings deposited via hybrid plasma process*. 4th International Symposium on Surface and Interface of Biomaterials, Rome, Italy, September 24-28 2013.

M. Cloutier, S. Turgeon, R. Tolouei, O. Lesage, A. Sarkissian, M. Tatoulian, D. Mantovani. *Synthesis and characterization of silver loaded DLC nanocoatings and their application as tunable, highly stable antibacterial surfaces*. 19th International Vacuum Congress, Paris, France, September 9-13 2013.

M. Cloutier, S. Turgeon, R. Tolouei, A. Sarkissian, F. Rosei, D. Mantovani. *Interfacial investigation of diamond-like carbon coatings for the creation of highly adherent antibacterial surfaces*. XXI International Materials Research Society (MRS) Congress, Cancún, Mexico, August 12-17 2012.

National and local conferences

M. Cloutier, S. Turgeon, P. Chevallier, M. Tatoulian, D. Mantovani. *Plasma-based approaches to tunable and highly stable antibacterial coatings*. Séminaires du LIOAD, Nantes, France, November 16 2015.

M. Cloutier, O. Seddiki, S. Turgeon, C. Harnagea, A. Sarkissian, F. Rosei, D. Mantovani. *Investigation of the adhesion of diamond-like carbon coatings on stainless steel for the development of functionalized antibacterial surfaces*. NanoQuébec 2012, Montréal, Canada 20-21 March 2012.

M. Cloutier, O. Lesage, L. Lévesque, R. Tolouei, P. Chevallier, S. Turgeon, M. Tatoulian, D. Mantovani. *Revêtements de Diamond-Like Carbon dopés à l'argent: Vers des surfaces antibactériennes ultrastables pour diverses applications*. Colloque Étudiant du CERMA, Québec, Canada, September 7 2012.

Poster presentations

M. Cloutier, M. Tatoulian, D. Mantovani. *Strategies for controlled release of biocidal silver ions from plasma-deposited antibacterial coatings*. 10th World Biomaterials Congress, Montréal, Canada, May 17-22 2016.

M. Cloutier, M. Tatoulian, D. Mantovani. *Silver-doped diamond-like carbon: towards highly stable antibacterial coatings*. BIOMAT 2015, Ile de Ré, France, October 12-14 2015.

M. Cloutier, R. Tolouei, S. Turgeon, M. Tatoulian, D. Mantovani. *Silver-doped diamond-like carbon: towards highly stable antibacterial coatings*. Commonwealth Science Conference, Bangalore, India, November 25-29 2014.

M. Cloutier, V. Montaña-Machado, M. Dorri, L. Angeloni, F. Anoooshepour, S. Díaz-Rodríguez, L. Hugoni, E. Michel, R. Tolouei, C. Paternoster, P. Chevallier, S. Turgeon, D.

Mantovani. *Nanocoatings and surface modifications at the LBB*. CHU symposium, Québec, Canada, October 17 2014.

M. Cloutier, R. Tolouei, O. Lesage, L. Lévesque, P. Chevallier, S. Turgeon, A. Sarkissian, F. Rosei, M. Tatoulian, D. Mantovani. *Design and Development of silver-doped DLC nanocoatings with improved operational stability*. 30th Annual Meeting Of The Canadian Biomaterials Society, Ottawa, Canada, May 29 – June 1 2013.